INAUGURAL-DISSERTATION

zur
Erlangung der Doktorwürde
der
Naturwissenschaftlich-Mathematischen Gesamtfakultät
der
Ruprecht-Karls-Universität
Heidelberg

vorgelegt von

M.Sc. Marcel Mohr

aus Gießen

Tag der mündlichen Prüfung: .....

Mathematical modelling of plasma cell dynamics in multiple myeloma

Gutachter: Professor Dr. Anna Marciniak-Czochra

.....

Dedicated to my parents, D. & D.

Abstract

Plasma cell dyscrasias are characterised by accumulation of malignant plasma cells in the bone marrow. Asymptomatic multiple myeloma (AMM) evolves from monoclonal gammopathy of unknown significance (MGUS) and progresses to symptomatic myeloma involving end organ damage. Three main questions are addressed by mathematical modelling. Firstly, how is growth of malignant plasma cells characterised? Secondly, how fast does progression from early asymptomatic stages (MGUS, AMM) to symptomatic myeloma happen? Thirdly, how many malignant plasma cells initially arrive at the bone marrow?

New mathematical models consisting of piecewise-smooth ordinary differential equations are formulated describing the dynamics of healthy and malignant plasma cells in the bone marrow and its niche. Model analysis refers to existence and uniqueness of solutions, characterisation of solutions within invariant sets, and existence and stability properties of equilibria. Partial equilibria are identified extending the classical notion of equilibria. The models are validated using clinical data consisting of serum and urine samples ($n = 8398$) of patients with AMM and MGUS ($n = 322$ and $n = 196$, respectively).

Model analysis and parameter estimation imply that accumulation of malignant plasma cells can be quantified by the doubling time. A faster doubling time relates to a higher probability of progression to symptomatic myeloma and correlates with a small initial number of malignant plasma cells. Instead of one single initial malignant plasma cell, initiation of myeloma can rather be explained by a „malignant wave“ comprised of a population of malignant plasma cells arriving at the bone marrow and perturbing healthy homoeostasis.

This thesis is the result of an interdisciplinary doctorate and the joint work with Prof. Dr. Anna Marciniak-Czochra (Institute of Applied Mathematics, Heidelberg University) as well as with PD Dr. Dr. Dirk Hose and Dr. Anja Seckinger (Multiple Myeloma Research Laboratory, Heidelberg University Hospital).

Zusammenfassung

Plasmazelldyskrasien sind gekennzeichnet durch Akkumulation maligner Plasmazellen im Knochenmark. Das asymptomatische Multiple Myelom (AMM) entwickelt sich aus einer Monoklonalen Gammopathie Unklarer Signifikanz (MGUS) und progrediert zum symptomatischen Myelom, welches mit Endorganschäden assoziiert ist. Drei grundsätzliche Fragen werden durch mathematische Modellierung thematisiert. Erstens, wie ist das Wachstum maligner Plasmazellen charakterisiert? Zweitens, wie schnell verläuft die Progression von asymptomatischen Stadien (MGUS, AMM) zum symptomatischen Myelom? Drittens, wie viele maligne Plasmazellen erreichen initial das Knochenmark?

Neue mathematische Modelle bestehend aus stückweise glatten gewöhnlichen Differentialgleichungen werden formuliert, welche die Dynamik gesunder und maligner Plasmazellen im Knochenmark und in seiner Nische beschreiben. Die Analyse der Modelle behandelt Existenz- und Eindeutigkeit von Lösungen, die Charakterisierung von Lösungen innerhalb invarianter Mengen und Existenz und Stabilitätseigenschaften von Gleichgewichtslösungen. Partielle Gleichgewichtslösungen, welche das klassische Konzept der Gleichgewichtslösungen erweitern, werden bestimmt. Die Modelle werden validiert durch klinische Daten bestehend aus Serum- und Urinproben ($n = 8398$) von Patienten mit AMM und MGUS ($n = 322$ bzw. $n = 196$).

Modellanalyse und Parameterschätzung implizieren, dass die Akkumulation maligner Plasmazellen durch die Verdopplungszeit quantifiziert werden kann. Eine schnellere Verdopplungszeit kann mit einer höheren Wahrscheinlichkeit der Progression zum symptomatischen Myelom in Beziehung gesetzt werden und korreliert mit einer kleineren initialen Anzahl maligner Plasmazellen. Anstatt durch eine einzige maligne Plasmazelle kann der Beginn der Myelomerkrankung vielmehr durch eine „maligne Welle“ bestehend aus einer Population maligner Plasmazellen erklärt werden, welche im Knochenmark ankommt und die gesunde Homöostase stört.

Diese Dissertation ist das Ergebnis einer interdisziplinären Promotion und der gemeinsamen Arbeit mit Prof. Dr. Anna Marciniak-Czochra (Institut für Angewandte Mathematik, Universität Heidelberg) sowie mit PD Dr. Dr. Dirk Hose und Dr. Anja Seckinger (Labor für Myelomforschung, Universitätklinikum Heidelberg).

Acknowledgements

Working on this dissertation and bridging mathematical theory and medical practice have been a challenging and exciting journey of intense learning for me, not only in the scientific area, but also on a personal level. I deeply appreciate the help and support of all people who accompanied me during this time. I owe particular thanks to the following people and organisations:

First and foremost, I would like to express my gratitude to my supervisor Prof. Dr. Anna Marciniak-Czochra, who offered me the chance to do my doctorate in the area of mathematical modelling in medicine. Not only did she initiate the development of the interdisciplinary project, but also provided an open space for research which I appreciate much. I especially thank her for introducing me into the field of mathematical biology, for encouraging me to participate in international meetings, and for her help and expert advise in all situations.

I am grateful to my medical supervisors PD Dr. Dr. Dirk Hose and Dr. Anja Seckinger for their openness to start this project, and their persistence and patience during many exciting hours of discussions. I deeply acknowledge their commitment to introduce me to the field of multiple myeloma, and their constructive cooperation. I am particularly grateful to Dirk for his helpful suggestions improving this thesis.

Gratitude is owed to the Heidelberg Graduate School of Mathematical and Computational Methods for the Sciences (HGS MathComp) for its financial support during my work on this project. I am very thankful for having experienced various international conferences, meetings and workshops, which otherwise would not have been possible.

I appreciate the interest and the willingness of Dr. Johannes P. Schlöder for giving me theoretical insights into the field of parameter estimation and model identifiability.

I sincerely thank all present and former members of the working group "Applied Analysis and Modelling in Biosciences" for a pleasant working atmosphere. In particular, I am indebted to Dr. Maria Vittoria Barbarossa for being a mentor since my Master's degree. I have been fortunate that she accepted to carefully proofread this dissertation. Moreover, I would like to thank my colleague Jan-Erik Busse for several discussions that helped me to focus on analytical details. Special thanks go to Dr. Frederik Ziebell for many suggestions helping me with parameter estimation.

This dissertation would not have been possible without the encouragement of my family and friends. Heartfelt thanks to my parents for always believing in me, and to David Cordas dos Santos for his incalculable support. I am especially thankful to Julien Neubert who kept a sense of humour when I had lost mine.

Heidelberg, August 2016

Contents

1 Introduction

1.1 Healthy plasma cell biology and function

1.1.1 Healthy plasma cell function

Antibody molecules or **immunoglobulins (Ig)** are an essential part of the adaptive immune response. These are synthesised by specialised white blood cells known as **plasma cells (PCs)** [101].

Production of antibodies

The role of antibodies within the immune system is to recognise and bind to foreign proteins derived from microorganisms. Any protein that can be bound by an antibody is known as an antigen. The interaction between an antibody and an antigen is a key principle in immunology. When an antigen enters the body, it binds to specific B cell receptors. B cells whose receptors have bound the antigen receive a triggering signal which induces a prolific generation of PCs. These PCs massively produce specific antibodies reflecting an integral part of the humoral immune response [101, 131].

Antibody molecules are composed of two identical heavy chains and two light chains. This results in each antibody molecule possessing two antigen binding sites, see Figure 1.1. Antibodies can be classified into five broad types based on the characteristics of their heavy chain constant regions. These fives classes are known as antibody isotypes and include IgM, IgD, IgG, IgA and IgE [131, Chapter 3].

Longevity of immunity

PCs are mostly located in the bone marrow where they represent 0.25% of bone marrow cells [60]. They interact with the bone marrow and its local environment, termed the **niche**, providing growth and survival factors. Being resident in the niche,

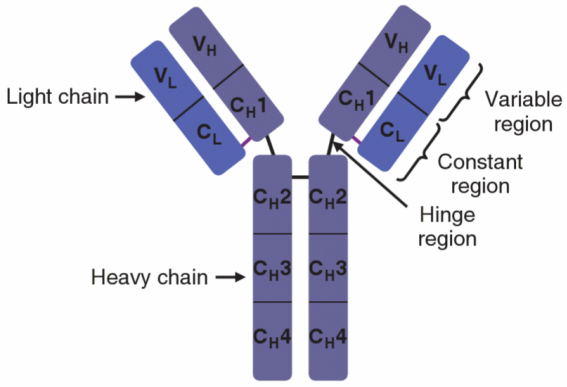

Figure 1.1: Structure of an antibody molecule of type IgA or IgG. Antibodies are composed of two light and two heavy chains linked together by disulphide bonds and divided into variable and constant regions. The variable region is responsible for the antigen-binding capacity of antibodies. Figure adapted from Williams [131, Chapter 3]. For details, see text.

PC survival is not limited owing to survival signals that are derived from the niche [94]. This yields a long-term immunity of $10 - 30$ years [84, 117]. Interaction with the niche is essential since otherwise PCs are prone to die [9, 57, 94].

1.1.2 Healthy plasma cell development

Before PCs can exert their effector functions, they undergo a highly controlled series of developmental stages. The bone marrow is essential for this process. It is located within the long bones in the human body and consists of a fatty substance surrounding a stroma of dividing stem cells [131, Chapter 1].

B cells are derived from the bone marrow. They leave the bone marrow to mature in the spleen, lymph nodes and secondary lymphoid organs. Each B cell produces antibodies that selectively bind to a particular antigen. Within secondary lymphoid tissues, only those B cells that produce antibodies with the highest affinity to the exposed antigen are selected [131, Chapter 2]. Mature B cells further differentiate into plasma blasts being the direct precursors of PCs. Plasma blasts are proliferative with doubling times in the range of days [57]. The migratory phase of plasma blasts lasts one week [94]. Further differentiation yields non-proliferating PCs that enter

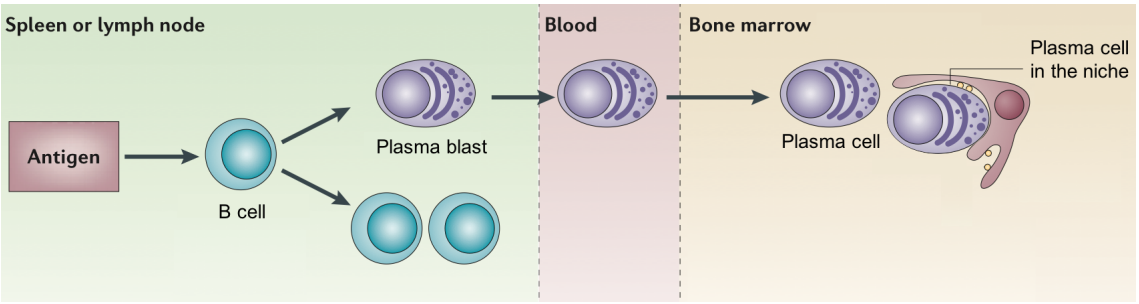

Figure 1.2: Development and maintenance of plasma cells (PCs). Antigen encounter induces B cell differentiation and clonal expansion. Non-proliferative PCs enter the bone marrow and reside in the niche for long term survival. Figure adapted from Radbruch et al. [94]. For details, see text.

the bone marrow through the peripheral blood and produce significant amounts of antibodies. For a visualisation, see Figure 1.2.

Clonal expansion

A primary immune response is triggered if the body encounters a new antigen the first time. It takes $10 - 14$ days for B cells to produce a significant amount of antibodies that can be detected in the bloodstream. The reason for this timespan is that the B cell population requires sufficient time to recognise the antigen and start proliferating in order to produce sufficient numbers of antigen-specific clones [131, Chapter 3]. This clonal expansion of PC precursors (such as plasma blasts) generates a population of non-proliferating PCs arriving at the bone marrow.

Antibody diversity

During B cell development, a number of changes in the genetic locus of the B cell receptor takes place. Two heavy chains and two light chains form the major components of the B cell receptor. The antibody repertoire in any given individual is vast, so that many different kinds of antigen are able to be bound (about 10^7 different antigen specificities). Since the genome is unable to accommodate so many individual Ig genes, immunological diversity is created by a mechanism known as genetic recombination. This allows individual genetic components to be stitched

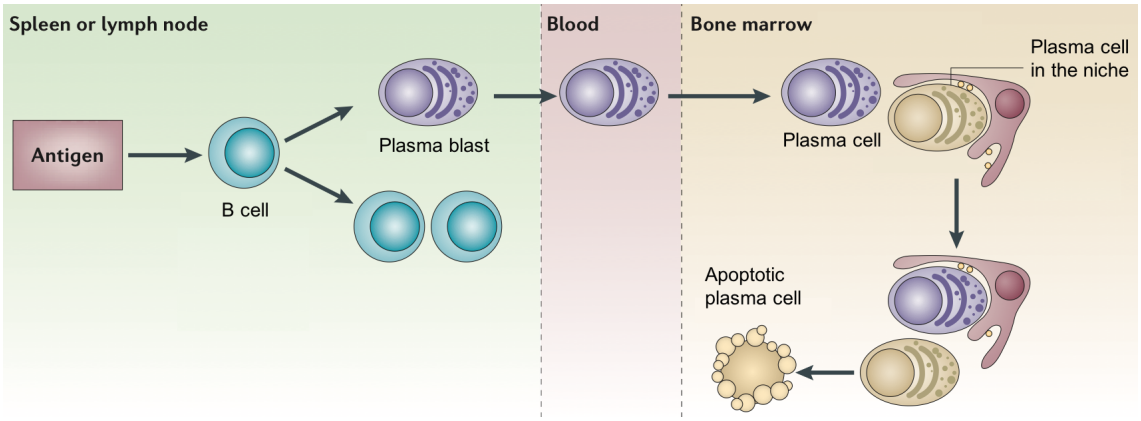

Figure 1.3: Competition of plasma cells (PCs) for occupancy of niches. Antigen encounter induces the production of plasma blasts. Clonal expansion creates a wave of PCs arriving at the bone marrow through the peripheral blood. They may dislocate resident PCs from the niche being able to survive for decades. PCs not being in contact with a niche are prone to die. Figure adapted from Radbruch et al. [94]. For details, see text.

together, enabling the recombination of many different genetic components in order to generate diversity.

The largest element of combinatorial diversity arises from the random recombination of three different gene segments, which occurs in the bone marrow during early B cell development. The heavy chains of B cell receptor genes are comprised of a variable region (V), diversity region (D) and joining region (J), while light chain genes are comprised of a V and J region. Three separate gene segments recombine to form heavy chains, while two gene segments recombine to form light chains. Each Ig heavy and light chain locus has several V, (D) and J gene segments. The combination of V-(D)-J gene segments is a vital and tightly regulated process in generating immunological diversity and is referred to as V(D)J recombination [131, Chapter 3].

Vaccination-induced immune response

Vaccination denotes the exposure of antigens to induce an immune response in order to generate specific antibodies. It can thus be seen as model for physiological antigen encounter (for example by microorganisms). About one week after vaccination, a wave of migrating plasma blasts specific for the vaccinated antigen is found in the blood, whereby PCs are mobilised into the blood being specific for antigens that were

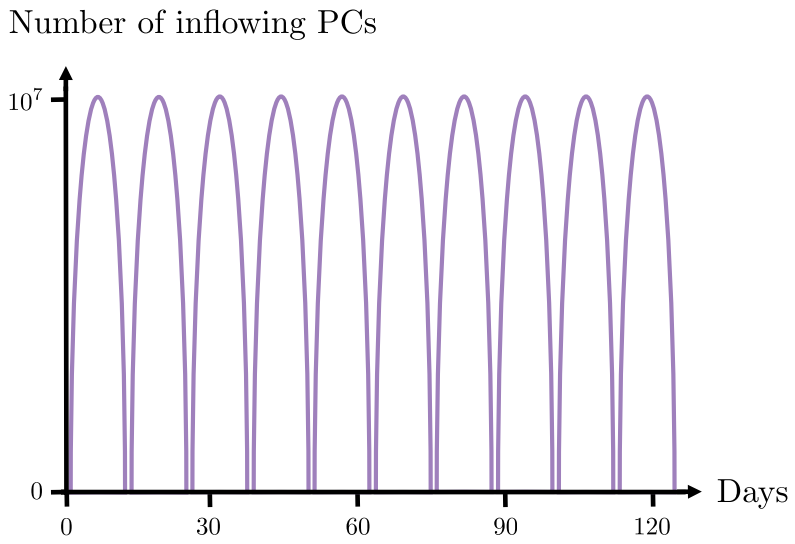

Figure 1.4: Sketch of the time-dependent inflow of plasma cells (PCs) into the bone marrow. It is estimated that about 30 antigenic adoptions to humoral immunity per year occur, each inducing clonal expansion of B cells and the concomitant generation of a wave consisting of a population of about 10^7 PCs arriving at the bone marrow [94]. For details, see text.

encountered previously [94]. This observation fosters the mechanism of competitive dislocation of PCs residing in the niche caused by a population of vaccination-induced PCs arriving at the bone marrow, i.e. „old“ PCs are replaced by vaccination-induced PCs. Being dislocated from the niche, PCs are prone to die. As a result of clonal expansion of PC precursors, the number of arriving vaccination-induced PCs is estimated to be in the magnitude of 10^7 cells [94]. After the immune response, the recruited PCs comprise $0.1 - 1\%$ of the resident PC pool [9, 94]. For a visualisation, see Figure 1.3.

As for vaccination-induced antigen encounter, this mechanism of humoral immunity likewise applies to the case of a natural antigen encounter induced by a pathogen with an extrapolated frequency of antigenic adoptions to humoral immunity of 30 per year. This translates into 30 waves of PCs per year (see Figure 1.4) arriving at the bone marrow and inducing competitive dislocation of PCs resident in the niche. This changes the PC content in the bone marrow leading to long-term immunity with about 1000 populations of PCs comprising 10^6 cells, respectively [94].

1.1.3 Surrogates and measurements

Antibodies are present in the blood serum. The concentration ranges of the five major human Ig classes are summarised in Table 1.1 with considerable inter-individual variety. With a proportional relationship between the number of PCs in the bone marrow and the level of Ig in the serum, the latter can be used as surrogate for the number of PCs (or for the tumour mass in case of PC dyscrasias) in an individual. Levels of Ig are fairly constant in an individual healthy adult. In particular, a constant level of Ig implies a constant number of PCs [101, Chapter 3].

1.2 Malignant plasma cell biology and pathogenesis

1.2.1 Plasma cell dyscrasias

PC dyscrasias are characterised by accumulation of **malignant PCs** in the bone marrow [108]. As their healthy counterpart, malignant PCs depend for survival on interactions with the bone marrow niche. They produce one type of Ig referred to as monoclonal protein. Malignant PCs harbour a high median number of chromosomal aberrations [28, 89] and multiple changes in gene expression compared to healthy PCs [48–50, 110]. In contrast to healthy PCs, malignant PCs proliferate [107].

Table 1.1: Concentration ranges of major human immunoglobulin classes in healthy serum [101, Chapter 3].

Immunoglobulin	**Concentration range** (g/l)
IgG	$8 - 16$
IgA	$1.4 - 4$
IgM	$0.5 - 2$
IgD	$0 - 0.4$
IgE	$17 \cdot 10^{-6} - 450 \cdot 10^{-6}$

Multiple myeloma (MM) is characterised by accumulation of malignant PCs in the bone marrow, causing clinical signs and symptoms related to bone disease (including hypercalcaemia), production of monoclonal protein (renal impairment), and displacement of normal haematopoiesis (anaemia, proneness to infection) [47, 109]. Before progression to these end organ damages (abbreviated with CRAB-criteria) [51], the disease is termed „asymptomatic“ myeloma (AMM). Traditionally synonymously used with „smoldering“ myeloma [70, 72], the latter designation is now restricted to asymptomatic patients without imminent risk of progression [72, 74, 95]. Asymptomatic myeloma evolves in all patients from a monoclonal gammopathy of unknown significance (MGUS) [76]. According to criteria defined by the International Myeloma Working Group (IMWG) [51, 95], the two disease stages are delineated solely by surrogates of tumour mass, i.e. serum monoclonal protein $\geq 30\,\mathrm{g/l}$ or urinary monoclonal protein $\geq 0.5\,\mathrm{g/die}$ and/or bone marrow PC infiltration of $\geq 10\%$.

The type of myeloma is determined by the type of the monoclonal protein aberrantly produced by malignant PCs. It comprises the major human Ig classes. In about 20% of the patients, malignant PCs only produce parts of the Ig, i.e. light chains (predominant light chain myeloma). If they are found in the urine, the disease is termed Bence-Jones myeloma [68, 71, 95]. Light chains are only occasionally liberated by healthy PCs.

Standard procedures for the diagnostic evaluation are imaging techniques to assess involvement of bone, laboratory assessment in combination with bone marrow investigation to evaluate the extent of PC infiltration and the influence on the haematopoietic system as well as renal function analysis [7, 44]. In laboratory assessment, the overproduction of a specific antibody due to the presence of malignant PCs is visible by a spike in the normal distribution of a serum protein electrophoresis. This spike is referred to as the M-gradient, which reflects the „malignant portion“ of the monoclonal Ig [44].

1.2.2 Pathogenesis of myeloma

Pathogenesis of myeloma involves molecular alterations in precursors of bone marrow PCs. Malignant PCs appear in the bone marrow. Their capabilities are to a large degree explainable by physiological functions of their healthy counterpart, i.e. healthy

PCs in the bone marrow [110]. They interact with the bone marrow microenvironment being dependent on growth and survival factors provided by the niche, which they share with healthy PCs [61]. Malignant PCs not being resident in the niche are prone to die. Competition for the niche yields displacement of healthy PCs. Further accumulation as a result of proliferation leads to MGUS and AMM. Malignant PCs induce the transformation of the bone marrow microenvironment which influences bone remodelling and generates bone disease. Ongoing accumulation of malignant PCs leads to therapy-requiring MM [47, 60, 110]. For details, see Klein et al. [60].

1.2.3 Surrogates and measurements

Changes in the levels of IgG (IgA, light chain) can be used as surrogates for changes in the number of malignant PCs for patients classified as IgG-myeloma (IgA-myeloma, predominant light chain myeloma), assuming that the categorisation of each patient according to the type of the monoclonal protein is distinct. This is not satisfied in case of patients with a biclonal gammopathy or a light chain escape. The former refers to the uncommon event of myeloma characterised by the presence of two monoclonal proteins [69, 73]. The latter is characterised by a change in the production of complete Ig molecules (IgA, IgG) to only remaining parts thereof (for example, light chain). In contrast to IgG, the M-gradient for IgA is technically more error-prone. This makes it impractical as a surrogate in case of IgA-myeloma.

1.3 Previous modelling approaches in multiple myeloma

1.3.1 Models of population dynamics of malignant plasma cells

Different mathematical approaches for modelling the growth of malignant PCs have been undertaken since 1969.

Hobbs [46] investigates the time course of the number of malignant PCs using serial measurements of monoclonal protein. Starting from one malignant PC, he assumes constant exponential growth. His findings suggest that it takes over as much as $15 - 20$ years for the clinical emergence of myeloma. Salmon and Smith [102, 103] observe that the number malignant PCs appears to be at least $0.5 \cdot 10^{12}$ at time

of clinical diagnosis, indicating that there is an enormous bulk of malignant PCs with prolonged proliferation occurring asymptomatically before the disease becomes clinically apparent. In contrast to Hobbs, the authors argue that constant exponential growth may not be the optimal assumption. They propose a Gompertzian growth model [75] in which growth is initially exponential but slows progressively before diagnosis or early in the period of clinical observation, see also Sullivan and Salmon [115] and Durie and Salmon [24]. Starting from one malignant PC, the model captures the dynamics of malignant PCs at the time of clinical presentation of a patient (doubling times of $4-6$ months). Back calculation implies short doubling times of the initial malignant PC (doubling times of $1-3$ days), suggesting about 5 years for the clinical emergence of myeloma. The retardation effect in the growth of malignant PCs induced by the Gompertzian model is thought to be due to a shift in the proportion of malignant PCs in the proliferative cycle [115]. A potential criticism could be seen that no biological reasoning for the severe retardation in the growth kinetics of malignant PCs could be identified. However, such a growth behaviour could be explained if the initial event of pathogenesis of myeloma would either appear before or during the clonal expansion of plasma blasts (i.e. proliferation with doubling times in the range of days versus observed doubling times of PCs in the range of months [57]).

In comparison to the exponential and the Gompertzian growth models, Jákó [53, Chapter 8] proposes a model, where another rapidly growing population of „induced“ malignant PCs is assumed, generating a bulk of 10^{12} cells, see Figure 1.5. Yet the author owes the biological justification for his assumption.

1.3.2 Further models

Zabalo [133] investigates the influence of the immune system on early development of myeloma by means of a model capturing the interaction between healthy and malignant PCs, stromal and immune cells. Growth of malignant PCs follows a logistic model. However, a decrease in the growth is not clinically observed [47]. Jonsson et al. [56] present a tumour growth inhibition model which uses ordinary differential equations (ODEs) for describing the dynamics of the monoclonal protein and its shrinkage rate due to treatment. The model is restricted to the population of malignant PCs and applies solely for refractory or relapsed myeloma. Tang et al. [116]

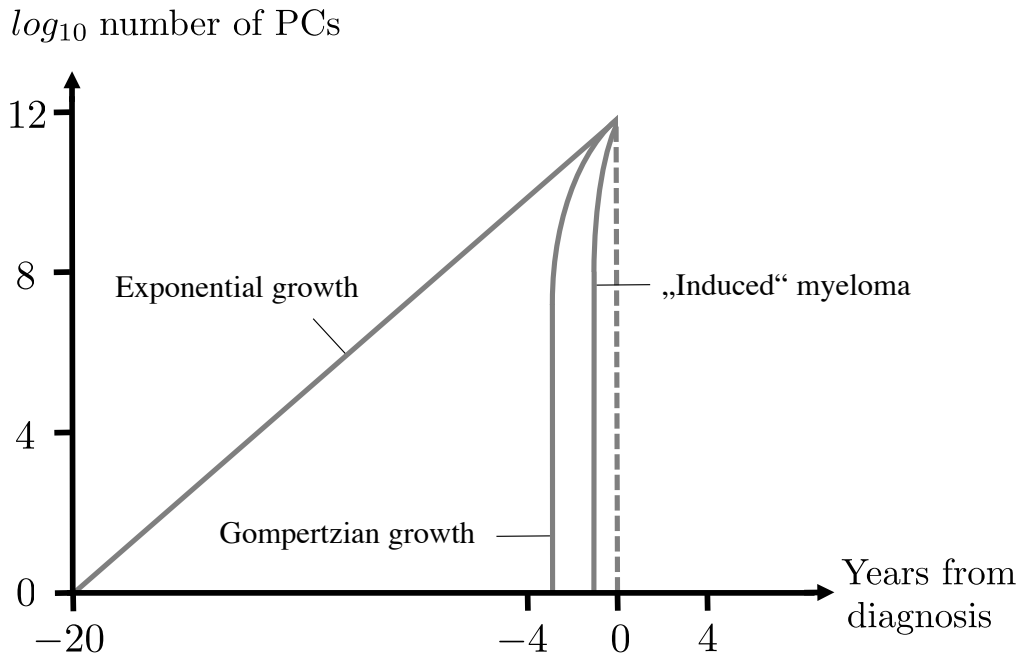

Figure 1.5: Models of the growth dynamics of malignant plasma cells (PCs). Starting from one malignant PC, exponential growth, Gompertzian growth and growth induced by a rapidly growing population of malignant PCs („induced“ myeloma) are sketched on a common logarithmic scale reaching the level of 10^{12} cells for clinical diagnosis. Figure adapted from Jákó [53, Chapter 8]. For details, see text.

propose a hierarchical and a clonal evolution model for malignant PCs tailored to investigate response after treatment. Incorporated rates are density-dependent.
Beside existing models capturing the mechanisms involved in long-term persistence of humoral immunity after natural infections or vaccinations (see for example [3, 122]), further models for myeloma focus on the dynamics of bone interactions in myeloma bone disease, where signalling between cells responsible for bone resorption and formation and their interactions with malignant PCs is considered [5, 54, 63, 64, 93, 128]. Such models are not in the scope of this thesis.

1.4 Aims of the thesis

The primary aims of this thesis are to investigate and provide answers to the following open questions in myeloma biology addressable by modelling:

1. Characterisation of the growth of malignant plasma cells

The aim is to provide biologically plausible models of the growth of malignant PCs allowing investigating whether growth is continuous (such as in an exponential model) or associated with a change in the growth pattern (such as in a Gompertzian growth model).

2. Characterisation of progression to symptomatic myeloma

The analysis addresses the question of how fast progression from early asymptomatic stages (MGUS, AMM) to therapy-requiring myeloma (MM) happens.

3. Quantification of the initial number of malignant plasma cells

Associated with myeloma growth, the study investigates how many malignant PCs initiate myeloma. Hypothesising that initiation of myeloma is due to a population of malignant PCs arriving at the bone marrow similar to the dynamics occurring within a natural immune response (see Figure 1.6), the analysis addresses the question whether one malignant PC is (or can be) able to induce accumulation in the bone marrow as it is assumed by the existing model, see Section 1.3.

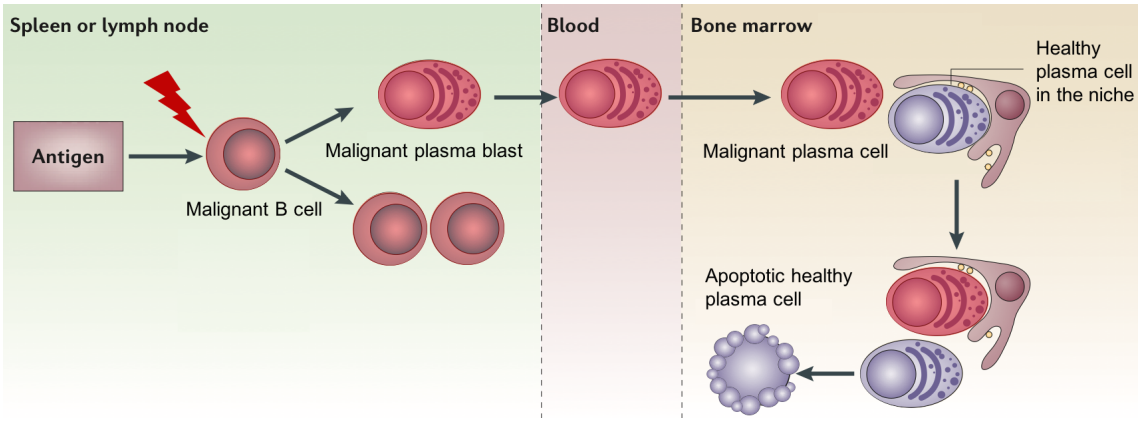

Figure 1.6: Hypothesised model of pathogenesis of myeloma. Molecular alterations in precursors of bone marrow plasma cells (PCs) induce the generation of malignant PCs arriving at the bone marrow and dislocating resident healthy PCs from the niche. PCs not being in contact with a niche are prone to die. Figure adapted from Radbruch et al. [94]. For details, see text.

1.5 Outline of the thesis

This thesis is structured in three parts. The first part (Chapter 2 - Chapter 5) focuses on the derivation of mathematical models capturing the dynamics of healthy and malignant PC accumulation in the bone marrow. The derived models are based on the current understanding of the mechanisms responsible for the development and maintenance of healthy PCs, and accumulation of malignant PCs in myeloma. The second part of the thesis (Chapter 6 - Chapter 8) is devoted to mathematical analysis of the models. Results of the analysis enable further understanding of the underlying mechanisms described by the systems of piecewise-smooth equations. The last part (Chapter 9 - Chapter 11) addresses a quantitative application of the mathematical models using clinical data. Data consist of serum and urine samples ($n = 8398$) of patients with AMM and MGUS ($n = 322$ and $n = 196$, respectively) being the largest worldwide available cohort of myeloma patient samples. A parameter estimation procedure is defined which allows extracting information about the growth of malignant PC population and identifying the initial number of malignant PCs arriving at the bone marrow at the beginning of myeloma.

Chapter 12 provides an integrated discussion and indicates directions for future research. The work is summarised in Chapter 13. Mathematical methods and contributions are stated in the Appendix.

This thesis is the result of an interdisciplinary doctorate and the joint work with Prof. Dr. Anna Marciniak-Czochra from the Institute of Applied Mathematics at Heidelberg University as well as with PD Dr. Dr. Dirk Hose and Dr. Anja Seckinger from the Multiple Myeloma Research Laboratory at Heidelberg University Hospital.

Part I

Mathematical models of healthy and malignant plasma cell dynamics

2 Simple model of exponential growth

At first, the dynamics of the growth of malignant PCs in the bone marrow are considered, neglecting the population of healthy PCs and the bone marrow niche. A simplistic exponential model is proposed, where the following assumptions are made:

Assumption 2.1 (Assumptions for the exponential model)**.**

(1) There is only one population of malignant PCs in the bone marrow.

(2) The rate of change of the number of malignant PCs is constant.

(3) Growth of the number of malignant PCs is independent of the number of healthy PCs.

Let $m(t)$ be the number of malignant PCs in the bone marrow at time t, and

$$m(t) = be^{at}, \quad a \in \mathbb{R},\ b > 0 \ \text{ for } \ t \geq 0. \tag{2.0.1}$$

The model captures exponential growth of $m(t)$ (if $a > 0$) as well as exponential decay of $m(t)$ (if $a < 0$).

Definition 2.2 (Doubling time (DT))**.** Consider the exponential model (2.0.1). For $a \neq 0$, let

$$\tau = \frac{\ln(2)}{|a|}. \tag{2.0.2}$$

If $a > 0$, then τ is the doubling time (DT) of $m(t)$, i.e. the period of time needed for the number of malignant PCs $m(t)$ to double in value. For $a < 0$, τ is the half-value time of $m(t)$, i.e. the period of time needed for $m(t)$ to halve in value.

3 Basic model of healthy plasma cell dynamics

In this chapter, the dynamics of healthy PCs in the bone marrow are considered. Based on healthy PC biology (see Section 1.1), PCs being located outside the niche are distinguished from those being located inside the niche. The following assumptions are made:

Assumption 3.1 (Assumptions for healthy PCs)**.**

(1) There is a constant inflow of healthy PCs per unit of time coming from the peripheral blood and arriving at the bone marrow.

(2) Healthy PCs outside the niche die at a constant rate.

(3) Healthy PCs inside the niche do not die.

(4) At healthy PC homoeostasis, there is a constant distribution between healthy PCs inside and outside the niche where there are more PCs inside than outside the niche.

(5) Transitions into and out of the niche depend on the distribution of healthy PCs within the bone marrow: If there are more PCs outside than inside the niche relative to homoeostasis, then PCs go into the niche at a constant rate. By contrast, if there are more PCs inside than outside the niche relative to homoeostasis, then PCs exit the niche at a constant rate. Rates can be different allowing PCs „sticking“ within the niche.

(6) The niche possesses an unbounded capacity.

Remark 3.2 (Comments on assumptions)**.**

(i) Vaccination exemplifies what happens physiologically if an infection takes place. A wave of a population of vaccination-induced PCs arrives at the bone marrow inducing competitive dislocation of PCs residing in the niche. The number of these antigen encounters can be estimated to be 30 per year [94]. As a simplification, the wave-like inflow of healthy PCs into the bone marrow is approximated by a constant inflow per unit of time, see Figure 3.1.

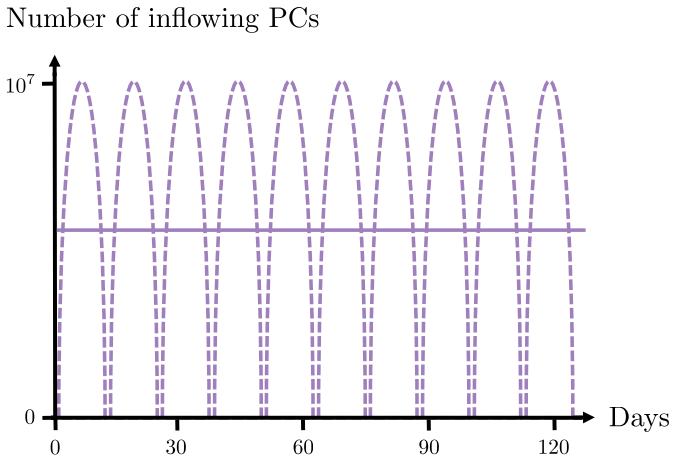

Figure 3.1: Approximation of the time-dependent inflow of healthy plasma cells (PCs) into the bone marrow by a constant inflow, i.e. 30 waves of healthy PCs arriving at the bone marrow per year (dashed) are approximated by a constant inflow of PCs per year (bold). For details, see text.

(ii) Healthy PCs not being resident in the niche are prone to die [9, 57, 94]. As a simplification, the death rate is assumed to be constant.

(iii) The lifespan of healthy PCs inside the niche (decades) is significantly longer than the lifespan of healthy PCs outside the niche (a few weeks) [9, 57, 94]. As a simplification, healthy PCs inside the niche are assumed not to die.

(iv) The total number of healthy PCs remains fairly constant in adulthood as determined by the constant level of immunoglobulin, see Section 1.1.

(v) At homoeostasis, the fraction of healthy PCs inside (outside) the niche is constant, where an increase in the number of PCs outside the niche yields an

increase in the number of PCs inside the niche. Vice versa, an increase in the number of PCs inside the niche yields an increase in the number of PCs outside the niche. For simplification, transition rates are constant. Biologically, the former may be due to antigen encounter and the concomitant arrival of a population of PCs in the bone marrow (outside of the niche). The latter can biologically be justified by death of PCs inside the niche (at a low rate) or PCs leaving the niche and then die.

(vi) Imposing a constant or dynamical carrying capacity [37, 88] for the bone marrow microenvironment is not justified by biological evidence. In case of myeloma, the growth of malignant PCs is unlimited as clinical data reflect, see Chapter 9.

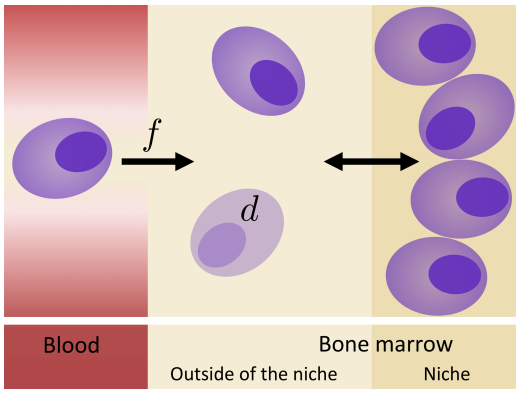

Figure 3.2: Illustration of the basic model of plasma cell (PC) dynamics in the bone marrow. Purple cells represent healthy PCs entering the bone marrow through the peripheral blood. PCs in the bone marrow are either located outside or inside the niche. Transitions between both compartments are possible. The light purple cell represents a dying healthy PC. For details, see text.

Table 3.1 on page 26 lists the variables and parameters used for modelling. Figure 3.2 gives a graphical representation of the basic model of PC dynamics in the bone marrow. A constant number $f > 0$ of healthy PCs, represented by purple cells, enters the bone marrow via the peripheral blood per unit of time. PCs are either located outside or inside the bone marrow niche, i.e. belonging to the x_h-compartment or to the y_h-compartment, respectively. In the former case, PCs die at a constant rate

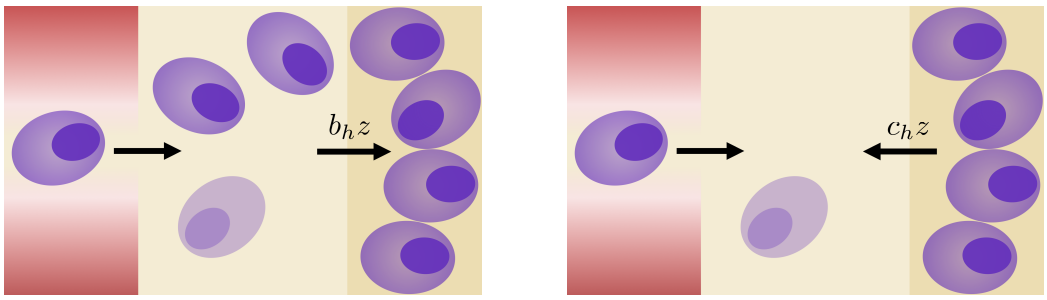

(a) Transition into the niche. (b) Transition out of the niche.

Figure 3.3: Transitions of healthy plasma cells (PCs) described by the basic model. If there is a surplus of PCs outside the niche ($z > 0$), then PCs enter the niche at rate b_h, see (a). If there is a surplus of PCs inside the niche ($z < 0$), then PCs leave the niche at rate c_h, see (b). For details, see text.

$d > 0$, indicated by a light purple cell. Furthermore, cells migrate between the two bone marrow compartments at rates b_h or c_h.

In the following, the dynamic equations for the variables $x_h(t)$ and $y_h(t)$ are formulated in terms of an ODE system corresponding to the illustration given by Figure 3.2. At first, it is clarified how transitions of PCs between the two bone marrow compartments are modelled. Define the function

$$\begin{aligned} z(t) :&= \#\text{ PCs outside the niche } - \#\text{ PCs inside the niche } + n \\ &= x_h(t) - y_h(t) + n, \end{aligned}$$

that is to say, the (positive or negative) **surplus of PCs relative to the niche balance**, where $n > 0$. If $z(t) = 0$, the niche is referred to as being in balance. If the latter holds for all times t, then this accounts for the constant distribution of PC numbers at homoeostasis where there are n more PCs inside than outside the niche. In this case, no transitions occur. If $z(t) > 0$, there are $z(t)$ more PCs outside than inside the niche relative to the niche balance. This surplus of PCs outside the niche migrates into the niche at a constant rate $b_h > 0$, see Figure 3.3 (a). Vice versa, if $z(t) < 0$, there are $-z(t)$ more PCs inside than outside the niche relative to the niche balance. This surplus of PCs inside the niche migrates out of the niche at a constant rate $c_h > 0$, see Figure 3.3 (b).

Remark 3.3. The capacity of the niche is not limited due to Assumption 3.1 (6). It varies with time in the following sense: If $z(t) > 0$, the surplus of PCs relative to the niche balance, which enters the niche, causes a simultaneous stretching of the niche. Consequently, the capacity of the niche increases. If $z(t) < 0$, the surplus of PCs inside the niche, which leaves the niche, causes a simultaneous shrinking of the niche. This results in a decrease of the capacity of the niche.

The previous analysis leads to the following definition of the **transition rates** for the surplus of healthy PCs $z(t)$, which are given by the function

$$\beta_h(z(t)) := \begin{cases} b_h & \text{if } z(t) \geq 0 \\ c_h & \text{if } z(t) < 0. \end{cases}$$

Having characterised the number of healthy PCs which either enter or exit the niche per unit of time depending on the sign of $z(t)$, the dynamic equations for $x_h(t)$ and $y_h(t)$ are formulated:

- The change in the number of healthy PCs in the bone marrow outside the niche per unit of time, $x_h'(t)$, is given by the number of PCs entering via the peripheral blood, f, minus PCs which die, dx_h, plus or minus those PCs which either enter or leave the compartment due to transitions, $\beta_h(z)z$. The mathematical equation reads

  $$x_h'(t) = f - \beta_h(z(t))z(t) - dx_h(t).$$

  For an illustration, see Figure 3.4 (a).

- The change in the number of healthy PCs in the bone marrow inside the niche per unit of time, $y_h'(t)$, is given by those PCs which either enter or leave the compartment due to transitions, $\beta_h(z)z$. The mathematical equation reads

  $$y_h'(t) = \beta_h(z(t))z(t).$$

  For an illustration, see Figure 3.4 (b).

All things considered, the complete mathematical model of healthy PC dynamics in the bone marrow is resumed:

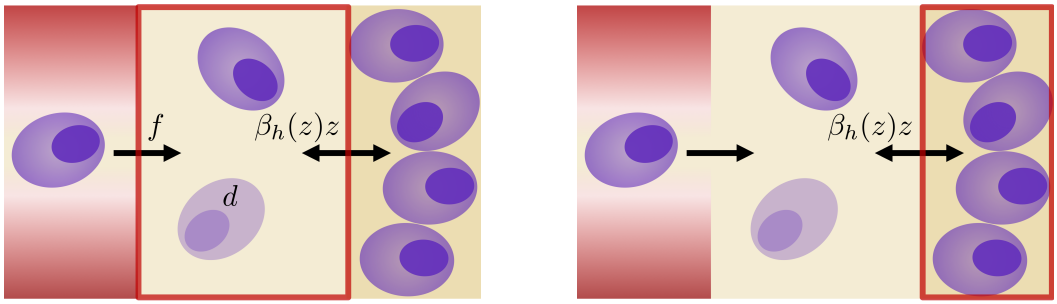

(a) Dynamics within the bone marrow compartment outside of the niche.

(b) Dynamics within the bone marrow compartment inside of the niche.

Figure 3.4: Dynamics of healthy plasma cells within the bone marrow compartments described by the basic model. For details, see text.

The **basic model of healthy PC dynamics in the bone marrow** (abbreviation: **basic model**) is given by the following system of ODEs for times $t \geq t_0 \geq 0$:

$$\begin{aligned} x_h'(t) &= f - \beta_h(z(t))z(t) - dx_h(t) \\ y_h'(t) &= \beta_h(z(t))z(t) \end{aligned} \tag{3.0.1}$$

with surplus of PCs relative to the niche balance $z(t)$ given by

$$z(t) = x_h(t) - y_h(t) + n, \tag{3.0.2}$$

transition rates $\beta_h(z(t))$ given by

$$\beta_h(z(t)) = \begin{cases} b_h & \text{if } z(t) \geq 0 \\ c_h & \text{if } z(t) < 0 \end{cases} \tag{3.0.3}$$

and non-negative initial conditions

$$\begin{aligned} x_h(t_0) &= x_h^0 \geq 0 \\ y_h(t_0) &= y_h^0 \geq 0. \end{aligned} \tag{3.0.4}$$

Variables and parameters are listed in Table 3.1 on page 26.

Remark 3.4. The basic model (3.0.1) (or system (3.0.1)) possesses exactly one equilibrium: Solving the system of equations

$$\begin{aligned} 0 &= f - \beta_h(z)z - dx_h \\ 0 &= \beta_h(z)z \end{aligned}$$

for x_h and y_h yields $z = 0$ and therefore $x_h = \frac{f}{d}$. It follows that $y_h = \frac{f}{d} + n$ due to (3.0.2). This implies that the niche is in balance for all times, and PC homoeostasis is characterised by the equilibrium of system (3.0.1). The occurrence of such an equilibrium is in accordance with the observation that the total number of healthy PCs remains constant in adulthood, see Section 1.1. This finding backs up Assumption 3.1 (4).

Definition 3.5 (Healthy equilibrium)**.** Consider the basic model (3.0.1). Let

$$E_h := \left(x_h^{E_h}, y_h^{E_h}\right)^T := \left(\frac{f}{d}, \frac{f}{d} + n\right)^T$$

be referred to as healthy equilibrium.

Table 3.1: Description of variables and parameters of the basic model of healthy plasma cell (PC) dynamics (3.0.1). All parameters are real and positive unless it is stated differently.

Symbol	**Description**	**Unit**
$x_h(t)$	Number of healthy PCs outside the niche at time t	# PCs
$y_h(t)$	Number of healthy PCs inside the niche at time t	# PCs
f	Number of healthy PCs entering the compartment outside of the niche via the blood per unit of time	# PCs $\cdot$ time^{-1}
d	Death rate of healthy PC outside the niche	time^{-1}
b_h	Transition rate of healthy PCs outside the niche into the niche	time^{-1}
c_h	Transition rate of healthy PCs inside the niche out of the niche	time^{-1}
n	Difference in number of PCs between PCs inside and outside the niche at healthy homoeostasis	# PCs

4 Extended model of healthy plasma cell dynamics

In this chapter, the model equations (3.0.1) of the basic model are extended in order to capture the dynamics of two distinct populations of healthy PCs in the bone marrow. Using a vaccination scenario, a regular antigen encounter induced by a pathogen and the concomitant production of a population of healthy PCs is exemplified. Vaccination can be interpreted as inducing one of the waves arriving at the bone marrow due to natural antigen encounter and causing dislocation of resident healthy PCs, see Chapter 1. Along these lines, **vaccination-induced** healthy PCs are distinguished from **pathogen-induced** healthy PCs within the total population of healthy PCs.

Assumption 4.1 (Assumptions for vaccination-induced healthy PCs)**.**

(1) There is a time $T \geq 0$ at which a certain number of vaccination-induced healthy PCs is added to the compartment of healthy PCs outside of the niche. In particular, there is no constant inflow of vaccination-induced healthy PCs.

(2) Vaccination-induced healthy PCs possess the same properties as pathogen-induced healthy PCs (because they are healthy PCs).

Remark 4.2 (Comment on assumptions)**.** Inflow of vaccination-induced PCs is described by one of the estimated 30 waves arriving at the bone marrow per year [94]. For simplification, it is approximated by a discrete-in-time event.

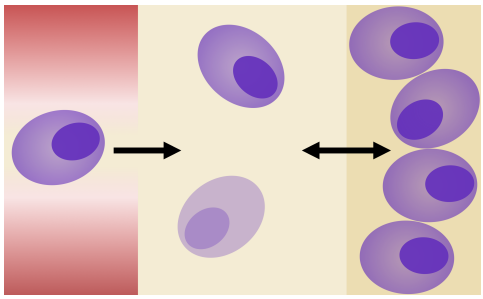

(a) Healthy equilibrium of pathogen-induced healthy PCs.

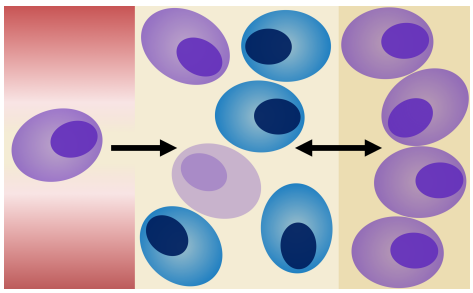

(b) Perturbation of the healthy equilibrium by vaccination-induced healthy PCs.

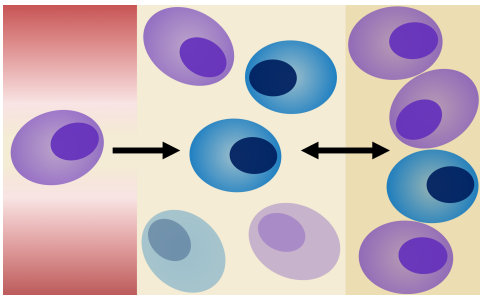

(c) Onset of the dynamics.

Figure 4.1: Perturbation of the healthy equilibrium due to vaccination. Purple cells represent pathogen-induced healthy plasma cells (PCs), whereas blue cells represent vaccination-induced healthy PCs. Homoeostasis is perturbed by a population of vaccination-induced healthy PCs arriving at the bone marrow in a discrete-in-time event (depicted as blue cells appearing outside the niche). For details, see text.

Figure 4.1 illustrates the scenario of a **vaccination-induced perturbation of the healthy equilibrium**: At time T, a certain number of vaccination-induced healthy PCs arrives at the bone marrow and is therefore added to the compartment of healthy PCs outside the niche. This discontinuous perturbation of the healthy equilibrium causes the onset of dynamical interactions.

The basic model is extended by two additional equations describing the number of vaccination-induced healthy PCs in the bone marrow outside and inside the niche, respectively. In order to distinguish between pathogen-induced and vaccination-induced healthy PCs, new notations for the model variables are introduced, see Table 4.1 on page 34. Note that there is no need to introduce further parameters since biologically both populations are the same as depicted in Assumption 4.1. Yet transitions need to be modified.

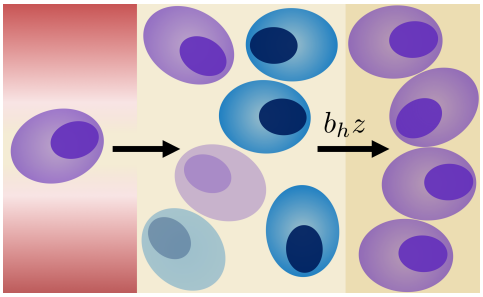

Figure 4.2: Transition of plasma cells (PCs) into the niche at time t is due to a surplus of PCs outside the niche at time t, i.e. $z(t) > 0$. This surplus of PCs composed of pathogen-induced and vaccination-induced healthy PCs enters the niche at rate b_h. For details, see Example 4.3.

At first, the surplus of PCs relative to the niche balance (3.0.2) is refined, i.e.

$$z(t) = \underbrace{x_{h,0}(t) + x_{h,v}(t)}_{\#\text{ PCs outside the niche}} - \underbrace{(y_{h,0}(t) + y_{h,v}(t))}_{\#\text{ PCs inside the niche}} + n, \quad n > 0.$$

Since $z(t)$ describes the surplus of the total healthy PCs relative to the niche balance, the proportion of each PC type (pathogen-induced or vaccination-induced) within each compartment has to be taken into account. This results in an additional factor in the transition term $\beta_h(z)z$ reflecting the proportionality.

Example 4.3 (Dynamics for $z(t) > 0$)**.** To give an illustration, consider the situation immediately after the perturbation of the healthy equilibrium. Since the number of PCs outside the niche abruptly increases at time T, it follows that $z(t) > 0$ for at least $t \in [T, T + \varepsilon)$, $\varepsilon > 0$. Thus, there is a surplus of PCs outside the niche relative to the niche balance, which migrates into the niche at constant rate b_h, see Figure 4.2. Assuming that the portion of each PC type (pathogen-induced or vaccination-induced) within the surplus $z(t)$ is the same as the portion of each PC type (pathogen-induced or vaccination-induced) within the compartment of PCs outside the niche, it follows that

$$\frac{x_{h,0}(t)}{x_{h,0}(t) + x_{h,v}(t)} z(t) \quad \text{and} \quad \frac{x_{h,v}(t)}{x_{h,0}(t) + x_{h,v}(t)} z(t)$$

describe the numbers of pathogen-induced healthy, respectively of vaccination-induced healthy PCs outside the niche migrating into the niche at rate b_h.

The rate function β_h is extended as follows:

$$\beta_{h,j}(z(t)) := \begin{cases} b_h \frac{x_{h,j}(t)}{x_{h,0}(t)+x_{h,v}(t)} & \text{if } z(t) \geq 0 \\ c_h \frac{y_{h,j}(t)}{y_{h,0}(t)+y_{h,v}(t)} & \text{if } z(t) < 0, \end{cases}$$

where $j \in \{0, v\}$. This allows formulating the dynamic equations for $x_{h,0}(t), x_{h,v}(t)$ and $y_{h,0}(t), y_{h,v}(t)$ based on the previous discussion:

- The change in the number of pathogen-induced and vaccination-induced healthy PCs in the bone marrow outside the niche per unit of time, $x'_{h,0}(t)$ and $x'_{h,v}(t)$, respectively, is given by

$$\begin{aligned} x'_{h,0}(t) &= f - \beta_{h,0}(z(t))z(t) - dx_{h,0}(t) \\ x'_{h,v}(t) &= -\beta_{h,v}(z(t))z(t) - dx_{h,v}(t). \end{aligned}$$

- The change in the number of pathogen-induced and vaccination-induced healthy PCs in the bone marrow inside the niche per unit of time, $y'_{h,0}(t)$ and $y'_{h,v}(t)$, respectively, is given by

$$\begin{aligned} y'_{h,0}(t) &= \beta_{h,0}(z(t))z(t) \\ y'_{h,v}(t) &= \beta_{h,v}(z(t))z(t). \end{aligned}$$

All things considered, the extended mathematical model of healthy PC dynamics in the bone marrow is resumed:

The **extended model of healthy PC dynamics in the bone marrow** (abbreviation: **extended model**) is given by the following system of ODEs for times $t \geq t_0 \geq 0$:

$$\begin{aligned} x'_{h,0}(t) &= f - \beta_{h,0}(z(t))z(t) - dx_{h,0}(t) \\ x'_{h,v}(t) &= -\beta_{h,v}(z(t))z(t) - dx_{h,v}(t) \\ y'_{h,0}(t) &= \beta_{h,0}(z(t))z(t) \\ y'_{h,v}(t) &= \beta_{h,v}(z(t))z(t) \end{aligned} \tag{4.0.1}$$

with surplus of PCs relative to the niche balance $z(t)$ given by

$$z(t) = x_{h,0}(t) + x_{h,v}(t) - (y_{h,0}(t) + y_{h,v}(t)) + n, \tag{4.0.2}$$

transition rates $\beta_{h,j}(z(t)),\ j \in \{0, v\}$, given by

$$\beta_{h,j}(z(t)) = \begin{cases} b_h \frac{x_{h,j}(t)}{x_{h,0}(t)+x_{h,v}(t)} & \text{if } z(t) \geq 0 \\ c_h \frac{y_{h,j}(t)}{y_{h,0}(t)+y_{h,v}(t)} & \text{if } z(t) < 0 \end{cases} \tag{4.0.3}$$

and non-negative initial conditions

$$\begin{aligned} x_{h,0}(t_0) &= x^0_{h,0} \geq 0 \\ x_{h,v}(t_0) &= x^0_{h,v} \geq 0 \\ y_{h,0}(t_0) &= y^0_{h,0} \geq 0 \\ y_{h,v}(t_0) &= y^0_{h,v} \geq 0. \end{aligned} \tag{4.0.4}$$

Variables and parameters are listed in Table 4.1 on page 34.

Observe that the healthy equilibrium of the basic model stated in Definition 3.5 can be formulated as an equilibrium of the extended model (4.0.1) (or system (4.0.1)), i.e.

$$E_h = \left(x_h^{E_h}, 0, y_h^{E_h}, 0\right)^T.$$

Definition 4.4 (Vaccination-induced perturbation of the healthy equilibrium)**.** Consider the extended model (4.0.1) and its healthy equilibrium E_h. Let $T \geq 0$. For $0 \leq t < T$, let (4.0.1) be at the healthy equilibrium E_h, i.e.

$$(x_{h,0}(t), x_{h,v}(t), y_{h,0}(t), y_{h,v}(t))^T = E_h.$$

Then, at $t = T$,

$$(x_{h,0}(T), x_{h,v}(T), y_{h,0}(T), y_{h,v}(T))^T = \left(x_h^{E_h}, x_{h,v}^0, y_h^{E_h}, 0\right)^T \quad \text{with} \quad x_{h,v}^0 > 0 \tag{4.0.5}$$

defines a vaccination-induced perturbation of the healthy equilibrium at time T as described in Assumption 4.1, which can be interpreted as initial condition for system (4.0.1) with $t_0 = T$.

Remark 4.5. The extended model (4.0.1) is a refinement of the basic model (3.0.1) in the following sense: It is

$$\begin{aligned}
(x_{h,0} + x_{h,v})'(t) &= x_{h,0}'(t) + x_{h,v}'(t) \\
&= f - \beta_{h,0}(z(t))z(t) - dx_{h,0}(t) - \beta_{h,v}(z(t))z(t) - dx_{h,v}(t) \\
&= f - (\beta_{h,0}(z(t)) + \beta_{h,v}(z(t)))\, z(t) - d\,(x_{h,0}(t) + x_{h,v}(t)) \\
&= f - \beta_h(z(t))z(t) - d\,(x_{h,0}(t) + x_{h,v}(t))
\end{aligned}$$

and

$$\begin{aligned}
(y_{h,0} + y_{h,v})'(t) &= y_{h,0}'(t) + y_{h,v}'(t) \\
&= \beta_{h,0}(z(t))z(t) + \beta_{h,v}(z(t))z(t) \\
&= \beta_h(z(t))z(t)
\end{aligned}$$

with $\beta_h(z)$ given by (3.0.3). By $x_h(t) = x_{h,0}(t) + x_{h,v}(t)$ and $y_h(t) = y_{h,0}(t) + y_{h,v}(t)$, the dynamics of $x_h(t)$ and $y_h(t)$ are adequately characterised by the basic model (3.0.1).

Remark 4.6. After the vaccination-induced perturbation of the healthy equilibrium, the dynamics of system (4.0.1) re-establishes the healthy equilibrium with the same total number of healthy PCs outside and inside the niche as before. However, the composition of healthy PCs within the niche is different, see Figure 4.3. In Section 8.1, it is investigated that system (4.0.1) possesses, in addition to the healthy

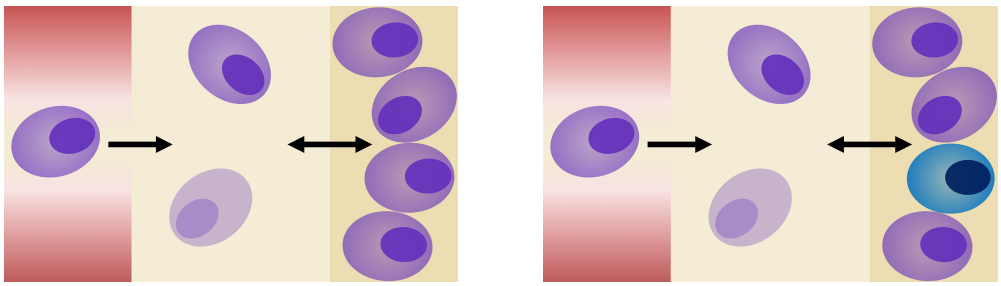

(a) Healthy equilibrium before vaccination.

(b) Healthy equilibrium after vaccination.

Figure 4.3: Healthy equilibrium of plasma cells (PCs) before and after vaccination. Vaccination-induced healthy PCs (blue) partially replace pathogen-induced healthy PCs (purple), yielding a new composition of the healthy equilibrium. The total number of PCs out- and inside the niche is unchanged compared to the previous equilibrium. For details, see Remark 4.6.

equilibrium E_h, a one-dimensional manifold of non-isolated equilibria, justifying that the extended model is able to explain qualitatively the long-term persistence of an additional immunity characteristic. In Section 10.2, a verification in terms of a quantification of this dynamical process is provided.

Table 4.1: Description of variables and parameters of the extended model of healthy plasma cell (PC) dynamics (4.0.1). All parameters are real and positive unless it is stated differently.

Symbol	**Description**	**Unit**
$x_{h,0}(t)$	Number of pathogen-induced healthy PCs outside the niche at time t	# PCs
$y_{h,0}(t)$	Number of pathogen-induced healthy PCs inside the niche at time t	# PCs
$x_{h,v}(t)$	Number of vaccination-induced healthy PCs outside the niche at time t	# PCs
$y_{h,v}(t)$	Number of vaccination-induced healthy PCs inside the niche at time t	# PCs
f	Number of healthy PCs entering the compartment outside of the niche via the blood per unit of time	# PCs $\cdot$ time^{-1}
d	Death rate of healthy PC outside the niche	time^{-1}
b_h	Transition rate of healthy PCs outside the niche into the niche	time^{-1}
c_h	Transition rate of healthy PCs inside the niche out of the niche	time^{-1}
n	Difference in number of PCs between PCs inside and outside the niche at healthy homoeostasis	# PCs

5 Model of healthy and malignant plasma cell dynamics

In this chapter, a mathematical model is derived which describes the dynamics of healthy and malignant PCs in the bone marrow. Derivation is based on the extended model, where malignant PCs are considered as a population of "vaccination-induced" PCs with the difference of being able to proliferate. They further may possess different properties compared with healthy PCs. Along these lines, **healthy** PCs are distinguished from **malignant** PCs within the total population of PCs.

Assumption 5.1 (Assumptions for malignant PCs)**.**

(1) There is a time $T \geq 0$ at which a certain number of malignant PCs is added to the bone marrow compartment outside of the niche. In particular, there is no constant inflow of malignant PCs.

(2) Malignant PCs are able to grow within both compartments, where the growth can be positive (i.e. accumulation by proliferation) or negative (i.e. death),

(3) Malignant PCs possess the same transition properties as healthy PCs, possibly at other rates.

Figure 5.1 illustrates the scenario of a **malignancy-induced perturbation of the healthy equilibrium**: At time T, a certain number of malignant PCs arrives at the bone marrow and is therefore added to the compartment of PCs outside the niche. Consequently, the healthy equilibrium is perturbed. Proliferation of malignant PCs is illustrated by a „dividing" cell.

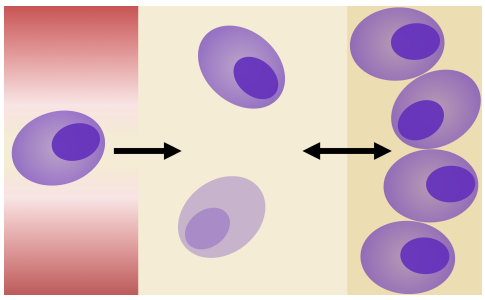

(a) Healthy equilibrium.

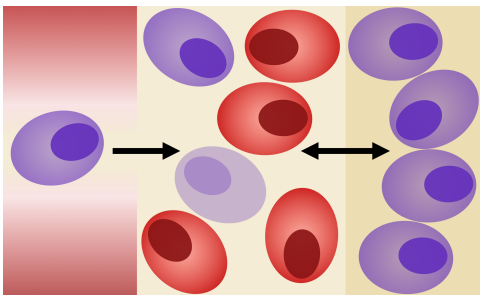

(b) Perturbation of the healthy equilibrium by malignant PCs.

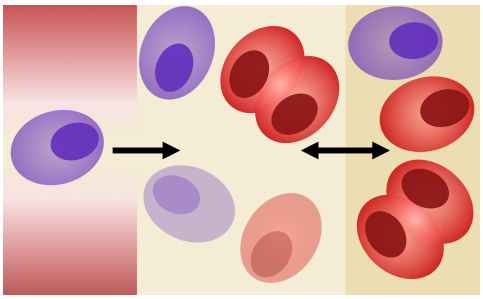

(c) Onset of malignant growth.

Figure 5.1: Perturbation of the healthy equilibrium due to malignancy. Purple cells represent healthy plasma cells (PCs), whereas red cells represent malignant PCs. Homoeostasis is perturbed by a population of malignant PCs arriving at the bone marrow in a discrete-in-time event (depicted as red cells appearing outside the niche). For details, see text.

The basic model is extended by two additional equations describing the number of malignant PCs in the bone marrow outside and inside the niche, respectively. Since parameter values of malignant PCs may differ from those of healthy PCs due to Assumption 5.1, new parameters for malignant PCs are introduced. Notations for the model variables and parameters are stated in Table 5.1 on page 40.

At first, the surplus of PCs relative to the niche balance (3.0.2) is refined, i.e.

$$z(t) = \underbrace{x_h(t) + x_m(t)}_{\#\text{ PCs outside the niche}} - \underbrace{(y_h(t) + y_m(t))}_{\#\text{ PCs inside the niche}} + n, \quad n > 0.$$

We not only have to take into account that the transition rates differ between healthy and malignant PCs but also the proportion of each type of PCs within each compartment. Similar to (4.0.3) in the extended model, the function for the

transition rates is defined as

$$\beta_j(z(t)) := \begin{cases} b_j \frac{x_j(t)}{x_h(t)+x_m(t)} & \text{if } z(t) \geq 0 \\ c_j \frac{y_j(t)}{y_h(t)+y_m(t)} & \text{if } z(t) < 0, \end{cases}$$

where $j \in \{h, m\}$. This allows formulating dynamic equations for x_h, x_m and y_h, y_m based on the previous discussion:

- The change in the number of healthy and malignant PCs in the bone marrow outside the niche per unit of time, $x_h'(t)$ and $x_m'(t)$, respectively, is given by

$$\begin{aligned} x_h'(t) &= f - \beta_h(z(t))z(t) - dx_h(t) \\ x_m'(t) &= p_1 x_m(t) - \beta_m(z(t))z(t). \end{aligned}$$

- The change in the number of healthy and malignant PCs in the bone marrow inside the niche per unit of time, $y_h'(t)$ and $y_m'(t)$, respectively, is given by

$$\begin{aligned} y_h'(t) &= \beta_h(z(t))z(t) \\ y_m'(t) &= p_2 y_m(t) + \beta_m(z(t))z(t). \end{aligned}$$

Parameters p_1 and p_2 are net growth rates, i.e. they include both proliferation and death of cells:

$$p_i = \text{proliferation rate} \quad - \quad \text{death rate}, \quad i \in \{1, 2\}.$$

The sign of p_1 and p_2, respectively, gives information about the predominance of either proliferation or death. If $p_1 > 0$ (respectively, $p_2 > 0$), cells accumulate, i.e. the proliferation rate exceeds the death rate, whereas if $p_1 < 0$ (respectively, $p_2 < 0$), cells rather die than proliferate. In particular, no advantage for malignant PCs being inside the niche is postulated as it has been done for healthy PCs. That is to say, the model allows malignant PCs to die both outside and inside the niche.

Thereby, the model of healthy and malignant PC dynamics in the bone marrow is resumed:

The **model of healthy and malignant PC dynamics in the bone marrow** (abbreviation: **myeloma model**) is given by the following system of ODEs for times $t \geq t_0 \geq 0$:

$$\begin{aligned} x_h'(t) &= f - \beta_h(z(t))z(t) - dx_h(t) \\ x_m'(t) &= p_1 x_m(t) - \beta_m(z(t))z(t) \\ y_h'(t) &= \beta_h(z(t))z(t) \\ y_m'(t) &= p_2 y_m(t) + \beta_m(z(t))z(t) \end{aligned} \tag{5.0.1}$$

with surplus of PCs relative to the niche balance $z(t)$ given by

$$z(t) = x_h(t) + x_m(t) - (y_h(t) + y_m(t)) + n, \tag{5.0.2}$$

transition rates $\beta_j(z(t)),\ j \in \{h, m\}$, given by

$$\beta_j(z(t)) = \begin{cases} b_j \frac{x_j(t)}{x_h(t)+x_m(t)} & \text{if } z(t) \geq 0 \\ c_j \frac{y_j(t)}{y_h(t)+y_m(t)} & \text{if } z(t) < 0, \end{cases} \tag{5.0.3}$$

and non-negative initial conditions

$$\begin{aligned} x_h(t_0) &= x_h^0 \geq 0 \\ x_m(t_0) &= x_m^0 \geq 0 \\ y_h(t_0) &= y_h^0 \geq 0 \\ y_m(t_0) &= y_m^0 \geq 0. \end{aligned} \tag{5.0.4}$$

Variables and parameters are listed in Table 5.1 on page 40.

The healthy equilibrium of the basic model as stated in Definition 3.5 can be formulated as an equilibrium of the myeloma model (5.0.1) (or system (5.0.1)), i.e.

$$E_h = \left(x_h^{E_h}, 0, y_h^{E_h}, 0\right)^T.$$

Definition 5.2 (Malignancy-induced perturbation of the healthy equilibrium)**.** Consider the myeloma model (5.0.1) and its healthy equilibrium E_h. Let $T \geq 0$. For $0 \leq t < T$, let (5.0.1) be at the healthy equilibrium E_h, i.e.

$$(x_h(t), x_m(t), y_h(t), y_m(t))^T = E_h.$$

Then, at $t = T$,

$$(x_h(T), x_m(T), y_h(T), y_m(T))^T = \left(x_h^{E_h}, x_m^0, y_h^{E_h}, 0\right)^T \quad \text{with} \quad x_m^0 > 0 \tag{5.0.5}$$

defines a malignancy-induced perturbation of the healthy equilibrium at time T as described in Assumption 5.1, which can be interpreted as initial condition for system (5.0.1) with $t_0 = T$.

The perturbation of the healthy equilibrium by a population of malignant PCs of a number to be determined (see Chapter 11) can be seen as recapitulation of the 30 episodes of inflow by physiological antigen exposure per year [94] with the main difference that malignant PCs continue to proliferate, whereas healthy PCs do not.

Remark 5.3 (Myeloma model related to previous models)**.** Unlike the extended model (4.0.1), the myeloma model (5.0.1) is not a refinement of the basic model. No closed system of differential equations describing the dynamics of $x_h(t) + x_m(t)$ and $y_h(t) + y_m(t)$ can be deduced. This is due to the additional growth terms and different transition rates in the equations for malignant PCs. Observe that the myeloma model generalises the extended model (4.0.1): Setting $p_1 = -d$, $p_2 = 0$ and $b_m = b_h,\ c_m = c_h$ yields the extended model, where the model variables have to be renamed appropriately.

Table 5.1: Description of variables and parameters of the model of healthy and malignant plasma cell (PC) dynamics (5.0.1). All parameters are real and positive unless it is stated differently.

Symbol	**Description**	**Unit**
$x_h(t)$	Number of healthy PCs outside the niche at time t	# PCs
$y_h(t)$	Number of healthy PCs inside the niche at time t	# PCs
$x_m(t)$	Number of malignant PCs outside the niche at time t	# PCs
$y_m(t)$	Number of malignant PCs inside the niche at time t	# PCs
f	Number of healthy PCs entering the compartment outside of the niche via the blood per unit of time	# PCs $\cdot$ time^{-1}
d	Death rate of healthy PCs outside the niche	time^{-1}
$p_1 \in \mathbb{R}$	Net growth rate of malignant PCs outside the niche	time^{-1}
$p_2 \in \mathbb{R}$	Net growth rate of malignant PCs inside the niche	time^{-1}
b_h	Transition rate of healthy PCs outside the niche into the niche	time^{-1}
b_m	Transition rate of malignant PCs outside the niche into the niche	time^{-1}
c_h	Transition rate of healthy PCs inside the niche out of the niche	time^{-1}
c_m	Transition rate of malignant PCs inside the niche out of the niche	time^{-1}
n	Difference in number of PCs between PCs inside and outside the niche at healthy homoeostasis	# PCs

Part II

Analysis of mathematical models of healthy and malignant plasma cell dynamics

6 Analysis of the basic model

The basic model of healthy PC dynamics in the bone marrow is recapitulated, see Chapter 3. For all $t \geq t_0$, the system of ODEs is given by

$$\begin{aligned} x_h'(t) &= f - \beta_h(z(t))z(t) - dx_h(t) \\ y_h'(t) &= \beta_h(z(t))z(t) \end{aligned} \tag{3.0.1}$$

with surplus of PCs relative to the niche balance $z(t)$ given by

$$z(t) = x_h(t) - y_h(t) + n, \tag{3.0.2}$$

transition rates $\beta_h(z(t))$ given by

$$\beta_h(z(t)) = \begin{cases} b_h & \text{if } \ z(t) \geq 0 \\ c_h & \text{if } \ z(t) < 0 \end{cases} \tag{3.0.3}$$

and non-negative initial conditions

$$\begin{aligned} x_h(t_0) &= x_h^0 \geq 0 \\ y_h(t_0) &= y_h^0 \geq 0. \end{aligned} \tag{3.0.4}$$

In general, the function $\beta_h(z)$ is not continuous in z, whereas the term $\beta_h(z)z$ in the dynamic equations is continuous, yet not differentiable in $z = 0$. Since the vector field of system (3.0.1) is smooth for $z > 0$ and $z < 0$, respectively, the associated dynamical system is of piecewise-smooth continuous conformation. The basic model (3.0.1) is reformulated using the framework of piecewise-smooth continuous dynamical systems. For details, see Appendix A.1 providing a compendium of relevant theoretical results.

For that, let

$$\mathcal{S}_1 := \{(x_h, y_h)^T \in \mathbb{R}^2 \colon z \geq 0\}$$
$$\mathcal{S}_2 := \{(x_h, y_h)^T \in \mathbb{R}^2 \colon z < 0\},$$

which yields a single switching manifold given by

$$\Sigma := \{(x_h, y_h)^T \in \mathbb{R}^2 \colon z = 0\}.$$

With the initial conditions (3.0.4), the reformulated system for $t \geq t_0$ reads

$$\begin{aligned}\begin{pmatrix} x_h'(t) \\ y_h'(t) \end{pmatrix} = g(x_h(t), y_h(t)) &= \begin{cases} g_1(x_h(t), y_h(t)) & \text{if } (x_h(t), y_h(t))^T \in \mathcal{S}_1 \\ g_2(x_h(t), y_h(t)) & \text{if } (x_h(t), y_h(t))^T \in \mathcal{S}_2 \end{cases} \\ &:= \begin{cases} \begin{pmatrix} f - b_h z(t) - d x_h(t) \\ b_h z(t) \end{pmatrix} & \text{if } (x_h(t), y_h(t))^T \in \mathcal{S}_1 \\ \begin{pmatrix} f - c_h z(t) - d x_h(t) \\ c_h z(t) \end{pmatrix} & \text{if } (x_h(t), y_h(t))^T \in \mathcal{S}_2. \end{cases} \end{aligned} \tag{6.0.1}$$

Remark 6.1. Since $g_1(x_h, y_h) = g_2(x_h, y_h)$ for all $(x_h, y_h)^T \in \Sigma$, the assignment of Σ belonging to $\mathcal{S}_1$ (instead of $\mathcal{S}_2$) is arbitrary but in accordance with the definition of the transition rate function $\beta_h(z)$ in (3.0.3).

For sake of simplicity, the index h is skipped in all model variables and parameters in the sequel of this chapter.

6.1 Existence and uniqueness of solutions

In the following, existence and uniqueness of solutions of the basic model are investigated. Referring to system (6.0.1), the right-hand side g is continuous. Thus, Theorem A.6 (i) immediately implies the following result about local existence of solutions:

Theorem 6.2 (Local existence of solutions)**.** *Consider the basic model* (3.0.1) *with initial conditions* (3.0.4)*. There exist solutions $x(t)$ and $y(t)$ which are defined for all t on an open maximal interval of existence $I_{max} \subseteq \mathbb{R}$ with $t_0 \in I_{max}$.*

Knowing that solutions $x(t)$ and $y(t)$ exist for all $t \in I_{max}$ for given initial condition, sufficient conditions for their non-negativity are evaluated. This is important since solutions describe cell counts. For approaching the problem, the concept of invariant sets is applied [130].

Proposition 6.3 (Non-negativity of solutions for $f \geq bn$)**.** *Consider the basic model* (3.0.1)*. Let $f \geq bn$. Then, it follows that $x(t), y(t) \geq 0$ for all $t \in I_{max}$.*

Proof. Define $h_j : \mathbb{R}^2 \to \mathbb{R},\ j = 1, 2$, by

$$\begin{aligned} h_1(x, y) &= f - \beta(z)z - dx \\ h_2(x, y) &= \beta(z)z, \end{aligned} \tag{6.1.1}$$

which represent the (non-smooth) right-hand sides of the ODEs for x and y within system (3.0.1), respectively. Positive invariance of the set $\mathbb{R}^2_+ = \{(x, y)^T \in \mathbb{R}^2 \mid x, y \geq 0\}$ under the vector field of system (3.0.1) is proven. It is

$$h_1(0, y) \geq 0 \ \Leftrightarrow \ \begin{cases} f - b(-y + n) \geq 0 & \text{if } \ n \geq y \\ f - c(-y + n) \geq 0 & \text{if } \ n < y. \end{cases} \tag{6.1.2}$$

For $n \geq y$, equation (6.1.2) is true due to $f \geq bn$. For $n < y$, it is $f - c(n - y) > 0$. Since $h_2(x, 0) = b(x + n) > 0$, the proof is complete. □

If $f < bn$, the previous result does not guarantee non-negativity of solutions. However, the set $\mathbb{R}^2_+$ can be restricted such that non-negativity of solutions holds true also in this case.

Proposition 6.4 (Non-negativity of solutions for $f \leq bn$)**.** *The set*

$$\mathcal{A} = \left\{ (x, y)^T \in \mathbb{R}^2 \colon x \geq 0,\ y \geq n - \frac{f}{b} \right\}$$

is (positively) invariant under the vector field of the basic model (3.0.1)*. In particular, if $f \leq bn$, then $\mathcal{A} \subseteq \mathbb{R}^2_+$.*

Proof. Consider h_1, h_2 which were defined in the previous proof, see (6.1.1). First, consider (6.1.2). For $n \geq y$, it is $f - bn + by \geq f - bn + b(n - \frac{f}{b}) = 0$. If $n < y$, it is $f - c(-y + n) > 0$. Since $h_2(x, n - \frac{f}{b}) = b(x + \frac{f}{b}) > 0$, this shows (positive) invariance of $\mathcal{A}$. Observe that $f \leq bn$ implies $y \geq 0$. This completes the proof. □

Remark 6.5. Due to the strict positivity of $h_2(x, \cdot),\ x \geq 0$, evaluated at the boundary of the corresponding invariant set of both Proposition 6.3 and 6.4, it follows that $y(t_0) \geq 0$ implies $y(t) > 0$ for all $t \in I_{max},\ t \neq t_0$.

Propositions 6.3 and 6.4 state sufficient conditions under which the solutions of the basic model are expected to stay non-negative. Therefore, non-negativity of solutions can be assumed in the remaining part of this section. In the forthcoming investigation, the result about local existence stated in Theorem 6.2 are extended.

Theorem 6.6 (Global existence of solutions)**.** *Consider the basic model* (3.0.1) *with initial conditions* (3.0.4)*. Assume that either $f \geq bn$ and $(x^0, y^0)^T \in \mathbb{R}^2_+$, or $f \leq bn$ and $(x^0, y^0)^T \in \mathcal{A}$. Then, there exist non-negative solutions $x(t)$ and $y(t)$ which are defined for all $t \geq t_0$.*

Proof. By Theorem 6.2 and Propositions 6.3 and 6.4 it follows that $x(t), y(t) \geq 0$ for all $t \in I_{max}$, where I_{max} is the maximal interval of existence. Then $x'(t) + y'(t) = f - dx(t) \leq f$, which implies that $x(t) + y(t) \leq ft + \tilde{c}$ with $\tilde{c} \in \mathbb{R}$ being a constant. Therefore, $x(t) + y(t)$ is bounded for each finite time point $t \in I_{max}$. Similarly, due to the non-negativity of each $x(t)$ and $y(t)$, boundedness holds also for each solution. Hence, the solutions can be extended globally in time, i.e. for all $t \geq t_0$. □

In the remaining part of this section, results on uniqueness of solutions are deduced. For further investigation of Lipschitz continuity (see Definition A.5) of the right-hand side of the basic model, observe the following: To check if a function $g : \mathcal{U} \to \mathbb{R}^n$ with $\mathcal{U} \subseteq \mathbb{R} \times \mathbb{R}^n$ and $g : (t, x) \mapsto g(t, x)$ is Lipschitz continuous in x, uniformly in t, it suffices to check that the component functions $g_i : \mathcal{U} \to \mathbb{R},\ i = 1, \ldots, n$, are Lipschitz continuous. Using the 1-norm $\| \cdot \|_1$, this is true because

$$|g_i(t, x) - g_i(t, y)| \leq L_i \|x - y\|_1 \ \text{ for } \ (t, x), (t, y) \in \mathcal{V}$$

for any closed bounded set $\mathcal{V} \subseteq \mathcal{U}$ and $L_i > 0,\ i = 1, \ldots, n$, implies

$$\|g(t,x) - g(t,y)\|_1 = \sum_{i=1}^{n} |g_i(t,x) - g_i(t,y)| \leq \sum_{i=1}^{n} L_i \|x - y\|_1 =: L\|x - y\|_1 \quad (6.1.3)$$

for $(t,x), (t,y) \in \mathcal{V}$.

Lemma 6.7. *Let a, b be real numbers such that $a \leq 0 \leq b$. Then, $|a - b| = |a| + |b|$.*

Proof. Let $a \leq 0 \leq b$. Then, $|a - b| = -(a - b) = -a + b = |a| + |b|$. This proves the claim. □

Theorem 6.8 (Global existence and uniqueness)**.** *Consider the basic model* (3.0.1) *with initial conditions* (3.0.4)*. Then, there exist unique solutions $x(t)$ and $y(t)$ which are defined for all $t \geq t_0$.*

Proof. Consider the functions h_1 and h_2 defined by (6.1.1) and proof Lipschitz continuity in $(x,y)^T \in \mathbb{R}^2$, respectively. That is to say, global Lipschitz continuity. Let $(x_1, y_1)^T,\ (x_2, y_2)^T \in \mathbb{R}^2$, and $z_1 = x_1 - y_1 + n,\ z_2 = x_2 - y_2 + n$. It follows that

$$\begin{aligned} |h_1(x_1,y_1) - h_1(x_2,y_2)| &= |f - \beta(z_1)z_1 - dx_1 - (f - \beta(z_2)z_2 - dx_2)| \\ &= |d(x_2 - x_1) + \beta(z_2)z_2 - \beta(z_1)z_1| \\ &\leq d|x_1 - x_2| + |\beta(z_1)z_1 - \beta(z_2)z_2|. \end{aligned}$$

For further analysis of the term $|\beta(z_1)z_1 - \beta(z_2)z_2|$, three cases for $(x_1, y_1)^T,\ (x_2, y_2)^T \in \mathbb{R}^2$ are considered:

(1) $z_1, z_2 \geq 0$, that is to say, $(x_1, y_1)^T,\ (x_2, y_2)^T \in \mathcal{S}_1$

(2) $z_1, z_2 < 0$, that is to say, $(x_1, y_1)^T,\ (x_2, y_2)^T \in \mathcal{S}_2$

(3) $z_2 < 0 \leq z_1$ or $z_1 < 0 \leq z_2$, that is to say, $(x_1, y_1)^T \in \mathcal{S}_1$ and $(x_2, y_2)^T \in \mathcal{S}_2$, or vice versa, respectively. Without loss of generality, assume that $z_2 < 0 \leq z_1$.

In case (1), it is $\beta(z_1) = \beta(z_2) = b$, thus $|\beta(z_1)z_1 - \beta(z_2)z_2| = b|z_1 - z_2|$. This yields

$$|h_1(x_1,y_1) - h_1(x_2,y_2)| \leq d|x_1 - x_2| + b|z_1 - z_2|.$$

In case (2), it is $\beta(z_1) = \beta(z_2) = c$. Thus $|\beta(z_1)z_1 - \beta(z_2)z_2| = c|z_1 - z_2|$. This yields

$$|h_1(x_1, y_1) - h_1(x_2, y_2)| \leq d|x_1 - x_2| + c|z_1 - z_2|.$$

In case (3), it is $\beta(z_1) = b$ and $\beta(z_2) = c$. Using Lemma 6.7 implies that

$$\begin{aligned} |\beta(z_1)z_1 - \beta(z_2)z_2| &= |\beta(z_1)z_1| + |\beta(z_2)z_2| \\ &\leq \max\{b, c\}\,(|z_1| + |z_2|) \\ &= \max\{b, c\}|z_1 - z_2|. \end{aligned}$$

This yields

$$|h_1(x_1, y_1) - h_1(x_2, y_2)| \leq d|x_1 - x_2| + \max\{b, c\}|z_1 - z_2|.$$

Thus, the following estimate is true for all $(x_1, y_1)^T, (x_2, y_2)^T \in \mathbb{R}^2$:

$$\begin{aligned} |h_1(x_1, y_1) - h_1(x_2, y_2)| &\leq d|x_1 - x_2| + \max\{b, c\}|z_1 - z_2| \\ &\leq d|x_1 - x_2| + \max\{b, c\}\Big(|x_1 - x_2| + |y_1 - y_2|\Big) \\ &\leq \Big(d + \max\{b, c\}\Big)\|(x_1, y_1)^T - (x_2, y_2)^T\|_1. \end{aligned}$$

Let $L_1 = d + \max\{b, c\}$. For h_2 it follows in the same fashion that

$$\begin{aligned} |h_2(x_1, y_1) - h_2(x_2, y_2)| &= |\beta(z_1)z_1 - \beta(z_2)z_2| \\ &\leq \max\{b, c\}|z_1 - z_2| \\ &\leq \max\{b, c\}\Big(|x_1 - x_2| + |y_1 - y_2|\Big) \\ &= \max\{b, c\}\|(x_1, y_1)^T - (x_2, y_2)^T\|_1. \end{aligned}$$

Let $L_2 = \max\{b, c\}$. With $L = L_1 + L_2 = 2\max\{b, c\} + d$ and (6.1.3), it follows that

$$\|(h_1(x_1, y_1), h_2(x_1, y_1))^T - (h_1(x_2, y_2), h_2(x_2, y_2))^T\|_1 \leq L\|(x_1, y_1)^T - (x_2, y_2)^T\|_1.$$

This implies global Lipschitz continuity of the right-hand side of system (3.0.1).

By Theorem A.6 and Remark A.7, this yields global existence and uniqueness of solutions. □

6.2 Stability of the healthy equilibrium

Remark 3.4 shows that there exists exactly one equilibrium of system (3.0.1), which is referred to as healthy equilibrium (see Definition 3.5),

$$E_h = \left(x^{E_h}, y^{E_h}\right)^T = \left(\frac{f}{d}, \frac{f}{d} + n\right)^T.$$

Further, $E_h \in \Sigma$, where a solution $(x(t), y(t))^T$ of system (3.0.1) attains the healthy equilibrium, i.e. $(x(t), y(t))^T = E_h$, if $(x(t), y(t))^T \in \Sigma$ for all t. Moreover, the following result holds:

Proposition 6.9 (Transversal intersection of Σ)**.** *Consider the basic model* (3.0.1)*. Every solution* $(x(t), y(t))^T$ *which reaches* $\Sigma \setminus E_h$ *intersects* Σ *transversally.*

Proof. To prove this statement, consider $(x, y)^T \in \Sigma \setminus E_h$ and $n(x, y)$, the normal to Σ at $(x, y)^T$. It holds that

$$n(x, y) = \frac{1}{\sqrt{2}} (1, -1)^T,$$

which yields the projections of $g_1(x, y)$ and $g_2(x, y)$ (see (6.0.1)) onto the normal to the switching manifold Σ,

$$n(x, y)^T g_1(x, y) = \frac{1}{\sqrt{2}} (f - dx) = n(x, y)^T g_2(x, y).$$

It follows that

$$\left[n(x, y)^T g_1(x, y)\right] \cdot \left[n(x, y)^T g_2(x, y)\right] = \frac{1}{2} (f - dx)^2 > 0,$$

which implies that a trajectory leaves $\Sigma \setminus E_h$. In particular, it enters $\mathcal{S}_1$ when $n(x, y)^T g_1(x, y) > 0$, and it enters $\mathcal{S}_2$ when $n(x, y)^T g_1(x, y) < 0$. This completes the proof. □

In more general problems of discontinuous dynamical systems, the above analysis is embedded in the so-called Filippov first order theory [23]. Depending on the chosen initial conditions, there may exist a finite time at which the solution $(x(t), y(t))^T$ reaches the switching manifold $\Sigma \setminus E_h$. In the forthcoming section, it is deduced that there exists at most one such time.

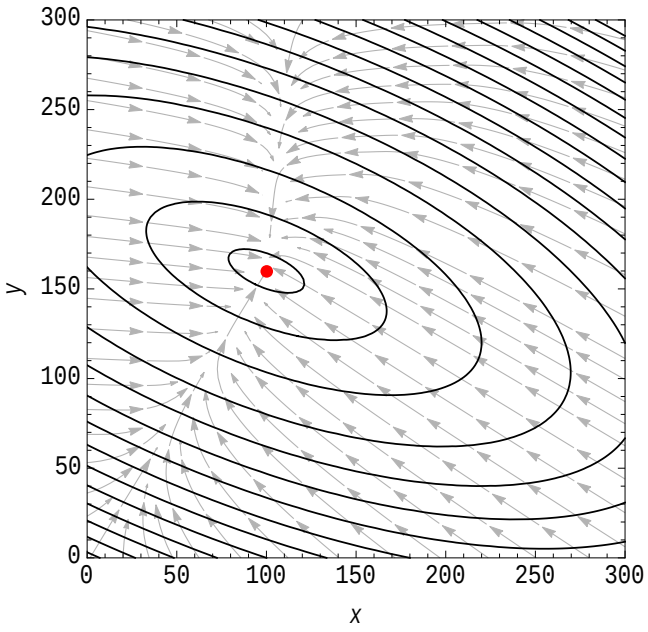

Figure 6.1: Contour plot showing level sets of the Lyapunov function V (black) given by (6.2.1). The flow of the basic model (light gray) and the healthy equilibrium E_h (red) are also shown, implying that all trajectories eventually reach E_h. Chosen parameter values are listed in Table 6.1 on page 65. For details, see text.

Next, global stability of the healthy equilibrium $E_h \in \Sigma$ is analysed. As exemplified in Appendix A.1.2, deducing stability properties of E_h from stability properties of E_h within each $\mathcal{S}_1$ and $\mathcal{S}_2$ can be misleading. Instead, proving the existence of a common strict Lyapunov function for both sub-systems guarantees global asymptotic stability.

Theorem 6.10 (Global asymptotic stability of E_h)**.** *Consider the basic model* (3.0.1)*. The healthy equilibrium E_h is globally asymptotically stable.*

Proof. In order to apply Theorem A.14, consider the function $V : \mathbb{R}^2 \mapsto \mathbb{R}$ defined by

$$V(x,y) := \frac{1}{2d}\left(x+y-2\frac{f}{d}-n\right)^2 + \frac{1}{2\max\{b,c\}}\left(y-\frac{f}{d}-n\right)^2. \tag{6.2.1}$$

V is shown to be a strict Lyapunov function of system (3.0.1) satisfying the conditions stated in Theorem A.14 (ii). Note that V is continuously differentiable. A straightforward calculation yields

$$V(x^{E_h}, y^{E_h}) = 0 \text{ and } V(x,y) > 0 \text{ for all } (x,y)^T \neq (x^{E_h}, y^{E_h})^T.$$

Calculating the Lie derivative of V along the vector field of system (3.0.1) yields

$$\begin{aligned}
\dot{V}(x,y) &= \frac{1}{d}\left(x+y-2\frac{f}{d}-n\right)(f-\beta(z)z-dx) + \frac{\beta(z)}{\max\{b,c\}}\left(y-\frac{f}{d}-n\right)z \\
&\quad + \frac{\beta(z)}{d}\left(x+y-2\frac{f}{d}-n\right)z \\
&= \frac{1}{d}\left(x+y-2\frac{f}{d}-n\right)(f-dx) + \underbrace{\frac{\beta(z)}{\max\{b,c\}}}_{\leq 1}\left(y-\frac{f}{d}-n\right)(x-y+n) \\
&\leq \left(x+y-2\frac{f}{d}-n\right)\left(\frac{f}{d}-x\right) + \left(y-\frac{f}{d}-n\right)(x-y+n) \\
&= -\left(\left(x-\frac{f}{d}\right)^2 + \left(y-\frac{f}{d}-n\right)^2\right) \\
&< 0
\end{aligned}$$

for all $(x,y)^T \neq (x^{E_h}, y^{E_h})^T$. Thus, E_h is globally asymptotically stable. □

Figure 6.1 illustrates the level sets of the Lyapunov function V for an arbitrary choice of parameter values given by Table 6.1 on page 65, which guarantees non-negativity of solutions according to Proposition 6.3.

6.3 Invariant sets

The previous analysis revealed that solutions of the basic model may intersect the switching manifold transversally if they reach $\Sigma \setminus E_h$, see Proposition 6.9. It was shown that E_h is globally asymptotically stable, see Theorem 6.10. In particular, that is $\lim_{t\to\infty}(x(t), y(t))^T = (x^{E_h}, y^{E_h})^T$. In this section, further analysis investigates how often a trajectory may cross the switching manifold at most, i.e. the maximal number of possible switches in the sign of the function $z(t)$ is examined.

Definition 6.11 (Sign switch)**.** A change in the sign of the value of $z(t)$ during time evolution, either from strictly positive to strictly negative, or vice versa, is denoted as sign switch of $z(t)$.

6.3.1 Two invariant sets of no sign switch of z

Regarding formulation (6.0.1), the basic model is a piecewise-linear inhomogeneous system with constant coefficient matrices within each $\mathcal{S}_1$ and $\mathcal{S}_2$, respectively. A straightforward calculation yields related eigenvectors

$$\left(\frac{\pm\sqrt{4b^2+d^2}-d}{2b}, 1\right)^T \quad \text{and} \quad \left(\frac{\pm\sqrt{4c^2+d^2}-d}{2c}, 1\right)^T,$$

respectively. Since eigenspaces are invariant under the corresponding linear (homogeneous) vector field [127], this motivates the following definition.

Definition 6.12 (Sets $\mathcal{R}_1$ and $\mathcal{R}_2$)**.** Let $R_i : \mathbb{R}^2 \to \mathbb{R},\ i = 1, 2, 3, 4$, be given by

$$\begin{aligned}
R_1(x,y) &:= y + \frac{\sqrt{4b^2+d^2}-d}{2b}x - \left(1 + \frac{\sqrt{4b^2+d^2}-d}{2b}\right)\frac{f}{d} - n \\
R_2(x,y) &:= y - x - n \\
R_3(x,y) &:= -y - \frac{\sqrt{4c^2+d^2}-d}{2c}x + \left(1 + \frac{\sqrt{4c^2+d^2}-d}{2c}\right)\frac{f}{d} + n \\
R_4(x,y) &:= -R_2(x,y).
\end{aligned}$$

Then, define

$$\mathcal{R}_1 := \bigcap_{i=1}^{2} \{(x,y)^T \in \mathbb{R}^2 \colon R_i(x,y) \leq 0\} \subset \mathcal{S}_1$$
$$\mathcal{R}_2 := \bigcap_{i=3}^{4} \{(x,y)^T \in \mathbb{R}^2 \colon R_i(x,y) \leq 0\} \subset \mathcal{S}_2 \cup \Sigma.$$

The boundary of the respective set is denoted as $\partial\mathcal{R}_j,\ j = 1,2$. That is to say,

$$\partial\mathcal{R}_1 = \{(x,y)^T \in \mathcal{R}_1 \colon R_1(x,y) = 0\} \cup \{(x,y)^T \in \mathcal{R}_1 \colon R_2(x,y) = 0\}$$
$$\partial\mathcal{R}_2 = \{(x,y)^T \in \mathcal{R}_2 \colon R_3(x,y) = 0\} \cup \{(x,y)^T \in \mathcal{R}_2 \colon R_4(x,y) = 0\}.$$

Observe that $E_h \in \partial\mathcal{R}_j$ for $j = 1,2$, and

$$\bigcap_{i=1}^{4} \{R_i(x,y) = 0\} = \{E_h\}.$$

Since E_h is an equilibrium of the basic model, it follows that the Lie derivatives $\dot{R}_i(E_h) = 0$ for all $i = 1,2,3,4$. Further it holds:

Theorem 6.13 (Invariant sets $\mathcal{R}_1$ and $\mathcal{R}_2$)**.** *The sets $\mathcal{R}_1$ and $\mathcal{R}_2$ are (positively) invariant under the vector field of the basic model* (3.0.1)*.*

Proof. First, consider the set $\mathcal{R}_1$. Let $(x,y)^T \in \partial\mathcal{R}_1 \setminus E_h$. Sketching $R_i(x,y) = 0$ for $i = 1,2$ in the phase plane (see Figure 6.2) shows that the boundary of $\mathcal{R}_1$ splits up into two parts, i.e.

(1) $R_1(x,y) = 0$ with $x > \frac{f}{d}$, and

(2) $R_2(x,y) = 0$ with $x < \frac{f}{d}$.

Note that if $x = \frac{f}{d}$, then $y = \frac{f}{d} + n$, and thus $(x,y)^T = E_h$. For the first part, straightforward calculation shows that

$$\dot{R}_1(x,y) \quad = \quad b(x-y+n) + \frac{\sqrt{4b^2+d^2}-d}{2b}\Big(f - b(x-y+n) - dx\Big)$$
$$\overset{(R_1=0)}{=} 0,$$

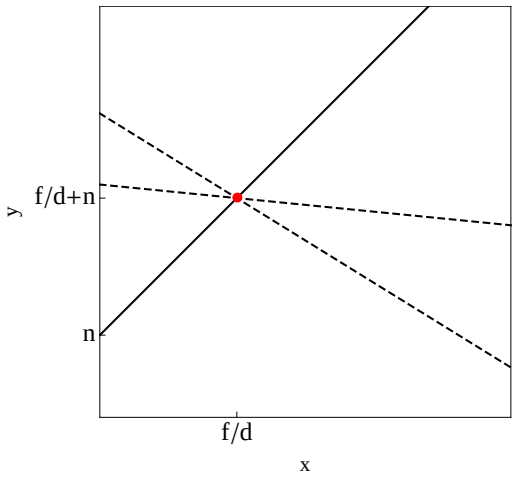

Figure 6.2: Sketch of relative positions of boundary lines in the phase plane of the basic model. The healthy equilibrium E_h (red), the sets $R_2(x,y) = 0 = R_4(x,y)$ (bold) and $R_1(x,y) = 0$ and $R_3(x,y) = 0$ (dashed) are visualised. For details, see proof of Theorem 6.13.

and for the second part, it is

$$\begin{aligned} \dot{R}_2(x,y) &= b(x-y+n) - \Big(f - b(x-y+n) - dx\Big) \\ &\overset{(R_2=0)}{=} dx - f \\ &< 0. \end{aligned}$$

This implies (positive) invariance of the set $\mathcal{R}_1$.

Next, consider the set $\mathcal{R}_2$. Let $(x,y)^T \in \partial\mathcal{R}_2 \setminus E_h$. Again, sketching $R_i(x,y) = 0$ for $i = 3,4$ in the phase plane (see Figure 6.2) shows that the boundary of $\mathcal{R}_2$ splits up into two parts, i.e.

(1) $R_3(x,y) = 0$ with $x < \frac{f}{d}$, and

(2) $R_4(x,y) = 0$ with $x > \frac{f}{d}$.

Note that if $x = \frac{f}{d}$, then $y = \frac{f}{d} + n$, and thus $(x,y)^T = E_h$. For the first part, an

immediate calculation gives

$$\begin{aligned}\dot{R}_3(x,y) &= -c(x-y+n) - \frac{\sqrt{4c^2+d^2}-d}{2c}\Big(f - c(x-y+n) - dx\Big)\\ &\overset{(R_3=0)}{=} 0,\end{aligned}$$

and for the second part, it is

$$\begin{aligned}\dot{R}_4(x,y) &= -c(x-y+n) + f - c(x-y+n) - dx\\ &\overset{(R_4=0)}{=} f - dx\\ &< 0.\end{aligned}$$

This implies (positive) invariance of the set $\mathcal{R}_2$. □

Remark 6.14. In fact, the proof of Theorem 6.13 shows that the sets

$$\{(x,y)^T \in \mathbb{R}^2 \colon R_1(x,y) = 0\}$$
$$\{(x,y)^T \in \mathbb{R}^2 \colon R_3(x,y) = 0\}$$

are (positively) invariant.

Figure 6.3 illustrates the invariant sets $\mathcal{R}_1$ and $\mathcal{R}_2$ in the phase plane. Parameter values are stated in Table 6.1 on page 65.

Assuming non-negativity of solutions using Proposition 6.3 or 6.4 guarantees (positive) invariance of $\mathcal{R}_1 \cap \mathbb{R}^2_+$ and $\mathcal{R}_2 \cap \mathbb{R}^2_+$. Since $\mathcal{R}_1 \subset \mathcal{S}_1$, the dynamics of a trajectory $(x(t), y(t))^T$ starting in $\mathcal{R}_1$ are thoroughly determined by the flow of system (3.0.1) within $\mathcal{S}_1$. Likewise, since $\mathcal{R}_2 \subset \mathcal{S}_2 \cup \Sigma$, the dynamics of a trajectory $(x(t), y(t))^T$ starting in $\mathcal{R}_2$ are thoroughly determined by the flow of system (3.0.1) within $\mathcal{S}_2 \cup \Sigma$. In both cases, there does not occur any switch in the sign of $z(t)$. The following implication holds:

Corollary 6.15. *The function $z(t)$ may switch its sign at most once.*

Proof. As a consequence of the definitions of $\mathcal{R}_1$ and $\mathcal{R}_2$, a switch in the sign of $z(t)$ is only possible for a solution starting in $\mathbb{R}^2 \setminus (\mathcal{R}_1 \cup \mathcal{R}_2)$, see also Figure 6.3. Let $(x^0, y^0)^T \in \mathbb{R}^2 \setminus (\mathcal{R}_1 \cup \mathcal{R}_2)$. Then, the corresponding trajectory $(x(t), y(t))^T$

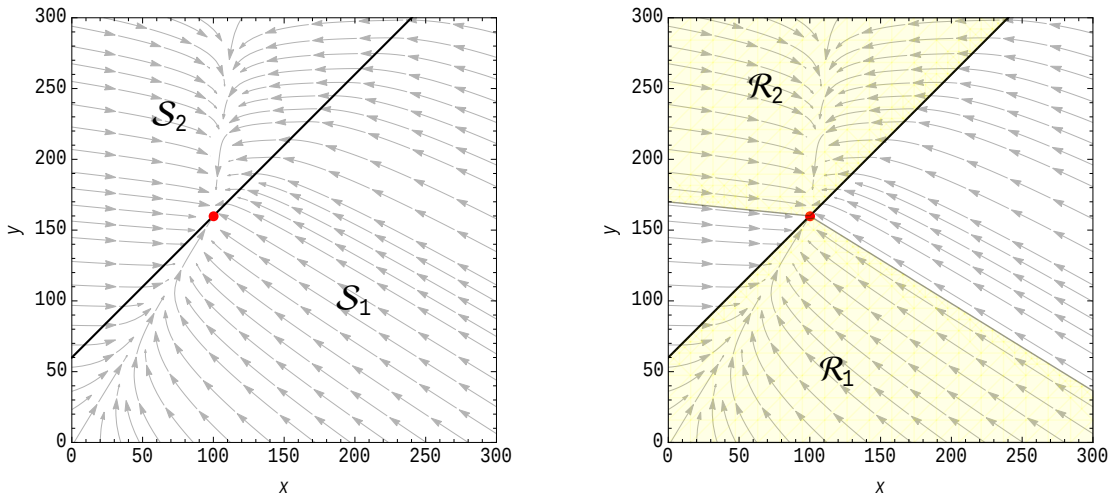

(a) Separation of the phase plane by Σ.

(b) Invariant sets $\mathcal{R}_1$ and $\mathcal{R}_2$.

Figure 6.3: Phase plane of the basic model visualising the corresponding vector field (light gray), the healthy equilibrium E_h (red) and the switching manifold Σ (black). The latter separates the set $\mathcal{S}_1$ from the set $\mathcal{S}_2$. Yellow regions mark invariant sets $\mathcal{R}_1$ and $\mathcal{R}_2$ given by Definition 6.12. Parameter values are stated in Table 6.1 on page 65. For details, see text.

eventually enters $\mathcal{R}_1 \cup \mathcal{R}_2$ as $t \to \infty$. This is due to global asymptotic stability of $E_h \in \mathcal{R}_1 \cup \mathcal{R}_2$, see Theorem 6.10. If $(x(t), y(t))^T$ enters $\mathcal{R}_1 \cup \mathcal{R}_2$ at a finite time $T > t_0$, then $(x(t), y(t))^T$ enters either $\mathcal{R}_1 \setminus E_h$ or $\mathcal{R}_2 \setminus E_h$. Note that E_h cannot be reached in finite time due to uniqueness of solutions, see Theorem 6.8. If this is attended by crossing Σ, Proposition 6.9 implies a sign switch in $z(t)$. Theorem 6.13 yields that $(x(t), y(t))^T \in \mathcal{R}_1 \cup \mathcal{R}_2$ for all times $t \geq T$, and no further switch in the sign of $z(t)$ occurs. This proves the claim. □

6.3.2 Two invariant sets of monotonicity of z

Having identified invariant sets of no sign switch of $z(t)$, further analysis investigates the dynamics of $z(t)$. By setting $x'(t) = y'(t)$, we search for solutions $(x(t), y(t))^T$ of the basic model where $x(t)$ and $y(t)$ possess equal growth behaviour. This condition immediately implies $z'(t) = 0$, which translates into $f - 2\beta(z(t))z(t) - dx(t) = 0$. If

$(x(t), y(t))^T \in \mathcal{S}_1$, then it follows that

$$f - 2b\,(x(t) - y(t) + n) - dx(t) = 0 \quad \Leftrightarrow \quad y(t) = \left(1 + \frac{d}{2b}\right) x(t) + n - \frac{f}{2b},$$

and if $(x(t), y(t))^T \in \mathcal{S}_2$, it is

$$f - 2c\,(x(t) - y(t) + n) - dx(t) = 0 \quad \Leftrightarrow \quad y(t) = \left(1 + \frac{d}{2c}\right) x(t) + n - \frac{f}{2c}.$$

This motivates the following definition.

Definition 6.16 (Sets $\mathcal{M}_1$ and $\mathcal{M}_2$)**.** Let $M_i : \mathbb{R}^2 \to \mathbb{R},\ i = 1, 2$, be given by

$$\begin{aligned} M_1(x, y) &:= y - \left(1 + \frac{d}{2b}\right)x - n + \frac{f}{2b} \\ M_2(x, y) &:= -y + \left(1 + \frac{d}{2c}\right)x + n - \frac{f}{2c}. \end{aligned}$$

Then, define

$$\begin{aligned} \mathcal{M}_1 &:= \{(x, y)^T \in \mathbb{R}^2 \colon R_1(x, y) \leq 0\} \cap \{(x, y)^T \in \mathbb{R}^2 \colon M_1(x, y) \leq 0\} \\ \mathcal{M}_2 &:= \{(x, y)^T \in \mathbb{R}^2 \colon R_3(x, y) \leq 0\} \cap \{(x, y)^T \in \mathbb{R}^2 \colon M_2(x, y) \leq 0\}. \end{aligned}$$

Observe that

$$\begin{aligned} \mathcal{M}_1 &= \mathcal{R}_1 \cap \{(x, y)^T \in \mathbb{R}^2 \colon M_1(x, y) \leq 0\} \subset \mathcal{R}_1 \subset \mathcal{S}_1 \\ \mathcal{M}_2 &= \mathcal{R}_2 \cap \{(x, y)^T \in \mathbb{R}^2 \colon M_2(x, y) \leq 0\} \subset \mathcal{R}_2 \subset \mathcal{S}_2 \cup \Sigma. \end{aligned}$$

By this definition, the next result is obtained:

Theorem 6.17 (Invariant sets $\mathcal{M}_1$ and $\mathcal{M}_2$)**.**

(i) The set $\mathcal{M}_1$ is (positively) invariant under the vector field of the basic model (3.0.1)*. In particular, the function $z(t)$ is monotonically decreasing within $\mathcal{M}_1$.*

(ii) The set $\mathcal{M}_2$ is (positively) invariant under the vector field of the basic model (3.0.1)*. In particular, the function $z(t)$ is monotonically increasing within $\mathcal{M}_2$.*

Proof. First, consider the set $\mathcal{M}_1$. Let $(x, y)^T \in \mathcal{M}_1$ such that $M_1(x, y) = 0$. Sketching $M_1(x, y) = 0$ in the phase plane (see Figure 6.4) shows that $x \leq \frac{f}{d}$. If

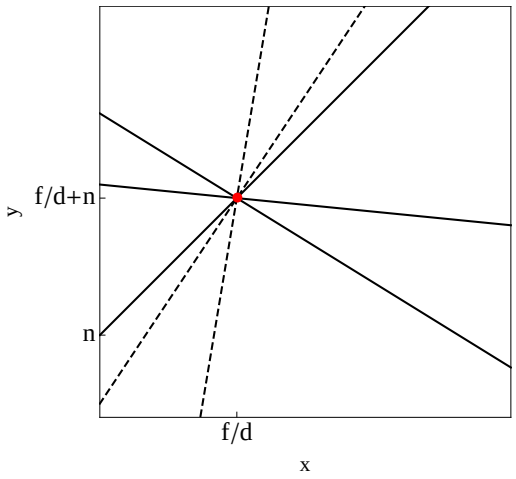

Figure 6.4: Sketch of relative positions of boundary lines in the phase plane of the basic model. The healthy equilibrium E_h (red), the sets $R_i(x,y) = 0$, $i = 1,2,3,4$ (bold) and $M_1(x,y) = 0$ and $M_2(x,y) = 0$ (dashed) are visualised. For details, see proof of Theorem 6.17.

$x = \frac{f}{d}$, then it follows that $(x,y)^T = E_h$. Thus, consider $x < \frac{f}{d}$. It is

$$\begin{aligned} \dot{M}_1(x,y) &= b(x-y+n) - \frac{(2b+d)}{2b}\Big(f - b(x-y+n) - dx\Big) \\ &\overset{(M_1=0)}{=} \frac{d}{4b}\Big(dx - f\Big) \\ &< 0. \end{aligned} \tag{6.3.1}$$

Using the result of Theorem 6.13 implies (positive) invariance of $\mathcal{M}_1$. Next, $z(t)$ is shown to be monotonically decreasing. For that, let $(x^0,y^0)^T \in \mathcal{M}_1$. It follows that $M_1(x(t),y(t)) \leq 0$ for all $t \geq t_0$. Therefore, it is

$$\begin{aligned} z'(t) &= f - 2bz(t) - dx(t) \\ &= f - 2bx(t) + 2by(t) - 2bn - dx(t) \\ &\leq f - 2bx(t) + 2b\left(\left(1 + \frac{d}{2b}\right)x(t) + n - \frac{f}{2b}\right) - 2bn - dx(t) \\ &= 0. \end{aligned}$$

This shows that $z'(t) \leq 0$ for all $t \geq t_0$ in $\mathcal{M}_1$. Observe that if $M_1(x^0,y^0) < 0$, then

$M_1(x(t), y(t)) < 0$ for all $t \geq t_0$ by the strict inequality in (6.3.1). Consequently, $z'(t) < 0$ for all $t \geq t_0$ in $\mathcal{M}_1$.

Next, consider the set $\mathcal{M}_2$. Let $(x, y)^T \in \mathcal{M}_2$ such that $M_2(x, y) = 0$. Sketching $M_2(x, y) = 0$ in the phase plane (see Figure 6.4) shows that $x \geq \frac{f}{d}$. If $x = \frac{f}{d}$, then it follows that $(x, y)^T = E_h$. Thus, consider $x > \frac{f}{d}$. It is

$$\begin{aligned} \dot{M}_2(x, y) &= -c(x - y + n) + \frac{2c + d}{2c}\Big(f - c(x - y + n) - dx\Big) \\ &\overset{(M_2=0)}{=} \frac{d}{4c}\Big(f - dx\Big) \\ &< 0. \end{aligned} \tag{6.3.2}$$

Using the result of Theorem 6.13 implies (positive) invariance of $\mathcal{M}_2$. Next, $z(t)$ is shown to be monotonically increasing. For that, let $(x^0, y^0)^T \in \mathcal{M}_2$. It follows that $M_2(x(t), y(t)) \leq 0$ for all $t \geq t_0$. Therefore, it is

$$\begin{aligned} z'(t) &= f - 2cz(t) - dx(t) \\ &= f - 2cx(t) + 2cy(t) - 2cn - dx(t) \\ &\geq f - 2bx(t) + 2b\left(\left(1 + \frac{d}{2c}\right)x(t) + n - \frac{f}{2c}\right) - 2bn - dx(t) \\ &= 0. \end{aligned}$$

This shows that $z'(t) \geq 0$ for all $t \geq t_0$ in $\mathcal{M}_2$. Observe that if $M_2(x^0, y^0) < 0$, then $M_2(x(t), y(t)) < 0$ for all $t \geq t_0$ by the strict inequality in (6.3.2). Consequently, $z'(t) > 0$ for all $t \geq t_0$ in $\mathcal{M}_2$. □

Corollary 6.18. *The function $z(t)$ possesses at most one maximum or minimum, respectively.*

Proof. As a consequence of the definitions of $\mathcal{M}_1$ and $\mathcal{M}_2$, the function $z(t)$ possesses an optimum at time $T \geq t_0$, i.e. $z'(T) = 0$, if and only if $M_1(x(T), y(T)) = 0$ or $M_2(x(T), y(T)) = 0$, respectively. By the proof of Theorem 6.17, the sets

$$\begin{aligned} &\{(x, y)^T \in \mathbb{R}^2 \colon M_1(x, y) = 0\} \setminus E_h \\ &\{(x, y)^T \in \mathbb{R}^2 \colon M_2(x, y) = 0\} \setminus E_h \end{aligned}$$

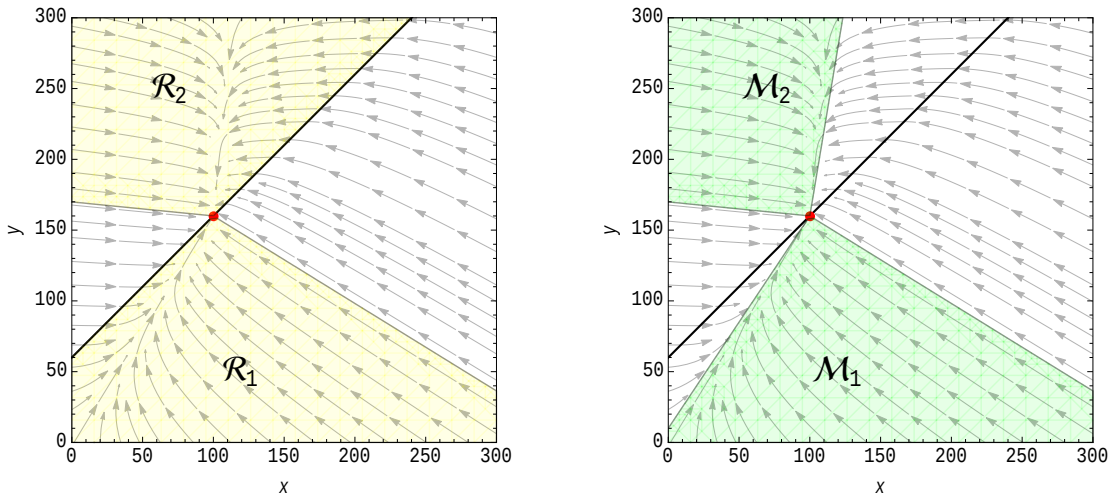

(a) Invariant sets of no sign switch of $z(t)$.

(b) Invariant sets of monotonicity of $z(t)$.

Figure 6.5: Phase plane of the basic model visualising the corresponding vector field (light gray), the healthy equilibrium E_h (red) and the switching manifold Σ (black). Yellow regions mark invariant sets $\mathcal{R}_1$ and $\mathcal{R}_2$ given by Definition 6.12. Green regions mark invariant sets $\mathcal{M}_1$ and $\mathcal{M}_2$ given by Definition 6.16. Parameter values are stated in Table 6.1 on page 65. For details, see text.

are repelling for the vector field of system (3.0.1) due to strict negativity of the respective Lie derivatives (6.3.1) and (6.3.2). More precisely, a trajectory reaching either of these sets crosses the respective set transversally such that $M_1(x(t), y(t)) < 0$ or $M_2(x(t), y(t)) < 0$ for all $t > T$, respectively. In particular, $z'(t) \neq 0$ for all $t > T$. This proves the claim. □

Figure 6.5 illustrates the invariant sets $\mathcal{M}_1$ and $\mathcal{M}_2$ along with the invariant sets $\mathcal{R}_1$ and $\mathcal{R}_2$ in the phase plane. Parameter values are stated in Table 6.1 on page 65.

6.4 Qualitative simulations

This chapter closes with simulations providing an illustration of previously derived results. The qualitative behaviour of solutions $(x(t), y(t))^T$ of the basic model (3.0.1) with different initial conditions $(x^0, y^0)^T$ is analysed in the phase plane. Used parameter values are stated in Table 6.1 on page 65. In the following, Figure 6.6 is

considered. By Theorem 6.10 and Theorem 6.13 a trajectory $(x(t), y(t))^T$ starting in one of the invariant sets $\mathcal{R}_1$ or $\mathcal{R}_2$ asymptotically approaches $(x^{E_h}, y^{E_h})^T$ without leaving $\mathcal{R}_1$ or $\mathcal{R}_2$, respectively. In particular, if a trajectory $(x(t), y(t))^T$ starts in one of the invariant sets $\mathcal{M}_1 \subset \mathcal{R}_1$ or $\mathcal{M}_2 \subset \mathcal{R}_2$, the function $z(t)$ is monotone, see Theorem 6.17.

(a) The depicted trajectory starts at $(0, 50)^T \in \mathcal{R}_1 \setminus \mathcal{M}_1$ and converges to E_h, where $z(t) \geq 0$ for all t. The dynamics of the solutions $x(t)$ and $y(t)$ reveal convergence to E_h. Observe that $z(t)$ is not monotone and possesses one maximum.

(b) The depicted trajectory starts at $(150, 0)^T \in \mathcal{M}_1$ and converges to E_h, where $z(t) \geq 0$ for all t. The dynamics of the solutions $x(t)$ and $y(t)$ reveal convergence to E_h. Observe that $z(t)$ is strictly monotonically decreasing.

(c) The depicted trajectory starts at $(150, 300)^T \in \mathcal{R}_2 \setminus \mathcal{M}_2$ and converges to E_h, where $z(t) \leq 0$ for all t. The dynamics of the solutions $x(t)$ and $y(t)$ reveal convergence to E_h. Observe that $z(t)$ is not monotone and possesses one minimum.

(d) The depicted trajectory starts at $(0, 250)^T \in \mathcal{M}_2$ and converges to E_h, where $z(t) \leq 0$ for all t. The dynamics of the solutions $x(t)$ and $y(t)$ reveal convergence to E_h. Observe that $z(t)$ is strictly monotonically increasing.

(e) The depicted trajectory starts at $(300, 200)^T \in \mathcal{S}_1 \setminus \mathcal{R}_1$ and converges to E_h, where $z(t)$ changes its sign one time. The dynamics of the solutions $x(t)$ and $y(t)$ reveal convergence to E_h. Observe that $z(t)$ is not monotone and possesses one minimum. $z(t)$ has exactly one root.

(f) The depicted trajectory starts at $(0, 100)^T \in \mathcal{S}_2 \setminus \mathcal{R}_2$ and converges to E_h, where $z(t)$ changes its sign one time. The dynamics of the solutions $x(t)$ and $y(t)$ reveal convergence to E_h. Observe that $z(t)$ is not monotone and possesses one maximum. $z(t)$ has exactly one root.

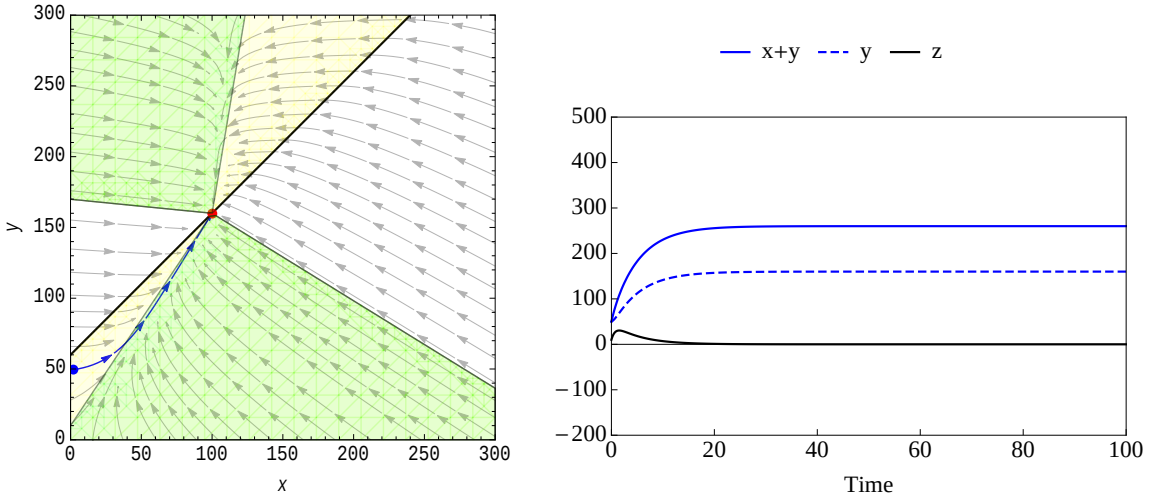

(a) Initial value $(x^0, y^0)^T = (0, 50)^T$.

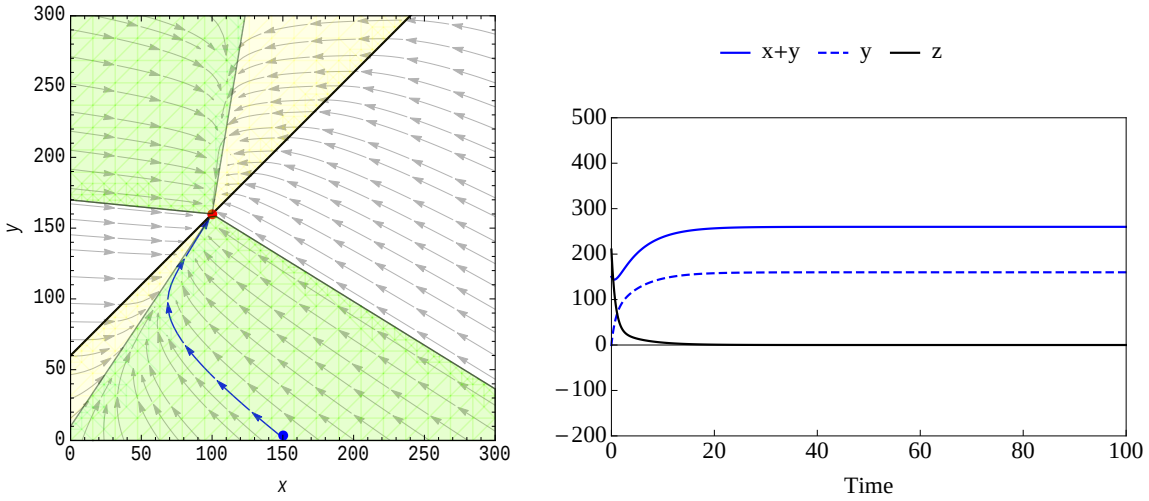

(b) Initial value $(x^0, y^0)^T = (150, 0)^T$.

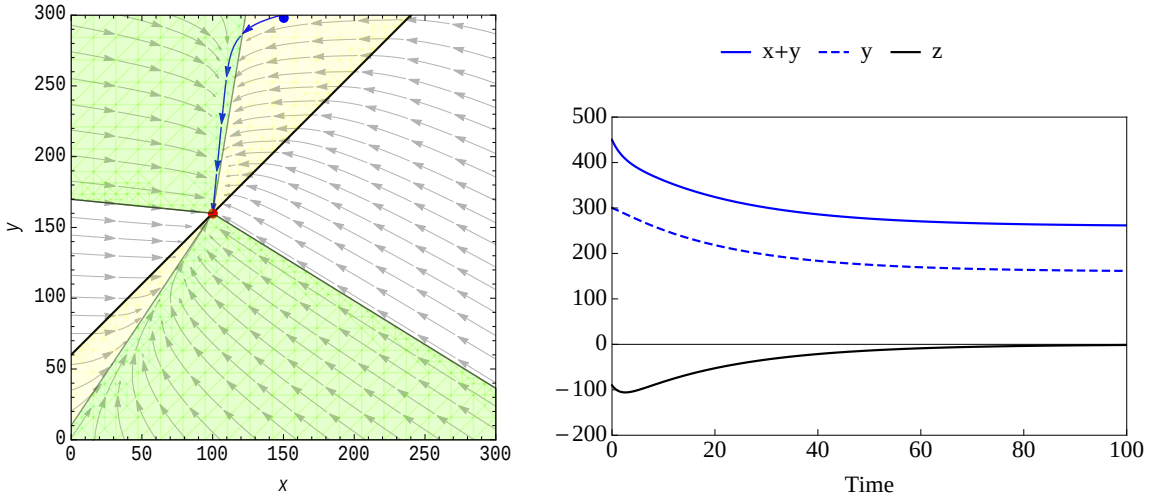

(c) Initial value $(x^0, y^0)^T = (150, 300)^T$.

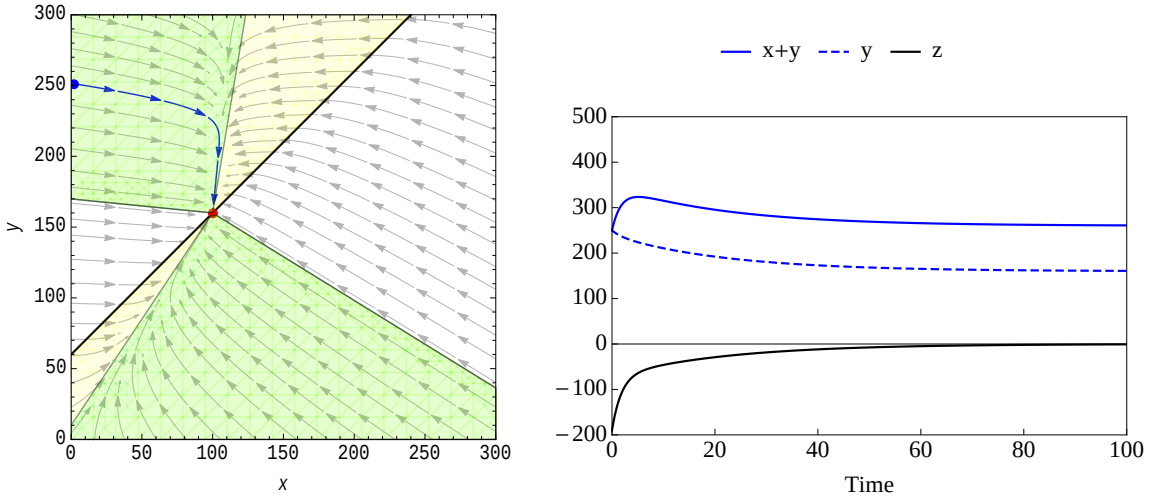

(d) Initial value $(x^0, y^0)^T = (0, 250)^T$.

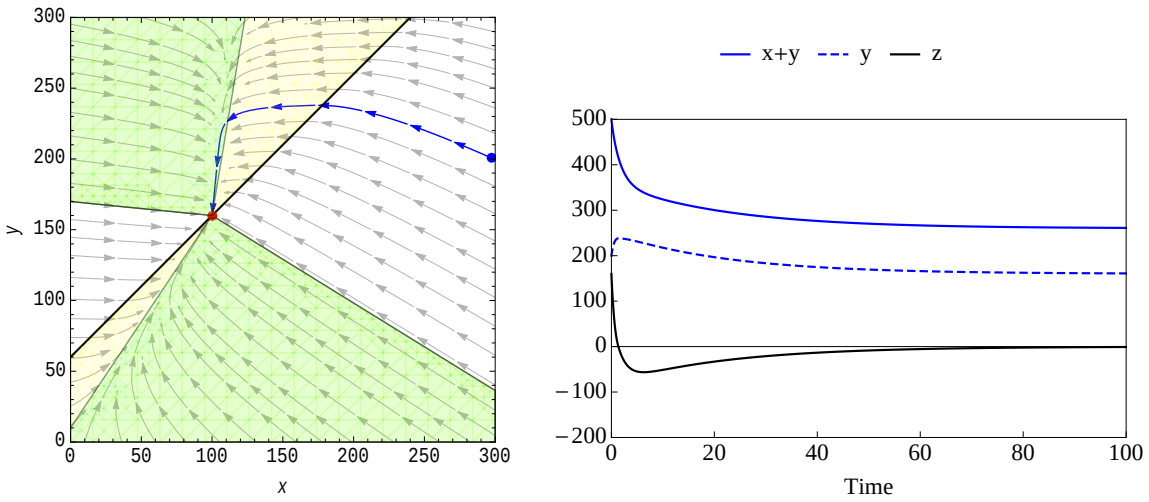

(e) Initial value $(x^0, y^0)^T = (300, 200)^T$.

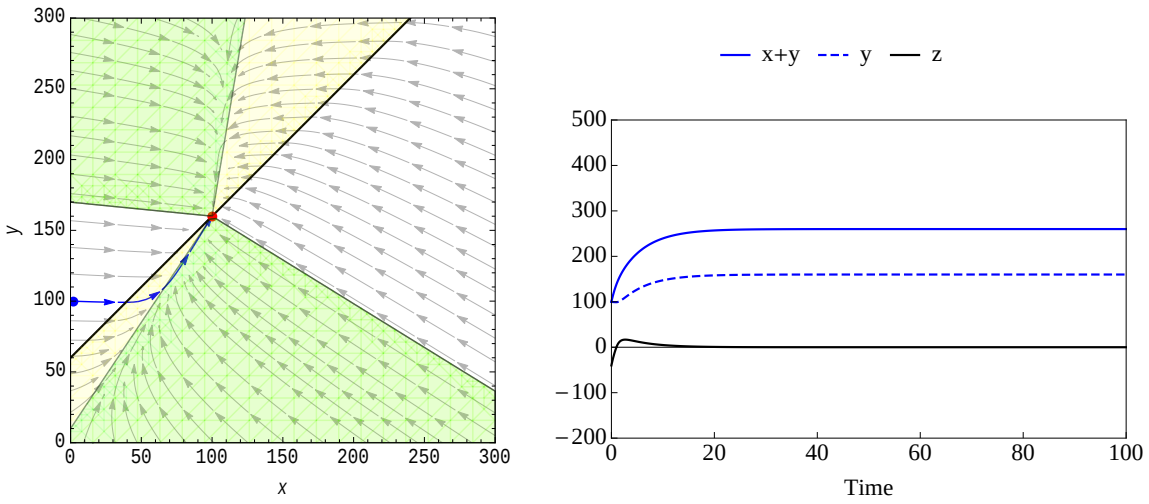

(f) Initial value $(x^0, y^0)^T = (0, 100)^T$.

Figure 6.6: Simulations of a trajectory in the phase plane and solutions of the basic model. Left: A trajectory (blue) in the phase plane of the basic model converging to E_h (red). The vector field (light gray) of the basic model is visualised. Yellow regions mark invariant sets $\mathcal{R}_1$ and $\mathcal{R}_2$ given by Definition 6.12. Green regions mark invariant sets $\mathcal{M}_1$ and $\mathcal{M}_2$ given by Definition 6.16. Right: Solutions $x(t) + y(t)$ (blue), $y(t)$ (dashed blue), and $z(t)$ (black). Parameter values are stated in Table 6.1. For details, see text.

Table 6.1: Parameter values for simulations in Chapter 6.

Parameter	**Value**
f	50
n	60
b	0.5
c	0.05
d	0.5

7 Analysis of the myeloma model

The model of healthy and malignant PC dynamics in the bone marrow, or myeloma model, is recapitulated, see Chapter 5. For all $t \geq t_0$, the system of ODEs is given by

$$\begin{aligned} x_h'(t) &= f - \beta_h(z(t))z(t) - dx_h(t) \\ x_m'(t) &= p_1 x_m(t) - \beta_m(z(t))z(t) \\ y_h'(t) &= \beta_h(z(t))z(t) \\ y_m'(t) &= p_2 y_m(t) + \beta_m(z(t))z(t) \end{aligned} \tag{5.0.1}$$

with surplus of PCs relative to the niche balance $z(t)$ given by

$$z(t) = x_h(t) + x_m(t) - (y_h(t) + y_m(t)) + n, \tag{5.0.2}$$

transition rates $\beta_j(z(t)),\ j \in \{h, m\}$, given by

$$\beta_j(z(t)) = \begin{cases} b_j \frac{x_j(t)}{x_h(t)+x_m(t)} & \text{if } z(t) \geq 0 \\ c_j \frac{y_j(t)}{y_h(t)+y_m(t)} & \text{if } z(t) < 0 \end{cases} \tag{5.0.3}$$

and non-negative initial conditions

$$\begin{aligned} x_h(t_0) &= x_h^0 \ \geq 0 \\ x_m(t_0) &= x_m^0 \geq 0 \\ y_h(t_0) &= y_h^0 \ \geq 0 \\ y_m(t_0) &= y_m^0 \geq 0. \end{aligned} \tag{5.0.4}$$

Observe that the functions $\beta_j(z),\ j \in \{h, m\}$, given by (5.0.3) are undefined in case of $x_h + x_m = 0$ or $y_h + y_m = 0$, respectively. Assuming $x_h(t) + x_m(t) \neq 0$ and $y_h(t) + y_m(t) \neq 0$ for all $t \geq t_0$, they are continuous for all $z \in \mathbb{R},\ z \neq 0$. It

follows that the functions $\beta_j(z)z,\ j \in \{h, m\}$, are continuous, but in general not differentiable in $z = 0$. Since the vector field of system (5.0.1) is smooth for $z > 0$ and $z < 0$, respectively, the associated dynamical system is of piecewise-smooth conformation. For a reformulation of the myeloma model into the framework of piecewise-smooth continuous dynamical systems (see Appendix A.1), let

$$\mathcal{S}_1 := \{(x_h, x_m, y_h, y_m)^T \in \mathbb{R}^4 \colon z \geq 0\}$$
$$\mathcal{S}_2 := \{(x_h, x_m, y_h, y_m)^T \in \mathbb{R}^4 \colon z < 0\}$$

with a single switching manifold given by

$$\Sigma := \{(x_h, x_m, y_h, y_m)^T \in \mathbb{R}^4 \colon z = 0\}.$$

With the initial conditions (5.0.4), the reformulated system for $t \geq t_0$ reads

$$\begin{aligned}
\begin{pmatrix} x_h'(t) \\ x_m'(t) \\ y_h'(t) \\ y_m'(t) \end{pmatrix} &= g(x_h(t), x_m(t), y_h(t), y_m(t)) \\
&= \begin{cases} g_1(x_h(t), x_m(t), y_h(t), y_m(t)) & \text{if } (x_h(t), x_m(t), y_h(t), y_m(t))^T \in \mathcal{S}_1 \\ g_2(x_h(t), x_m(t), y_h(t), y_m(t)) & \text{if } (x_h(t), x_m(t), y_h(t), y_m(t))^T \in \mathcal{S}_2 \end{cases} \\
&:= \begin{cases} \begin{pmatrix} f - b_h \frac{x_h(t)}{x_h(t)+x_m(t)} z(t) - d x_h(t) \\ p_1 x_m(t) - b_m \frac{x_m(t)}{x_h(t)+x_m(t)} z(t) \\ b_h \frac{x_h(t)}{x_h(t)+x_m(t)} z(t) \\ p_2 y_m(t) + b_m \frac{x_m(t)}{x_h(t)+x_m(t)} z(t) \end{pmatrix} & \text{if } (x_h(t), x_m(t), y_h(t), y_m(t))^T \in \mathcal{S}_1 \\ \begin{pmatrix} f - c_h \frac{y_h(t)}{y_h(t)+y_m(t)} z(t) - d x_h(t) \\ p_1 x_m(t) - c_m \frac{y_m(t)}{y_h(t)+y_m(t)} z(t) \\ c_h \frac{y_h(t)}{y_h(t)+y_m(t)} z(t) \\ p_2 y_m(t) + c_m \frac{y_m(t)}{y_h(t)+y_m(t)} z(t) \end{pmatrix} & \text{if } (x_h(t), x_m(t), y_h(t), y_m(t))^T \in \mathcal{S}_2. \end{cases}
\end{aligned} \tag{7.0.1}$$

7.1 Domain of definition and non-negativity of solutions

In this section, a domain for the right-hand side g of the myeloma model (7.0.1) is introduced such that the non-linearities appearing in the transition rate functions $\beta_j(z(t)),\ j \in \{h, m\}$ given by (5.0.3) are defined for all $t \geq t_0$. That is $x_h(t) + x_m(t) \neq 0$ in $\mathcal{S}_1$ and $y_h(t) + y_m(t) \neq 0$ in $\mathcal{S}_2$ for all $t \geq t_0$, respectively. Since the fractions in (5.0.3) reflect proportions of PCs (see Chapter 5), their non-negativity needs to be ensured. This involves non-negativity of solutions.

Let $\mathbb{R}^4_+$ denote the set of vectors in $\mathbb{R}^4$ with non-negative components.

Definition 7.1 (Set $\mathcal{W}$)**.** Let $W_i : \mathbb{R}^4_+ \to \mathbb{R},\ i = 1, 2$, are given by

$$W_1(x_h, x_m, y_h, y_m) := -x_h - x_m$$
$$W_2(x_h, x_m, y_h, y_m) := n - y_h - y_m.$$

Then, define

$$\mathcal{W} := \bigcap_{i=1}^{2} \{(x_h, x_m, y_h, y_m)^T \in \mathbb{R}^4_+ : W_i(x_h, x_m, y_h, y_m) \leq 0\}. \tag{7.1.1}$$

Assuming existence of solutions, the following result holds true:

Theorem 7.2 (Domain of definition and non-negativity of solutions)**.** *Consider the myeloma model* (5.0.1) *and assume that solutions exist. Then, the set $\mathcal{W}$ is (positively) invariant under the vector field of the myeloma model. In particular, if the initial conditions* (5.0.4) *satisfy $x_h^0 + x_m^0 > 0$ and $y_h^0 + y_m^0 \geq n$, then the functions* (5.0.3) *are defined for all $t \geq t_0$. Moreover, it follows that $x_h(t), x_m(t), y_h(t), y_m(t) \geq 0$ for all $t \geq t_0$.*

Proof. At first, non-negativity of solutions $x_h(t), x_m(t), y_h(t), y_m(t)$ is proved. For that, let $h_j : \mathbb{R}^4 \to \mathbb{R},\ j = 1, 2, 3, 4$, by

$$\begin{aligned} h_1(x_h, x_m, y_h, y_m) &= f - \beta_h(z)z - dx_h \\ h_2(x_h, x_m, y_h, y_m) &= p_1 x_m - \beta_m(z)z \\ h_3(x_h, x_m, y_h, y_m) &= \beta_h(z)z \\ h_4(x_h, x_m, y_h, y_m) &= p_2 y_m + \beta_m(z)z. \end{aligned} \tag{7.1.2}$$

These functions are the component functions of g representing the right-hand side of system (7.0.1). It follows that

$$h_1(0, x_m, y_h, y_m) = f - \beta_h(z) = \begin{Bmatrix} f & \text{if } z \geq 0 \\ f - c_h \frac{y_h}{y_h + y_m} z & \text{if } z < 0 \end{Bmatrix} > 0$$

$$h_2(x_h, 0, y_h, y_m) = -\beta_m(z)z = \begin{Bmatrix} 0 & \text{if } z \geq 0 \\ -c_m \frac{y_m}{y_h + y_m} z & \text{if } z < 0 \end{Bmatrix} \geq 0$$

$$h_3(x_h, x_m, 0, y_m) = \beta_h(z)z = \begin{Bmatrix} b_h \frac{x_h}{x_h + x_m} z & \text{if } z \geq 0 \\ 0 & \text{if } z < 0 \end{Bmatrix} \geq 0$$

$$h_4(x_h, x_m, y_h, 0) = \beta_m(z)z = \begin{Bmatrix} b_m \frac{x_h}{x_h + x_m} z & \text{if } z \geq 0 \\ 0 & \text{if } z < 0 \end{Bmatrix} \geq 0.$$

Consequently, since $x_h^0, x_m^0, y_h^0, y_m^0 \geq 0$, it follows that $x_h(t), x_m(t), y_h(t), y_m(t) \geq 0$ for all $t \geq t_0$. In other words, the set $\mathbb{R}^4_+$ is (positively) invariant under the vector field of system (5.0.1).

Next, the set $\mathcal{W}$ given by (7.1.1) is shown to be (positively) invariant under the vector field of system (5.0.1). At first, choose $(x_h, x_m, y_h, y_m)^T \in \mathcal{W}$ such that $W_2(x_h, x_m, y_h, y_m) = 0$. It follows that $z = x_h + x_m - y_h - y_m + n = x_h + x_m \geq 0$. Consequently,

$$\begin{aligned} \dot{W}_2(x_h, x_m, y_h, y_m) &= -h_3(x_h, x_m, y_h, y_m) - h_4(x_h, x_m, y_h, y_m) \\ &= -\beta_h(z)z - p_2 y_m - \beta_m(z)z \\ &\leq 0. \end{aligned}$$

Next, let $(x_h, x_m, y_h, y_m)^T \in \mathcal{W}$ such that $W_1(x_h, x_m, y_h, y_m) = 0$. It follows that $z = x_h + x_m - y_h - y_m + n = -y_h - y_m + n \leq 0$. Consequently,

$$\begin{aligned}
\dot{W}_1(x_h, x_m, y_h, y_m) &= -h_1(x_h, x_m, y_h, y_m) - h_2(x_h, x_m, y_h, y_m) \\
&= -f + \beta_h(z)z + dx_h - p_1 x_m + \beta_m(z)z \\
&\leq -f + dx_h - p_1 x_m \\
&\leq \begin{cases} -f + d\,(x_h + x_m) & \text{if } p_1 \geq 0 \\ -f + \max\{d, |p_1|\}\,(x_h + x_m) & \text{if } p_1 < 0 \end{cases} \qquad (7.1.3) \\
&\overset{(W_1=0)}{=} -f \\
&< 0.
\end{aligned}$$

Since $\mathbb{R}^4_+$ is (positively) invariant, it follows that the set $\mathcal{W}$ is (positively) invariant. The strict negativity of the Lie derivative $\dot{W}_1$ in (7.1.3) implies that choosing initial conditions

$$(x_h^0, x_m^0, y_h^0, y_m^0)^T \in \mathcal{W} \cap \{(x_h, x_m, y_h, y_m)^T \in \mathbb{R}^4_+ \colon W_1(x_h, x_m, y_h, y_m) < 0\}$$

yields $x_h(t) + x_m(t) > 0$ for all $t \geq t_0$. This completes the proof. □

Remark 7.3 (Perturbations of the healthy equilibrium)**.** With Remark 5.3, an analogue statement of Theorem 7.2 holds true for the extended model (4.0.1). Choosing a malignancy-induced perturbation of the healthy equilibrium as initial condition for the myeloma model (see Definition 5.2), it holds that $x_h^0 + x_m^0 = x_h^{E_h} + x_m^0 > 0$ and $y_h^0 + y_m^0 = y_h^{E_h} = \frac{f}{d} + n \geq n$. Thus, the requirements of Theorem 7.2 are not restrictive from a biological point of view but suited for the setting of investigation. The same holds true for the case of the vaccination-induced perturbation of the healthy equilibrium in the framework of the extended model (4.0.1) as introduced by Definition 4.4. The extended model (4.0.1) will be discussed in Chapter 8.

Consequently, in the subsequent considerations, the myeloma model is considered to be defined on the (positively) invariant set $\mathcal{W}$. That is to say, we only consider solutions of the myeloma model with initial conditions (5.0.4) located in $\mathcal{W}$.

7.2 Existence and uniqueness of solutions

Existence results for solutions of the myeloma model in $\mathcal{W}$ can be inferred from continuity of the right-hand side g in system (7.0.1) yielding a local statement, compare Theorem 6.2. By boundedness of a linear combination of non-negative solutions for all finite times $t \geq t_0$, existence extends for a global statement, compare Theorem 6.6. The latter holds true due to

$$\begin{aligned} x_h'(t) + y_h'(t) &= f - dx_h(t) \leq f \\ x_m'(t) + y_m'(t) &= p_1 x_m(t) + p_2 y_m(t) \leq \max\{p_1, p_2\} \left(x_m(t) + y_m(t)\right). \end{aligned}$$

Next, the main result about global existence and uniqueness of solutions of the myeloma model is formulated and proven.

Theorem 7.4 (Global existence and uniqueness)**.** *Consider the myeloma model* (5.0.1) *defined on $\mathcal{W}$, i.e. let $(x_h^0, x_m^0, y_h^0, y_m^0)^T \in \mathcal{W}$. Then, there exists a unique solution $(x_h(t), x_m(t), y_h(t), y_m(t))^T \in \mathcal{W}$ for all $t \geq t_0$.*

Proof. The aim is to show Lipschitz continuity of the right-hand side g of the system (7.0.1). Therefore, consider the functions h_1, h_2, h_3 and h_3 defined by (7.1.2) and restrict them to the set $\mathcal{W}$. Moreover, let $X = (x_h, x_m, y_h, y_m)^T \in \mathcal{W}$. Choose $X_1 = (x_{h,1}, x_{m,1}, y_{h,1}, y_{m,1})^T \in \mathcal{W}$ and $X_2 = (x_{h,2}, x_{m,2}, y_{h,2}, y_{m,2})^T \in \mathcal{W}$ and set $z_1 = x_{h,1} + x_{m,1} - y_{h,1} - y_{m,1} + n$ and $z_2 = x_{h,2} + x_{m,2} - y_{h,2} - y_{m,2} + n$. For further analysis, three cases for $X_1, X_2 \in \mathcal{W}$ are considered:

(1) $z_1, z_2 > 0$, that is to say, $X_1, X_2 \in \mathcal{W} \cap (\mathcal{S}_1 \setminus \Sigma)$

(2) $z_1, z_2 < 0$, that is to say, $X_1, X_2 \in \mathcal{W} \cap \mathcal{S}_2$

(3) $z_2 \leq 0 \leq z_1$ or $z_1 \leq 0 \leq z_2$, that is to say, $X_1 \in \mathcal{W} \cap \mathcal{S}_1$ and $X_2 \in \mathcal{W} \cap (\mathcal{S}_2 \cup \Sigma)$, or vice versa, respectively. Without loss of generality, consider $z_2 \leq 0 \leq z_1$.

In cases (1) and (2), it follows that $h_j(X) \in C^1(\Omega, \mathbb{R})$, $j = 1, 2, 3, 4$, where $\Omega = \mathcal{W} \cap (\mathcal{S}_1 \setminus \Sigma)$ or $\Omega = \mathcal{W} \cap \mathcal{S}_2$, respectively. Thus, showing that the gradients $\nabla h_j(X)$ are bounded for all $X \in \Omega$ implies Lipschitz continuity of $h_j(X)$ in $X \in \Omega$ [91, 119]. In case (3), Lipschitz continuity is directly proven. It will be useful to observe that

for $X \in \mathcal{W}$, it is

$$0 \leq \frac{x_j}{x_h + x_m} \leq 1, \quad j \in \{h, m\}, \quad \text{and} \quad 0 \leq \frac{y_j}{y_h + y_m} \leq 1, \quad j \in \{h, m\}.$$

Moreover, if $z \geq 0$, then

$$0 \leq \frac{z}{x_h + x_m} = \frac{x_h + x_m - y_h - y_m + n}{x_h + x_m} = 1 + \frac{n - y_h - y_m}{x_h + x_m} \leq 1$$

due to $n - y_h - y_m \leq 0$. In case of $z \leq 0$, it follows that

$$0 \leq \frac{-z}{y_h + y_m} = \frac{-(x_h + x_m - y_h - y_m + n)}{y_h + y_m} = 1 - \frac{x_h + x_m + n}{y_h + y_m} < 1$$

due to

$$0 < \frac{x_h + x_m + n}{y_h + y_m} \leq 1.$$

Lipschitz continuity of h_1: For case (1), let $X \in \mathcal{W} \cap (\mathcal{S}_1 \setminus \Sigma)$. With

$$\nabla h_1(X) = \begin{pmatrix} -b_h \frac{x_h}{x_h + x_m} + b_h \frac{x_h z}{(x_h + x_m)^2} - b_h \frac{z}{x_h + x_m} - d \\ b_h \frac{x_h}{x_h + x_m} \\ -b_h \frac{x_h}{x_h + x_m} + b_h \frac{x_h z}{(x_h + x_m)^2} \\ b_h \frac{x_h}{x_h + x_m} \end{pmatrix},$$

it follows that

$$\|\nabla h_1(X)\|_1 \leq 4 b_h \frac{x_h}{x_h + x_m} + 2 b_h \frac{x_h z}{(x_h + x_m)^2} + b_h \frac{z}{x_h + x_m} + d \leq 7 b_h + d.$$

This implies Lipschitz continuity of $h_1(X)$ in $X \in \mathcal{W} \cap (\mathcal{S}_1 \setminus \Sigma)$ with Lipschitz

constant $L_{1,1} = 7b_h + d$. For case (2), let $X \in \mathcal{W} \cap \mathcal{S}_2$. With

$$\nabla h_1(X) = \begin{pmatrix} -c_h \frac{y_h}{y_h+y_m} - d \\ c_h \frac{y_h}{y_h+y_m} + c_h \frac{y_h z}{(y_h+y_m)^2} - c_h \frac{z}{y_h+y_m} \\ -c_h \frac{y_h}{y_h+y_m} \\ c_h \frac{y_h}{y_h+y_m} + c_h \frac{y_h z}{(y_h+y_m)^2} \end{pmatrix},$$

it follows that

$$\|\nabla h_1(X)\|_1 \leq 4c_h \frac{y_h}{y_h+y_m} + 2c_h \frac{y_h(-z)}{(y_h+y_m)^2} + c_h \frac{-z}{y_h+y_m} + d < 7c_h + d.$$

This implies Lipschitz continuity of $h_1(X)$ in $X \in \mathcal{W} \cap \mathcal{S}_2$ with Lipschitz constant $L_{1,2} = 7c_h + d$. For case (3), choose $X_1 \in \mathcal{W} \cap \mathcal{S}_1$ and $X_2 \in \mathcal{W} \cap (\mathcal{S}_2 \cup \Sigma)$. It follows that

$$\begin{aligned} |h_1(X_1) - h_1(X_2)| &= |f - \beta_h(X_1)z_1 - dx_{h,1} - f + \beta_h(X_2)z_2 + d_h x_{h,2}| \\ &\leq |\beta_h(X_1)z_1 - \beta_h(X_2)z_2| + d|x_{h,1} - x_{h,2}| \\ &\leq \max\{b_h, c_h\}|z_1 - z_2| + d|x_{h,1} - x_{h,2}| \\ &\leq (\max\{b_h, c_h\} + d)\,\|X_1 - X_2\|_1 \end{aligned}$$

due to Lemma 6.7, i.e.

$$\begin{aligned} |\beta_h(X_1)z_1 - \beta_h(X_2)z_2| &= \left| b_h \frac{x_{h,1}}{x_{h,1}+x_{m,1}} z_1 \right| + \left| c_h \frac{y_{h,2}}{y_{h,2}+y_{m,2}} z_2 \right| \\ &\leq b_h|z_1| + c_h|z_2| \\ &\leq \max\{b_h, c_h\}|z_1 - z_2| \\ &\leq \max\{b_h, c_h\}\|X_1 - X_2\|_1. \end{aligned} \tag{7.2.1}$$

We define $L_{1,3} = \max\{b_h, c_h\} + d$ and conclude that

$$\begin{aligned} |h_1(X_1) - h_1(X_2)| \leq L_1\|X_1 - X_2\|_1 \text{ with } L_1 &= \max\{L_{1,1}, L_{1,2}, L_{1,3}\} \\ &= 7\max\{b_h, c_h\} + d \end{aligned}$$

is true for all $X_1, X_2 \in \mathcal{W}$. Thus, $h_1(X)$ is (globally) Lipschitz continuous in $X \in \mathcal{W}$.

Lipschitz continuity of h_2: For case (1), let $X \in \mathcal{W} \cap (\mathcal{S}_1 \setminus \Sigma)$. With

$$\nabla h_2(X) = \begin{pmatrix} -b_m \frac{x_m}{x_h + x_m} + b_m \frac{x_m z}{(x_h + x_m)^2} \\ b_m \frac{x_m}{x_h + x_m} \\ p_1 - b_m \frac{x_m}{x_h + x_m} + b_m \frac{x_m z}{(x_h + x_m)^2} - b_m \frac{z}{x_h + x_m} \\ b_m \frac{x_m}{x_h + x_m} \end{pmatrix},$$

it follows that

$$\|\nabla h_2(X)\|_1 \leq 4b_m \frac{x_m}{x_h + x_m} + 2b_m \frac{x_m z}{(x_h + x_m)^2} + b_m \frac{z}{x_h + x_m} + |p_1| \leq 7b_m + |p_1|.$$

This implies Lipschitz continuity of $h_2(X)$ in $X \in \mathcal{W} \cap (\mathcal{S}_1 \setminus \Sigma)$ with Lipschitz constant $L_{2,1} = 7b_m + |p_1|$. For case (2), let $X \in \mathcal{W} \cap \mathcal{S}_2$. With

$$\nabla h_2(X) = \begin{pmatrix} -c_m \frac{y_m}{y_h + y_m} \\ c_m \frac{y_m z}{(y_h + y_m)^2} + c_m \frac{y_m}{y_h + y_m} \\ p_1 - c_m \frac{y_m}{y_h + y_m} \\ c_m \frac{y_m z}{(y_h + y_m)^2} - c_m \frac{z}{y_h + y_m} + c_m \frac{y_m}{y_h + y_m} \end{pmatrix},$$

it follows that

$$\|\nabla h_2(X)\|_1 \leq 4c_m \frac{y_m}{y_h + y_m} + 2c_m \frac{y_m(-z)}{(y_h + y_m)^2} + c_m \frac{-z}{y_h + y_m} + |p_1| < 7c_m + |p_1|.$$

This implies Lipschitz continuity of $h_2(X)$ in $X \in \mathcal{W} \cap \mathcal{S}_2$ with Lipschitz constant $L_{2,2} = 7c_m + |p_1|$. For case (3), choose $X_1 \in \mathcal{W} \cap \mathcal{S}_1$ and $X_2 \in \mathcal{W} \cap (\mathcal{S}_2 \cup \Sigma)$. It

follows that

$$\begin{aligned}|h_2(X_1) - h_2(X_2)| &= |p_1 x_{m,1} - \beta_m(X_1) z_1 - p_1 x_{m,2} + \beta_m(X_2) z_2| \\ &\leq |p_1||x_{m,1} - x_{m,2}| + |\beta_m(X_1) z_1 - \beta_m(X_2) z_2| \\ &\leq |p_1||x_{m,1} - x_{m,2}| + \max\{b_m, c_m\}|z_1 - z_2| \\ &\leq (|p_1| + \max\{b_m, c_m\}) \, \|X_1 - X_2\|_1\end{aligned}$$

due to Lemma 6.7, i.e.

$$\begin{aligned}|\beta_m(X_1) z_1 - \beta_m(X_2) z_2| &= \left| b_m \frac{x_{m,1}}{x_{h,1} + x_{m,1}} z_1 \right| + \left| c_m \frac{y_{m,2}}{y_{h,2} + y_{m,2}} z_2 \right| \\ &\leq b_m |z_1| + c_m |z_2| \\ &\leq \max\{b_m, c_m\}|z_1 - z_2| \\ &\leq \max\{b_m, c_m\} \|X_1 - X_2\|_1.\end{aligned} \tag{7.2.2}$$

We define $L_{2,3} = |p_1| + \max\{b_m, c_m\}$ and conclude that

$$\begin{aligned}|h_2(X_1) - h_2(X_2)| \leq L_2 \|X_1 - X_2\|_1 \;\text{ with }\; L_2 &= \max\{L_{2,1}, L_{2,2}, L_{2,3}\} \\ &= 7 \max\{b_m, c_m\} + |p_1|\end{aligned}$$

is true for all $X_1, X_2 \in \mathcal{W}$. Thus, $h_2(X)$ is (globally) Lipschitz continuous in $X \in \mathcal{W}$.

Lipschitz continuity of h_3: For case (1), let $X \in \mathcal{W} \cap (\mathcal{S}_1 \setminus \Sigma)$. With

$$\nabla h_3(X) = \begin{pmatrix} b_h \frac{x_h}{x_h + x_m} - b_h \frac{x_h z}{(x_h + x_m)^2} + b_h \frac{z}{x_h + x_m} \\ -b_h \frac{x_h}{x_h + x_m} \\ b_h \frac{x_h}{x_h + x_m} - b_h \frac{x_h z}{(x_h + x_m)^2} \\ -b_h \frac{x_h}{x_h + x_m} \end{pmatrix},$$

it follows that

$$\|\nabla h_3(X)\|_1 \leq 4 b_h \frac{x_h}{x_h + x_m} + 2 b_h \frac{x_h z}{(x_h + x_m)^2} + b_h \frac{z}{x_h + x_m} \leq 7 b_h.$$

This implies Lipschitz continuity of $h_3(X)$ in $X \in \mathcal{W} \cap (\mathcal{S}_1 \setminus \Sigma)$ with Lipschitz constant $L_{3,1} = 7b_h$. For case (2), let $X \in \mathcal{W} \cap \mathcal{S}_2$. With

$$\nabla h_3(X) = \begin{pmatrix} c_h \frac{y_h}{y_h+y_m} \\ -c_h \frac{y_h}{y_h+y_m} - c_h \frac{y_h z}{(y_h+y_m)^2} + c_h \frac{z}{y_h+y_m} \\ c_h \frac{y_h}{y_h+y_m} \\ -c_h \frac{y_h}{y_h+y_m} - c_h \frac{y_h z}{(y_h+y_m)^2} \end{pmatrix},$$

it follows that

$$\|\nabla h_3(X)\|_1 \leq 4c_h \frac{y_h}{y_h+y_m} + 2c_h \frac{y_h(-z)}{(y_h+y_m)^2} + c_h \frac{-z}{y_h+y_m} < 7c_h.$$

This implies Lipschitz continuity of $h_3(X)$ in $X \in \mathcal{W} \cap \mathcal{S}_2$ with Lipschitz constant $L_{3,2} = 7c_h$. For case (3), choose $X_1 \in \mathcal{W} \cap \mathcal{S}_1$ and $X_2 \in \mathcal{W} \cap (\mathcal{S}_2 \cup \Sigma)$. By (7.2.1), it follows that

$$|h_3(X_1) - h_3(X_2)| = |\beta_h(X_1)z_1 - \beta_h(X_2)z_2| \leq \max\{b_h, c_h\}\|X_1 - X_2\|_1.$$

We define $L_{3,3} = \max\{b_h, c_h\}$ and conclude that

$$\begin{aligned} |h_3(X_1) - h_3(X_2)| \leq L_3\|X_1 - X_2\|_1 \text{ with } L_3 &= \max\{L_{3,1}, L_{3,2}, L_{3,3}\} \\ &= 7\max\{b_h, c_h\} \end{aligned}$$

is true for all $X_1, X_2 \in \mathcal{W}$. Thus, $h_3(X)$ is (globally) Lipschitz continuous in $X \in \mathcal{W}$.

Lipschitz continuity of h_4: For case (1), let $X \in \mathcal{W} \cap (\mathcal{S}_1 \setminus \Sigma)$. With

$$\nabla h_4(X) = \begin{pmatrix} b_m \frac{x_m}{x_h+x_m} - b_m \frac{x_m z}{(x_h+x_m)^2} \\ -b_m \frac{x_m}{x_h+x_m} \\ b_m \frac{x_m}{x_h+x_m} - b_m \frac{x_m z}{(x_h+x_m)^2} + b_m \frac{z}{x_h+x_m} \\ p_2 - b_m \frac{x_m}{x_h+x_m} \end{pmatrix},$$

it follows that

$$\|\nabla h_4(X)\|_1 \leq 4b_m \frac{x_m}{x_h + x_m} + 2b_m \frac{x_m z}{(x_h + x_m)^2} + b_m \frac{z}{x_h + x_m} + |p_2| \leq 7b_m + |p_2|.$$

This implies Lipschitz continuity of $h_4(X)$ in $X \in \mathcal{W} \cap (\mathcal{S}_1 \setminus \Sigma)$ with Lipschitz constant $L_{4,1} = 7b_m + |p_2|$. For case (2), let $X \in \mathcal{W} \cap \mathcal{S}_2$. With

$$\nabla h_4(X) = \begin{pmatrix} c_m \frac{y_m}{y_h + y_m} \\ -c_m \frac{y_m z}{(y_h + y_m)^2} - c_m \frac{y_m}{y_h + y_m} \\ c_m \frac{y_m}{y_h + y_m} \\ p_2 - c_m \frac{y_m z}{(y_h + y_m)^2} + c_m \frac{z}{y_h + y_m} - c_m \frac{y_m}{y_h + y_m} \end{pmatrix},$$

it follows that

$$\|\nabla h_4(X)\|_1 \leq 4c_m \frac{y_m}{y_h + y_m} + 2c_m \frac{y_m(-z)}{(y_h + y_m)^2} + c_m \frac{-z}{y_h + y_m} + |p_2| < 7c_m + |p_2|.$$

This implies Lipschitz continuity of $h_4(X)$ in $X \in \mathcal{W} \cap \mathcal{S}_2$ with Lipschitz constant $L_{4,2} = 7c_m + |p_2|$. For case (3), choose $X_1 \in \mathcal{W} \cap \mathcal{S}_1$ and $X_2 \in \mathcal{W} \cap (\mathcal{S}_2 \cup \Sigma)$. By (7.2.2), it follows that

$$\begin{aligned} |h_4(X_1) - h_4(X_2)| &= |p_2 y_{m,1} + \beta_m(X_1) z_1 - p_2 y_{m,2} - \beta_m(X_2) z_2| \\ &\leq |p_2||y_{m,1} - y_{m,2}| + |\beta_m(X_1) z_1 - \beta_m(X_2) z_2| \\ &\leq (|p_2| + \max\{b_m, c_m\}) \, \|X_1 - X_2\|_1. \end{aligned}$$

We define $L_{4,3} = |p_2| + \max\{b_m, c_m\}$ and conclude that

$$\begin{aligned} |h_4(X_1) - h_4(X_2)| \leq L_4 \|X_1 - X_2\|_1 \text{ with } L_4 &= \max\{L_{4,1}, L_{4,2}, L_{4,3}\} \\ &= 7 \max\{b_m, c_m\} + |p_2| \end{aligned}$$

is true for all $X_1, X_2 \in \mathcal{W}$. Thus, $h_4(X)$ is (globally) Lipschitz continuous in $X \in \mathcal{W}$.

Lipschitz continuity of g: In a final step, let

$$L := L_1 + L_2 + L_3 + L_4 = 14\,(\max\{b_h, c_h\} + \max\{b_m, c_m\}) + |p_1| + |p_2| + d$$

and conclude that

$$\|g(X_1) - g(X_2)\|_1 = \sum_{j=1}^{4} |h_j(X_1) - h_j(X_2)| \leq L\|X_1 - X_2\|_1$$

for all $X_1, X_2 \in \mathcal{W}$, which implies (global) Lipschitz continuity of the right-hand side $g(X)$ of system (7.0.1) in $X \in \mathcal{W}$. By Theorem A.6 and Remark A.7, this yields global existence and uniqueness of solutions. □

Remark 7.5. With Remark 5.3, an analogue statement of Theorem 7.4 holds true for the extended model (4.0.1).

7.3 Equilibria

The following analysis distinguishes between isolated and non-isolated equilibria.

Definition 7.6 (Isolated and non-isolated equilibrium, adapted from Chapter 1 in [20])**.** If an equilibrium is contained in an open subset of the phase space in which there is no other equilibrium, then it is referred to as an isolated equilibrium. Otherwise, it is a non-isolated equilibrium.

For investigation of equilibria of the myeloma model, set $g(x_h, x_m, y_h, y_m) = 0$ in system (7.0.1), and solve for (constant) x_h, x_m, y_h and y_m. In particular, consider $g_1(x_h, x_m, y_h, y_m) = 0$ in $\mathcal{W} \cap \mathcal{S}_1$ and $g_2(x_h, x_m, y_h, y_m) = 0$ in $\mathcal{W} \cap \mathcal{S}_2$.

Theorem 7.7 (Equilibria)**.** *Consider the myeloma model* (5.0.1) *defined on* $\mathcal{W}$*.*

(i) If $p_1 \neq 0$ *and* $p_2 \neq 0$*, then there exists the healthy equilibrium*

$$E_h = \left(x_h^{E_h}, 0, y_h^{E_h}, 0\right)^T \in \mathcal{W} \cap \Sigma.$$

Additionally, a further well-defined isolated equilibrium

$$E_m := \left(x_h^{E_m}, x_m^{E_m}, 0, y_m^{E_m}\right)^T \in \mathcal{W} \cap \mathcal{S}_2$$

exists if and only if $p_1 < 0$ *and* $0 < p_2 < \frac{c_m p_1}{p_1 - c_m}$, *where*

$$\begin{aligned} x_h^{E_m} &= \frac{f}{d} \\ x_m^{E_m} &= \frac{c_m p_2}{p_1 p_2 - c_m p_2 - c_m p_1} \left(\frac{f}{d} + n \right) \\ y_m^{E_m} &= \frac{-c_m p_1}{p_1 p_2 - c_m p_2 - c_m p_1} \left(\frac{f}{d} + n \right). \end{aligned}$$

No further equilibria exist.

(ii) If $p_1 = 0$ *and* $p_2 \neq 0$, *then there exists a one-dimensional manifold of non-isolated equilibria given by*

$$\mathcal{E}_1 = \left\{ \begin{pmatrix} x_h^{E_1} \\ x_m^{E_1} \\ y_h^{E_1} \\ y_m^{E_1} \end{pmatrix} \in \mathcal{W} : \begin{pmatrix} \frac{f}{d} \\ 0 \\ \frac{f}{d} + n \\ 0 \end{pmatrix} + x_m^{E_1} \begin{pmatrix} 0 \\ 1 \\ 1 \\ 0 \end{pmatrix} \right\} \subset \mathcal{W} \cap \Sigma.$$

No further equilibria exist.

(iii) If $p_1 \neq 0$ *and* $p_2 = 0$, *then there exists a one-dimensional manifold of non-isolated equilibria given by*

$$\mathcal{E}_2 = \left\{ \begin{pmatrix} x_h^{E_2} \\ x_m^{E_2} \\ y_h^{E_2} \\ y_m^{E_2} \end{pmatrix} \in \mathcal{W} : \begin{pmatrix} \frac{f}{d} \\ 0 \\ \frac{f}{d} + n \\ 0 \end{pmatrix} + y_m^{E_2} \begin{pmatrix} 0 \\ 0 \\ -1 \\ 1 \end{pmatrix} \right\} \subset \mathcal{W} \cap \Sigma.$$

No further equilibria exist.

(iv) If $p_1 = 0$ *and* $p_2 = 0$, *then there exists a two-dimensional manifold of non-*

isolated equilibria given by

$$\mathcal{E}_3 = \left\{ \begin{pmatrix} x_h^{E_3} \\ x_m^{E_3} \\ y_h^{E_3} \\ y_m^{E_3} \end{pmatrix} \in \mathcal{W} : \begin{pmatrix} \frac{f}{d} \\ 0 \\ \frac{f}{d} + n \\ 0 \end{pmatrix} + x_m^{E_3} \begin{pmatrix} 0 \\ 1 \\ 1 \\ 0 \end{pmatrix} + y_m^{E_3} \begin{pmatrix} 0 \\ 0 \\ -1 \\ 1 \end{pmatrix} \right\} \subset \mathcal{W} \cap \Sigma.$$

No further equilibria exist.

Proof. At first, observe that solving $g_1(x_h, x_m, y_h, y_m) = 0$ immediately implies $x_h = \frac{f}{d}$ and $z = 0$, whereas solving $g_2(x_h, x_m, y_h, y_m) = 0$ implies $x_h = \frac{f}{d}$, and either $y_h = 0$ or $z = 0$. In the following, each case (i) - (iv) is investigated:

Case (i): Let $p_1 \neq 0$ and $p_2 \neq 0$. Solving $g_1(x_h, x_m, y_h, y_m) = 0$ in $\mathcal{S}_1$ yields the healthy equilibrium E_h as the only equilibrium. For $g_2(x_h, x_m, y_h, y_m) = 0$, it follows that $x_h = \frac{f}{d}$, and either $y_h = 0$ or $z = 0$. In the latter case, E_h is obtained. For $y_h = 0$, it follows that

$$\begin{aligned} p_1 x_m - c_m \left(\frac{f}{d} + n + x_m - y_m \right) &= 0 \\ p_2 y_m + c_m \left(\frac{f}{d} + n + x_m - y_m \right) &= 0. \end{aligned}$$

Significantly, this system obtains a unique solution if and only if $p_1 \neq 0$ and $p_2 \neq 0$. Solving this system yields

$$\begin{aligned} x_m^{E_m} &= \frac{c_m p_2}{p_1 p_2 - c_m p_2 - c_m p_1} \left(\frac{f}{d} + n \right) \\ y_m^{E_m} &= \frac{-c_m p_1}{p_1 p_2 - c_m p_2 - c_m p_1} \left(\frac{f}{d} + n \right). \end{aligned}$$

We need to show that $x_m^{E_m}$ and $y_m^{E_m}$ are well-defined (i.e. the denominators are non-zero) and non-negative.

(1) If $p_2 > 0$, then it must hold that $p_1 p_2 - c_m p_2 - c_m p_1 > 0$ and $p_1 < 0$. This is true if and only if $p_1 < 0$ and $0 < p_2 < \frac{c_m p_1}{p_1 - c_m}$.

(2) If $p_2 < 0$, then it must hold that $p_1p_2 - c_mp_2 - c_mp_1 < 0$ and $p_1 > 0$. This is true if and only if $0 < p_1 < c_m$ and $\frac{c_mp_1}{p_1-c_m} < p_2 < 0$.

Furthermore, it must hold that $E_m \in \mathcal{S}_2$. A straightforward calculation gives

$$z = \left(\frac{f}{d} + n\right) \frac{p_1p_2}{p_1p_2 - c_mp_2 - c_mp_1}$$

at E_m, which is negative only in case (1). Consequently, case (2) can be excluded. At last, it must hold that $E_m \in \mathcal{W}$. Clearly, $W_1(x_h^{E_m}, x_m^{E_m}, y_h^{E_m}, y_m^{E_m}) \leq 0$. Moreover, it is

$$\begin{aligned} W_2(x_h^{E_m}, x_m^{E_m}, y_h^{E_m}, y_m^{E_m}) = \frac{(p_1p_2 - c_mp_2)n + \frac{f}{d}c_mp_1}{p_1p_2 - c_mp_2 - c_mp_1} \leq 0 \\ \Leftrightarrow \ \frac{f}{d}c_mp_1 \leq (c_m - p_1)p_2n, \end{aligned}$$

which is true due to $p_1 < 0$ and $p_2 > 0$.

Case (ii): Let $p_1 = 0$ and $p_2 \neq 0$. This implies $y_m = 0$. Let $(x_h, x_m, y_h, y_m) \in \mathcal{S}_2$. If $g_2(x_h, x_m, y_h, y_m) = 0$ and $z \neq 0$, it follows that $y_h = 0$, which implies $z = \frac{f}{d} + n + x_m > 0$ for $x_m \geq 0$ and consequently $(x_h, x_m, y_h, y_m) \notin \mathcal{S}_2$. It follows that $z = 0$. This implies $y_h = \frac{f}{d} + n + x_m$. Choosing $x_m \geq 0$ yields a uniquely determined $y_h \geq \frac{f}{d} + n$. Thus, $E \in \mathcal{E}_1 \subset \mathcal{W} \cap \Sigma$ is an equilibrium.

Case (iii): Let $p_1 \neq 0$ and $p_2 = 0$. This implies $x_m = 0$. Let $(x_h, x_m, y_h, y_m) \in \mathcal{S}_2$. If $g_2(x_h, x_m, y_h, y_m) = 0$ and $z \neq 0$, then $y_h = 0 = y_m$, which implies $z = \frac{f}{d} + n > 0$ and consequently $(x_h, x_m, y_h, y_m) \notin \mathcal{S}_2$. It follows that $z = 0$. This implies $y_h = \frac{f}{d} + n - y_m$. Choosing $y_h \in [0, \frac{f}{d} + n]$ yields a uniquely determined $y_h \geq 0$. Thus, $E \in \mathcal{E}_2 \subset \mathcal{W} \cap \Sigma$ is an equilibrium.

Case (iv): Let $p_1 = 0$ and $p_2 = 0$. Let $(x_h, x_m, y_h, y_m) \in \mathcal{S}_2$. If $g_2(x_h, x_m, y_h, y_m) = 0$ and $z \neq 0$, then $y_h = 0 = y_m$, which implies $z = \frac{f}{d} + n > 0$ and consequently $(x_h, x_m, y_h, y_m) \notin \mathcal{S}_2$. It follows that $z = 0$. This implies $y_h = \frac{f}{d} + n + x_m - y_m$. Choosing appropriate x_m and y_m (i.e. such that $(x_h, x_m, y_h, y_m) \in \mathcal{W}$) yields a uniquely determined y_h. Thus, $E \in \mathcal{E}_3 \subset \mathcal{W} \cap \Sigma$ is an equilibrium. □

Observe that $E_h \in \mathcal{E}_1 \cap \mathcal{E}_2 \cap \mathcal{E}_3$. By contrast to smooth dynamical systems for which the theory of manifolds of equilibria can be extended to non-isolated equilibria [4], a deduction of stability for $E \in \mathcal{E}_1 \cup \mathcal{E}_2 \cup \mathcal{E}_3 \subset \Sigma$ from that within $\mathcal{S}_1$ and $\mathcal{S}_2$ might be misleading. Classical theory of smooth dynamical systems [36] can be applied for analysing the stability of $E_m \in \mathcal{W} \cap \mathcal{S}_2$.

Theorem 7.8 (Stability of E_m)**.** *Consider the myeloma model* (5.0.1) *defined on* $\mathcal{W}$*. The equilibrium* E_m *is locally asymptotically stable whenever it exists.*

Proof. Since $E_m \in \mathcal{S}_2$, consider the vector field with right-hand side g_2 of system (7.0.1). Linearisation of $g_2 = g_2(x_h, x_m, y_h, y_m)$ about E_m yields the Jacobian matrix

$$\begin{pmatrix} -d & \frac{c_h}{c_m}p_2 & 0 & 0 \\ 0 & -\frac{c_h}{c_m}p_2 & 0 & 0 \\ -c_m & c_m - p_2 & p_1 - c_m & c_m \\ c_m & -c_m + p_2 & c_m & p_2 - c_m \end{pmatrix}.$$

Due to the block form, its eigenvalues are $\lambda_1 = -d < 0$, $\lambda_2 = -\frac{c_h}{c_m}p_2 < 0$ (by Theorem 7.7), and the solutions of

$$\begin{vmatrix} p_1 - c_m - \lambda_{3,4} & c_m \\ c_m & p_2 - c_m - \lambda_{3,4} \end{vmatrix} = 0, \tag{7.3.1}$$

which are given by

$$\lambda_{3,4} = \frac{p_1 + p_2 - 2c_m}{2} \pm \sqrt{\frac{(p_1 + p_2 - 2c_m)^2}{4} - \big(p_1p_2 - p_1c_m - c_mp_2\big)}.$$

A straightforward calculation shows that the radicand is always non-negative. Moreover, it is $\Re(\lambda_{3,4}) < 0$ if and only if $2c_m - p_1 - p_2 > 0$ and $p_1p_2 - p_1c_m - c_mp_2 > 0$. The latter is fulfilled by definition of $E_m \in \mathcal{W}$ (see Theorem 7.7), and it implies the

former condition due to

$$2c_m - p_1 - p_2 > 2c_m - \frac{p_1 p_2}{c_m} > 0.$$

Since $\Re(\lambda_i) < 0$ for all $i = 1, 2, 3, 4$, the theorem of Hartman and Grobman [36, Theorem 1.4.1] implies the claim. □

7.4 Partial equilibria

Using (5.0.1), the time evolution of the total number of malignant PCs $x_m(t) + y_m(t)$ satisfies

$$x_m'(t) + y_m'(t) = p_1 x_m(t) + p_2 y_m(t). \tag{7.4.1}$$

Observe that the growth of the total number of malignant PCs does not directly depend on the healthy PC population. If $p_1, p_2 > 0$, it follows by equation (7.4.1) that

$$x_m'(t) + y_m'(t) \geq \min\{p_1, p_2\} \left(x_m(t) + y_m(t)\right).$$

This implies

$$x_m(t) + y_m(t) \geq \left(x_m^0 + y_m^0\right) e^{\min\{p_1,p_2\}(t-t_0)} \quad \text{with} \quad x_m^0, y_m^0 \geq 0.$$

Therefore, $\lim_{t\to\infty} \left(x_m(t) + y_m(t)\right) = \infty$.

Remark 7.9 (Declining total number of malignant PCs)**.** If $p_1, p_2 < 0$, equation (7.4.1) implies

$$x_m(t) + y_m(t) \leq \left(x_m^0 + y_m^0\right) e^{\max\{p_1,p_2\}(t-t_0)}.$$

With $x_m^0, y_m^0 \geq 0$, it follows that $\lim_{t\to\infty} \left(x_m(t) + y_m(t)\right) = 0$.

This describes that if $p_1, p_2 > 0$ the total number of malignant PCs grows in time rather than converging to an equilibrium (such as E_m). In contrast, the total number of healthy PCs is supposed to decline during the development of myeloma [60], potentially approaching a (rather low) equilibrium state. This observation motivates the subsequent investigation of so-called partial equilibria [124].

Definition 7.10 (Partial equilibrium)**.** Consider a dynamical system generated by the flow

$$\begin{aligned} x'(t) &= f(x(t), y(t)) \\ y'(t) &= g(x(t), y(t)). \end{aligned} \tag{7.4.2}$$

Assume f, g such that solutions $(x(t), y(t))^T \in \mathcal{U} \times \mathcal{V} \subseteq \mathbb{R}^m \times \mathbb{R}^n$ exist and are unique for all $t \geq t_0$. If $f(x, y(t)) = 0$ with $x(t) = x$ is constant for all $t \geq t_0$, then $E_p(t) = (x, y(t))^T$ is called partial equilibrium of the system (7.4.2).

Observe that a partial equilibrium $E_p(t) = (x, y(t))^T$ of the system (7.4.2) according to Definition 7.10 extends the notion of an equilibrium: If $y(t) = y$ is constant for all $t \geq t_0$, then the partial equilibrium is an equilibrium in the classical sense, i.e. $E_p(t) = E_p = (x, y)^T$, delineated as **total equilibrium** [124]. Distinguish partial equilibria from **quasi-steady states**. Latter arise in mathematical modelling due to different time scales of the involved processes [120]. At a quasi-steady state, it holds $x'(t) = 0$ for all $t \geq t_0$. This is likewise the case at a partial equilibrium $E_p(t)$. Both concepts differ in that $x(t) = x$ is constant at a partial equilibrium.

In the following investigation, let the healthy components of system (5.0.1) satisfy the **partial equilibrium condition**

$$\begin{aligned} x_h'(t) = 0,\ x_h(t) = x_h \quad &\text{for all } \ t \geq t_0 \\ y_h'(t) = 0,\ y_h(t) = y_h \quad &\text{for all } \ t \geq t_0. \end{aligned} \tag{7.4.3}$$

The following two lemmas prepare the main result about existence and characterisation of partial equilibria of the myeloma model, which satisfy the partial equilibrium conditions (7.4.3). Firstly, the equations (7.4.3) are characterised in terms of the sign of the function $z(t)$.

Lemma 7.11. *Consider the myeloma model* (5.0.1) *defined on* $\mathcal{W}$*. The partial equilibrium condition* (7.4.3) *holds true if and only if either*

(i) $x_h = \frac{f}{d}$ *with* $z(t) = 0$ *for all* $t \geq t_0$*, or*

(ii) $x_h = \frac{f}{d}$ *and* $y_h = 0$ *with* $z(t) \leq 0$ *for all* $t \geq t_0$*.*

Proof. Assume that equations (7.4.3) hold true. From $y_h'(t) = 0$, it follows that

$$0 = \begin{cases} b_h \frac{x_h}{x_h + x_m(t)} z(t) & \text{if } z(t) \geq 0 \\ c_h \frac{y_h}{y_h + y_m(t)} z(t) & \text{if } z(t) < 0 \end{cases} \tag{7.4.4}$$

for all $t \geq t_0$. From $x_h'(t) = 0$, it follows that $x_h = \frac{f}{d}$. Observe that equation (7.4.4) cannot be true if $z(t) > 0$ for any time $t \geq t_0$. Consequently, $z(t) \leq 0$ for all $t \geq t_0$. There are two cases: Firstly, if $z(t) = 0$ for all $t \geq t_0$, then equation (7.4.4) is satisfied for all $t \geq t_0$ regardless of the exact value of y_h. Secondly, if there exists at least one time $t \geq t_0$ such that $z(t) < 0$, then $y_h = 0$. The back-implication follows by insertion. This proves the claim. □

Secondly, the solutions $x_m(t)$ and $y_m(t)$ are characterised if equations (7.4.3) hold true. The forthcoming result implies that there do not exist partial equilibria at which additionally either $x_m'(t) = 0,\ x_m(t) = x_m$ is constant for all $t \geq t_0$, or $y_m'(t) = 0,\ y_m(t) = y_m$ is constant for all $t \geq t_0$.

Lemma 7.12. *Consider the myeloma model* (5.0.1) *defined on* $\mathcal{W}$. *Let the partial equilibrium condition* (7.4.3) *hold true. It follows that either* $x_m(t) = x_m$ *and* $y_m(t) = y_m$ *are constant for all* $t \geq t_0$ *(i.e. a total equilibrium is attained), or* $x_m(t)$ *and* $y_m(t)$ *are non-constant for all* $t \geq t_0$.

Proof. The partial equilibrium condition (7.4.3) and Lemma 7.11 imply $x_h = \frac{f}{d}$ and y_h is constant. Moreover, $z(t) \leq 0$ for all $t \geq t_0$. Consequently, the flow of system (5.0.1) is restricted to $\mathcal{S}_2 \cup \Sigma$, where the dynamics of $x_m(t)$ and $y_m(t)$ are described by a planar linear system of ODEs,

$$\begin{aligned} x_m'(t) &= p_1 x_m(t) - c_m \left(x_m(t) - y_m(t) + \frac{f}{d} + n - y_h \right) \\ y_m'(t) &= p_2 y_m(t) + c_m \left(x_m(t) - y_m(t) + \frac{f}{d} + n - y_h \right). \end{aligned} \tag{7.4.5}$$

Observe that solutions of system (7.4.5) exist and are unique. Furthermore, if $x_m'(t) = 0$ and $x_m(t) = x_m$ is constant for all $t \geq t_0$, it follows from the first equation

of (7.4.5) that

$$y_m(t) = \left(1 - \frac{p_1}{c_m}\right) x_m + \frac{f}{d} + n - y_h$$

is constant for all $t \geq t_0$. Similarly, if $y_m'(t) = 0$ and $y_m(t) = y_m$ is constant for all $t \geq t_0$, it follows that $x_m(t) = x_m$ is constant for all $t \geq t_0$. Thus, the only partial equilibrium of system (7.4.5) is a total equilibrium. Due to uniqueness of solutions, this cannot be reached at a finite time. This proves the claim. □

Theorem 7.7 characterises the complete set of possible total equilibria of the myeloma model. The next theorem states necessary and sufficient conditions for existence of partial equilibria satisfying (7.4.3) in terms of the net growth rates p_1 and p_2 and the initial conditions x_m^0 and y_m^0. Further, it delineates total equilibria from the set of partial equilibria. By Lemma 7.12, this guarantees existence of partial equilibria with non-constant malignant components $x_m(t)$ and $y_m(t)$.

Theorem 7.13 (Partial equilibria)**.** *Consider the myeloma model* (5.0.1) *defined on* $\mathcal{W}$*. There exist exactly two partial equilibria of the form* $E_p(t) = (x_h, x_m(t), y_h, y_m(t))^T \in \mathcal{W}$ *with initial conditions* $x_m(t_0) = x_m^0$ *and* $y_m(t_0) = y_m^0$*, which are given by*

$$E_{p,1}(t) = \begin{pmatrix} \frac{f}{d} \\ x_m^0 e^{p_1(t-t_0)} \\ \frac{f}{d} + n \\ y_m^0 e^{p_2(t-t_0)} \end{pmatrix} \in \mathcal{W} \cap \Sigma \quad \text{and} \quad E_{p,2}(t) = \begin{pmatrix} \frac{f}{d} \\ x_m(t) \\ 0 \\ y_m(t) \end{pmatrix} \in \mathcal{W} \cap (\mathcal{S}_2 \cup \Sigma)$$

for all $t \geq t_0$*. They expand the set of total equilibria by possessing non-constant malignant components* $x_m(t)$ *and* $y_m(t)$ *for all* $t \geq t_0$*:*

(i) $E_{p,1}(t)$ *has non-constant* $x_m(t)$ *and* $y_m(t)$ *for all* $t \geq t_0$ *if and only if* $p_1 = p_2 \neq 0$ *and* $x_m^0 = y_m^0 > 0$*.*

(ii) $E_{p,2}(t)$ *has non-constant* $x_m(t)$ *and* $y_m(t)$ *for all* $t \geq t_0$ *if and only if* $p_1 \leq p_2$*,* $p_2 \geq 0$ *and* $E_{p,2}(t_0) \in \mathcal{W} \cap (\mathcal{S}_2 \cup \Sigma)$*, where*

- $E_{p,2}(t_0) \notin \mathcal{E}_2$ *in case of* $p_1 \neq 0$ *and* $p_2 = 0$*,*

– $E_{p,2}(t_0) \notin \mathcal{E}_3$ *in case of* $p_1 = 0 = p_2$,

– $E_{p,2}(t_0) \neq E_m$ *in case of* $p_1 < 0$ *and* $0 < p_2 < \frac{c_m p_1}{p_1 - c_m}$.

Proof. In order to obtain partial equilibria of the form $E_p(t) = (x_h, x_m(t), y_h, y_m(t))^T$, assume that the partial equilibrium condition (7.4.3) holds true. By Lemma 7.11 this is equivalent to either

(i) $x_h = \frac{f}{d}$ with $z(t) = 0$ for all $t \geq t_0$, or

(ii) $x_h = \frac{f}{d}$ and $y_h = 0$ with $z(t) \leq 0$ for all $t \geq t_0$.

In the following, the conditions for the function $z(t)$ stated in each case (i) and (ii), respectively, are translated into equivalent conditions for the model parameters p_1 and p_2 and for the initial conditions x_m^0 and y_m^0. Distinguishing total equilibria from those with non-constant malignant components $x_m(t)$ and $y_m(t)$ completely characterises the respective set of partial equilibria $E_p(t)$ in each case, see Lemma 7.12.

Case (i): Let $x_h = \frac{f}{d}$. It is shown that $z(t) = 0$ for all $t \geq t_0$ if and only if the solution of the myeloma model (5.0.1) is a total equilibrium satisfying $E_{p,1}(t_0) \in \mathcal{E}_1 \cup \mathcal{E}_2 \cup \mathcal{E}_3$, or it is a partial equilibrium $E_{p,1}(t)$ characterised by $p_1 = p_2 \neq 0$ with $x_m^0 = y_m^0 \neq 0$ (i.e. with non-constant $x_m(t)$ and $y_m(t)$ for all $t \geq t_0$).

Consider $E_{p,1}(t)$. Assuming $E_{p,1}(t_0) \in \mathcal{E}_1 \cup \mathcal{E}_2 \cup \mathcal{E}_3$ immediately implies $z(t) = 0$ for all $t \geq t_0$ due to Theorem 7.7. If $p_1 = p_2 \neq 0$ with $x_m^0 = y_m^0 \neq 0$, a straightforward calculation shows that $z(t) = 0$ for all $t \geq t_0$.

Let $z(t) = 0$ for all $t \geq t_0$. This is equivalent to $0 = z'(t) = x_m'(t) - y_m'(t)$ with $y_h = \frac{f}{d} + n + x_m(t) - y_m(t)$ for all $t \geq t_0$. Further, $x_m'(t) = p_1 x_m(t)$ and $y_m'(t) = p_2 y_m(t)$ for all $t \geq t_0$. This implies $x_m(t) = x_m^0 e^{p_1(t-t_0)}$ and $y_m(t) = y_m^0 e^{p_2(t-t_0)}$. Moreover, it is

$$x_m'(t) = y_m'(t) \;\Leftrightarrow\; p_1 x_m(t) = p_2 y_m(t) \;\Leftrightarrow\; p_1 x_m^0 e^{p_1(t-t_0)} = p_2 y_m^0 e^{p_2(t-t_0)}.$$

On the one hand, the following total equilibria are found:

- If $p_1 = 0$ and $p_2 \neq 0$, it follows that $x_m(t) = x_m^0$ and $y_m(t) = 0$ for all $t \geq t_0$,

where $y_h = \frac{f}{d} + n + x_m^0$. Thus, we obtain $E_{p,1}(t) \in \mathcal{E}_1$ for all $t \geq t_0$, which is a total equilibrium.

- If $p_1 \neq 0$ and $p_2 = 0$, it follows that $x_m(t) = 0$ and $y_m(t) = y_m^0$ for all $t \geq t_0$, where $y_h = \frac{f}{d} + n - y_m^0$. Thus, we obtain $E_{p,1}(t) \in \mathcal{E}_2$ for all $t \geq t_0$, which is a total equilibrium.

- If $p_1 = 0 = p_2$, it follows that $x_m(t) = x_m^0$ and $y_m(t) = y_m^0$ for all $t \geq t_0$, where $y_h = \frac{f}{d} + n + x_m^0 - y_m^0$. Thus, we obtain $E_{p,1}(t) \in \mathcal{E}_3$ for all $t \geq t_0$, which is a total equilibrium.

On the other hand, assume that $p_1 \neq 0 \neq p_2$. If $x_m^0 = 0$ ($y_m^0 = 0$), then $x_m(t) = 0$ ($y_m(t) = 0$) for all $t \geq t_0$ and therefore $y_m(t) = 0$ ($x_m(t) = 0$) for all $t \geq t_0$. Thus, we obtain $E_{p,1}(t) = E_h$ for all $t \geq t_0$, which is the healthy equilibrium. As a consequence, assume $x_m^0 \neq 0 \neq y_m^0$. It follows that

$$p_1 x_m^0 e^{p_1(t-t_0)} = p_2 y_m^0 e^{p_2(t-t_0)} \quad \Leftrightarrow \quad x_m^0 = \frac{p_2}{p_1} y_m^0 e^{(p_2-p_1)(t-t_0)},$$

which holds true for all $t \geq t_0$ if and only if $p_1 = p_2$ and $x_m^0 = y_m^0$. Since solutions are considered to be in the (positively) invariant set $\mathcal{W}$, it is $x_m^0 = y_m^0 > 0$. Consequently, $x_m(t) = x_m^0 e^{p_1(t-t_0)} = y_m(t)$ for all $t \geq t_0$, and therefore $y_h = \frac{f}{d} + n$. Observe that $x_m(t)$ and $y_m(t)$ are non-constant for all $t \geq t_0$.

Case (ii): Let $x_h = \frac{f}{d}$ and $y_h = 0$. That is to say, consider $E_{p,2}(t)$. First, it is shown that $\mathcal{W} \cap (\mathcal{S}_2 \cup \Sigma)$ is (positively) invariant under the vector field of the myeloma model (5.0.1) if and only if $p_1 \leq p_2$ and $p_2 \geq 0$.

Let $\mathcal{W} \cap (\mathcal{S}_2 \cup \Sigma)$ be (positively) invariant under the vector field of system (5.0.1), and let $E_{p,2}(t_0) \in \mathcal{W} \cap (\mathcal{S}_2 \cup \Sigma)$. Thus, let $z(t) \leq 0$ for all $t \geq t_0$. This is equivalent to $x_m'(t) \geq p_1 x_m(t)$ and $y_m'(t) \leq p_2 y_m(t)$ for all $t \geq t_0$, implying $x_m(t) \geq x_m^0 e^{p_1(t-t_0)}$ and $y_m(t) \leq y_m^0 e^{p_2(t-t_0)}$. Observe that $x_m(t), y_m(t) \geq 0$ for all $t \geq t_0$ due to $E_{p,2}(t) \in \mathcal{W}$. It follows that

$$0 \geq z(t) = \frac{f}{d} + n + x_m(t) - y_m(t) \geq \frac{f}{d} + n + x_m^0 e^{p_1(t-t_0)} - y_m^0 e^{p_2(t-t_0)}$$

for all $t \geq t_0$, which implies

$$y_m^0 \geq \left(\frac{f}{d} + n\right) e^{-p_2(t-t_0)} + x_m^0 e^{(p_1-p_2)(t-t_0)}. \tag{7.4.6}$$

This holds true if and only if it holds true at $t = t_0$ and both terms of the right-hand side of the inequality are non-increasing in t. Otherwise, there exists a finite time such that the inequality is no longer satisfied due to (positive) exponential growth of either terms. In other words, (7.4.6) holds true for all $t \geq t_0$ if and only if $\frac{f}{d} + n + x_m^0 - y_m^0 \leq 0$ and $p_1 \leq p_2,\ p_2 \geq 0$.

Next, assume that $p_1 \leq p_2$ and $p_2 \geq 0$. It is shown that $\mathcal{W} \cap (\mathcal{S}_2 \cup \Sigma)$ is (positively) invariant under the vector field of system (5.0.1). Since $\mathcal{W}$ is (positively) invariant (see Theorem 7.2), it suffices to show that $\mathcal{S}_2 \cup \Sigma$ is (positively) invariant. Let

$$U \colon \mathbb{R}^2_+ \to \mathbb{R},\ \ U(x_m, y_m) := \frac{f}{d} + n + x_m - y_m. \tag{7.4.7}$$

Choosing $(\frac{f}{d}, x_m, 0, y_m)^T \in \mathcal{W} \cap (\mathcal{S}_2 \cup \Sigma)$ such that $U(x_m, y_m) = 0$ implies

$$\begin{aligned} \dot{U}(x_m, y_m) &= h_2(x_h, x_m, y_h, y_m) - h_4(x_h, x_m, y_h, y_m) \\ &\overset{(U=0)}{=} p_1 x_m - p_2 y_m \\ &\overset{(U=0)}{=} (p_1 - p_2) x_m - p_2 \left(\frac{f}{d} + n\right) \\ &\leq 0 \end{aligned} \tag{7.4.8}$$

due to the assumption.

It follows that $E_{p,2}(t) \in \mathcal{W} \cap (\mathcal{S}_2 \cup \Sigma)$ for all $t \geq t_0$ if and only if $p_1 \leq p_2,\ p_2 \geq 0$ and $E_{p,2}(t_0) \in \mathcal{W} \cap (\mathcal{S}_2 \cup \Sigma)$. By differentiating total equilibria from the set of partial equilibria, Lemma 7.12 yields that $x_m(t)$ and $y_m(t)$ are non-constant for all $t \geq t_0$. Observe that contemplable total equilibria are given by

- $E_{p,2}(t_0) = (\frac{f}{d}, 0, 0, \frac{f}{d} + n)^T \in \mathcal{E}_2$ in case of $p_1 \neq 0$ and $p_2 = 0$,
- $E_{p,2}(t_0) = (\frac{f}{d}, x_m^0, 0, y_m^0)^T \in \mathcal{E}_3$ with $y_m^0 = \frac{f}{d} + n + x_m^0$ in case of $p_1 = 0 = p_2$,
- $E_{p,2}(t_0) = E_m$ in case of $p_1 < 0$ and $0 < p_2 < \frac{c_m p_1}{p_1 - c_m}$.

This proves the theorem. □

Observe that the inequality (7.4.8) in the proof of Theorem 7.13 (ii) is strict in case of $p_2 \neq 0$. This implies the following result:

Corollary 7.14. *Consider the myeloma model* (5.0.1) *defined on* $\mathcal{W}$. *Let* $p_1 \leq p_2$ *and* $p_2 > 0$. *If* $E_{p,2}(t_0) \in \mathcal{W} \cap (\mathcal{S}_2 \cup \Sigma)$, *then* $E_{p,2}(t) \in \mathcal{W} \cap \mathcal{S}_2$ *for all* $t > t_0$.

As for total equilibria, the aim is to characterise partial equilibria with respect to their stability. In the following, an adequate definition of stability for partial equilibria is provided.

Definition 7.15 (Stability of a partial equilibrium)**.** Consider a dynamical system generated by the flow

$$\begin{aligned} x'(t) &= f(x(t), y(t)) \\ y'(t) &= g(x(t), y(t)). \end{aligned} \tag{7.4.2}$$

Assume f, g such that solutions $(x(t), y(t))^T \in \mathcal{U} \times \mathcal{V} \subseteq \mathbb{R}^m \times \mathbb{R}^n$ exist and are unique for all $t \geq t_0$. Let $E_p(t) = (x, y(t))^T$ be a partial equilibrium of the system (7.4.2). Then, $E_p(t)$ is (asymptotically) stable within the system (7.4.2) if $x(t) = x$ is (asymptotically) stable within the system $x'(t) = f(x(t), y_0)$ for all $y_0 \in \mathcal{V}$.

Note that since $E_{p,1}(t) \in \Sigma$ for all $t \geq t_0$, the deduction of stability properties of $E_{p,1}(t)$ from those within both sub-systems $\mathcal{S}_1$ and $\mathcal{S}_2$ is not straightforward. However, the following stability result for $E_{p,2}(t)$ with $E_{p,2}(t_0) \in \mathcal{S}_2$ can be deduced:

Theorem 7.16 (Stability of $E_{p,2}(t)$)**.** *Consider the myeloma model* (5.0.1) *defined on* $\mathcal{W}$. *Let* $p_1 \leq p_2$ *and* $p_2 > 0$. *If* $E_{p,2}(t_0) \in \mathcal{W} \cap \mathcal{S}_2$, *then the partial equilibrium* $E_{p,2}(t)$ *is locally asymptotically stable.*

Proof. By assumption, it is $z(t) < 0$ for all $t \geq t_0$, see Corollary 7.14. The dynamics of the equilibrium components of $E_{p,2}(t)$ within $\mathcal{S}_2$ are described by the system

$$\begin{aligned} x_h'(t) &= f - c_h \frac{y_h(t)}{y_h(t) + y_m(t)} z(t) - d x_h(t) \\ y_h'(t) &= c_h \frac{y_h(t)}{y_h(t) + y_m(t)} z(t). \end{aligned} \tag{7.4.9}$$

Since solutions of the myeloma model (5.0.1) are considered within $\mathcal{W}$, it follows that $x_m(t) \geq 0$ and $y_m(t) > \frac{f}{d} + n$ for all $t \geq t_0$. Note that $(x_h, y_h)^T = \left(\frac{f}{d}, 0\right)^T$ is an

equilibrium of system (7.4.9). Since

$$\begin{aligned}\frac{\partial}{\partial y_h}\left(\frac{y_h}{y_h+y_m}z\right) &= \frac{\partial}{\partial y_h}\left(\frac{y_h}{y_h+y_m}(x_h+x_m-y_h-y_m+n)\right)\\ &= \frac{y_h+y_m-y_h}{(y_h+y_m)^2}(x_h+x_m-y_h-y_m+n)+\frac{y_h}{y_h+y_m}(-1)\\ &= \frac{y_m}{(y_h+y_m)^2}z-\frac{y_h}{y_h+y_m},\end{aligned}$$

it follows that the Jacobian matrix of the right-hand side of system (7.4.9) evaluated at $(x_h, y_h)^T = \left(\frac{f}{d}, 0\right)^T$

$$\begin{pmatrix} -d & -c_h\frac{z(t)}{y_m(t)} \\ 0 & c_h\frac{z(t)}{y_m(t)} \end{pmatrix}.$$

Therefore, the well-defined (time-dependent) eigenvalues of the Jacobian matrix are given by

$$\lambda_1 = -d < 0 \ \text{ and } \ \lambda_2 = c_h\frac{z(t)}{y_m(t)} < 0 \ \text{ for all } \ t \geq t_0.$$

In particular, $\lambda_1, \lambda_2 < 0$ for all fixed $x_m(t) = x_{m,0} \geq 0$ and $y_m(t) = y_{m,0} > \frac{f}{d} + n$ for all $t \geq t_0$. Consequently, the theorem of Hartman and Grobman [36, Theorem 1.4.1] implies local asymptotic stability of $(x_h, y_h)^T = \left(\frac{f}{d}, 0\right)^T$ within the system (7.4.9) with $x_m(t) = x_{m,0}$ and $y_m(t) = y_{m,0}$. By Definition 7.15, this implies local asymptotic stability of $E_{p,2}(t)$ within the myeloma model (5.0.1). □

Remark 7.17. The assumptions of Theorem 7.16 include the case where $E_{p,2}(t) = E_m$. Observe that the stability result is in accordance with Theorem 7.8.

Beside stating conditions on the net growth parameters and on initial conditions to guarantee existence of partial equilibria, Theorem 7.13 explicitly characterises the shape of the malignant components $x_m(t)$ and $y_m(t)$ in case of the partial equilibrium $E_{p,1}(t)$ for all $t \geq t_0$. That is to say,

$$x_m(t) = x_m^0 e^{p_1(t-t_0)} = y_m(t).$$

Observe that this arises from the knowledge about the dynamics of the function $z(t)$, i.e. $z'(t) = 0$ for all $t \geq t_0$. Yet less is known about the dynamics of $z(t)$ and consequently about the malignant components at the partial equilibrium $E_{p,2}(t)$.

The following investigation focuses on the asymptotic behaviour of $x_m(t)$ and $y_m(t)$ at the partial equilibrium $E_{p,2}(t)$.

Theorem 7.18 (Asymptotics of $x_m(t)$ and $y_m(t)$ at $E_{p,2}(t)$)**.** *Consider the myeloma model* (5.0.1) *defined on* $\mathcal{W}$*. Let* $p_1 \leq p_2$*,* $p_2 \geq 0$ *and* $E_{p,2}(t_0) \in \mathcal{W} \cap (\mathcal{S}_2 \cup \Sigma)$*.*

(i) If $p_1 < 0$ *and* $0 < p_2 < \frac{c_m p_1}{p_1 - c_m}$*, then* $\lim_{t\to\infty} E_{p,2}(t) = E_m$*.*

(ii) If $p_1 \leq 0$ *and* $p_2 = 0$*, then* $x_m(t) + y_m(t) \leq x_m^0 + y_m^0$ *for all* $t \geq t_0$*.*

(iii) Otherwise, i.e. if $p_1 < 0$ *and* $p_2 \geq \frac{c_m p_1}{p_1 - c_m}$*, or* $p_1 = 0$ *and* $p_2 > 0$*, or* $p_1 > 0$ *and* $p_2 \geq p_1$*, then* $\lim_{t\to\infty} x_m(t) = \infty$ *and* $\lim_{t\to\infty} y_m(t) = \infty$*.*

Proof. Theorem 7.13 (ii) implies that $E_{p,2}(t) \in \mathcal{W} \cap (\mathcal{S}_2 \cup \Sigma)$ for all $t \geq t_0$ if $p_1 \leq p_2$ and $p_2 \geq 0$. Observe that if $E_{p,2}(t)$ is a total equilibrium, the claim is trivially satisfied. Further, since $x_h = \frac{f}{d}$ and $y_h = 0$ for all $t \geq t_0$, the dynamics for the non-constant malignant components $x_m(t)$ and $y_m(t)$ are given by the planar linear system (7.4.5) with $y_h = 0$, that is to say,

$$\begin{aligned} x_m'(t) &= (p_1 - c_m)x_m(t) + c_m y_m(t) - c_m\left(\frac{f}{d} + n\right) =: k_1(x_m(t), y_m(t)) \\ y_m'(t) &= (p_2 - c_m)y_m(t) + c_m x_m(t) + c_m\left(\frac{f}{d} + n\right) =: k_2(x_m(t), y_m(t)). \end{aligned} \tag{7.4.10}$$

For $p_1 \leq p_2$ and $p_2 \geq 0$, a straightforward calculation yields the following case analysis for total equilibria $E = (x_m, y_m)^T$ of system (7.4.10):

Case (i): If $p_1 < 0$ and $0 < p_2 < \frac{c_m p_1}{p_1 - c_m}$, then $x_m = x_m^{E_m}$ and $y_m = y_m^{E_m}$, see also Theorem 7.7. This implies $\left(\frac{f}{d}, x_m, 0, y_m\right)^T = E_m \in \mathcal{W} \cap \mathcal{S}_2$. The coefficient matrix of the linear system (7.4.10) reads

$$\begin{pmatrix} p_1 - c_m & c_m \\ c_m & p_2 - c_m \end{pmatrix}.$$

By means of (7.3.1) within the proof of Theorem 7.8, the real parts of its eigenvalues are strictly negative. Consequently, E is globally asymptotically stable within system (7.4.10). This implies $\lim_{t\to\infty}(x_m(t), y_m(t))^T = E$ and as a result $\lim_{t\to\infty} E_{p,2}(t) = E_m$.

Case (ii): If $p_1 < 0$ and $p_2 = 0$, then $x_m = 0$ and $y_m = \frac{f}{d} + n$. This implies $\left(\frac{f}{d}, x_m, 0, y_m\right)^T \in \mathcal{E}_2 \subset \mathcal{W} \cap \Sigma$. If $p_1 = 0$ and $p_2 = 0$, then $y_m = \frac{f}{d} + n + x_m$. This implies $\left(\frac{f}{d}, x_m, 0, y_m\right)^T \in \mathcal{E}_3 \subset \mathcal{W} \cap \Sigma$. Thus, stability analysis of E within system (7.4.10) could be misleading. However, since $x_m'(t) + y_m'(t) = p_1 x_m(t) + p_2 y_m(t) \leq 0$ for $p_1 \leq 0$ and $p_2 = 0$, it follows that $x_m(t) + y_m(t) \leq x_m^0 + y_m^0$ for all $t \geq t_0$, where $x_m^0, y_m^0 \in \mathcal{W} \cap (\mathcal{S}_2 \cup \Sigma)$.

Case (iii): Otherwise (i.e. if $p_1 < 0$ and $p_2 \geq \frac{c_m p_1}{p_1 - c_m}$, or $p_1 = 0$ and $p_2 > 0$, or $p_1 > 0$ and $p_2 \geq p_1$), no equilibrium exists in $\mathcal{W} \cap (\mathcal{S}_2 \cup \Sigma)$. Since

$$\frac{\partial}{\partial y_m} k_1(x_m, y_m) = c_m > 0$$
$$\frac{\partial}{\partial x_m} k_2(x_m, y_m) = c_m > 0$$

for all $\left(\frac{f}{d}, x_m, 0, y_m\right)^T \in \mathcal{W} \cap (\mathcal{S}_2 \cup \Sigma)$, system (7.4.10) is strictly cooperative, i.e. the growth of $x_m(t)$ increases the growth rate of $y_m(t)$ and vice versa. Then, all trajectories $(x_m(t), y_m(t))^T$ of system (7.4.10) converge either to an equilibrium or to boundary points of $\mathcal{W} \cap (\mathcal{S}_2 \cup \Sigma)$, including infinity [119, Theorem 7.4]. In the remaining part of the proof, it is shown that the boundary of $\mathcal{W} \cap (\mathcal{S}_2 \cup \Sigma)$ is repelling for the vector field of system (7.4.10). This implies convergence of $x_m(t)$ and $y_m(t)$

to infinity. Observe that

$$(x_m, y_m)^T \in \mathcal{W} \cap (\mathcal{S}_2 \cup \Sigma) \quad \Leftrightarrow \quad \frac{f}{d} + n + x_m - y_m \leq 0 \ \text{ and } \ x_m \geq 0.$$

With (7.4.7), it follows that

$$\begin{aligned} \dot{U}(x_m, y_m) &= (p_1 - c_m)x_m(t) + c_m y_m(t) - c_m \left(\frac{f}{d} + n\right) \\ &\quad - \left((p_2 - c_m)y_m(t) + c_m x_m(t) + c_m \left(\frac{f}{d} + n\right)\right) \\ &\overset{(U=0)}{=} p_1 x_m - p_2 y_m \\ &\overset{(U=0)}{=} (p_1 - p_2)x_m - p_2 \left(\frac{f}{d} + n\right) \\ &< 0 \end{aligned} \tag{7.4.11}$$

due to $p_1 \leq p_2$ and $p_2 > 0$. Note that if $U(x_m(t_0), y_m(t_0)) = 0$, then the strict inequality in (7.4.11) implies that $U(x_m(t), y_m(t)) < 0$ for all $t > t_0$, i.e. $\frac{f}{d} + n + x_m - y_m < 0$ for all $t > t_0$. By this result, it follows that

$$k_1(0, y_m) = c_m y_m - c_m \left(\frac{f}{d} + n\right) = -c_m \left(\frac{f}{d} + n - y_m\right) > 0$$

for all $t > t_0$. This implies that the boundary of $\mathcal{W} \cap (\mathcal{S}_2 \cup \Sigma)$ is repelling for the vector field of system (7.4.10). As a consequence, it is $\lim_{t\to\infty} x_m(t) = \infty$ and $\lim_{t\to\infty} y_m(t) = \infty$. □

7.5 Qualitative simulations

In this section, simulations are provided which qualitatively illustrate previously derived results on existence and stability of partial equilibria satisfying (7.4.3) in the framework of the myeloma model (5.0.1). Chosen parameter values are listed in Table 7.1 on page 98. In the following, Figure 7.1 is considered visualising partial equilibria $E_{p,1}(t)$ and $E_{p,2}(t)$:

(a) It is $E_{p,1}(t)$ with $p_1 = 0.5$, $p_2 = 0.5$, and $x_m^0 = 1 = y_m^0$ at $t_0 = 0$. It follows that $x_m(t) = x_m^0 e^{p_1 t} = y_m(t)$ by Theorem 7.13 (i).

(b) It is $E_{p,2}(t)$ with $p_1 = -0.1$, $p_2 = 0.05$, and $x_m^0 = 0$, $y_m^0 = \frac{f}{d} + n + 1$ at $t_0 = 0$. It follows that $\lim_{t\to\infty} x_m(t) = x_m^{E_m}$ and $\lim_{t\to\infty} y_m(t) = y_m^{E_m}$ by Theorem 7.18 (i).

(c) It is $E_{p,2}(t)$ with $p_1 = 0.1$, $p_2 = 1$, and $x_m^0 = 0$, $y_m^0 = \frac{f}{d} + n + 1$ at $t_0 = 0$. It follows that $\lim_{t\to\infty} x_m(t) = \infty$ and $\lim_{t\to\infty} y_m(t) = \infty$ by Theorem 7.18 (iii).

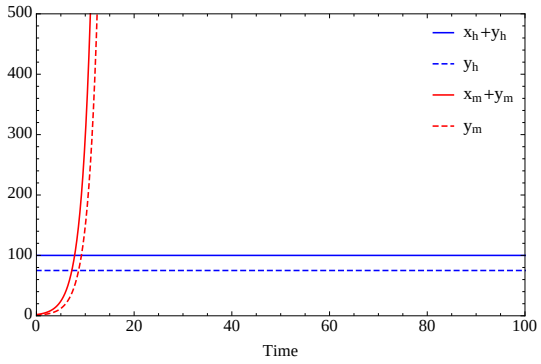

(a) Partial equilibrium $E_{p,1}(t)$.

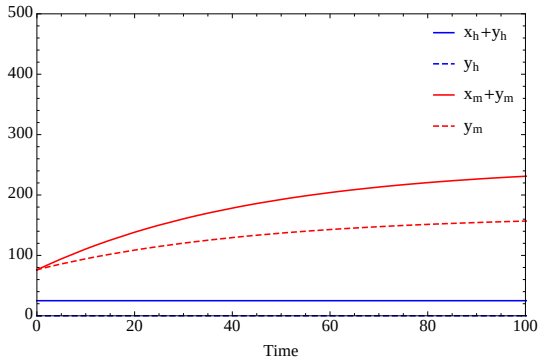

(b) Partial equilibrium $E_{p,2}(t)$, where $x_m(t)$ and $y_m(t)$ converge.

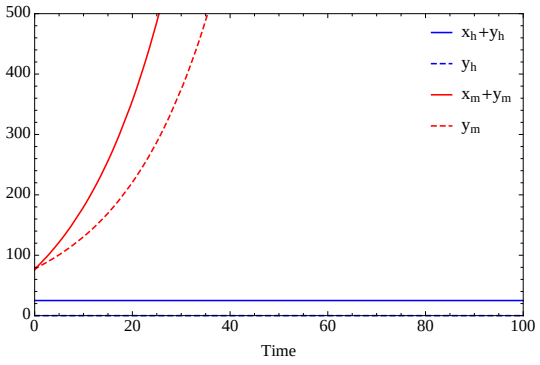

(c) Partial equilibrium $E_{p,2}(t)$, where $x_m(t)$ and $y_m(t)$ increase to infinity.

Figure 7.1: Simulations of partial equilibria of the myeloma model. Solutions $x_h(t) + y_h(t)$ (blue), $y_h(t)$ (dashed blue), $x_m(t) + y_m(t)$ (red), $y_m(t)$ (dashed red) are visualised. Existence and characterisation of partial equilibria are due to Theorem 7.13. Parameter values are stated in Table 7.1 and in the text.

Next, different scenarios for a malignancy-induced perturbation of the healthy equilibrium as introduced by Definition 5.2 are considered, i.e. choosing initial conditions $(x_h^0, x_m^0, y_h^0, y_m^0)^T = \left(x_h^{E_h}, x_m^0, y_h^{E_h}, 0\right)^T$ with $x_m^0 > 0$. In the following, Figure 7.3 on page 99 is considered:

(a) It is $p_1 = -0.1 < 0$ and $p_2 = -0.1 < 0$ with $x_m^0 = 500$. This implies absent (positive) growth $x_m(t) + y_m(t)$. The solution converges to the healthy equilibrium E_h.

(b) It is $p_1 = -1 < 0$ and $p_2 = 0.55$ with $x_m^0 = 1$. Observe that $p_2 < \frac{c_m p_1}{p_1 - c_m} = 0.5$. The solution converges to the total equilibrium E_m, which exists and is locally asymptotically stable, see Theorems 7.7 and 7.8.

(c) It is $p_1 = -1 < 0$ and $p_2 = 0.55$ with $x_m^0 = 1$. Observe that $p_2 > \frac{c_m p_1}{p_1 - c_m} = 0.5$ The solution approaches the partial equilibrium $E_{p,2}(t)$, which exists and is locally asymptotically stable, see Theorems 7.13 and 7.16. Figure 7.4 visualises the corresponding dynamics of $z(t)$. Observe that $z(t)$ possesses one zero and eventually strictly decreases.

(d) It is $p_1 = 0.2$ and $p_2 = 0.1 < p_1$ with $x_m^0 = 1$. The solution increases.

The scaling of the time axes is chosen to represent realistic timespans, i.e. age of a patient in years. Solutions of the myeloma model can be interpreted as reflecting numbers of healthy and malignant PCs, see part three of this thesis.

Numerical simulations imply that growth of $x_m(t) + y_m(t)$ depends on the parameters p_1 and p_2. If $p_1 \leq p_2$ and $p_2 > 0$, then $x_m(t) + y_m(t)$ increases, whereas $x_h(t) + y_h(t)$ decreases. In particular, if $p_1 < 0$ and $p_2 \leq \frac{c_m p_1}{p_1 - c_m}$, it follows that growth of $x_m(t) + y_m(t)$ is retarded approaching E_m. For a visualisation in the plane of net growth rates, see Figure 7.2.

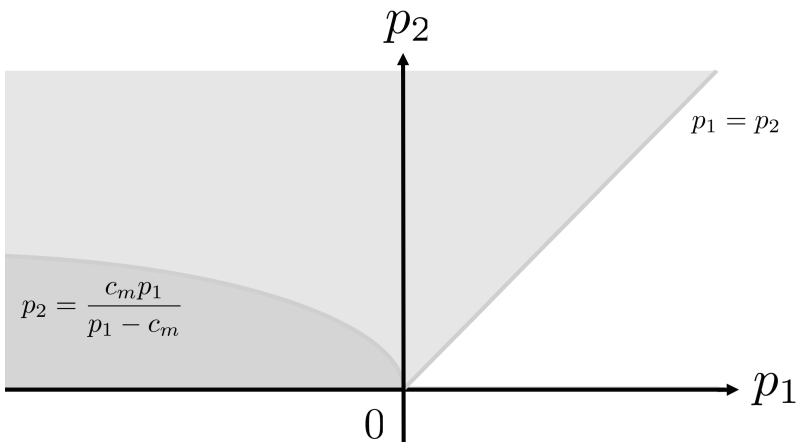

Figure 7.2: Plane of net growth rates visualising regions (gray) where $x_m(t) + y_m(t)$ representing the total number of malignant plasma cells (PCs) in the bone marrow increases and $x_h(t) + y_h(t)$ representing the total number of healthy PCs in the bone marrow decreases. Increase of $x_m(t) + y_m(t)$ is either retarded (dark) implying convergence of the solution of the myeloma model to the total equilibrium E_m, or unbounded (light) implying that a partial equilibrium is reached. For details, see text.

Table 7.1: Parameter values for simulations in Section 7.5.

Parameter	**Value**
f	25
n	25
b_h	1
b_m	1
c_h	1
c_m	1
d	1

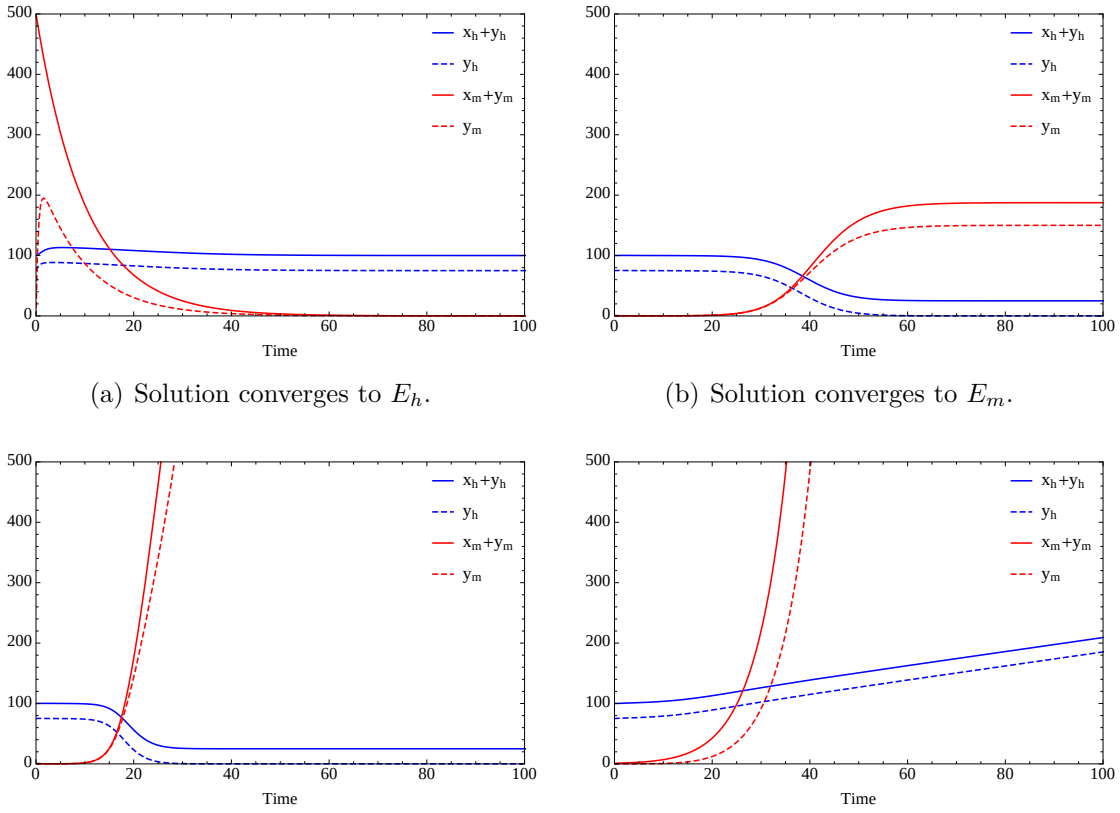

(a) Solution converges to E_h.

(b) Solution converges to E_m.

(c) Solution converges to $E_{p,2}$.

(d) Solution increases.

Figure 7.3: Dynamics of solutions of the myeloma model due to malignancy-induced perturbations of the healthy equilibrium. $x_h(t) + y_h(t)$ (blue), $y_h(t)$ (dashed blue), $x_m(t) + y_m(t)$ (red), $y_m(t)$ (dashed red). Depending on the choice of the malignancy-induced perturbation of the healthy equilibrium x_m^0 and net growth rates p_1 and p_2, different dynamic behaviour of solutions is observed. Parameter values are stated in Table 7.1 and in the text.

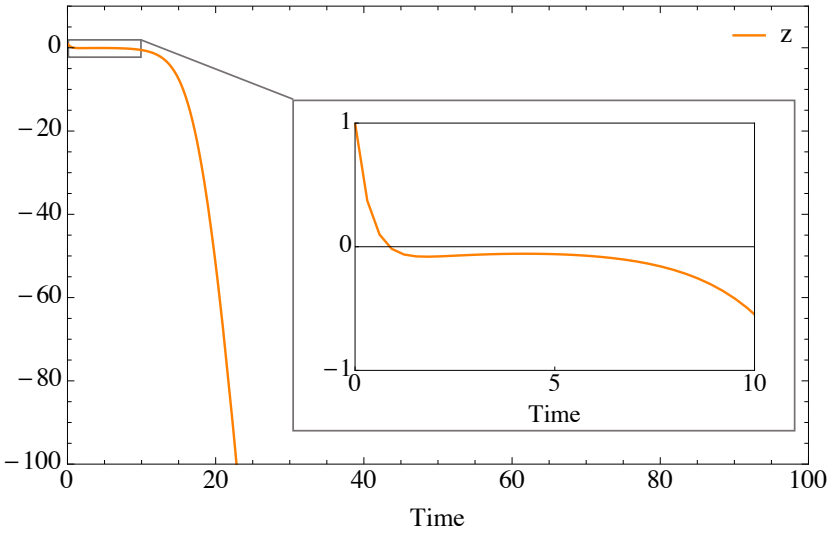

Figure 7.4: Dynamics of the function $z(t)$ due to a malignancy-induced perturbation of the healthy equilibrium corresponding to Figure 7.3 (c). $z(t)$ is positive at the beginning. The snapshot visualises $z(t) = 0$ and shows that $z(t)$ switches the sign once, being negative and strictly decreasing. For details, see text.

8 Analysis of the extended model

The extended model of healthy PC dynamics in the bone marrow is recapitulated, see Chapter 4. For $t \geq t_0$, the system of ODEs is given by

$$\begin{aligned} x'_{h,0}(t) &= f - \beta_{h,0}(z(t))z(t) - dx_{h,0}(t) \\ x'_{h,v}(t) &= -\beta_{h,v}(z(t))z(t) - dx_{h,v}(t) \\ y'_{h,0}(t) &= \beta_{h,0}(z(t))z(t) \\ y'_{h,v}(t) &= \beta_{h,v}(z(t))z(t) \end{aligned} \tag{4.0.1}$$

with surplus of PCs relative to the niche balance $z(t)$ given by

$$z(t) = x_{h,0}(t) + x_{h,v}(t) - (y_{h,0}(t) + y_{h,v}(t)) + n, \tag{4.0.2}$$

transition rates $\beta_{h,j}(z(t)),\ j \in \{0, v\}$, given by

$$\beta_{h,j}(z(t)) = \begin{cases} b_h \frac{x_{h,j}(t)}{x_{h,0}(t)+x_{h,v}(t)} & \text{if } z(t) \geq 0 \\ c_h \frac{y_{h,j}(t)}{y_{h,0}(t)+y_{h,v}(t)} & \text{if } z(t) < 0 \end{cases} \tag{4.0.3}$$

and non-negative initial conditions

$$\begin{aligned} x_{h,0}(t_0) &= x^0_{h,0} \geq 0 \\ x_{h,v}(t_0) &= x^0_{h,v} \geq 0 \\ y_{h,0}(t_0) &= y^0_{h,0} \geq 0 \\ y_{h,v}(t_0) &= y^0_{h,v} \geq 0. \end{aligned} \tag{4.0.4}$$

Similar to the myeloma model, the functions $\beta_{h,j}(z),\ j \in \{0, v\}$, given by (4.0.3) are undefined in case of $x_{h,0} + x_{h,v} = 0$ or $y_{h,0} + y_{h,v} = 0$, respectively. Assuming $x_{h,0}(t) + x_{h,v}(t) \neq 0$ and $y_{h,0}(t) + y_{h,v}(t) \neq 0$ for all $t \geq t_0$, they are continuous for all

$z \in \mathbb{R},\ z \neq 0$. It follows that the functions $\beta_{h,j}(z)z,\ j \in \{0, v\}$, are continuous, but in general not differentiable in $z = 0$. Observe that the reformulated system for the extended model (4.0.1) is similar to (7.0.1), where

$$\mathcal{S}_1 := \{(x_{h,0}, x_{h,v}, y_{h,0}, y_{h,v})^T \in \mathbb{R}^4 \colon z \geq 0\}$$
$$\mathcal{S}_2 := \{(x_{h,0}, x_{h,v}, y_{h,0}, y_{h,v})^T \in \mathbb{R}^4 \colon z < 0\}$$

yielding a single switching manifold given by

$$\Sigma := \{(x_{h,0}, x_{h,v}, y_{h,0}, y_{h,v})^T \in \mathbb{R}^4 \colon z = 0\}.$$

By Remark 5.3, previously derived results for the myeloma model (5.0.1) about a suitable domain of definition and non-negativity of solutions (see Theorem 7.2) as well as existence and uniqueness of solutions (see Theorem 7.4) likewise hold true in case of the extended model (4.0.1). In the following, the set $\mathcal{W}$ (see Definition 7.1) is interpreted in the setting of the variables of the extended model (4.0.1), i.e.

$$\mathcal{W} := \bigcap_{i=1}^{2} \{(x_{h,0}, x_{h,v}, y_{h,0}, y_{h,v})^T \in \mathbb{R}^4_+ \colon W_i(x_{h,0}, x_{h,v}, y_{h,0}, y_{h,v}) \leq 0\}.$$

The following results can be deduced:

Theorem 8.1 (Domain of definition and non-negativity of solutions)**.** *Consider the extended model* (4.0.1) *and assume that solutions exist. Then, the set $\mathcal{W}$ is (positively) invariant under the vector field of the extended model. In particular, if the initial conditions* (4.0.4) *satisfy $x^0_{h,0} + x^0_{h,v} > 0$ and $y^0_{h,0} + y^0_{h,v} \geq n$, then the functions* (4.0.3) *are defined for all $t \geq t_0$. Moreover, it follows that $x_{h,0}(t), x_{h,v}(t), y_{h,0}(t), y_{h,v}(t) \geq 0$ for all $t \geq t_0$.*

Consequently, in the subsequent considerations, the extended model is considered to be defined on the (positively) invariant set $\mathcal{W}$. That is to say, we only consider solutions of the extended model with initial conditions (4.0.4) located in $\mathcal{W}$.

Theorem 8.2 (Global existence and uniqueness)**.** *Consider the extended model* (4.0.1) *defined on $\mathcal{W}$, i.e. let $(x^0_{h,0}, x^0_{h,v}, y^0_{h,0}, y^0_{h,v})^T \in \mathcal{W}$. Then, there exists a unique solution $(x_{h,0}(t), x_{h,v}(t), y_{h,0}(t), y_{h,v}(t))^T \in \mathcal{W}$ for all $t \geq t_0$.*

8.1 Non-isolated equilibria

In this section, equilibria of system (4.0.1) are investigated. Beside the healthy equilibrium $E_h = \left(x_h^{E_h}, 0, y_h^{E_h}, 0\right)^T$, there exists a manifold of non-isolated equilibria.

Theorem 8.3 (Non-isolated equilibria)**.** *Consider the extended model* (4.0.1) *defined on* $\mathcal{W}$*. There exists a one-dimensional manifold of non-isolated equilibria given by*

$$\mathcal{E} = \left\{ \begin{pmatrix} x_{h,0}^E \\ x_{h,v}^E \\ y_{h,0}^E \\ y_{h,v}^E \end{pmatrix} \in \mathcal{W} : \begin{pmatrix} \frac{f}{d} \\ 0 \\ \frac{f}{d} + n \\ 0 \end{pmatrix} + y_{h,v}^E \begin{pmatrix} 0 \\ 0 \\ -1 \\ 1 \end{pmatrix} \right\} \subset \mathcal{W} \cap \Sigma.$$

No further equilibria exist.

Proof. With Remark 5.3, this follows by Theorem 7.7 (iii). □

Remark 8.4. Observe that choosing $y_{h,v}^E = 0$ yields the healthy equilibrium. Thus, $E_h \in \mathcal{E}$.

Next, stability properties of the one-dimensional manifold of non-isolated equilibria $\mathcal{E}$ are analysed. By contrast to the myeloma model, the observation is used that the extended model is a refinement of the basic model in the sense of Remark 4.5. This enables an appropriate deduction of stability despite the fact that $\mathcal{E} \subset \mathcal{W} \cap \Sigma$.

Theorem 8.5 (Stability of $\mathcal{E}$)**.** *Consider the extended model* (4.0.1) *defined on* $\mathcal{W}$*. The one-dimensional manifold of non-isolated equilibria* $\mathcal{E}$ *is globally asymptotically stable. That is solutions of system* (4.0.1) *asymptotically approach* $\mathcal{E}$*.*

Proof. By Remark 4.5, it holds that

$$\begin{aligned} x_h(t) &= x_{h,0}(t) + x_{h,v}(t) \\ y_h(t) &= y_{h,0}(t) + y_{h,v}(t), \end{aligned}$$

where $x_h(t)$ and $y_h(t)$ are solutions of the basic model (3.0.1). Due to Theorem 6.10,

$E_h = (x_h^{E_h}, y_h^{E_h})^T$ is globally asymptotically stable within system (3.0.1). This implies

$$\lim_{t\to\infty} (x_{h,0}(t) + x_{h,v}(t)) = x_h^{E_h} = \frac{f}{d}$$
$$\lim_{t\to\infty} (y_{h,0}(t) + y_{h,v}(t)) = y_h^{E_h} = \frac{f}{d} + n$$

and in particular

$$\lim_{t\to\infty} z(t) = 0.$$

It remains to show that $\lim_{t\to\infty} x_{h,v}(t) = 0$. Then, every solution of the extended model (4.0.1) asymptotically approaches $E = (x_{h,0}^E, x_{h,v}^E, y_{h,0}^E, y_{h,v}^E)^T \in \mathcal{E}$ due to

$$x_{h,0}^E + x_{h,v}^E = 0 + \frac{f}{d}$$
$$y_{h,0}^E + y_{h,v}^E = \left(\frac{f}{d} + n - y_{h,v}^E\right) + y_{h,v}^E = \frac{f}{d} + n.$$

Let $\varepsilon > 0$ arbitrary but fixed. Since $\lim_{t\to\infty} z(t) = 0$, it follows that for

$$0 < \tilde{\varepsilon} < \frac{\varepsilon d}{2\max\{b_h, c_h\}}$$

there exists a $\tilde{T} > t_0$ such that $|z(t)| < \tilde{\varepsilon}$ for all $t \geq \tilde{T}$. Thus, for all $t \geq \tilde{T}$, it is

$$x'_{h,v}(t) = -\beta_{h,v}(z(t))z(t) - dx_{h,v}(t) < \max\{b_h, c_h\}\tilde{\varepsilon} - dx_{h,v}(t).$$

Next, consider the following ODE with initial condition,

$$w'(t) = \max\{b_h, c_h\}\tilde{\varepsilon} - dw(t)$$
$$w(\tilde{T}) \geq x_{h,v}^0 \text{ and } w(\tilde{T}) > \frac{\max\{b_h, c_h\}\tilde{\varepsilon}}{d}$$

for all $t \geq \tilde{T}$. It follows that

$$w(t) = \underbrace{\frac{\max\{b_h, c_h\}\tilde{\varepsilon}}{d}}_{<\varepsilon/2} + e^{-d(t-\tilde{T})}\left(w(\tilde{T}) - \frac{\max\{b_h, c_h\}\tilde{\varepsilon}}{d}\right)$$

for all $t \geq \tilde{T}$. Using the comparison principle for ODEs [42, Chapter 3], this implies

$$x_{h,v}(t) < w(t) < \frac{\varepsilon}{2} + \frac{\varepsilon}{2} = \varepsilon.$$

Observe that the first inequality is true for all $t \geq \tilde{T}$, whereas the second holds for all $t \geq T$, where $T > \tilde{T}$ is chosen such that the second term in $w(t)$,

$$e^{-d(t-\tilde{T})}\left(w(\tilde{T}) - \frac{\max\{b_h, c_h\}\tilde{\varepsilon}}{d}\right), \tag{8.1.1}$$

is smaller than $\frac{\varepsilon}{2}$. This can be achieved since (8.1.1) is positive and exponentially decreasing in time. Due to non-negativity of $x_{h,v}(t)$ for all $t \geq t_0$, it follows that $\lim_{t\to\infty} x_{h,v}(t) = 0$. This proves the claim. □

In the remaining part of this section, the influence of a vaccination-induced perturbation of the healthy equilibrium as introduced by Definition 4.4 on the composition of the re-established healthy equilibrium is investigated, see Chapter 4. Theorem 8.5 provides the mathematical confirmation of this biological observation. That is to say, every solution of the extended model eventually reaches the manifold $\mathcal{E}$ again after such a perturbation. However, it does not provide a characterisation of the exact composition of the equilibrium, i.e. of the value of $y^E_{h,v}$, at the limit. For further analysis, recapitulate the definition of the vaccination-induced perturbation of the healthy equilibrium at time $T > 0$,

$$(x_{h,0}(T), x_{h,v}(T), y_{h,0}(T), y_{h,v}(T))^T = \left(x_h^{E_h}, x^0_{h,v}, y_h^{E_h}, 0\right)^T \quad \text{with} \quad x^0_{h,v} > 0. \tag{4.0.5}$$

As stated in Definition 4.4, (4.0.5) is interpreted as initial condition for the extended model (4.0.1), i.e. $t_0 = T$. Without loss of generality, set $T = 0$. Observe that the corresponding solution is located in $\mathcal{W}$ due to Remark 7.3. In the following, an upper estimate for the solution $y_{h,v}(t)$ for all $t \geq 0$ is derived, and consequently for its limit $\lim_{t\to\infty} y_{h,v}(t) = y^E_{h,v}$.

Theorem 8.6 (Upper bound for vaccination-induced healthy PCs inside the niche)**.** *Consider the extended model* (4.0.1) *defined on* $\mathcal{W}$*. Let initial conditions be given by*

(4.0.5) *for* $T = 0$. *Then, it is* $0 \leq y_{h,v}(t) \leq y_{h,v}^{upper}(\bar{t})$ *for all* $t \geq 0$, *where*

$$\begin{aligned} y_{h,v}^{upper}(t) &:= (1 - e^{-2b_h t})\frac{1}{2}x_{h,v}^0 \\ \bar{t} &:= \frac{1}{\sqrt{4b_h^2 + d^2}} \ln\left(\frac{4b_h^2 + 2b_h d + d^2 + (2b_h + d)\sqrt{4b_h^2 + d^2}}{2b_h d}\right). \end{aligned} \tag{8.1.2}$$

Proof. By Remark 4.5, it is

$$\begin{aligned} x_h(0) &= x_{h,0}(0) + x_{h,v}(0) = x_h^{E_h} + x_{h,v}^0 = \frac{f}{d} + x_{h,v}^0 \\ y_h(0) &= y_{h,0}(0) + y_{h,v}(0) = y_h^{E_h} = \frac{f}{d} + n, \end{aligned}$$

which implies $z(0) > 0$. Observe that $(x_h(0), y_h(0))^T \notin \mathcal{R}_1 \cup \mathcal{R}_2$. Consequently, $z(t)$ is zero if either the solution has reached the equilibrium (which can only happen at infinite time due to the uniqueness of solutions, see Theorem 8.2), or the function is to switch its sign (in finite time). In any case, there is at most one (finite or infinite) time $\bar{t} > 0$ with $z(\bar{t}) = 0$ due to Corollary 6.15.

The proof consists of two steps: In the first step, it is used that the flow induced by system (4.0.1) is located within $\mathcal{S}_1$ for $0 \leq t \leq \bar{t}$. This enables the derivation of upper estimates for the solutions $y_{h,0}(t)$ and $y_{h,v}(t)$ of system (4.0.1) within $\mathcal{S}_1$, respectively. In the second step, evaluation of these estimates at the switching time $t = \bar{t}$ yields upper estimates for $y_{h,0}(t)$ and $y_{h,v}(t)$ for all $t \geq 0$, respectively, due to the following reasoning: On the one hand, it is $z(t) \geq 0$ for all $0 \leq t \leq \bar{t}$ implying $y'_{h,0}(t) \geq 0$ and $y'_{h,v}(t) \geq 0$ for all $0 \leq t \leq \bar{t}$. On the other hand, it is $z(t) \leq 0$ for all $t \geq \bar{t}$, and consequently $y'_{h,0}(t) \leq 0$ and $y'_{h,v}(t) \leq 0$ for all $t \geq \bar{t}$.

Step 1: Consider system (4.0.1) within $\mathcal{S}_1$. Since

$$\begin{aligned} x'_{h,0}(t) &= f - \beta_{h,0}(z(t))z(t) - dx_{h,0}(t) \leq f - dx_{h,0}(t) \\ x'_{h,v}(t) &= -\beta_{h,v}(z(t))z(t) - dx_{h,v}(t) \leq -dx_{h,v}(t) \end{aligned}$$

with $x_{h,0}(0) = x_h^{E_h} = \frac{f}{d}$ and $x_{h,v}(0) = x_{h,v}^0 > 0$, it follows that

$$x_{h,0}(t) \leq \frac{f}{d}, \quad x_{h,v}(t) \leq x_{h,v}^0.$$

Consequently, the following estimates hold true:

$$\begin{aligned} y'_{h,0}(t) &= \beta_{h,0}(z(t))z(t) \leq b_h z(t) \leq u(y_{h,0}(t), y_{h,v}(t)) \\ y'_{h,v}(t) &= \beta_{h,v}(z(t))z(t) \leq b_h z(t) \leq u(y_{h,0}(t), y_{h,v}(t)), \end{aligned}$$

where

$$u(y_{h,0}(t), y_{h,v}(t)) := b_h \left(\frac{f}{d} + x^0_{h,v} - y_{h,0}(t) - y_{h,v}(t) + n \right).$$

Due to the comparison principle for systems of ODEs (see for instance [59, Proposition 1.4], it follows that

$$\begin{aligned} y_{h,0}(t) &\leq y^{upper}_{h,0}(t) \\ y_{h,v}(t) &\leq y^{upper}_{h,v}(t), \end{aligned}$$

where $y^{upper}_{h,0}(t)$ and $y^{upper}_{h,v}(t)$ are solutions of the system of ODEs

$$\begin{aligned} \frac{d}{dt} y^{upper}_{h,0}(t) &= u(y^{upper}_{h,0}(t), y^{upper}_{h,v}(t)), \quad y^{upper}_{h,0}(0) = y_{h,0}(0) = \frac{f}{d} + n \\ \frac{d}{dt} y^{upper}_{h,v}(t) &= u(y^{upper}_{h,0}(t), y^{upper}_{h,v}(t)), \quad y^{upper}_{h,v}(0) = y_{h,v}(0) = 0. \end{aligned} \tag{8.1.3}$$

Solving system (8.1.3) gives

$$\begin{aligned} y^{upper}_{h,0}(t) &= \frac{f}{d} + n + \frac{1}{2} x^0_{h,v} \left(1 - e^{-2b_h t} \right) \\ y^{upper}_{h,v}(t) &= (1 - e^{-2b_h t}) \frac{1}{2} x^0_{h,v}. \end{aligned}$$

Observe that the solutions are strictly positive for $t > 0$.

Step 2: The switching time $\bar{t}$ is calculated using explicit solution formulae for solutions $x_h(t)$ and $y_h(t)$ of the basic model (3.0.1) within $\mathcal{S}_1$,

$$\begin{aligned} x_h(t) &= \frac{1}{2ds} e^{-\frac{1}{2}(2b_h + d + s)t} \left(2se^{\frac{1}{2}(2b_h + d + s)t} f + d(d+s)x^0_{h,v} + d(-d+s)e^{st} x^0_{h,v} \right) \\ y_h(t) &= \frac{f}{d} + \frac{b_h x^0_{h,v}}{s} \left(e^{st} - 1 \right) e^{-\frac{1}{2}(2b_h + d + s)t} + n, \end{aligned} \tag{8.1.4}$$

where $s = \sqrt{4b_h^2 + d^2}$ with initial conditions $x_h(0) = \frac{f}{d} + x^0_{h,v}$ and $y_h(0) = \frac{f}{d} + n$.

They are derived via elementary calculation. Using (8.1.4) implies that

$$z(t) = 0 \quad \Leftrightarrow \quad t = \bar{t} \text{ with } \bar{t} = \frac{1}{s} \ln \left(\frac{4b_h^2 + 2b_h d + d^2 + (2b_h + d)s}{2b_h d} \right)$$

Note that $\bar{t} > 0$ is well-defined. In particular, $\bar{t}$ only depends on the parameters b_h and d. As a consequence, a switch in the sign of $z(t)$ occurs at $t = \bar{t}$.

By the remark at the beginning of the proof, combining steps 1 and 2 yields that $y_{h,v}^{upper}(\bar{t})$ provides an upper estimate for $y_{h,v}(t)$ for all $t \geq 0$. This proves the claim. □

Remark 8.7. Note that the proof of Theorem 8.6 additionally implies

$$0 \leq y_{h,0}(t) \leq y_{h,0}^{upper}(\bar{t}) = y_{h,v}^{upper}(\bar{t}) + \frac{f}{d} + n,$$

i.e. an upper bound for the number of healthy PCs inside the niche after vaccination. Yet it does not provide new information since $y_{h,0}^{upper}(\bar{t}) > y_h^{E_h}$.

Theorem 8.6 shows the existence of one sign switch of the function $z(t)$ by stating the time point at which this switch occurs. In this regard, it extends the previously derived result of Corollary 6.15 for a particular set of initial conditions for the basic model, i.e.

$$\{(x_h^0, y_h^0)^T \in \mathbb{R}^2 \colon x_h^0 > \frac{f}{d},\ y_h^0 = \frac{f}{d} + n\} \notin \mathcal{R}_1 \cup \mathcal{R}_2.$$

8.2 Qualitative simulations

Concluding this chapter, simulations are provided to visualise the qualitative dynamics of the re-establishment of the healthy equilibrium after a vaccination-induced perturbation at time $T > 0$ (see Definition 4.4) within the framework of the extended model (4.0.1). Values of chosen parameters are stated in Table 8.1 on page 109. In the following, Figure 8.1 is considered:

- For $0 \leq t < 200$, the system is at healthy equilibrium E_h, where $x_{h,0}^{E_h} = 10$ and $y_{h,0}^{E_h} = 90$. In particular, it is $z(t) = 0$ for all $0 \leq t < 200$.

- At $t = 200$, the system is perturbed by $x^0_{h,v} = 84$. This is attended by an increase of $z(t)$. In particular, it is $z(t) > 0$ for all $200 \leq t < \bar{t} \approx 202.65$, and $z(\bar{t}) = 0$, see Theorem 8.6.

- For all $t > \bar{t}$, it is $z(t) < 0$. This results in a decrease of both $y_{h,0}(t)$ and $y_{h,v}(t)$. Theorem 8.5 implies that the solution asymptotically approaches $E \in \mathcal{E}$. Observe that $E \neq E_h$ but $x^E_{h,0} + x^E_{h,v} = 10$ ($x^E_{h,0} = 10$, $x^E_{h,v} = 0$) and $y^E_{h,0} + y^E_{h,v} = 90$ ($y^E_{h,0} = 65$, $y^E_{h,v} = 25$). Theorem 8.6 implies that $y^E_{h,v}$ can be estimated from above by $y^{upper}_{h,v}(\bar{t}) \approx 41.8$.

The scaling of the axes is due to reasons of visualisation. In Chapter 10, a realistic quantification is presented, where time can be interpreted as lifetime of a patient, and solutions represent numbers of PCs.

Remark 8.8. By (8.1.2) in Theorem 8.6 it follows that $y^{upper}_{h,v}(\bar{t}) \leq \frac{1}{2}x^0_{h,v}$. Observe that the right-hand side of the latter inequality provides an upper estimate for $y^E_{h,v}$ independently from the switching time $\bar{t}$. By comparison, for $y^{upper}_{h,v}(\bar{t}) \ll \frac{1}{2}x^0_{h,v}$, significantly more information on the composition of the re-established healthy equilibrium can be extracted, since the set of possible values for $y^E_{h,v}$ gets smaller. Here it holds that $y^{upper}_{h,v}(\bar{t}) \approx 41.8 < 42 = \frac{1}{2}x^0_{h,v}$. Along these lines, $y^{upper}_{h,v}(\bar{t})$ is an upper estimate of rather minor value.

Table 8.1: Parameter values for simulations in Section 8.2.

Parameter	**Value**
f	0.2
n	80
b_h	1
c_h	1
d	0.02
$x^0_{h,v}$	84
T	200

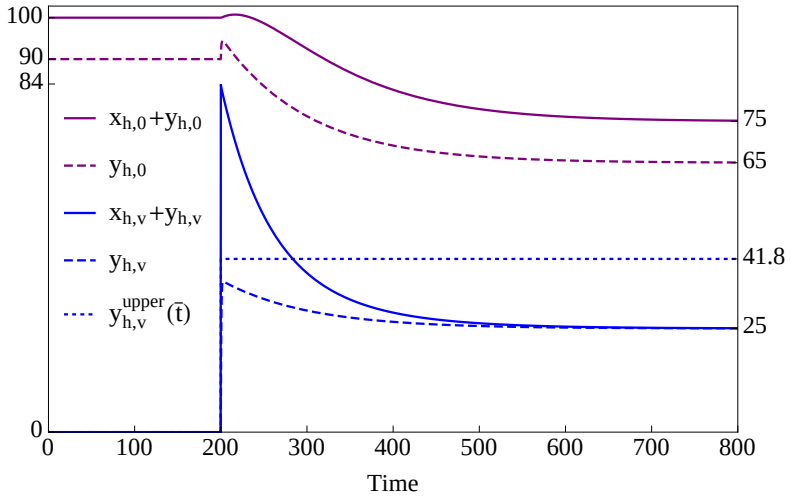

(a) Dynamics of solution of the extended model.

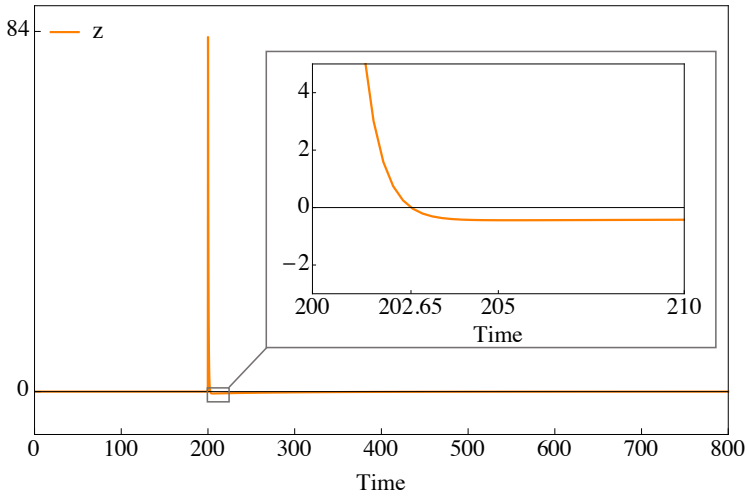

(b) Dynamics of $z(t)$.

Figure 8.1: Vaccination-induced perturbation of the healthy equilibrium. (a) The qualitative dynamics of a vaccination-induced perturbation of the healthy equilibrium at $t = 200$ and the concomitant re-establishment of a newly composed healthy equilibrium are depicted. $x_{h,0}(t) + y_{h,0}(t)$ (purple) represents the total number of pathogen-induced healthy PCs in the bone marrow, $y_{h,0}(t)$ (dashed purple) is the number of pathogen-induced healthy PCs inside the niche, $x_{h,v}(t) + y_{h,v}(t)$ (blue) represents the total number of vaccination-induced healthy PCs in the bone marrow, and $y_{h,v}(t)$ (dashed blue) is the number of vaccination-induced healthy PCs inside the niche. $y_{h,v}^{upper}(\bar{t})$ (dotted blue) is the upper estimate derived in Theorem 8.6. (b) Dynamics of the function $z(t)$. The vaccination-induced perturbation of the healthy equilibrium causes a sudden increase of $z(t)$ and a concomitant decrease. The snapshot visualises $z(t)$ changing the sign from positive to negative at $t = \bar{t} \approx 202.65$. Then, $z(t)$ approaches zero. Parameter values are stated in Table 8.1.

Part III

Quantitative application of mathematical models of healthy and malignant plasma cell dynamics using clinical data

9 Data analysis

9.1 Doubling time of malignant plasma cells

Two sets of patient data have been provided by the Multiple Myeloma Research Laboratory at Heidelberg University Hospital. These consist of consecutive serum and/or urine samples from 338 AMM-patients and 305 MGUS-patients. Relevant attributes of each patient data set consist of

- an anonymised identification number,
- the class of myeloma (IgA, IgG, light chain or asecretory)
- the timespan (in days) between birth and PC purification at bone marrow aspiration,
- the date of progression to symptomatic disease according to the IMWG criteria [51, 95], or last follow-up without progression,
- time series of concentrations of IgA, IgG, IgM and M-gradient in the serum (in g/l) and of light chains in the urine (LCU, in mg/die).

Not each of these concentrations is available for each patient because measurements were only performed for clinical follow-up. Patients received treatment only after disease progression to symptomatic MM.

Time series serve as surrogates for the malignant growth dynamics, where a linear dependence of the Ig and light chain concentration on the number of malignant PCs is assumed, see Chapter 1. IgG measurements for patients classified as IgG-myeloma, IgA measurements for patients classified as IgA-myeloma, and LCU for patients classified as light chain myeloma are used. With few exceptions, categorisation of each patient according to the type of the monoclonal protein is distinct, see Section 1.2.

The exponential model (2.0.1) is used to describe the growth of malignant PCs. Observe that the growth of the malignant PC population is thereby considered autonomous, i.e. without being impacted by healthy PCs, see Chapter 2.

Remark 9.1 (Limitations of the exponential model)**.** Growth of malignant PCs is quantified by parameter a, whereas parameter b represents the initial value of the respective surrogate. A limitation in the accuracy of estimation of the initial number of malignant PCs is given by the fact that IgG and IgA are also produced by healthy PCs. For IgG-myeloma, the potential error is higher, since normal values of IgG (IgA) are between $8 - 16$ g/l ($1.4 - 4$ g/l), see Chapter 1. The error is smallest in the M-gradient as it reflects the portion of monoclonal protein. However, it is less often measured. A further limitation is given due to the sensitivity of turbidostatic measurements of IgG and IgA and determination of the M-gradient, as a value of zero for the latter does not imply absence of malignant PCs [108].

For fitting the model (2.0.1) to data, at least three measurements of the respective surrogate are required to reduce the influence of fluctuations of serum and urine measurements by chance. Not to falsely exclude patients with fast progression, two measurements are allowed if additionally time interval between these two measurements is long enough, or the surrogate increases significantly:

Definition 9.2 (Inclusion criteria for the exponential model)**.** Consider data sets of AMM- and MGUS-patients with time series consisting of at least two measurements of either serum (for IgA- or IgG-myeloma) and/or urine (for Bence-Jones and predominant light chain myeloma) with a time interval between the first and the last measurement of one month. Furthermore, one of the following criteria has to be fulfilled:

(i) At least three measurements are available.

(ii) If only two measurements are available, then the time interval between the measurements is at least three months.

(iii) If only two measurements are available and the time interval between the measurements is shorter than three months, then the increase of involved IgA/IgG/M-gradient is $> 5\,\mathrm{g/l}$ or 24-hour light chain excretion $> 200\,\mathrm{mg/die}$. These are the progress criteria for AMM according to the IMWG [51, 95].

With such criteria the trade-off between minimising the uncertainty of the estimates for a and b and preventing the exclusion of patients with fast growing malignant PCs is balanced.

To proceed with parameter estimation for model (2.0.1), a logarithmic transformation of the time series of measurements which represent the surrogate of malignant PCs is performed. Then, the linear model

$$\tilde{y} = \tilde{b} + at, \;\; \tilde{y} = \ln(y), \; \tilde{b} = \ln(b)$$

is fitted to the transformed data using least squares methods [105]. The quality of the fit regarding the data is evaluated using the coefficient of determination R^2 [105]. Calculations and simulations are performed using the computation software programme *Mathematica, Version 9* by Wolfram Research. For further information on parameter estimation, see Appendix A.3.

Results

Data sets of 518 patients (196 MGUS- and 322 AMM-patients) fulfil the inclusion criteria stated in Definition 9.2. The total analysis comprises 4674 serum and 3724 urine samples. Mean follow-up is 4.8 years for MGUS- and 3.8 years for AMM-patients, respectively. Having obtained the estimates for each patient within the data sets allows calculating the DT (in years) according to (2.0.2). Median DT in patients with MGUS is 64.9 years compared to 10.4 years in patients with AMM ($P < 0.001$), see Figure 9.1 (a). Progressing patients show an even faster DT ($P < 0.001$), see Figure 9.1 (b). Statistical evaluation was performed using a Wilcoxon rank-sum test [16].

Next, patients are grouped in terms of their DTs. To avoid data-adapted thresholds, a geometric row as cut-offs is applied.

Definition 9.3 (DT-groups)**.** By means of the DT τ (in years), the following groups of malignant PC accumulation are delineated: very fast ($0 < \tau < 2$), fast ($2 \leq \tau < 4$), intermediate ($4 \leq \tau < 16$), and almost no (or not visible) accumulation ($\tau \geq 16$ or $\tau \leq 0$).

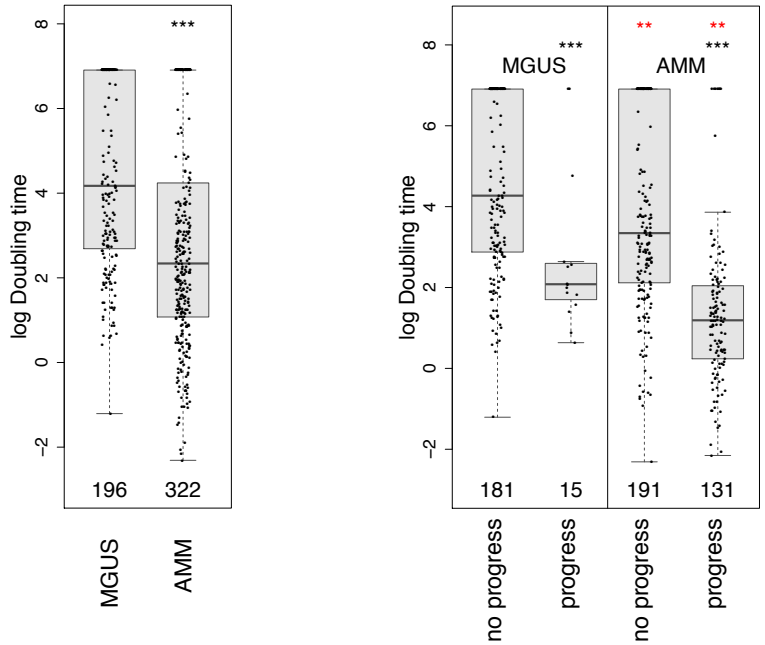

Figure 9.1: Box-Whisker plot of doubling times (DTs) of patients with MGUS versus AMM. The ordinate axis shows the natural logarithm of DTs. Negative DTs are set to 1000. Significant difference between the groups is depicted by two asterisks for a level of $P < 0.01$ and three asterisks for a level of $P < 0.001$. Red asterisks mark significant differences between respective groups of MGUS and AMM. Significance testing was performed using a Wilcoxon rank-sum test [16]. For details, see [109].

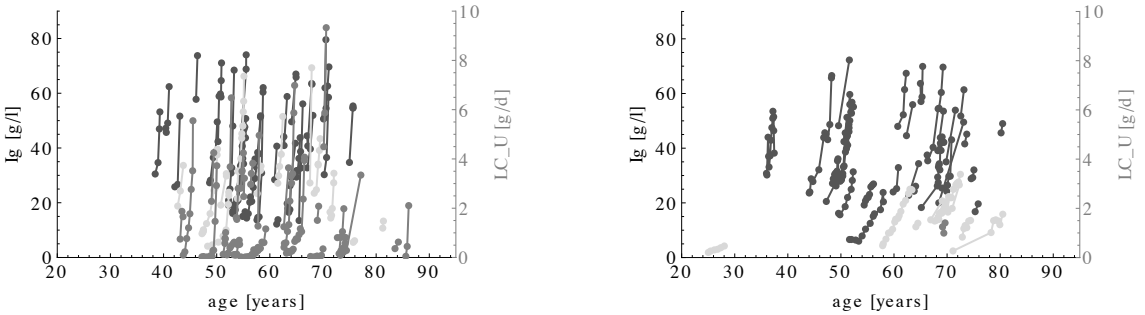

(a) $0 < \tau < 2$ (66/322).

(b) $2 \leq \tau < 4$ (36/322).

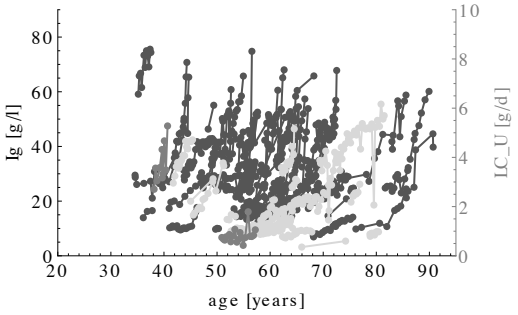

(c) $4 \leq \tau < 16$ (84/322).

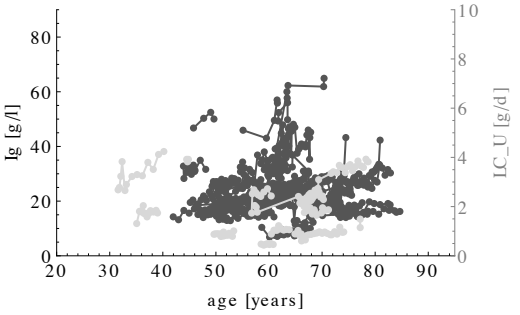

(d) $\tau \geq 16$ (71/322).

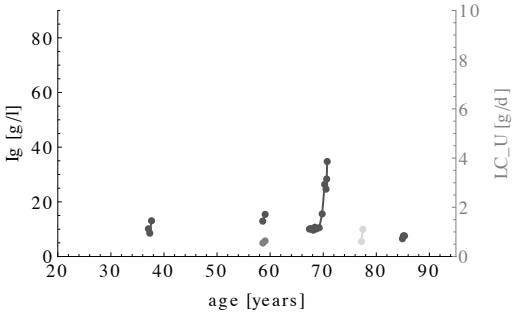

(e) $0 < \tau < 2$ (6/196).

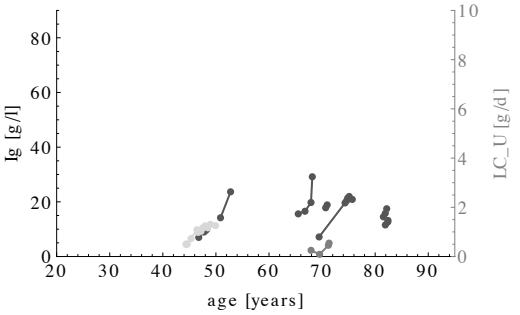

(f) $2 \leq \tau < 4$ (10/196).

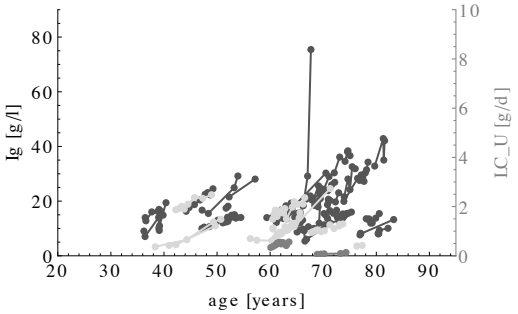

(g) $4 \leq \tau < 16$ (39/196).

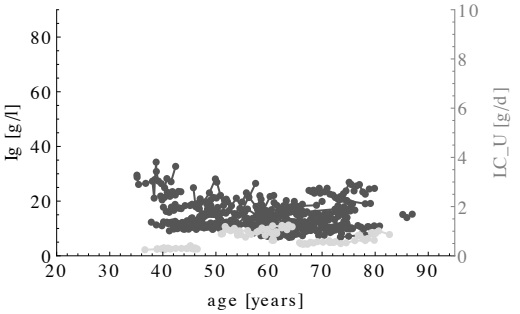

(h) $\tau \geq 16$ (68/196).

Figure 9.2: Patterns of malignant plasma cell accumulation according to Definition 9.3 for 322 AMM- and 196 MGUS-patients, see (a)-(d) and (e)-(h), respectively. Patients with $\tau \leq 0$ (65/322 AMM, 73/196 MGUS) are not shown. IgA: Light gray. IgG: Dark gray. Light chains (LCU): Medium gray.

Results

Three main accumulation patterns of malignant PCs can be observed: a fast increase in patients within the DT-groups satisfying $0 < \tau < 2$ or $2 \leq \tau < 4$ (102/322 AMM-patients, 16/196 MGUS-patients), an intermediate increase when $4 \leq \tau < 16$ (84/322 AMM-patients, 39/196 MGUS-patients), and an infinitesimal increase in patients with $\tau \geq 16$ or $\tau \leq 0$ (136/322 AMM-patients, 141/196 MGUS-patients). Figure 9.2 illustrates the three patterns for AMM- and MGUS-patients by means of plotting the malignant surrogate for patients within each of the four DT-groups $0 < \tau < 2$, $2 \leq \tau < 4$, $4 \leq \tau < 16$ and $\tau \geq 16$.

Next, it is investigated how many patients in each DT-group progress to MM. In order to use the DT to infer a prognostic value for the time to progression, measurements which were taken at time of progression are excluded, and accordingly patients who do not fulfil the inclusion criteria according to Definition 9.2. This enables the calculation of a DT on which a clinical decision would have been drawn.

Results

For the AMM-cohort, 302 patient data sets fulfil the inclusion criteria given by Definition 9.2. Within this cohort, significantly different numbers of progressing patients are delineated with $P < 0.001$, $P = 0.003$, and $P < 0.001$ for the subsequent comparisons between the four DT-groups of patients with very fast ($0 < \tau < 2$), fast ($2 \leq \tau < 4$), intermediate ($4 \leq \tau < 16$), and almost no ($\tau \geq 16$ or $\tau \leq 0$) accumulation of malignant PCs, respectively, using a Log-rank test [40]. In particular, progression rates of 73%, 36%, 26% and 7% at 2 years, and 97%, 76%, 57% and 18% at 5 years, respectively, are observed. The corresponding Kaplan-Meier survival plot [27] is given by Figure 9.3. For details, see [109].

Remark 9.4. One caveat regarding the association of progression with the accumulation rate of malignant PCs is that the latter is linked to disease progression. Performing a landmark analysis [123] by defining alternative starting points (instead of the date of bone marrow aspiration) still delineates the prognostic impact of the DT. For details, see [109].

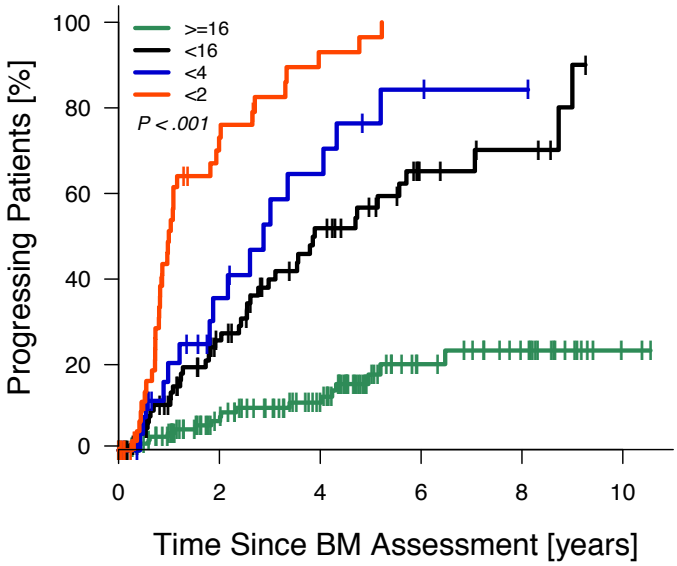

138	92	65	26	17	2	16
84	45	24	8	5		<16
28	12	6	2	1		<4
52	9	2				<2

Figure 9.3: Association of progression since bone marrow (BM) assessment with the accumulation rate of malignant plasma cells. Doubling times in years, very fast (red), fast (blue), intermediate (black), and almost no (green) accumulation, respectively, as assessed by exponentially modelling the increase in tumour mass in subsequent serum and urine samples for 302 AMM-patients. Computation of survival curves and median time to progression are based on non-parametric survival estimates for censored data using Kaplan-Meier estimation [27]. Differences between the curves were tested using a Log-rank test [40]. For details, see [109].

Discussion

In clinical practice, the DT allows delineation of patients with very different time to progression. Once (at least two) measurements of the monoclonal protein have been taken, calculation of the DT at each presentation of the patient is readily obtainable. Figure 9.4 shows a screen shot of the interface of a user-friendly tool (executable in Microsoft *Excel* and Apache *Open Office*) for the calculation of the DT given the measurements. The program also calculates the standard error of the DT by using the error propagation formula for a transformed estimate [10]. This enables

further evaluation of uncertainties regarding the categorisation into one of the defined DT-groups. Thus, the DT turns out to be a strong prognostic parameter correlated to progression. Its prediction is dynamic and can vary after each presentation of the patient, possibly inferring a modified prediction.

Further, it was shown that tumour mass and molecular characteristics determine progression to symptomatic disease (see [109]):

- High-risk groups in gene expression-based risk stratifications and presence of any progression-associated chromosomal aberration are associated with shorter DT. Tumour mass surrogates are in turn significantly associated with higher DT.

- Light chain asymptomatic myeloma shows a significantly faster progression to symptomatic myeloma compared to IgG- and IgA-myelomas. This is consistent with the observation that more than half of the patients with light chain myeloma appear in the group of very fast accumulation of malignant PCs.

- On the basis of additional (sequencing) data being beyond the scope of this thesis, it was shown that progression is driven by the initial set of aberrations, not their *de novo* appearance.

DTs are incompatible with common *de novo* appearance of progression-driving aberrations in evolution and progression of AMM. In fact, unlike the previous concept that a gain of progression-associated chromosomal aberrations between the stages of MGUS, AMM and MM drives progression [81], evolution and progression of AMM can be explained by accumulation rate, tumour mass and molecular characteristics without necessity of *de novo* appearance of genetic alterations [109].

Doubling Time Calculation

Insert at least 2 measurements in the columns „Date“ and „Measurement“. Guarantee that the units of the values in „Measurement“ are the same. The tool calculates the Doubling Time (DT) and its Standard Error (SE) based on the given data and the fitting results.

1. DT: Click on the green cell (Fit Parameter) and follow the commented instruction. The DT (years) is listed in the green cell „DT (y)“. A negative value has to be interpreted as half-value time.

2. SE: Click on the orange cell (Fit SE) and follow the commented instruction. The SE (years) of the DT is listed in the orange cell „SE (y)“.

# Patient	Date (MM/DD/YY)	Measurement	Time Points	Fit Parameter	DT (y)
1			0		
2			0	Fit SE	SE (y)
3			0		
4			0		
5			0		
6			0		
7			0		
8			0		
9			0		
10			0		
11			0		
12			0		
13			0		
14			0		
15			0		
16			0		
17			0		
18			0		
19			0		
20			0		

Example:

# Patient	Date (MM/DD/YY)	Measurement	Time Points	Fit Parameter	DT (y)
1	08.20.08	35,32	0	1,000397017	**4,784202144**
2	05.20.09	42,53	273	Fit SE	SE (y)
3	07.22.09	44,75	336	3,69646E-05	**0,445525749**
4	04.14.10	47,62	602		
5	09.29.10	52,21	770		
6	06.08.11	57,07	1022		
7	03.07.12	60,13	1295		

Figure 9.4: Excel tool for the calculation of the doubling time (DT) as a quantitative assessment of malignant plasma cell accumulation. For details, see [109].

9.2 Data transformation

In this section, a transformation of the data is defined in order to match them with the observable variables of the myeloma model (5.0.1). Identifying a relation between the measurements and PC counts allows drawing conclusions on the initial number of malignant PCs at the onset of myeloma.

In the following, IgA-myeloma and IgG-myeloma patients are considered. The exclusion of light chain myeloma patients is motivated by the amount of light chain excretion in the 24 h urine being dependent also on other parameters, including renal function. Light chains are only excreted once the renal resorption capacity is saturated. Thus, LCU measurements need to be taken as error-prone. Further, they cannot be taken as surrogate for the number of healthy PCs since they are only occasionally liberated by healthy PCs, see Section 1.2.

Assumption 9.5 (Ig as surrogate)**.** The level of normal Ig and monoclonal protein (i.e. Ig produced by malignant PCs) can be taken as surrogate for the number of healthy and malignant PCs in the bone marrow, respectively.

Remark 9.6. The assumption requires that the production of Ig in other sites except the bone marrow is unaffected by accumulation of PCs in the bone marrow and the vast majority of Ig is produced by PCs [8].

9.2.1 Average number of healthy plasma cells

From estimates based on large cohorts of adult normal-weighted healthy individuals [55] it can be deduced that about 95% of the Ig concentrations per litre of blood lie within the interval $(7.65, 20.13)$ (in g/l). The average Ig concentration can be estimated to comprise approximately 13 g/l (10 g/l IgG, 2 g/l IgA, 1 g/l IgM) [32, 55]. Ig types with marginal incidence, for instance IgD, are neglected. Assuming an average volume of 5 litres of blood [18] yields an average total amount of 65 g Ig (50 g IgG, 10 g IgA, 5 g IgM).

Estimates for the average total number of PCs in the bone marrow are deduced from two different approaches:

(1) *Proposed estimates:* Firstly, Radbruch et al. [94] estimate the total number of PCs in the human bone marrow to be about 10^9 cells. Secondly, the bone

marrow cellularity is estimated to comprise about 10^{12} cells [41]. Assuming a fraction of PCs of about $0.25 - 1\%$ [94, 118], the total number of PCs can be calculated to be in the range of $2.5 \cdot 10^9 - 10^{10}$ cells. A comparable result can be obtained starting from data by Sandkühler et al. [104] reporting that the number of PCs in the bone marrow comprises about $7.5 \cdot 10^9$ cells per litre of bone marrow. With a total bone marrow volume of $1.6 - 4.0$ litres [129], this implies an estimate of PC counts in the range of $1.2 - 3 \cdot 10^{10}$ cells.

Summarising reported values yields that the average total number of PCs in the human bone marrow lies in the order of $2.5 \cdot 10^9 - 3 \cdot 10^{10}$ cells.

(2) *Estimates based on Ig synthesis rates of PCs:* The total amount of IgG at healthy homoeostasis is assumed to be 50 g. The half-life time of IgG molecules can be estimated to be 20 days [14, 83, 86] and IgG synthesis rate is about 5 pg - 34 pg per PC per day [103]. In order to relate IgG synthesis to the total number of PCs, define $G(t)$ as the amount of IgG molecules (in gramme) at time t (in days). Taking into account Assumption 9.5, the production and degradation of IgG is modelled as follows:

$$G'(t) = sC(t) - d_g G(t),$$

where $C(t)$ is the total number of IgG-producing PCs at time t, s is the synthesis rate, and d_g is the death rate of IgG molecules (which is given by the reciprocal of the half-life time multiplied by $\ln(2)$). At homoeostasis, it holds

$$sC = d_g G,$$

where C and G are the total amount of IgG at equilibrium (which is known), and the total number of IgG-producing PCs at equilibrium, respectively. Inserting the extreme values for IgG synthesis rate and solving the equation for C yields two possibilities:

(a) If $s = 5 \cdot 10^{-12} \frac{g}{\text{PC}}$ (i.e. taking the lower bound of the synthesis rate), then

$$\begin{aligned} C = \frac{d_g G}{s} &= \frac{\ln(2)}{5 \cdot 20} \cdot 50 \cdot 10^{12} \text{ PCs} \\ &\approx 3.5 \cdot 10^{11} \text{ PCs}. \end{aligned}$$

(b) If $s = 34 \cdot 10^{-12} \frac{g}{\text{PCs}}$ (i.e. taking the upper bound of the synthesis rate), then

$$C = \frac{d_g G}{s} = \frac{\ln(2)}{34 \cdot 20} \cdot 50 \cdot 10^{12} \text{ PCs}$$
$$\approx 5 \cdot 10^{10} \text{ PCs}.$$

Taking into account that C is about 80% (more precisely, $10/13 \cdot 100\%$) of the total number of PCs, the total number of PCs in the human bone marrow can be estimated to range between $6 \cdot 10^{10} - 4.5 \cdot 10^{11}$ cells.

The estimate for the IgG synthesis rate, i.e. 5 pg - 34 pg per PC per day, varies between different individuals. At the same time, inter-individual physiological variation is observed in the level of Ig in healthy serum (see Chapter 1) implying inter-individual variation in the number of healthy PCs at healthy equilibrium. Being derived from malignant PCs with an average of 12 pg per PC per day [102, 103], this estimate for the IgG synthesis rate is lower compared to healthy PCs. Based on cultured PCs phenotypically resembling peripheral blood PCs, Jourdan et al. [57] report an IgG synthesis rate in a range of about 20 pg - 35 pg per PC per day with mean of 26 pg per PC per day. Using this mean synthesis rate implies

$$C = \frac{d_g G}{s} = \frac{\ln(2)}{26 \cdot 20} \cdot 50 \cdot 10^{12} \text{ PCs}$$
$$\approx 6.7 \cdot 10^{10} \text{ PCs}.$$

Further, the half-life time of disappearance of IgG in myeloma patients is shorter compared to healthy patients, likewise suggesting the IgG synthesis rate of malignant PCs to be lower compared to healthy PCs (if catabolic rates of normal and monoclonal IgG are the same) [103].

Combining both ways of estimation, a span of $2.5 \cdot 10^9 - 6.7 \cdot 10^{10}$ cells results. Taking the mean value motivates the following assumption:

Assumption 9.7 (Total amount of Ig and total number of PCs at healthy equilibrium)**.**

(1) The average total amount of Ig is 13 g per litre of blood (10 g/l IgG, 2 g/l IgA, 1 g/l IgM).

(2) The average total number of PCs in the human bone marrow comprises 10^{10} cells.

Assumptions 9.5 and 9.7 yield the following relation between Ig concentration in the blood and the total number of PCs in the bone marrow:

Consequence 9.8 (Transformation to PC number)**.** *Let Assumptions 9.5 and 9.7 be true. The following equivalence relation holds:*

$$1\,\text{g/l}\ \ Ig \mathrel{\widehat{=}} \frac{1}{13} \cdot 10^{10}\ \ PCs.$$

This relation is to be interpreted as the transformation of a measurement of 1 g/l *Ig to* $1/13 \cdot 10^{10}$ *PCs.*

Remark 9.9. Using this transformation for both healthy and malignant PCs implies an underestimation of the number of malignant PCs relative to the number of healthy PCs due to lower Ig secretion rate of the former [57, 103].

9.2.2 Surrogates for the number of plasma cells

In the following, plausible surrogates for the number of healthy and malignant PCs are discussed, distinguishing between IgA- and IgG-myeloma patients.

IgA-myeloma patients

In case of IgA-myeloma, malignant PCs secrete IgA and IgA concentration is used as surrogate for the number of malignant PCs. For the number of healthy PCs, IgG concentration is used as surrogate. Note that the measured IgG levels correspond to $10/13 \cdot 100\%$ of the total number of healthy PCs.

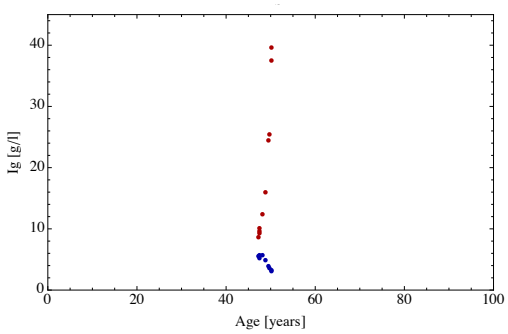

(a) IgG (blue) and IgA (red) measurements.

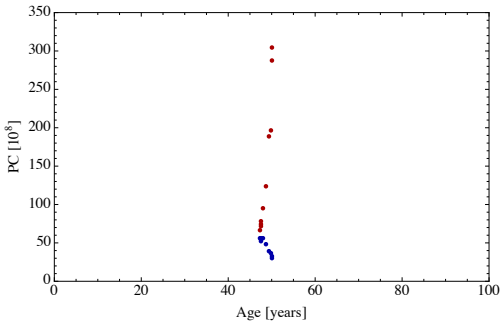

(b) Number of healthy (blue) and malignant (red) PCs.

Figure 9.5: Example for the transformation of immunoglobulin (Ig) measurements to plasma cell (PC) counts in case of an IgA-myeloma patient using Consequence 9.10. For details, see text.

Consequence 9.10 (Surrogates for IgA-myeloma patients)**.** *Consider an IgA-myeloma patient. Let Assumptions 9.5 and 9.7 be true. Using IgA concentration as surrogate for the number of malignant PCs and IgG concentration as surrogate for the number of healthy PCs, the following equivalence relations hold:*

$$1\,\mathrm{g/l}\ \ \mathit{IgA} \mathrel{\widehat{=}} \frac{1}{13} \cdot 10^{10}\ \ \mathit{malignant\ PCs}$$
$$1\,\mathrm{g/l}\ \ \mathit{IgG} \mathrel{\widehat{=}} \frac{10}{13} \cdot \frac{1}{13} \cdot 10^{10}\ \ \mathit{healthy\ PCs.}$$

These relations are to be interpreted as the transformation of a measurement of $1\,\mathrm{g/l}$ *IgA or IgG to the corresponding number of PCs.*

The transformation of Ig measurements to PC number is exemplified by means of an arbitrarily chosen patient data set. Figure 9.5 (a) shows Ig concentration measurements dependent on the age of the patient. The transformed data using Consequence 9.10 are visualised in Figure 9.5 (b).

Remark 9.11 (IgA as surrogate)**.** The healthy base level of IgA is low (range given by $1.4-4$ g/l, see Chapter 1). By using IgA concentration as surrogate for the number of malignant PCs, the production of IgA by healthy PCs is neglected, implying an overestimation of the number of malignant PCs relative to the number of healthy PCs, especially for low initial levels of IgA. Vice versa, the error is low in case of a high level of IgA.

IgG-myeloma patients

In case of IgG-myeloma, malignant PCs secrete IgG. Thus, IgG concentration is used as surrogate for the number of malignant PCs. In contrast to the usage of IgA for IgA-myeloma patients, the portion of IgG produced by healthy PCs cannot be neglected since the healthy base level of IgG reflects about 80% of the total number of healthy PCs, see Assumption 9.7. Alternatively, the M-gradient can be used as surrogate since it reflects the „malignant portion“ of the total IgG.

In the following, several options describing plausible surrogates for the numbers of healthy and malignant PCs are identified:

(1) The M-gradient is used as surrogate for the number of malignant PCs [51, 95]. Thus, applying Consequence 9.8 yields

$$1\,\mathrm{g/l}\ \text{ M-gradient } \mathrel{\widehat{=}} \frac{1}{13}\cdot 10^{10}\ \text{ malignant PCs.}$$

This relation is to be interpreted as the transformation of a measurement of 1 g/l M-gradient to $1/13{\cdot}10^{10}$ malignant PCs. The following possible surrogates for the number of healthy PCs are considered:

(1a) As surrogate for the number of healthy PCs, the difference of the IgG and the M-gradient concentrations (i.e. IgG value minus M-gradient value) is used. The latter allows isolating the „healthy portion“ of the total IgG. Since IgG constitutes $10/13 \cdot 100\%$ of the total Ig concentration (see Assumption 9.7), multiplication of the resulting concentration by 13/10 is necessary to represent 100% of healthy PCs. Hence

$$1\,\mathrm{g/l}\ \ (\mathrm{IgG} - \text{M-gradient}) \mathrel{\widehat{=}} \frac{13}{10}\cdot\frac{1}{13}\cdot 10^{10}\ \text{ healthy PCs.}$$

(1b) As surrogate for the number of healthy PCs, the sum of the difference of IgG and M-gradient concentrations (see Option 1 (a)) and the IgA and IgM concentrations is used. According to Assumption 9.7, this reflects the total Ig concentration. Hence

$$1\,\mathrm{g/l}\ \ (\mathrm{IgG} - \text{M-gradient} + \mathrm{IgA} + \mathrm{IgM}) \mathrel{\widehat{=}} \frac{1}{13}\cdot 10^{10}\ \text{ healthy PCs.}$$

(1c) As surrogate for the number of healthy PCs, the sum of IgA and IgM concentrations is used. Since IgA and IgM constitute $3/13 \cdot 100\%$ of the total Ig concentration (see Assumption 9.7), multiplication of the resulting concentration by 13/3 is necessary to represent 100% of healthy PCs. Hence

$$1\,\mathrm{g/l} \quad (\mathrm{IgA} + \mathrm{IgM}) \mathrel{\widehat{=}} \frac{13}{3} \cdot \frac{1}{13} \cdot 10^{10} \quad \text{healthy PCs.}$$

(1d) As surrogate for the number of healthy PCs, the IgA concentration is used. Since IgA constitutes $2/13 \cdot 100\%$ of the total Ig concentration (see Assumption 9.7), multiplication of the concentration by 13/2 is necessary to represent the total number of healthy PCs. Hence

$$1\,\mathrm{g/l} \quad \mathrm{IgA} \mathrel{\widehat{=}} \frac{13}{2} \cdot \frac{1}{13} \cdot 10^{10} \quad \text{healthy PCs.}$$

(2) Instead of using the M-gradient as surrogate for the number of malignant PCs, IgG concentration is chosen in the following approaches. For the number of healthy PCs, IgA concentration is used. As in option (1d), the following equivalence relation holds:

$$1\,\mathrm{g/l} \quad \mathrm{IgA} \mathrel{\widehat{=}} \frac{13}{2} \cdot \frac{1}{13} \cdot 10^{10} \quad \text{healthy PCs.}$$

The following possible surrogates for the number of malignant PCs are considered:

(2a) As surrogate for the number of malignant PCs, IgG concentration minus 10 is used, where 10 is the average concentration of IgG in healthy individuals, see Assumption 9.7. Hence

$$1\,\mathrm{g/l} \quad (\mathrm{IgG} - 10) \mathrel{\widehat{=}} \frac{1}{13} \cdot 10^{10} \quad \text{malignant PCs.}$$

(2b) To avoid subtraction of an average value, IgA concentration is used to derive an individual healthy level of IgG. For that, the IgA concentration

is multiplied by 13/2 and extrapolated to the value of IgG using that the portion of IgG in total Ig is 10/13, see Assumption 9.7. As surrogate for the number of malignant PCs, IgG concentration minus the extrapolated individual healthy IgG concentration is used. Hence

$$1\,\mathrm{g/l}\ \left(\mathrm{IgG} - \frac{10}{13}\cdot\frac{13}{2}\,\mathrm{IgA}\right) \mathrel{\widehat{=}} \frac{1}{13}\cdot 10^{10}\ \text{ malignant PCs.}$$

Applying the above transformations by means of three randomly chosen patient data sets yields the following observations, see Patients A, B and C in Figure 9.6:

Regarding Patient C, an increase in the number of healthy PCs is observed as suggested by the transformed data using option (1a) and (1b), which is biologically implausible but still could be explained by normal fluctuations either in the data or in the population of healthy PCs. Having a closer look on the results of option (1), observe that M-gradient measurements are not available for all IgG-myeloma patients at all measurement time points. This can be seen by a reduced number of transformed data points for the number of malignant PCs, see Patient A. Applying options (1) yields three transformed data points for the number of malignant PCs, whereas a transformation of the data using option (2a) or (2b) results in noticeably more data points. Yet a transformation based on option (2) implies drawbacks. Firstly, a constant IgG level due to secretion by healthy PCs as proposed by variant (2a) is not justified biologically. Secondly, variant (2b) uses an artificial derivation for the transformation. Lastly, negative values for the number of malignant PCs may occur, as for Patient A. The same holds true for options (1a) and (1b), see Patient B.

Consequently, either option (1c) or (1d) is chosen. Comparing options (1c) and (1d), observe that more information is included in (1c) compared to (1d), because concomitant to IgG measurements, those of IgM are available at all time points.

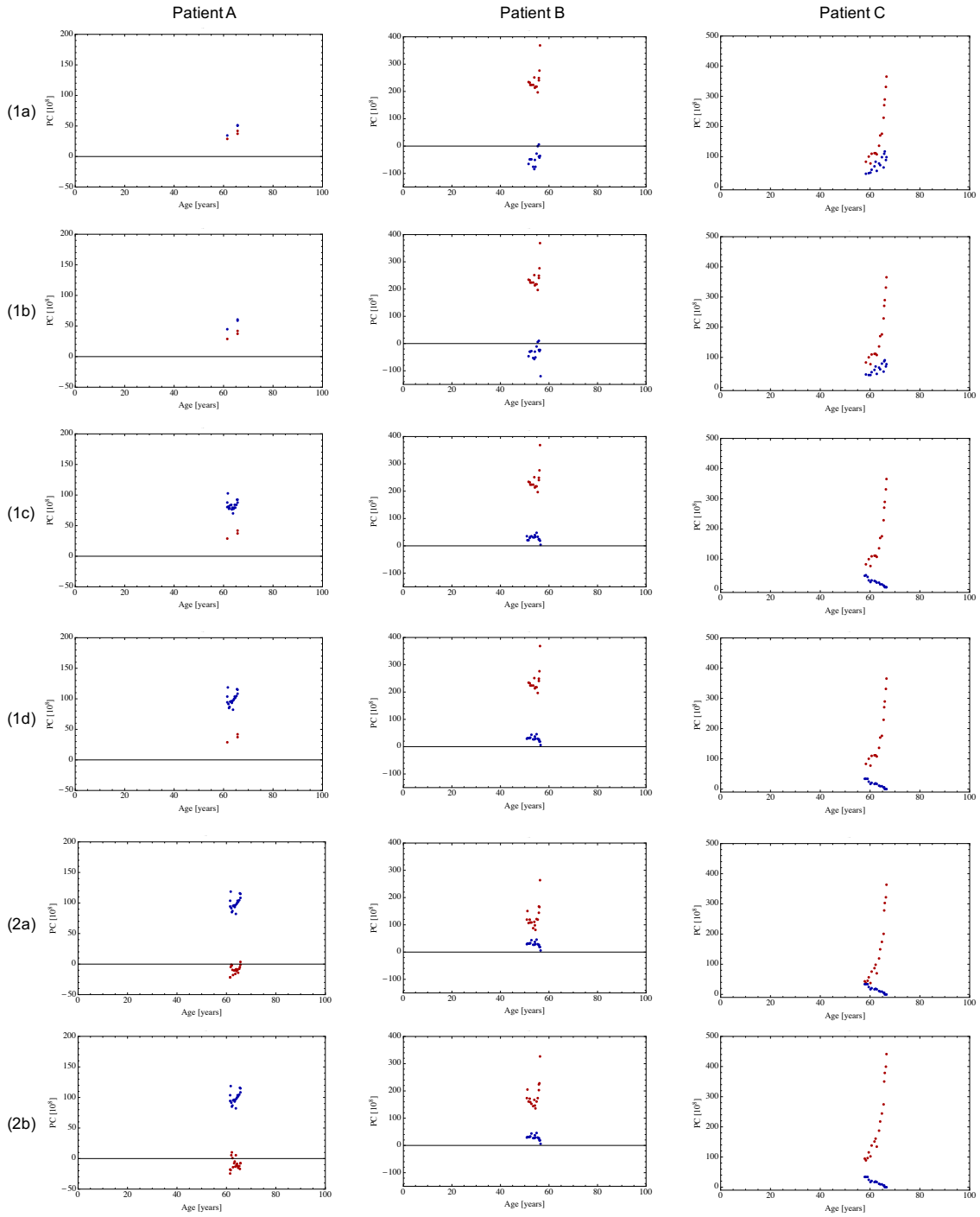

Figure 9.6: Variants for transforming data. Number of healthy (blue) and malignant (red) plasma cells (PCs) after application of different data transformation options (rows) for three selected Patients A, B and C (columns). For a discussion, see text.

Combining Assumptions 9.5, 9.7 and Consequence 9.8 yields

Consequence 9.12 (Surrogates for IgG-myeloma patients)**.** *Consider an IgG-myeloma patient. Let Assumptions 9.5 and 9.7 be true. Using M-gradient concentration as surrogate for the number of malignant PCs and the sum of IgA and IgM concentrations as surrogate for the number of healthy PCs, the following equivalence relations hold:*

$$1\,\mathrm{g/l}\ \ \textit{M-gradient} \mathrel{\widehat{=}} \frac{1}{13}\cdot 10^{10}\ \ \textit{malignant PCs}$$
$$1\,\mathrm{g/l}\ \ \textit{IgA} + \textit{IgM} \mathrel{\widehat{=}} \frac{13}{3}\cdot\frac{1}{13}\cdot 10^{10}\ \ \textit{healthy PCs.}$$

These relations are to be interpreted as the transformation of a measurement of 1 g/l *M-gradient or IgA plus IgM to the corresponding number of PCs.*

Remark 9.13 (M-gradient as surrogate)**.** As the M-gradient is the concentration of monoclonal protein, a change in its value reflects a change in the number of malignant PCs if the secretion rate of an individual malignant PC is constant. In contrast, the value of IgG includes the protein expressed by healthy PCs, see Chapter 1. Comparison of DTs based on IgG and M-gradient for those AMM-patients where both measurements are available yields that the DT based on IgG measurements is slower (56/105) than or within a 20% range (38/105) of the DT based on M-gradient measurements.

In contrast to IgG-myeloma, the M-gradient is less appropriate as surrogate for the number of malignant PCs in case of IgA-myeloma due to relative error-proneness in calculation, see Section 1.2.

By application of the transformations stated in Consequence 9.10 for IgA-myeloma patients, and in Consequence 9.12 for IgG-myeloma patients, respectively, the time series of each patient data set can be transformed into a time series of the form

$$\mathcal{D} = \{(t_1, h_1, m_1), \ldots, (t_j, h_j, m_j)\}$$

where $(t_k, h_k, m_k),\ k = 1, \ldots, j$, is the triple of data points reflecting the number of healthy PCs, h_k, and the number of malignant PCs, m_k, at the age t_k (in years) of the corresponding patient possessing measurements at j time points. Neglecting leap years one years is defined to comprise 365 days. Note that either h_k or m_k may

be empty due to a missing respective measurement at time t_k. This justifies the following reformulation of $\mathcal{D}$:

Definition 9.14 (Transformed time series of patient data sets)**.** The transformed time series of the data set of a patient is given by

$$\mathcal{D} = \{(t_{1_h}, h_1), \ldots, (t_{u_h}, h_u)\} \cup \{(t_{1_m}, m_1), \ldots, (t_{v_m}, m_v)\} \tag{9.2.1}$$

where u and v are the numbers of data points representing the numbers of healthy and malignant PCs, respectively. Moreover, $\{1_h, \ldots, u_h\} \subseteq \{1, \ldots, j\}$ and $\{1_m, \ldots, v_m\} \subseteq \{1, \ldots, j\}$ represent the index sets of time points at which numbers of healthy and malignant PCs are available, respectively. These time points are arranged as $t_{1_h} \leq t_{2_h} \leq \cdots \leq t_{u_h}$ and $t_{1_m} \leq t_{2_m} \leq \cdots \leq t_{v_m}$.

The transformed data do not differentiate between cells out- and inside the niche but give the total number of healthy and malignant PCs, respectively. Along these lines, the myeloma model (5.0.1) is only partially observed, see Appendix A.3.2.

10 Parameter estimation approach

10.1 Calibration of the healthy equilibrium

Before the population of malignant PCs arrives at the bone marrow and begins to accumulate, healthy PCs are at homoeostasis. Since PCs outside the niche are distinguished in the myeloma model from those inside the niche, an assumption on the fraction of PCs outside the niche at healthy equilibrium is required.

Referring Section 1.1, approximately 30 waves of about 10^7 PCs arrive at the bone marrow per year. Assuming that these waves are equally distributed over one year, such a wave arrives at the bone marrow after 12 days. It is known that PCs in the bone marrow may survive for month, whereas plasma blasts die within few days [57]. Taking a half-life time of PCs outside the niche of 40 days [2, 9, 94] implies an average number of PCs outside the niche being in the magnitude of at least 10^7 cells, which is 1% of 10^9 cells. The latter is the estimated total number of PCs in the bone marrow by Radbruch et al. [94]. This is in accordance with further observations reporting that that at least 90% of all PCs are located inside the niche [15, 121].

Assumption 10.1 (Healthy PCs outside the niche at healthy equilibrium)**.** At healthy equilibrium, it is assumed that

(1) the fraction of PCs outside the niche comprises 1% of the total number of healthy PCs in the bone marrow.

(2) the half-live time of PCs outside the niche is 40 days [2, 9, 94].

In Chapter 9, it was deduced that the total number of healthy PCs at healthy equilibrium is in the magnitude of 10^{10} cells, see Assumption 9.7. Due to inter-individual variability in the level of Ig and thus in the number of healthy PCs at equilibrium (see Section 1.1), taking this value for each individual patient may lead to large deviations between the model responses and the data. The patient-specific

number varies in a range around 10^{10} cells just as the total concentration of Ig varies in a range around 13 g/l, see Assumption 9.7.

Example 10.2. From Jolliff et al. [55] it can be deduced that about 95% of the Ig concentrations for adult normal-weighted healthy patients lie within the interval $(7.65, 20.13)$ (in g/l). Consequence 9.8 implies an (approximate) 95% interval for the total number of healthy PCs at healthy equilibrium given by $(3/5 \cdot 10^{10}, 8/5 \cdot 10^{10})$. Similar results can be deduced from [32].

Assumption 10.3 (Total number of healthy PCs at healthy equilibrium)**.** For each patient data set, there exists a $k = 1, \dots, 12$ such that the number of healthy PCs at healthy equilibrium can be approximated by $k/5 \cdot 10^{10}$ PCs.

Observe that Assumption 10.3 expands the interval described in Example 10.2 and implies a discretisation. Thereby, the value of k is chosen such that the resulting solutions of the myeloma model fit the data best for each patient data set. The exact procedure is explained in Section 10.5.

Considering the myeloma model at healthy equilibrium E_h (see Chapter 5), Assumptions 9.7, 10.1 and 10.3 imply the following model calibration at the healthy equilibrium E_h.

Consequence 10.4 (Calibration of the healthy equilibrium)**.** *Consider the myeloma model* (5.0.1) *at healthy equilibrium E_h. Let Assumption 9.7, 10.1 and 10.3 hold. Then, the following parametrisation holds true:*

$$\begin{aligned} x_h^{E_h} &= \frac{1}{100} \cdot \frac{k}{5} \cdot 10^{10} \text{ PCs} \\ y_h^{E_h} &= \frac{99}{100} \cdot \frac{k}{5} \cdot 10^{10} \text{ PCs} \\ n &= \frac{98}{100} \cdot \frac{k}{5} \cdot 10^{10} \text{ PCs} \\ d &= \frac{\ln(2)}{40} \text{ day}^{-1} \\ f &= \frac{1}{100} \cdot \frac{k}{5} \cdot \frac{\ln(2)}{40} \cdot 10^{10} \text{ PCs} \cdot \text{day}^{-1}, \end{aligned}$$

where $k = 1, \dots, 12$.

Remark 10.5. Observe that f is in the magnitude of 10^8 cells, whereas waves of healthy PCs arriving at the bone marrow are estimated to comprise about 10^7 cells [94]. The difference in the magnitudes arises from different assumptions on the total number of healthy PCs in the bone marrow (i.e. 10^9 cells in [94] versus 10^{10} cells in this work, see Section 9.2).

Calibration of the healthy equilibrium allows the values of the parameters d, f, and n in the myeloma model to be identified. However, this leaves the transition rates b_h, b_m, c_h and c_m to be determined.

The migratory phase of plasma blasts lasts one week [94]. Thus, once arrived at the bone marrow, the phase of PC transition into the niche may be estimated to take place on the time scale of a fraction of one week. The rates of transitions are assumed to be equal for healthy and malignant PCs. Transition into the niche is assumed to happen at the same rate as transition out of the niche. This leads to the following assumption.

Assumption 10.6 (Fixation of transition rates)**.** The transitions rates are assumed to be equal. In particular, $b_h = b_m = c_h = c_m = 1$ day^{-1}.

Remark 10.7. Assumption 10.6 implies no *a priori* advantage of PCs inside the niche compared to PCs outside the niche due to their adhesion to the niche. The influence of fixed transition rates on model solutions is investigated in Section 10.4.

10.2 Vaccination-induced dynamics as plausibility check

In this section it is tested whether the models are able to reproduce biological observations assuming that the calibration given by Consequence 10.4 and Assumption 10.6 holds true. For that, the extended model (4.0.1) with vaccination-induced perturbation of the healthy equilibrium (4.0.5) is considered, see Chapter 4. Without loss of generality, assume that $T = 0$. Further, let $k = 5$. Below, this setting is referred to as calibrated extended model.

At first, the number of vaccination-induced healthy PCs entering the bone marrow, $x^0_{h,v} > 0$, is varied and chosen to be $10^7, 10^8$ and 10^9. In the following, Figure 10.1 is considered:

(a) 10^7 vaccination-induced healthy PCs arrive at the bone marrow and perturb the healthy equilibrium. The fraction of vaccination-induced healthy PCs at the re-established healthy equilibrium is 0.004%.

(b) 10^8 vaccination-induced healthy PCs arrive at the bone marrow and perturb the healthy equilibrium. The fraction of vaccination-induced healthy PCs at the re-established healthy equilibrium is 0.241%.

(c) 10^9 vaccination-induced healthy PCs arrive at the bone marrow and perturb the healthy equilibrium. The fraction of vaccination-induced healthy PCs at the re-established healthy equilibrium is 4.21%.

By Theorem 8.6 it is $z(t) > 0$ for all $0 \leq t < \bar{t}$ and $z(t) \leq 0$ for all $t \geq \bar{t}$, where $\bar{t} = 2.73$. Thus, inflow of PCs into the niche happens until 3 days after the arrival of vaccination-induced PCs at the bone marrow. Observe that approaching the re-established healthy equilibrium takes longer time in case of a larger number of vaccination-induced PCs entering the bone marrow, compare Figure 10.1 (a) and (c).

Results and discussion

Radbruch et al. report that $0.1 - 1\%$ of the „old“ PC population is replaced by PCs created due to an antigen encounter [94]. Simulations indicate that the calibrated extended model is able to reproduce this observation assuming that the number of vaccination-induced PCs entering the bone marrow is between 10^7 and 10^9 cells. Further, knowing that about 10% of the vaccination-induced PCs entering the bone marrow persist in the niche providing humoral immunity for decades [65, 94], the calibrated extended model reproduces this observation choosing $x^0_{h,v}$ in the range of $2 - 3 \cdot 10^7$ (see Table 10.1) whereby $y^E_{h,v} = 33/100 \cdot 10^7$ PCs eventually reside inside the niche.

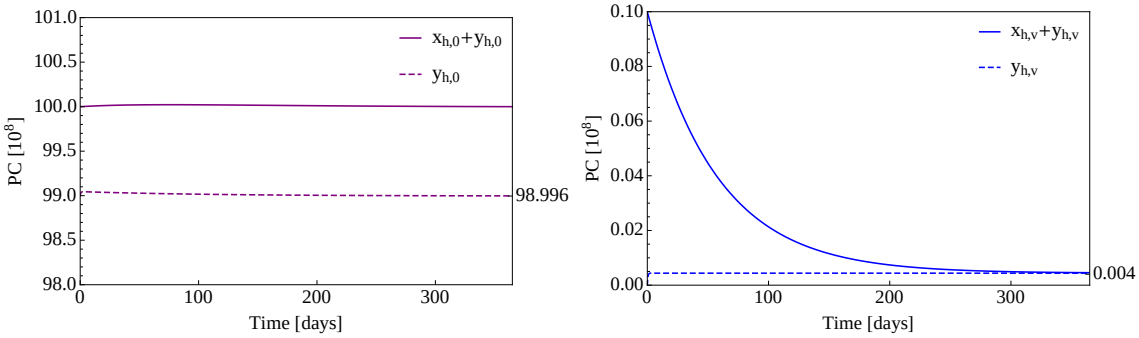

(a) $x^0_{h,v} = 10^7$

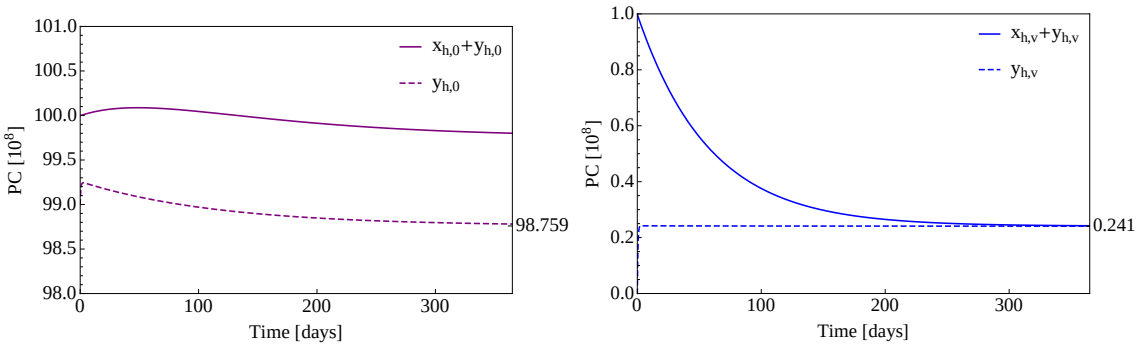

(b) $x^0_{h,v} = 10^8$

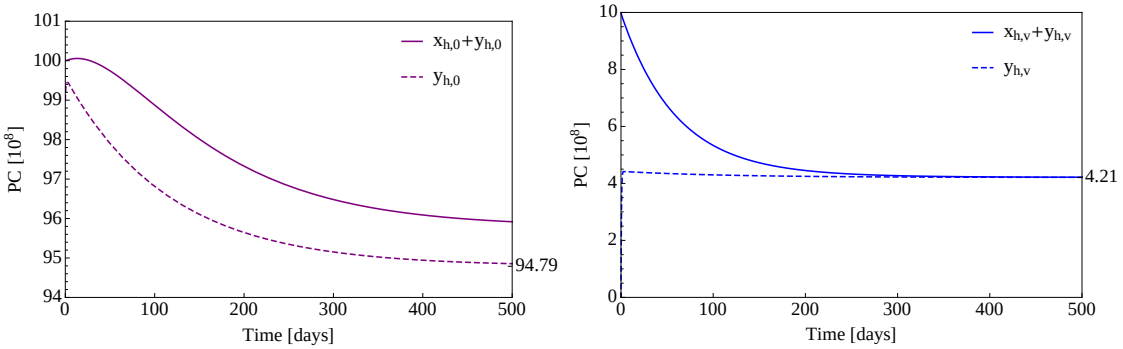

(c) $x^0_{h,v} = 10^9$

Figure 10.1: Vaccination-induced perturbation of the healthy equilibrium for $x^0_{h,v} \in \{10^7, 10^8, 10^9\}$. Left: Dynamics of the number of pathogen-induced healthy plasma cells (PCs) in total (purple) and inside the niche (dashed purple). Right: Dynamics of the number of vaccination-induced healthy PCs in total (blue) and inside the niche (dashed blue). Ranges of axes are adjusted for optimised visualisation of results. For details, see text.

Further investigation focuses on the question of how many vaccinations of a second antigen would be needed to decrease the newly established immunity characteristic $y^E_{h,v} = 33/100 \cdot 10^7$ PCs to 50%. For that, a simulation experiment is performed using the calibrated extended model. Having obtained the re-established healthy equilibrium $E \in \mathcal{E}$ with components $x^E_{h,0},\ x^E_{h,v}$ and $y^E_{h,0},\ y^E_{h,v}$, initial conditions $x^0_{h,0} = x^E_{h,0} + 3 \cdot 10^7,\ x^0_{h,v} = x^E_{h,v}$ and $y^0_{h,0} = y^E_{h,0},\ y^0_{h,v} = y^E_{h,v}$ are used to simulate a perturbation of E induced by a vaccination of an antigen different to the prior. This generates the next re-established healthy equilibrium $E_1 \in \mathcal{E}$, see Theorem 8.5. This procedure is repeated n times ($n \in \mathbb{N}$) until $y^{E_n}_{h,v} \leq y^E_{h,v} = 1/2 \cdot 33/100 \cdot 10^7$ PCs holds true for the first time.

Table 10.1: Portion of persisting vaccination-induced healthy plasma cells (PCs) after vaccination.

Initial condition $x^0_{h,v}$	**Persisting PCs**
10^4	$< 0.05\%$
10^5	0.05%
10^6	0.48%
10^7	4.39%
$2 \cdot 10^7$	8.04%
$3 \cdot 10^7$	11.13%
$4 \cdot 10^7$	13.78%
$5 \cdot 10^7$	16.08%
$6 \cdot 10^7$	18.08%
$7 \cdot 10^7$	19.85%
$8 \cdot 10^7$	21.42%
$9 \cdot 10^7$	22.82%
10^8	24.08%
10^9	42.10%

Results and discussion

About 480 antigen encounters would be necessary to cause the desired reduction. Assuming that 30 waves of PCs arrive at the bone marrow due to natural antigenic adoptions to humoral immunity [94], this translates into 16 years for the Ig production for a defined antigen to decrease by half on the assumption that no further exposure occurred. This time scale is in accordance with the observation of Radbruch et al. [94] stating that the serum concentration of an antibody specificity would decrease to 50% of the original equilibrium concentration within 23 years.

The observed dynamics are qualitatively in accordance with biological measurements of Bernasconi et al. [9], who report the time course of PCs secreting antibodies to tetanus toxoid after vaccination. Similarly, the results qualitatively match observations of Radbruch et at. [94] describing the kinetics of humoral immune response in mice and are in accordance with the (biological) stability of humoral immunity [94].

10.3 Selection of patient data sets

In order to define a suitable parameter estimation procedure which allows fitting the myeloma model to a transformed time series $\mathcal{D}$ of a corresponding patient given by (9.2.1), data is grouped according to the DT, see Section 9.1. Its calculation is based on the exponential model (2.0.1) which is fitted to data representing the number of malignant PCs.

Definition 10.8 (Associated DT)**.** Consider a patient data set with transformed time series $\mathcal{D}$ given by (9.2.1). The associated DT is the DT τ based on an exponential model (2.0.1) for the data $\{(t_{1_m}, m_1), \ldots, (t_{v_m}, m_v)\}$, see Section 9.1.

Remark 10.9 (Negative DT)**.** If $\tau > 0$, data indicate malignant growth. Biologically, one expects at the same time a decrease in the number of healthy PCs [60]. If $\tau < 0$, data indicates malignant decline. The *a priori* grouping of the patient data sets assists parameter estimation in two ways: Firstly, one may think of excluding patient data sets with a negative associated DT because it seems unlikely for the malignant PC population to decline, and consequently, the indication of an accumulation drop would only be due to normal fluctuations in the data or few data points. Secondly, if one aims to keep those patients with a negative associated DT, the information of a

decline in the data translates into an advantage in terms of a more efficient fitting procedure, see Remark 10.17.

The observation of $\tau < 0$ (or $\tau \approx \infty$) would be in agreement with almost all malignant PCs arriving at the bone marrow in the initial wave. Progression to symptomatic disease would still be possible if driven not by an increase in tumour mass but for example by the development of bone disease. Yet the investigated populations represent early stages of myeloma (AMM and MGUS) being less aggressive. A decrease in the number of malignant PCs could also be explained by competitive dislocation due to normal waves consisting of healthy PCs, possibly more likely to appear within early stages of myeloma. In contrast, such a growth behaviour would not be expected for therapy-requiring myeloma. In order to choose an unbiased approach, patients with $\tau < 0$ are included in the study.

Specifying inclusion criteria of patient data sets which are suitable for parameter estimation in the framework of the myeloma model (see also Definition 9.2), each data set is required at least three data points for both the number of healthy and malignant PCs in the time series $\mathcal{D}$. This is due to the higher complexity of the model and assures the estimation to be more reliable. Data sets with a data range shorter than one year are excluded as long as the growth of the malignant population mirrored by the data is not significantly fast. Referred to the DT-groups stated in Definition 9.3, the absolute value of the associated DT is required to be smaller than four years. To summarise,

Definition 10.10 (Inclusion criteria for the myeloma model)**.** Consider a patient data set with transformed time series $\mathcal{D}$ given by (9.2.1) and with associated DT τ given by Definition 10.8. The patient is included in the parameter estimation procedure of the myeloma model (5.0.1) if the following is satisfied:

(i) $u,\ v \geq 3$.

(ii) If $t_{v_m} - t_{1_m} \leq 1$, then $|\tau| \leq 4$.

10.4 Average healthy equilibrium

Before performing parameter estimation, the myeloma model with malignancy-induced perturbation of the healthy equilibrium is recalled, where the time $t \geq 0$ represents the age of a corresponding patients in years. The system of ODEs is given by

$$\begin{aligned} x_h'(t) &= f - \beta_h(z(t))z(t) - dx_h(t) \\ x_m'(t) &= p_1 x_m(t) - \beta_m(z(t))z(t) \\ y_h'(t) &= \beta_h(z(t))z(t) \\ y_m'(t) &= p_2 y_m(t) + \beta_m(z(t))z(t) \end{aligned} \tag{5.0.1}$$

with surplus of PCs relative to the niche balance $z(t)$ given by

$$z(t) = x_h(t) + x_m(t) - (y_h(t) + y_m(t)) + n, \tag{5.0.2}$$

transition rates $\beta_j(z(t)),\ j \in \{h, m\}$, given by

$$\beta_j(z(t)) = \begin{cases} b_j \frac{x_j(t)}{x_h(t)+x_m(t)} & \text{if } z(t) \geq 0 \\ c_j \frac{y_j(t)}{y_h(t)+y_m(t)} & \text{if } z(t) < 0, \end{cases} \tag{5.0.3}$$

and with malignancy-induced perturbation of the healthy equilibrium at age T, i.e.

$$(x_h(t), x_m(t), y_h(t), y_m(t))^T = \left(x_h^{E_h}, 0, y_h^{E_h}, 0\right)^T$$

for $0 \leq t < T$, and

$$(x_h(T), x_m(T), y_h(T), y_m(T))^T = \left(x_h^{E_h}, x_m^0, y_h^{E_h}, 0\right)^T \quad \text{with } x_m^0 > 0. \tag{5.0.5}$$

In the following, (5.0.5) is interpreted as initial condition for system (5.0.1) with $t_0 = T$. Recall that a corresponding solution is located in $\mathcal{W}$ due to Remark 7.3. The remaining freely selectable parameters are the total number of healthy PCs at equilibrium described by k (see Consequence 10.4), the age T of the patient at which the healthy equilibrium is perturbed by a certain number of malignant PCs x_m^0 arriving at the bone marrow, and the malignant growth parameters p_1 and p_2.

Remark 10.11. Observe that the myeloma model (5.0.1) with arbitrary parameters p_1, p_2 and arbitrary initial conditions k, x_m^0, T is not identifiable. In particular, this is constituted by spot tests revealing large confidence intervals for the estimates (results not shown). Details about identifiability can be found in Appendix A.4.2.

The prior observation suggests to fix the initial conditions k, x_m^0, T and estimate the parameters p_1 and p_2. Yet values for the initial conditions are unknown and cannot be deduced from literature or measurements. In particular, this is the case for the patient-specific malignancy-induced perturbation of the healthy equilibrium, i.e. x_m^0, which may differ greatly within the patient cohort.

At a first attempt, the number of healthy PCs at healthy equilibrium is fixed as the average value, i.e. $k = 5$. By this assumption, the following fitting procedure is defined:

Definition 10.12 (Fitting procedure for average healthy equilibrium)**.** Consider the myeloma model (5.0.1) with malignancy-induced perturbation of the healthy equilibrium (5.0.5) and a patient data set with transformed time series $\mathcal{D}$ given by (9.2.1). Let Consequence 10.4 and Assumption 10.6 hold. Let $k = 5$. This implies that the only freely selectable parameters are given by x_m^0, T and p_1, p_2. The values of the fixed parameters are shown in Table 10.2. Define the following algorithm based on a discretisation of x_m^0 and T:

```
let x_m^0 = 10^q with q = 0, 1, 2, ..., 11
let T = 5r with r = 0, 1, 2, ..., ⌊t̃/5⌋, where t̃ = min{t_{1_h}, t_{1_m}}
for each q do
    for each r do
        estimate p_1 and p_2 and evaluate the goodness of the fit
    end for
end for
```

The output consists of combinations of $\{x_m^0, T, p_1, p_2\}$.

The chosen values for the number of malignant PCs arriving at the bone marrow, $x_m^0 = 10^q$ with $q = 0, 1, 2, \ldots, 11$, represent orders of magnitudes which are biologically plausible and of interest. In particular, the discretisation covers one malignant PC, 10^7 PCs as observed after antigen encounter [94], and an upper limit of 10^{11} PC. For the discretisation in the age T, time steps of five years are chosen up to the maximal

Table 10.2: Fixed parameter values and units for parameter estimation with $k = 5$.

Parameter	**Value**	**Unit**
$x_h^{E_h}$	10^8	# PCs
$y_h^{E_h}$	$99 \cdot 10^8$	# PCs
f	$365 \cdot \frac{\ln(2)}{40} \cdot 10^8$	# PCs $\cdot$ year^{-1}
d	$365 \cdot \frac{\ln(2)}{40}$	year^{-1}
b_h	365	year^{-1}
b_m	365	year^{-1}
c_h	365	year^{-1}
c_m	365	year^{-1}
n	$98 \cdot 10^8$	# PCs

possible year limited by the age of the corresponding patient at the first measurement (as myeloma is initiated before MGUS and AMM are diagnosed). Note that there is a trade-off: A higher refinement implies higher precision in finding the best fit for a chosen initial number of malignant PCs. However, it enlarges the workload of the algorithm due to an increased amount of executions.

Estimation of the model parameters p_1 and p_2 is performed using least squares formulation [106] to minimise the errors between the data and the model output. The least squares cost functional $S(x_m^0, T, p_1, p_2)$ is given by

$$S(x_m^0, T, p_1, p_2) = \sum_{j=1}^{u} |x_h(t_{j_h}) + y_h(t_{j_h}) - h_j|^2 + \sum_{j=1}^{v} |x_m(t_{j_m}) + y_m(t_{j_m}) - m_j|^2.$$

Note that the myeloma model is partially observed, see Appendix A.3.2, i.e. the total number of healthy $(x_h(t) + y_h(t))$ and malignant $(x_m(t) + y_m(t))$ PCs in the bone marrow has to be taken into account, respectively. Optimisation is performed using the method of Nelder and Mead [90]. The estimated variance s^2 is used as

goodness-of-fit measure [106], i.e.

$$s^2 = s^2(x_m^0, T, p_1, p_2) = \frac{S(x_m^0, T, p_1, p_2)}{N-2},$$

where N is the total number of data points in $\mathcal{D}$, i.e. $N = |\mathcal{D}|$. The best fit for the time series $\mathcal{D}$ is obtained by choosing

$$(\bar{x}_m^0, \bar{T}, \bar{p}_1, \bar{p}_2) = \operatorname{argmin} s^2(x_m^0, T, p_1, p_2).$$

s^2 measures the average of the squares of the deviations. The smaller its value, the better the model fits the data. For more details on non-linear parameter estimation, see Appendix A.3.2.

Due to the discretisation in time (T) and initial number of malignant PCs (x_m^0), a variation of 10% in the estimated variance is permitted. This was proven to be adequate for simultaneously minimising the set of best fits and „smoothing“ the discretisation.

Definition 10.13 (Best-fit solutions)**.** Consider the output of the fitting procedure stated in Definition 10.12. Let the best fit for the time series $\mathcal{D}$ be obtained by $(\bar{x}_m^0, \bar{T}, \bar{p}_1, \bar{p}_2)$, and let $\bar{s}^2 = s^2(\bar{x}_m^0, \bar{T}, \bar{p}_1, \bar{p}_2)$ be the corresponding smallest estimated variance. Best-fit solutions are defined as those solutions with corresponding outputs of the fitting procedure satisfying

$$s^2(x_m^0, T, p_1, p_2) \in [\bar{s}^2, \bar{s}^2 + \frac{1}{10} \cdot \bar{s}^2].$$

10.4.1 Results and discussion

The output of the algorithm stated in Definition 10.12 is discussed for three exemplary AMM-patients. Results are shown in Figures 10.2, 10.3 and 10.4. For each figure, the table in part (a) lists the values of s^2 in a matrix, where each element (or box) stands for one parameter estimation problem of finding the best values of p_1 and p_2. Each column represents an initial number of malignant PCs x_m^0 ranging from 10^0 (E0) to 10^{11} (E11), whereas each row represents the age of the patient at which the initial number of malignant PCs appears in the bone marrow, i.e. age 0 up to

age 45 and 50, respectively. The yellow elements in the matrices mark elements corresponding to best-fit solutions according to Definition 10.13. Part (b) visualises best fits including statistical evaluations.

Figure 10.2 (IgA-myeloma Patient 1): The data set contains $N = 17$ data points for the number of healthy and malignant PCs, respectively. Best fits (related to green numbers) are obtained for three malignancy-induced perturbations of the healthy equilibrium of (from left to right) 10^5 malignant PCs arriving at the bone marrow at age 0, 10^6 malignant PCs arriving at the bone marrow at age 15, and 10^7 malignant PCs arriving at the bone marrow at age 30.

Figure 10.3 (IgG-myeloma Patient 2): The data set contains $N = 5$ data points for the number of healthy and malignant PCs, respectively. Best fits (related to green numbers) are obtained for two malignancy-induced perturbations of the healthy equilibrium of (from left to right) 10^9 malignant PCs arriving at the bone marrow at age 0, and 10^{10} malignant PCs arriving at the bone marrow at age 35.

Figure 10.4 (IgG-myeloma Patient 3): The data set contains $N = 3$ data points for the number of healthy and malignant PCs, respectively. Best fits (related to green numbers) are obtained for five malignancy-induced perturbations of the healthy equilibrium of (from left to right) 10^0 malignant PCs arriving at the bone marrow at age 30, 10^1 malignant PCs arriving at the bone marrow at age 35, 10^4 malignant PCs arriving at the bone marrow at age 45, 10^5 malignant PCs arriving at the bone marrow at age 50, and 10^6 malignant PCs arriving at the bone marrow at age 55.

Observe that the best-fit estimates for the net proliferation rates p_1 and p_2 are located within biologically plausible ranges. It is $p_1 \in (-0.01, 0.55)$ per year and $p_2 \in (0.07, 0.92)$ per year. In particular, p_1 can be negative while p_2 is always positive. Indeed, this is the case for all patients with a positive associated DT within the AMM- and MGUS-cohort. Confidence intervals of the estimated parameters p_1 and p_2 are narrow (magnitudes of the standard errors range from 10^{-5} to 10^{-2}) suggesting well-posedness of the parameter estimation problem in matters of parameter identifiability. For details, see Appendix A.4.2.

T \ xm0	E0	E1	E2	E3	E4	E5	E6	E7	E8	E9	E10	E11
0			454	274	112	61	148	373				
5				363	173	65	109	313				
10					269	91	78	250				
15					390	128	62	187	499			
20						179	72	128	418			
25						245	117	80	326			
30						329	183	62	228			
35						439	278	102	133			
40							409	199	69	405		
45								362	109	225		
50									316	81		
55										359		

(a)

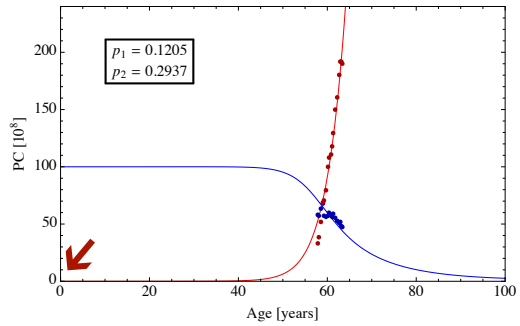

	Estimate	Standard Error	Confidence Interval
p1	0.1205315273727493434	0.0000576357	0.120414 0.120649
p2	0.2937168467988612880	0.000428284	0.292844 0.294589

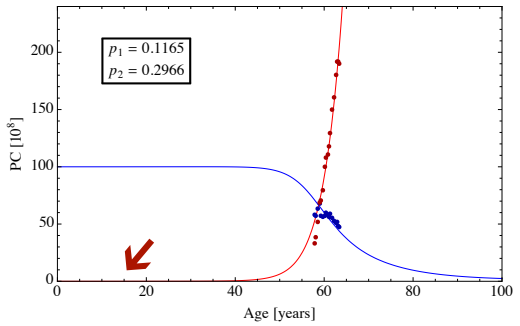

	Estimate	Standard Error	Confidence Interval
p1	0.1164525409825483864	0.000271783	0.115899 0.117006
p2	0.2966325499977927613	0.000113993	0.2964 0.296865

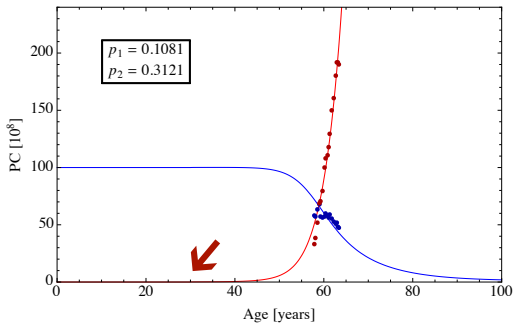

	Estimate	Standard Error	Confidence Interval
p1	0.1081445446766075508	0.000470588	0.107186 0.109103
p2	0.3121174481835264158	0.000392008	0.311319 0.312916

(b)

Figure 10.2: Analysis of the fitting procedure for Patient 1 according to Definition 10.12. (a) Matrix of values of s^2. All values are rounded to natural numbers. Green numbers mark smallest value within a column. Light gray elements mark values bigger than 500. Yellow elements mark best-fit solutions according to Definition 10.13, where $\bar{s}^2 = 61$. (b) Best fits (related to green numbers) of the data (points) are obtained for $x_m^0 = 10^5$ at $T = 0$, $x_m^0 = 10^6$ at $T = 15$, and $x_m^0 = 10^7$ at $T = 30$ (red arrows). The dynamics of the total number of healthy (blue) and malignant (red) plasma cells (PCs) in the bone marrow are shown. Estimated values of p_1 and p_2 are reported in the box and confidence intervals of the estimates are stated.

T \ xm0	E0	E1	E2	E3	E4	E5	E6	E7	E8	E9	E10	E11
0							761	424	250	205	256	396
5							931	506	276	205	251	406
10								623	315	208	246	419
15								796	378	216	240	436
20									479	233	233	460
25									649	269	225	493
30									953	344	216	543
35										512	207	627
40										941	208	792
45											274	
50												

(a)

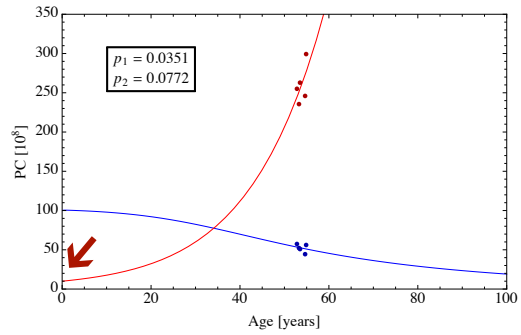

	Estimate	Standard Error	Confidence Interval
p1	0.0350536	0.00645703	0.0201636 0.0499435
p2	0.0771841	0.00282338	0.0706734 0.0836948

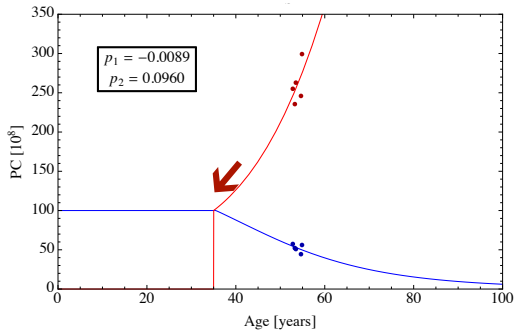

	Estimate	Standard Error	Confidence Interval
p1	-0.00887186	0.010288	-0.032596 0.0148524
p2	0.0960435	0.00603661	0.0821231 0.109964

(b)

Figure 10.3: Analysis of the fitting procedure for Patient 2 according to Definition 10.12. (a) Matrix of values of s^2. All values are rounded to natural numbers. Green numbers mark smallest value within a column. Light gray elements mark values bigger than 1000. Yellow elements mark best-fit solutions according to Definition 10.13, where $\bar{s}^2 = 205$. (b) Best fits (related to green numbers) of the data (points) are obtained for $x_m^0 = 10^9$ at $T = 0$, and $x_m^0 = 10^{10}$ at $T = 35$ (red arrows). The dynamics of the total number of healthy (blue) and malignant (red) plasma cells (PCs) in the bone marrow are shown. Estimated values of p_1 and p_2 are reported in the box and confidence intervals of the estimates are stated.

T \ xm0	E0	E1	E2	E3	E4	E5	E6	E7	E8	E9	E10	E11
0	698	717	895									
5	494	612	785									
10	426	505	668	884								
15	290	391	545	756								
20	190	282	417	618	869							
25	120	185	292	472	715							
30	93	112	180	325	547	842						
35	138	100	103	191	373	649						
40	315	199	109	101	208	438	787					
45	719	519	286	127	99	230	529	973				
50			842	436	187	95	259	654				
55					766	273	91	289	818			
60							604	104	295			
65								904	378	195		

(a)

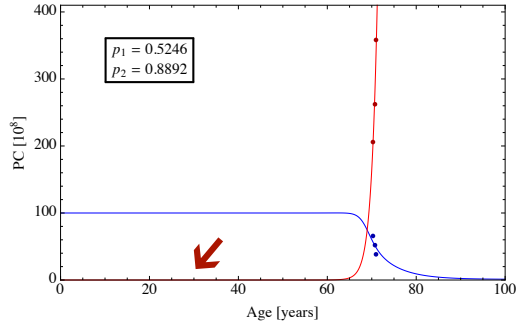

	Estimate	Standard Error	Confidence Interval
p1	0.52461	0.0153064	0.482112 0.567107
p2	0.889222	0.0492203	0.752565 1.02588

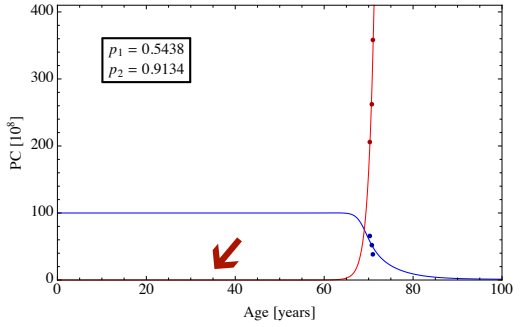

	Estimate	Standard Error	Confidence Interval
p1	0.543825	0.0174335	0.495422 0.592229
p2	0.913355	0.0534381	0.764987 1.06172

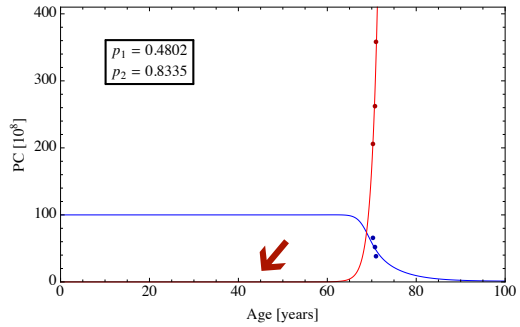

	Estimate	Standard Error	Confidence Interval
p1	0.480196	0.0283233	0.401558 0.558834
p2	0.833479	0.0414062	0.718517 0.948441

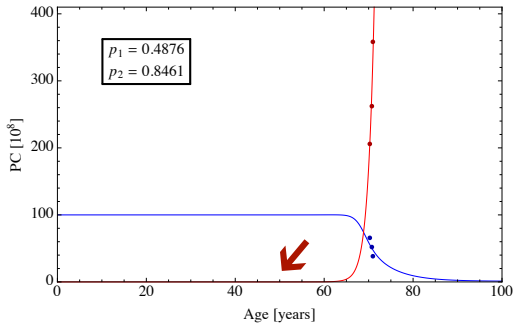

	Estimate	Standard Error	Confidence Interval
p1	0.487556	0.0329089	0.396186 0.578926
p2	0.846134	0.0361868	0.745664 0.946605

(b)

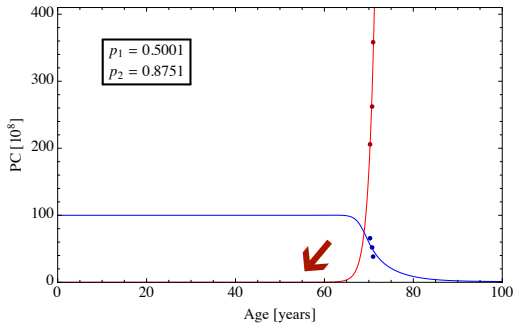

	Estimate	Standard Error	Confidence Interval
p1	0.500099	0.0132248	0.463381 0.536817
p2	0.875135	0.0145139	0.834838 0.915432

(b continued)

Figure 10.4: Analysis of the fitting procedure for Patient 3 according to Definition 10.12. (a) Matrix of values of s^2. All values are rounded to natural numbers. Green numbers mark smallest value within a column. Light gray elements mark values bigger than 1000. Yellow elements mark best-fit solutions according to Definition 10.13, where $\bar{s}^2 = 91$. (b) Best fits (related to green numbers) of the data (points) are obtained for $x_m^0 = 1$ at $T = 30$, $x_m^0 = 10$ at $T = 35$, $x_m^0 = 10^4$ at $T = 45$, $x_m^0 = 10^5$ at $T = 50$, and $x_m^0 = 10^6$ at $T = 55$ (red arrows). The dynamics of the total number of healthy (blue) and malignant (red) plasma cells (PCs) in the bone marrow are shown. Estimated values of p_1 and p_2 are reported in the box and confidence intervals of the estimates are stated.

As indicated by the yellow elements in the matrices in Figures 10.2, 10.3 and 10.4, a set of best-fit solutions is generated (see Definition 10.13) where the best-fit solutions differ marginally with respect to the goodness-of-fit measure s^2. In the following, the appearance of such sets of best-fit solutions is investigated using IgA-myeloma Patient 1 from the AMM-cohort as exemplary patient. Figure 10.5 is considered:

(a) Without loss of generality, a best-fit solution is given by $x_m^0 = 10^6$ at $T = 15$ and estimates $p_1 = 0.1165$ and $p_2 = 0.2966$. The gray-shaded area marks the time range of available data.

(b) Increasing $x_m^0 = 10^7$ while letting the other parameters fixed implies that the number of malignant PCs grows more rapidly, leading to an earlier decrease of the healthy PC population. Therefore, the solution is far away from being a good fit, i.e. approximating the bold curves.

(c) Increasing $T = 30$ while letting the other parameters fixed the solution approaches the best-fit solution. Yet improvement is possible.

(d) A decrease of p_1 combined with an increase of p_2 yields another best-fit solution. Both best-fit solutions coincide well in the gray-shaded area of the given data. There are marginal differences at the boundaries of the area. These deviations vanish in the sense that the solution still leads to a minimal estimate of the variance s^2, see Figure 10.2 (a). Deviations between both best-fit solutions slightly enlarge left and right aside of the gray-shaded area.

A change in the initial condition for the number of malignant PCs can be compensated by variation of the estimates in order to derive a best-fit solution to given data. Along these lines, the myeloma model comprises adequate variability to cope with such perturbations. The difference between two best-fit estimates for different initial conditions is marginal, see $p_1 = 0.1165$ (0.1081) and $p_2 = 0.2966$ (0.3121). This observation is in accordance with non-identifiability of the myeloma model with arbitrary parameters p_1, p_2 and T, x_m^0, see also Remark 10.11.

The previous examples demonstrated the output of the algorithm stated in Definition 10.12. In view of these findings, plausible estimates and best-fit solutions for patient data sets can be derived. However, in more than one third of the data sets the fitting

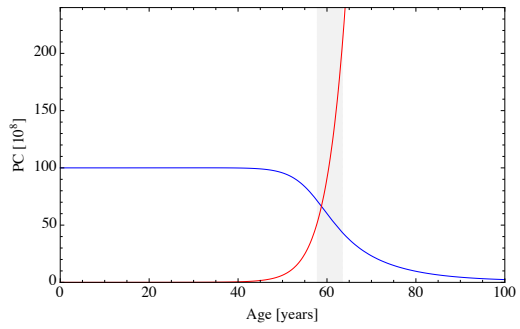

(a) Best fit for $x_m^0 = 10^6$ at $T = 15$ and $p_1 = 0.1165$, $p_2 = 0.2966$.

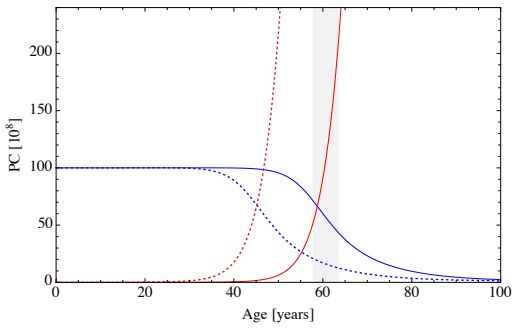

(b) x_m^0 is increased to 10^7.

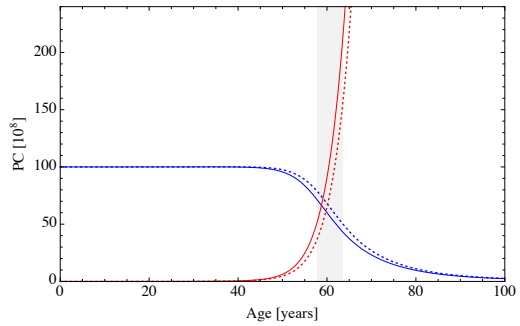

(c) T is increased to 30.

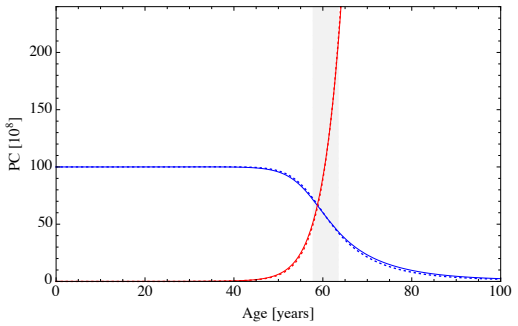

(d) Best fit for $x_m^0 = 10^7$ at $T = 30$ and $p_1 = 0.1081$, $p_2 = 0.3121$.

Figure 10.5: Relationship between two best-for solutions for IgA-myeloma Patient 1. Gray-shaded areas mark time range of given data. Dotted curves illustrate the perturbed solutions for the number of healthy (blue) and malignant (red) plasma cells (PCs) after a change of parameters described in the respective caption. For details, see text.

procedure yields apparently improvable (in the sense of a lower value for s^2) or even implausible fitting results. Figure 10.6 (a) shows an example suggesting a higher initial value for the healthy equilibrium. In contrast, the example in Figure 10.6 (b) suggests a lower healthy equilibrium in order to obtain better fits for the number of healthy PCs. Figure 10.6 (c) exemplifies that taking the average healthy equilibrium as initial condition leads to biologically implausible results. The population of healthy PCs grows, which contradicts clinical observations [60]. Observe that these findings are a consequence of the inter-individual biological variation of healthy Ig levels, see Chapter 1. In Section 10.5, an adequate adaptation of the presented algorithm is provided to deal with these observations.

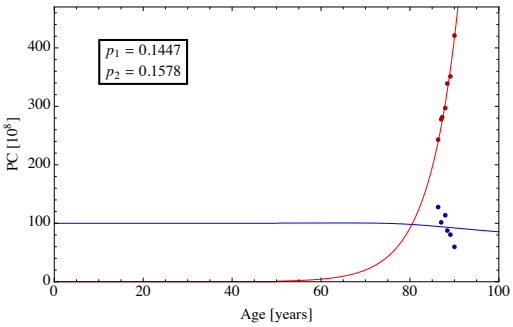

(a) Improvement of fitting results with a higher number of healthy PCs at healthy equilibrium.

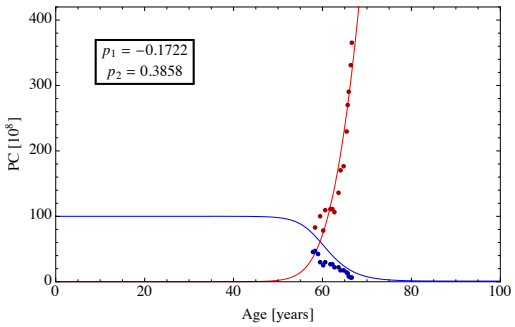

(b) Improvement of fitting results with a lower number of healthy PCs at healthy equilibrium.

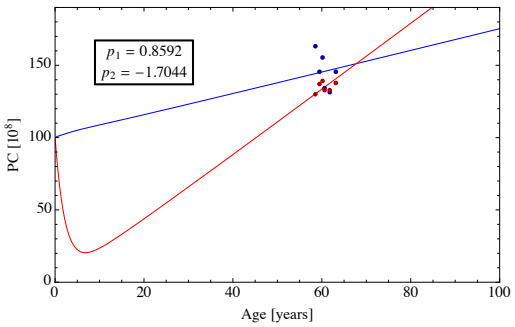

(c) Biologically implausible fitting results due to a low number of healthy PCs at healthy equilibrium.

Figure 10.6: Examples of improvable or implausible best-fit solutions for IgG-myeloma patients. The dynamics of the total number of healthy (blue) and malignant (red) plasma cells (PCs) are shown. For details, see text.

There are deviations which could suggest an increase instead of a decrease in the number of healthy PCs. To comply with clinical observations, the following assumption is used as a further criterion for best-fit solutions.

Assumption 10.14 (Malignant increase excludes healthy increase)**.** The number of healthy PCs does not increase above the healthy equilibrium if the number of malignant PCs increases.

10.4.2 Sensitivity of solutions to changes in the transition rates

The values of the estimates for p_1 and p_2 depend on the values of the fixed parameters listed in Table 10.2 on page 143, deduced from biological observations. It was assumed that transitions are all equal, i.e. $b_h = b_m = c_h = c_m = 1$ day^{-1}, see Assumption 10.6. To avoid arbitrary assumptions, parameter sensitivity of the best-fit solution to alterations in the transition rates are investigated. Details on sensitivity analysis can be found in Appendix A.4.1. Observe that the myeloma model is not continuously differentiable with respect to the parameters. As a consequence, methods of sensitivity analysis cannot directly be applied. However, the system may be approximated by a smooth version. Details are described in Appendix A.2.

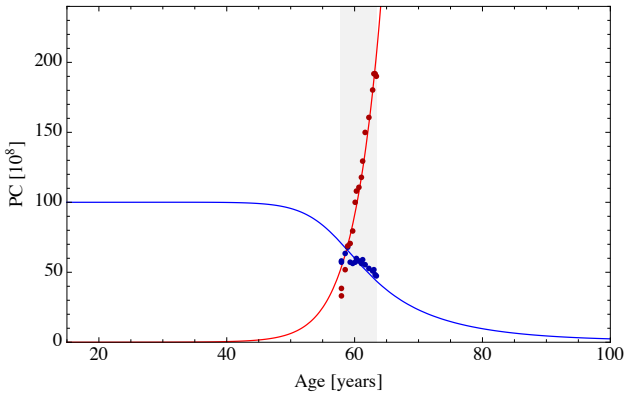

Figure 10.7: Approximated best-fit solution for the data set of Patient 1 with $x_m^0 = 10^6$ at $T = 15$, and estimates $p_1 = 0.1205$ and $p_2 = 0.2937$. The dynamics of the total number of healthy (blue) and malignant (red) plasma cells (PCs) are shown. For approximation, the smoothed model with $\varepsilon = 10^{12}$ is used. Details can be found in Appendix A.2.

In the following, it is shown how a best-fit solution changes if the values of the parameters b_h, b_m, c_h, c_m vary. Consider IgA-myeloma Patient 1 and a corresponding best-fit solution with malignancy-induced perturbation given by $x_m^0 = 10^6$ at $T = 15$. Only relevant time intervals are considered, i.e. starting from the onset of the malignancy at age $T = 15$, see Figure 10.7. The gray-shaded area marks the time range of given data. This area is of particular interest since large variations in the observations within this range affect the estimates, whereas marginal variations hardly have an influence.

Let p_1, p_2 and x_0, T be fixed, and investigate the deviation of the observations $x_h(t) + y_h(t)$ and $x_m(t) + y_m(t)$ from the best-fit solutions for different scenarios for the values of b_h, b_m, c_h, c_m. In the following, Figure 10.8 is considered:

(a) It is investigated how small simultaneous changes of the values of b_h, b_m, c_h, c_m influence the best-fit solutions $x_h(t)+y_h(t)$ and $x_m(t)+y_m(t)$. The sensitivities are normalised relative to the best-fit solutions.

(b) It is investigated how small simultaneous changes in the values of b_h, b_m or c_h, c_m influence the best-fit solutions $x_h(t)+y_h(t)$ and $x_m(t)+y_m(t)$, respectively, while keeping the other parameters fixed at their nominal value. The sensitivities are normalised relative to the best-fit solutions.

(c) It is investigate how small changes in the values of b_h or b_m or c_h or c_m influence the best-fit solutions $x_h(t)+y_h(t)$ and $x_m(t)+y_m(t)$, respectively, while keeping the other parameters fixed at their nominal value. The sensitivities are normalised relative to the best-fit solutions.

The graphs in Figure 10.8 indicate that the number of healthy and malignant PCs, $x_h(t) + y_h(t)$ and $x_m(t) + y_m(t)$, respectively, shows negligible sensitivity to small alterations in the parameters b_h, b_m, c_h, c_m. The highest sensitivities are observed in case (c), although relative sensitivity values are still far below 1%. In case of small changes of c_h or c_m, the number of healthy PCs shows a larger sensitivity compared to the number of malignant PCs. Sensitivity within the range of the data is low, indicating non-identifiability of the respective parameter. Reliable estimation of these parameters on the basis of the given data set would not have been possible. By contrast, sensitivities of the best-fit solutions on small changes in the values of the parameters p_1 and p_2 illustrate their identifiability, see Figure 10.10 on page 158. This is also indicated by narrow confidence intervals of the estimates.

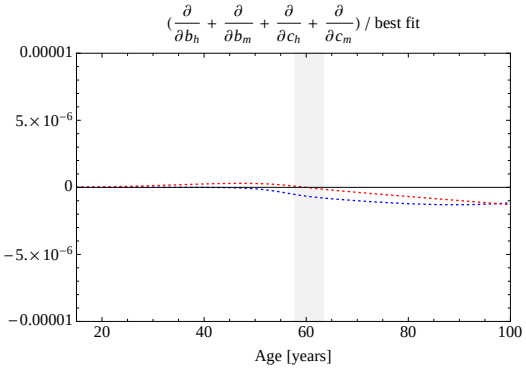

(a) Sensitivity to a simultaneous perturbation of b_h, b_m, c_h, c_m.

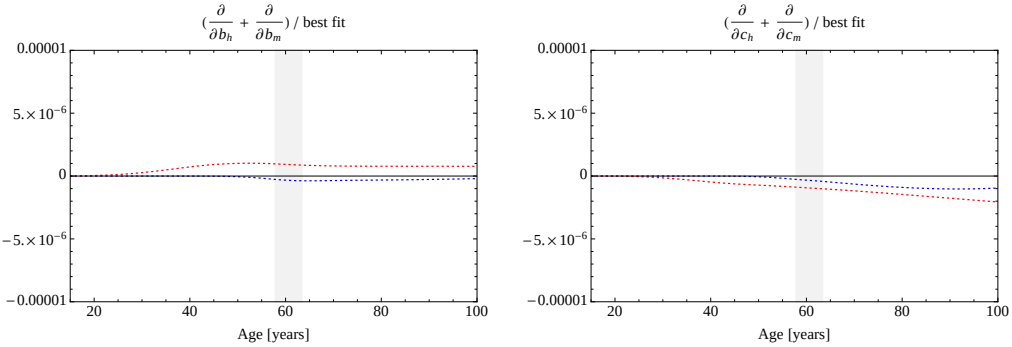

(b) Sensitivity to a simultaneous perturbation of b_h, b_m or c_h, c_m.

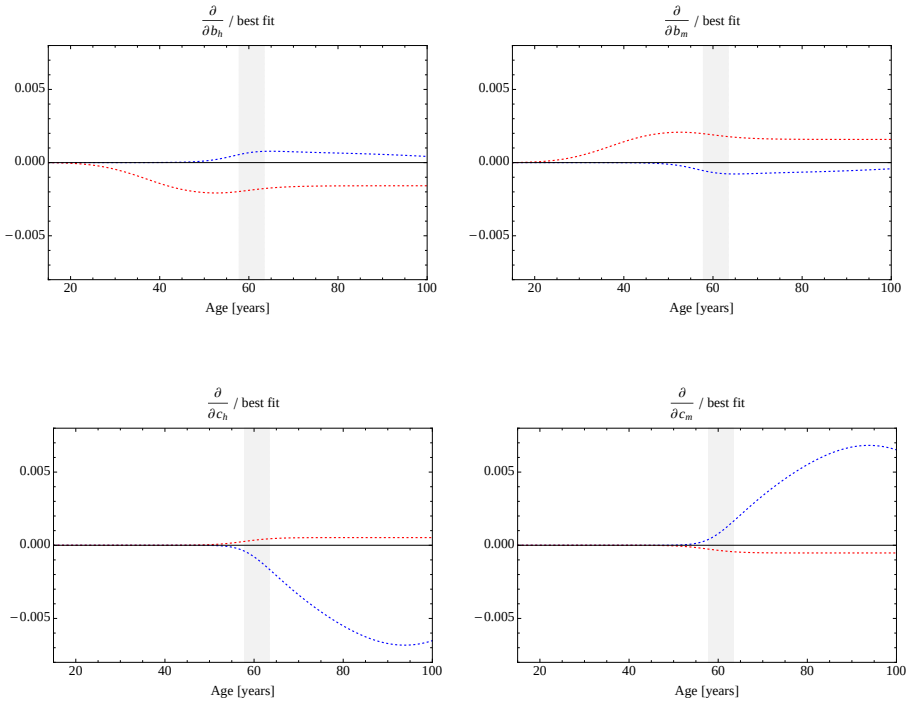

(c) Sensitivity to a perturbation of b_h, b_m, c_h or c_m.

Figure 10.8: Local sensitivity analysis of a best-fit solution of Patient 1: The parameter under investigation is infinitesimally perturbed. The gray area represents the range of the data. Blue dotted: Sensitivity of the total number of healthy plasma cells (PCs) relative to the best-fit solution. Red dotted: Sensitivity of the total number of malignant PCs relative to the best-fit solution.

In view of these findings, small deviations of the values of the transition rates b_h, b_m, c_h, c_m from their nominal value (i.e. $b_h = b_m = c_h = c_m = 1\,\text{day}^{-1}$) are in accordance with the best-fit solutions. To investigate the influence of larger changes in the parameters, the error in the observations is considered. In general, if θ is the parameter under consideration, the difference between the reference solution (i.e. the solution obtained with the nominal value of θ, typically the best-fit value) and the solution obtained with θ altered by $\Delta(\theta)$ needs to be analysed, see Appendix A.4.1. Again, different scenarios for the values of b_h, b_m, c_h, c_m are investigated. In the following, Figure 10.9 is considered:

(a) It is investigated how a simultaneous multiplication by either 10 or 1/10 of the value of b_h, b_m, c_h, c_m influence the best-fit solutions $x_h(t) + y_h(t)$ and $x_m(t) + y_m(t)$. The errors are normalised relative to the best-fit solutions.

(b) It is investigated how a simultaneous multiplication by either 10 or 1/10 of the value of b_h, b_m or c_h, c_m influence the best-fit solutions $x_h(t) + y_h(t)$ and $x_m(t) + y_m(t)$, respectively, while keeping the other parameters fixed at their nominal value. The errors are normalised relative to the best-fit solutions.

(c) It is investigated how a multiplication by either 10 or 1/10 of the value of b_h or b_m or c_h or c_m influence the best-fit solutions $x_h(t) + y_h(t)$ and $x_m(t) + y_m(t)$, respectively, while keeping the other parameters fixed at their nominal value. The errors are normalised relative to the best-fit solutions.

The graphs in Figure 10.9 indicate that larger changes of the parameter b_h, b_m, c_h or c_m cause a larger relative error in the model output up to 2500%, see case (c) (ranges not completely shown), compared to simultaneous changes of parameters as stated in cases (a) and (b). If b_h, b_m or c_h, c_m are simultaneously changed, the deviations are still small, i.e. the relative sensitivities are less than 0.4% for the number of healthy PCs and less than 0.5% for malignant PCs. If b_h, b_m, c_h, c_m are simultaneously changed, the deviations are less than 0.5%. Similar sensitivity analysis yields qualitatively similar results for Patients 2 and 3 (results not shown).

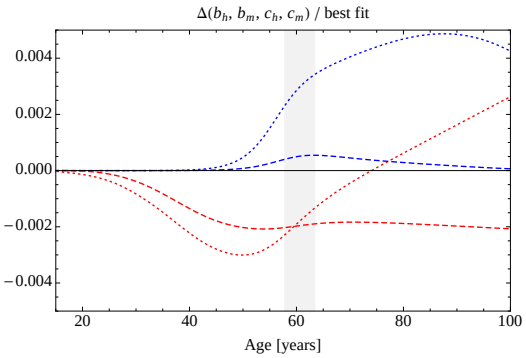

(a) Sensitivity to a simultaneous perturbation of b_h, b_m, c_h, c_m.

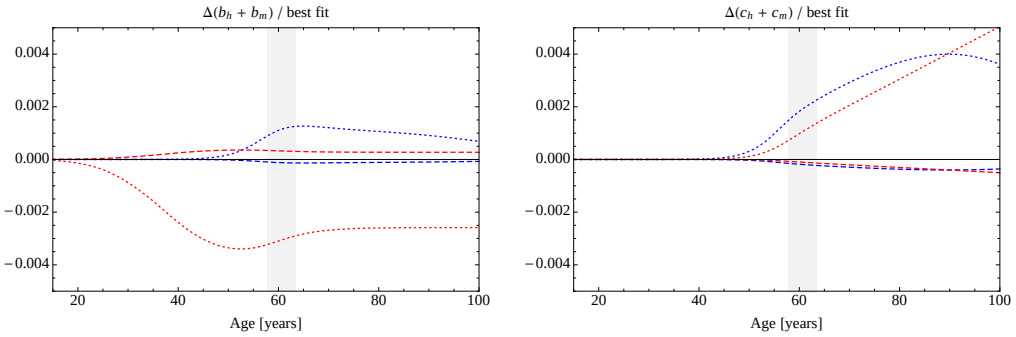

(b) Sensitivity to a simultaneous perturbation of b_h, b_m or c_h, c_m.

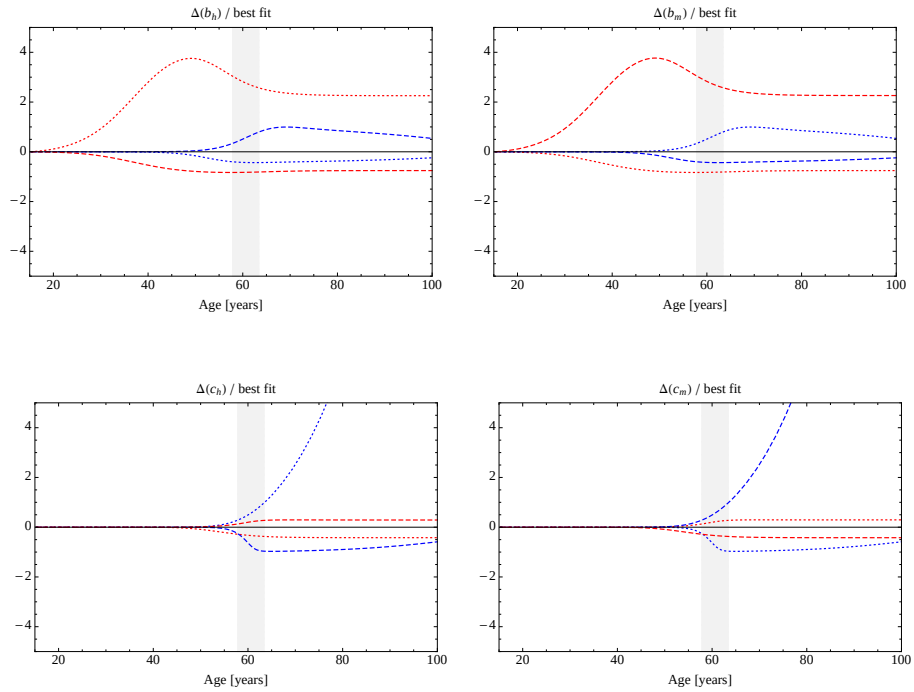

(c) Sensitivity to a perturbation of b_h, b_m, c_h or c_m.

Figure 10.9: Sensitivity analysis of a best-fit solution of Patient 1: The parameter under investigation is multiplied by 10 (dashed) or by 1/10 (dotted), respectively. The gray area represents the range of the data. Blue: Normalised error of the total number of healthy plasma cells (PCs) relative to the best-fit solution. Red: Normalised error of the total number of malignant PCs relative to the best-fit solution.

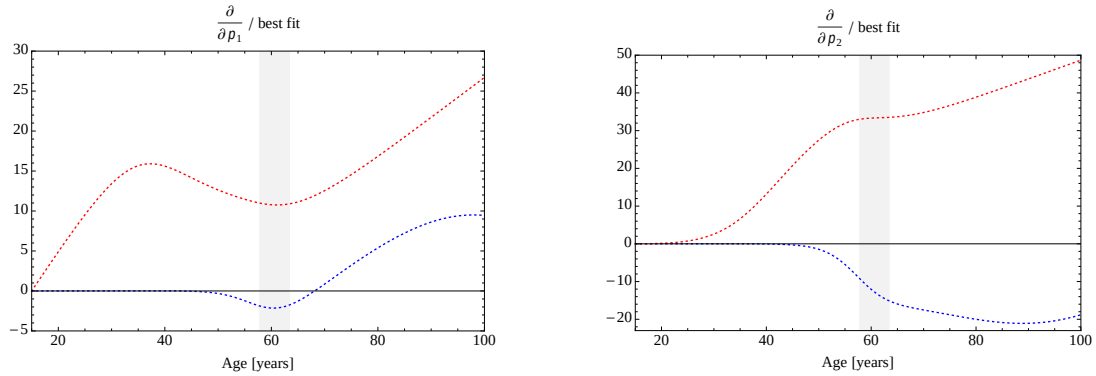

Figure 10.10: Local sensitivity analysis of a best-fit solution of Patient 1: The parameter under investigation is infinitesimally perturbed. The gray area represents the range of the data. Blue dotted: Sensitivity of the total number of healthy plasma cells (PCs) relative to the best-fit solution. Red dotted: Sensitivity of the total number of malignant PCs relative to the best-fit solution. Left: Sensitivity to a perturbation of p_1. Right: Sensitivity to a perturbation of p_2.

Dependent on the precision of the measurements or biological deviations in the measurements, the best-fit estimates still lead to a (biologically and mathematically) plausible fit for the given set of data using perturbations as in cases (a) or (b). Since it was assumed that $b_h = b_m = c_h = c_m$, this assumption can reasonably be loosened by letting $b_h = b_m$ and $c_h = c_m$, and vary either $b_h = b_m$ and/or $c_h = c_m$. Biologically, this implies that transition into and out of the niche may be different. Rates are assumed to be equal for healthy and malignant PCs. For example, $b_h = b_m = 1\,\text{day}^{-1}$ can be kept but $c_h = c_m = 0.5\,\text{day}^{-1}$. Biologically, this could be due to an increase of PC adhesion to the niche, which would imply a reduced transition rate out of the niche.

The results of the sensitivity analysis confirm that the best-fit solution obtained with $b_h = b_m = c_h = c_m = 1\,\text{day}^{-1}$ is still an excellent fit and a best-fit solution for the new parameter setting. Parameter estimation with altered transition rates as stated above yields best-fit solutions with marginal differences in s^2 and the estimates. This was confirmed for a spot test of patient data sets (results not shown). Along these lines, the best-fit solutions are characterised to be robust.

Remark 10.15. Instead of fixing the death rate d of healthy PCs, it could be estimated in addition to the net growth parameters p_1 and p_2. However, spot tests reveal non-identifiability in terms of large estimation errors (results not shown).

10.5 Individual healthy equilibrium

Next, an optimised fitting procedure is presented with an individualised choice of the parameter k. To exemplify the procedure, consider IgA-myeloma Patient 1. The fitting algorithm stated in Definition 10.12 is applied for different values of k. The results in form of the matrices of values of s^2 along with a best-fit solution for $k = 3, \dots, 8$ are shown in Figure 10.12 on page 164. In case of $k = 1, 2$, the fits are biologically implausible (see Assumption 10.14) and for $k = 9, 10, 11, 12$, the values of s^2 exceed 500, implying comparably bad fits.

As observed in case of $k = 5$, there are set of best-fit solutions, see Definition 10.13. For $k = 4$, the estimated variances s^2 exhibit the smallest values compared to all best-fit solutions, see Figure 10.12 (b). Consequently, the optimised choice for k is related to $k = 4$.

This observation enables a structured approach to optimise the fitting procedure stated in Definition 10.12 without the necessity to execute all parameter estimation procedures for each single scenario on the discrete grid $\{k, x_m^0, T\}$, where $k = 1, \dots, 12$ and x_m^0, T. Instead, with the results for $k = 5$, it suffices to identify those columns of the matrix of values of s^2 which possess the smallest values (i.e. where the green elements are the smallest). For this initial number of malignant PCs, the value for k is varied. The individual healthy equilibrium relates to the value of k which leads to the smallest value of s^2 within the chosen columns. For the exemplary Patient 1, column E6 may be chosen to investigate the values of s^2 for different values of k, see Figure 10.11 on page 161.

The adapted fitting algorithm is summarised:

Definition 10.16 (Fitting procedure for individual healthy equilibrium)**.** Consider the myeloma model (5.0.1) with malignancy-induced perturbation of the healthy equilibrium (5.0.5) and a patient data set with transformed time series $\mathcal{D}$ given by (9.2.1). Let Consequence 10.4 and Assumption 10.6 hold. For each $k = 1, \dots, 12$, the only freely selectable parameters are given by x_m^0, T and p_1, p_2. The values of the fixed parameters are shown in Table 10.2. Define the following algorithm based on a discretisation of x_m^0 and T:

1: let $x_m^0 = 10^q$ with $q = 0, 1, 2, \ldots, 11$
2: let $T = 5r$ with $r = 0, 1, 2, \ldots, \lfloor \frac{\tilde{t}}{5} \rfloor$, where $\tilde{t} = \min\{t_{1_h}, t_{1_m}\}$
3: fix k arbitrarily and execute algorithm stated in Definition 10.12
4: identify at least one value of q associated with a best fit; fix q
5: **for** each k **do**
6: **for** each r **do**
7: estimate p_1 and p_2 and evaluate the goodness of the fit
8: **end for**
9: **end for**
10: choose k associated with the best fit such that Assumption 10.14 is satisfied; fix k
11: execute algorithm stated in Definition 10.12

The value of k associated with the best fits is referred to as **individual healthy equilibrium**.

Observe that k is chosen as to the smallest estimated variance and regarding Assumption 10.14. Figure 10.13 on page 166 illustrates the output of the algorithm stated in Definition 10.16 by means of the three data sets of Patients 1, 2 and 3, each showing the matrix of values of s^2 for the individual healthy equilibrium and a best-fit solution. As selection criterion for the best-fit solutions, those scenarios are incorporated which deviate by at most 10% from the smallest s^2 (see Definition 10.13) indicated by the yellow elements.

The optimised fitting procedure given by Definition 10.16 remarkably improves the fits in Figure 10.14. Thus, the myeloma model (5.0.1) is able to reproduce data adequately.

Remark 10.17 (Practical procedure)**.** The fitting procedure consists of an individualised approach. Data-specific properties allow optimising the procedure and avoid long run-times or the occurrence of errors, for example, due to an inappropriate initial guess within the optimisation algorithm. Beside the range of the data, the growth behaviour of the population of malignant PCs is used to select which fitting scenarios on the grid $\{k, x_m^0, T\}$ can be neglected. For instance, if the associated DT is positive, a growing tendency of the malignant PC population in the myeloma model is expected. Thus, 10^{11} malignant PCs can be excluded to constitute the malignancy-induced perturbation if the corresponding data in $\mathcal{D}$ is located within the range 10^9

cells to 10^{10} cells. If the associated DT is negative, relevant malignancy-induced perturbations consist of 10^{10} or 10^{11} malignant PCs.

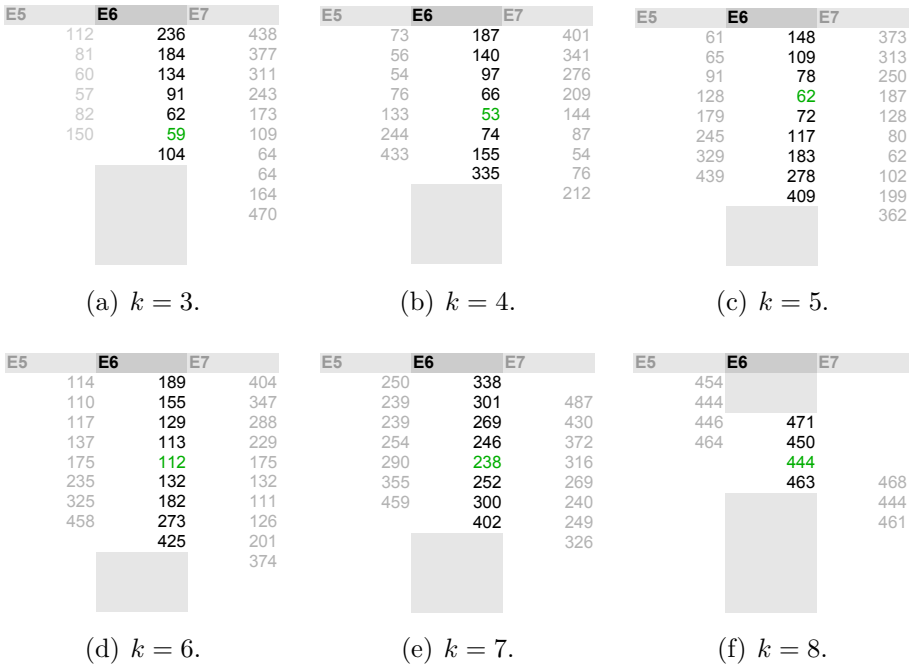

(a) $k = 3$. (b) $k = 4$. (c) $k = 5$.

(d) $k = 6$. (e) $k = 7$. (f) $k = 8$.

Figure 10.11: Visualisation of the parameter estimation approach given by Definition 10.16 for Patient 1. Column E6 (i.e. $q = 6$) is considered for different values of k. The smallest value within a column is obtained for $k = 4$. For details, see text.

T \ xm0	E0	E1	E2	E3	E4	E5	E6	E7	E8	E9	E10	E11
0					66	60	112	236	438			
5					93	57	81	184	377			
10						72	60	134	311			
15						113	57	91	243			
20							82	62	173	440		
25							150	59	109	347		
30								104	64	246		
35									64	144		
40									164	67	427	
45									470	86	241	
50										404	70	
55											281	

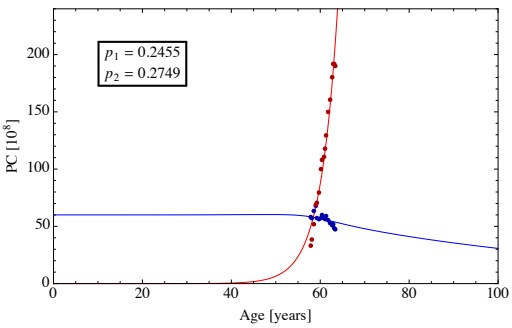

(a) $k = 3$.

T \ xm0	E0	E1	E2	E3	E4	E5	E6	E7	E8	E9	E10	E11
0		360	223	114	57	73	187	401				
5		483	314	172	77	56	140	341				
10			440	260	121	54	97	276				
15				386	198	76	66	209				
20					322	133	53	144	422			
25						244	74	87	330			
30						433	155	54	230			
35							335	76	131			
40								212	60	413		
45									95	228		
50									452	66		
55										324		

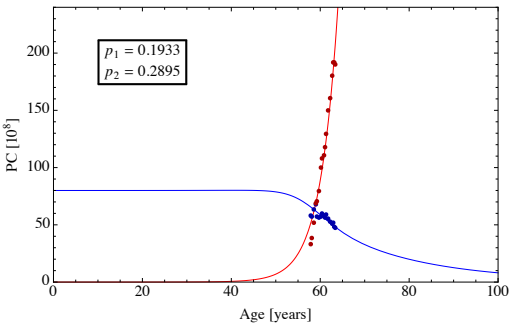

(b) $k = 4$.

T \ xm0	E0	E1	E2	E3	E4	E5	E6	E7	E8	E9	E10	E11
0			454	274	112	61	148	373				
5				363	173	65	109	313				
10					269	91	78	250				
15					390	128	62	187	499			
20						179	72	128	418			
25						245	117	80	326			
30						329	183	62	228			
35						439	278	102	133			
40							409	199	69	405		
45								362	109	225		
50									316	81		
55										359		

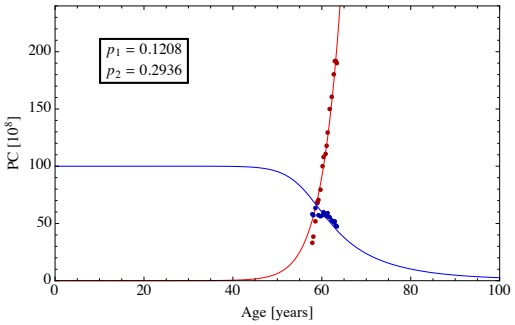

(a) $k = 5$.

T \ xm0	E0	E1	E2	E3	E4	E5	E6	E7	E8	E9	E10	E11
0		499	242	168	122	114	189	404				
5			376	203	141	110	155	347				
10				248	171	117	129	288				
15				308	215	137	113	229				
20				387	277	175	112	175	458			
25					363	235	132	132	369			
30					480	325	182	111	274			
35						458	273	126	182			
40							425	201	118	422		
45								374	133	251		
50									323	123		
55										379		

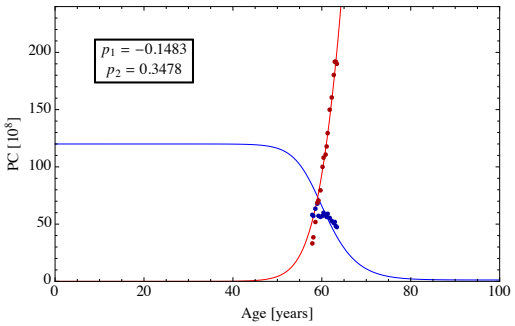

(b) $k = 6$.

T \ xm0	E0	E1	E2	E3	E4	E5	E6	E7	E8	E9	E10	E11
0		343	334	279	242	250	338					
5			427	313	256	239	301	487				
10				363	285	239	269	430				
15				448	331	254	246	372				
20					400	290	238	316				
25						355	252	269	496			
30						459	300	240	405			
35							402	249	316			
40								326	249			
45									257	348		
50										239		
55												

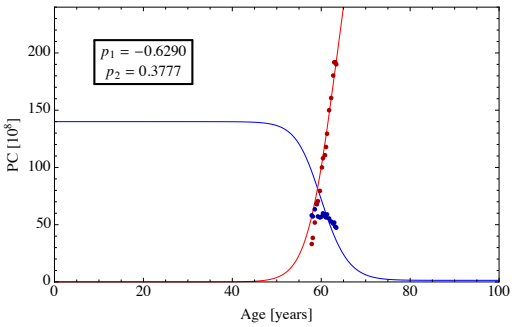

(a) $k = 7$.

T \ xm0	E0	E1	E2	E3	E4	E5	E6	E7	E8	E9	E10	E11
0				491	448	454						
5					465	444						
10					497	446	471					
15						464	450					
20							444					
25							463	468				
30								444				
35								461				
40										449		
45										474		
50											444	
55												

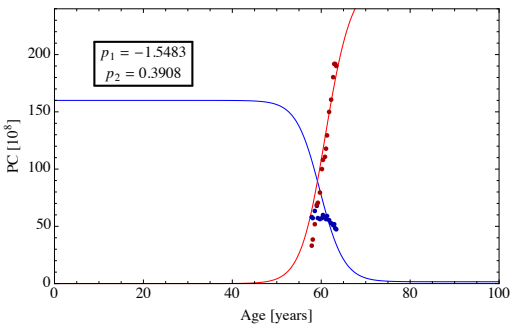

(b) $k = 8$.

Figure 10.12: Results of parameter estimation for Patient 1 for different values of k. Top: Matrix of values of s^2. All values are rounded to natural numbers. Green numbers mark smallest value within a column. Light gray elements either mark values higher than 500, or invalid results according to Assumption 10.14. Bottom: An arbitrarily chosen best-fit solution showing the dynamics of the total number of healthy (blue) and malignant (red) plasma cells (PCs). For details, see text.

T \ xm0	E0	E1	E2	E3	E4	E5	E6	E7	E8	E9	E10	E11
0		360	223	114	57	73	187	401				
5		483	314	172	77	56	140	341				
10			440	260	121	54	97	276				
15				386	198	76	66	209				
20					322	133	53	144	422			
25						244	74	87	330			
30						433	155	54	230			
35							335	76	131			
40								212	60	413		
45									95	228		
50									452	66		
55										324		

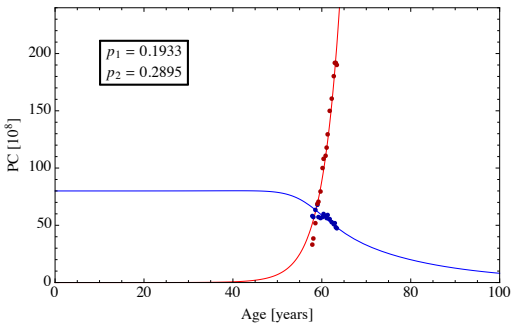

(a) Patient 1: $k = 4$.

T \ xm0	E0	E1	E2	E3	E4	E5	E6	E7	E8	E9	E10	E11
0						987	721	421	244	205	254	388
5							824	498	268	205	249	398
10							942	596	304	207	244	410
15								718	361	215	238	425
20								871	451	231	231	446
25									596	264	223	476
30									813	335	214	520
35										493	206	595
40										883	210	740
45											290	
50												

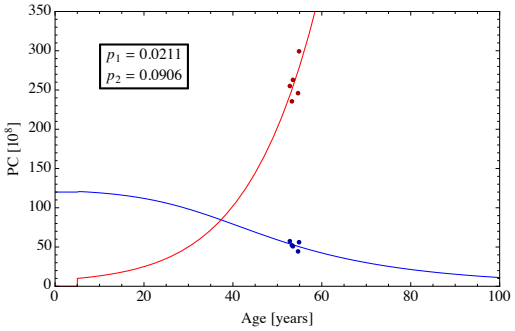

(b) Patient 2: $k = 6$.

T \ xm0	E0	E1	E2	E3	E4	E5	E6	E7	E8	E9	E10	E11
0	451	617	802									
5	357	514	693	918								
10	265	408	578	800								
15	181	311	458	673	935							
20	115	224	338	537	795							
25	82	150	223	397	642	954						
30	86	97	128	259	478	782						
35	153	85	80	141	310	590	971					
40	441	125	107	80	160	384	747					
45		513	259	121	80	188	491	962				
50			720	560	172	79	229	642				
55					609	196	79	279	835			
60					681	521	305	86	308			
65							844	595	223	203		

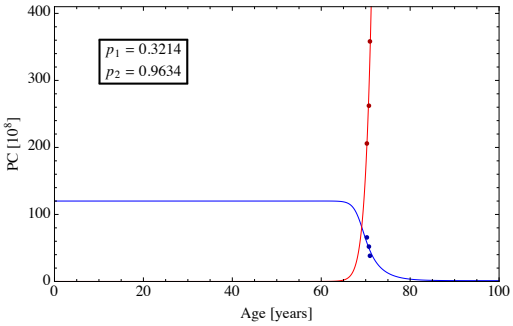

(a) Patient 3: $k = 6$.

Figure 10.13: Analysis of the fitting procedure according to Definition 10.16 yields the individual healthy equilibrium k and the respective matrix of values of s^2 (left) for Patients 1, 2 and 3. All values are rounded to natural numbers. Green numbers mark smallest value within a column. Light gray elements mark values higher than 500 (1000) for case (a) (for cases (b) and (c)). Yellow elements mark best-fit solutions according to Definition 10.13. Right: An arbitrarily chosen best-fit solution showing the dynamics of the total number of healthy (blue) and malignant (red) plasma cells (PCs). For details, see text.

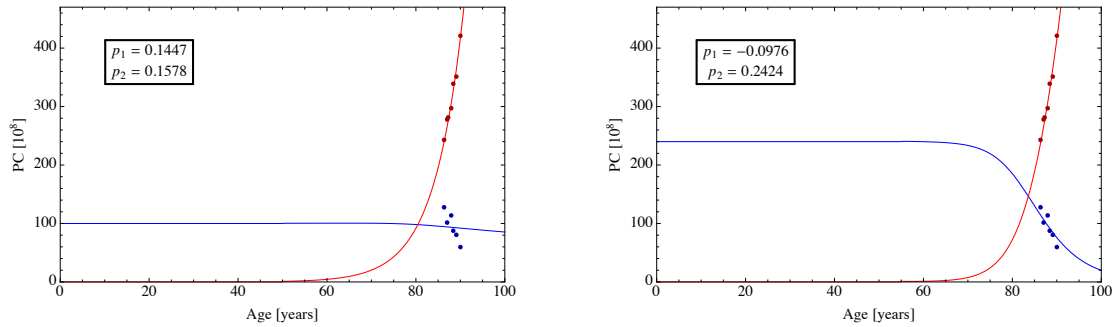

(a) $k = 12$ leads to an improvement of best-fit solutions.

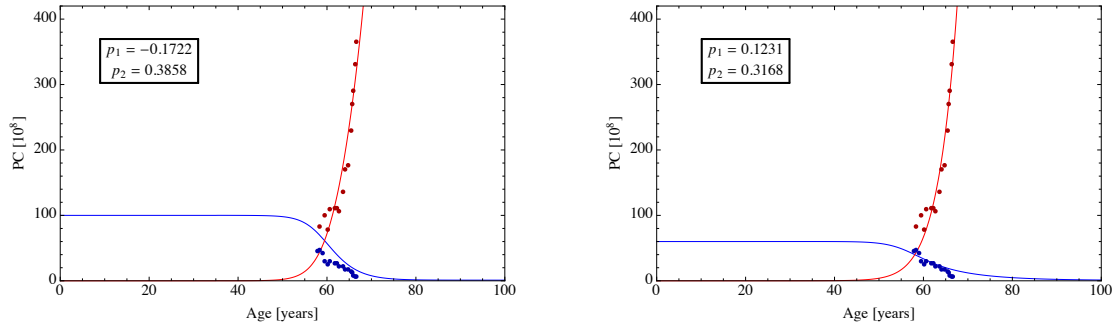

(b) $k = 3$ leads to an improvement of best-fit solutions.

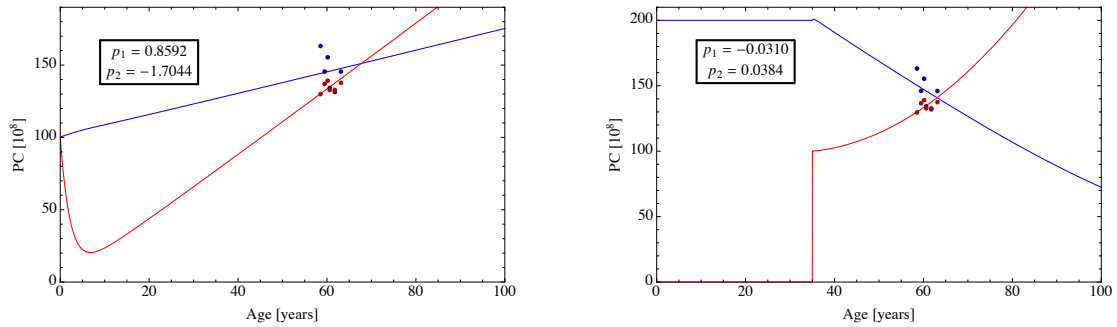

(c) $k = 10$ leads to an improvement of best-fit solutions.

Figure 10.14: Examples of improved best-fit solutions for IgG-myeloma patients due to the choice of an individual healthy equilibrium. The dynamics of the total number of healthy (blue) and malignant (red) plasma cells (PCs) are shown. Left: A best-fit solution for $k = 5$, see Figure 10.6. Right: A best-fit solution for the individual k. For details, see text.

11 Evaluation of parameter estimation

11.1 Statistical evaluation

Referring to Chapter 9, data sets of 254 AMM-patients (67 IgA-myeloma, 187 IgG-myeloma) and 156 MGUS-patients (31 IgA-myeloma, 125 IgG-myeloma) are qualified for parameter estimation. Applying the inclusion criteria given by Definition 10.10 results in 187 eligible AMM-patients (52 IgA-myeloma, 135 IgG-myeloma) and 104 MGUS-patients (27 IgA-myeloma, 77 IgG-myeloma). In about 80% of the 187 AMM-patients (43/52 IgA-myeloma, 110/135 IgG-myeloma) and in about 65% of the 104 MGUS-patients (18/27 IgA-myeloma, 52/77 IgG-myeloma), the surrogate for the number of malignant PCs indicates a growth of the malignant PC population with respect to a positive associated DT, see Definition 10.8.

In the following, the outcomes from parameter estimation are evaluated. Since inference should only be based on adequate fitting results, a further selection criterion is added for a data set being included into the evaluation process.

Definition 11.1 (Selection criterion for evaluation)**.** Consider a patient data set with transformed time series $\mathcal{D}$ given by (9.2.1) which was included into the parameter estimation procedure stated in Definition 10.16. Let $\bar{s}^2$ be the smallest estimated variance for the chosen individual healthy equilibrium. Then, this patient is included into the evaluation process if $\bar{s}^2 < 1000$, and denoted as **eligible patient**.

The additional selection criterion is chosen to exclude fits obtaining outliers or severe variations in the data, yielding 185 AMM-patients (52 IgA-myeloma, 133 IgG-myeloma) and 101 MGUS-patients (26 IgA-myeloma, 75 IgG-myeloma) considered appropriate for evaluation. Table 11.1 provides an overview of eligible AMM- and

MGUS-patients separated into IgA- and IgG-myeloma and positive/negative associated DT τ.

Table 11.1: Eligible patients within the AMM- and MGUS-cohort.

	AMM			**MGUS**		
	IgA	IgG		IgA	IgG	
Total	**52**	**133**		**26**	**75**	
$\tau > 0$	43	108	(82%)	18	51	(68%)
$\tau < 0$	9	25	(18%)	8	24	(32%)

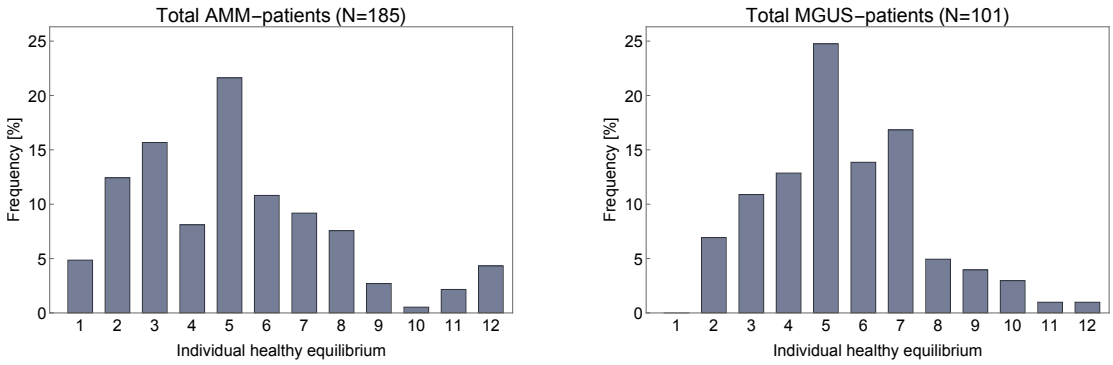

Figure 11.1: Frequencies of individual healthy equilibria within the AMM- and MGUS-cohort of eligible patients. N is the total number of patients within the respective cohort. Mean values are given by 5.1 for the AMM-cohort (left) and 5.5 for the MGUS-cohort (right).

Remark 11.2. In total, there are 2071 data points representing the number of healthy PCs, and 1753 data points representing the number of malignant PCs. In average, a time series is composed of 11 data points representing the number of healthy PCs for both IgA- and IgG-myeloma, and 11 and 9 data points representing the number of malignant PCs for IgA- and IgG-myeloma, respectively.

Figure 11.1 depicts the frequencies of the individual healthy equilibria as part of best-fit solutions of eligible patients, see fitting procedure stated in Definition 10.16 and Definition 10.13. These data-driven findings are in accordance with the Assumptions 9.5, 9.7 and 10.3 in regard to the average value given by $k = 5$ (mean values are 5.1 for the AMM-cohort and 5.5 for the MGUS-cohort).

In the remaining part of this chapter, best-fit solutions within the AMM- and MGUS-cohort are investigated. Firstly, evaluation of the estimates p_1 and p_2 is focused allowing characterising malignant growth. Secondly, information on the malignancy-induced perturbation of the healthy equilibrium (x_m^0 and T) corresponding to best-fit solutions is exploited. Thereby, the initial number of malignant PCs in myeloma is analysed. Histograms were generated using the software package *Mathematica, Version 10* by Wolfram Research.

11.2 Characterisation of malignant growth

Observe that for each patient there exists a set of best-fit solutions (see Definition 10.13) involving estimates for the net growth parameters of malignant PCs, i.e. p_1 for the growth of malignant PCs outside the niche, and p_2 for the growth of those inside the niche.

11.2.1 Growth patterns

Referring to the results of Section 7.5, the estimates p_1 and p_2 determine how the growth of the populations of healthy and malignant PCs is characterised expecting the solutions either to approach an equilibrium (i.e. E_m), a partial equilibrium (i.e. $E_{p,2}(t)$) or to decline. By means of six representative patients, Figure 11.2 visualises solutions types of the myeloma model which are identified as best-fit solutions within the AMM- and MGUS-cohort, respectively. For their frequencies, see Table 11.2.

Remark 11.3. To calculate the statistics in Table 11.2, a best-fit solution for each eligible patient was chosen. All best-fit solutions for one patient imply the same growth pattern as verified for a spot test of patients (results not shown).

Table 11.2: Frequencies of solution types of the myeloma model within the AMM- and MGUS-cohort of eligible patients.

	AMM			**MGUS**		
	IgA	IgG		IgA	IgG	
Solution type A	35	79	(62%)	13	43	(55%)
Solution type B	8	35	(23%)	7	16	(23%)
Solution type C	9	19	(15%)	6	16	(22%)

Solution type A: Figure 11.2 (a) shows the most common solution type, which is observed in the set of best-fit solutions for 62% and 55% of the patients within the AMM- and MGUS-cohort, respectively. Mathematically, the model solution approaches a partial equilibrium (see Chapter 7), i.e. the population of malignant PCs increases whereas the population of healthy PCs decreases not becoming entirely extinct (due to the constant inflow of healthy PCs into the bone marrow by model assumption). Note that unbounded growth of the total population of malignant PCs can be achieved even if $p_1 < 0$, i.e. malignant PCs outside the niche die. The estimates lie in a biologically plausible range. Regarding Patient A1, the estimates imply that the number of malignant PCs outside and inside the niche grows by about 19% or 29% per year, respectively.

Solution type B: Figure 11.2 (b) depicts a solution type which is observed in 23% of the patients within each cohort. Mathematically, the model solution approaches the total equilibrium E_m (see Chapter 7), i.e. the population of malignant PCs increases and approaches an equilibrium state whereas the population of healthy PCs decreases not becoming entirely extinct. The dynamics are due to relatively dominant negative growth of malignant PCs outside the niche, whereby proliferation inside the niche cannot compensate for growth inhibition, i.e. $p_2 < \frac{c_m p_1}{p_1 - c_m}$. In contrast to Patient B2, the equilibrium is approached relatively fast in case of Patient B1.

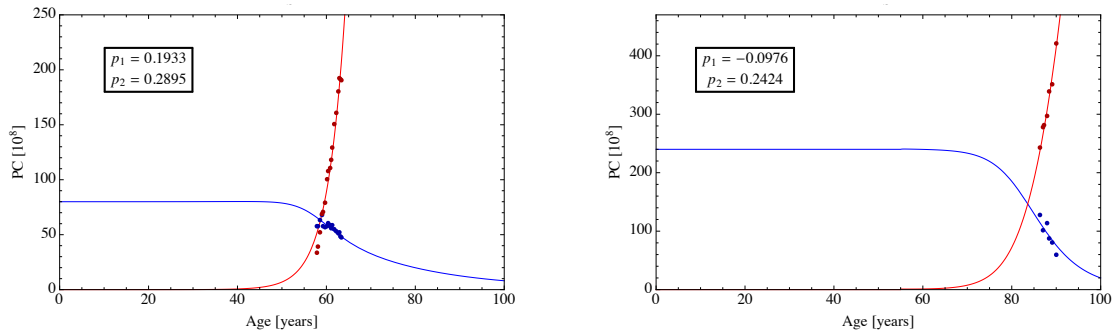

(a) Solution type A: Increase in the number of malignant PCs. Left: Patient A1. Right: Patient A2.

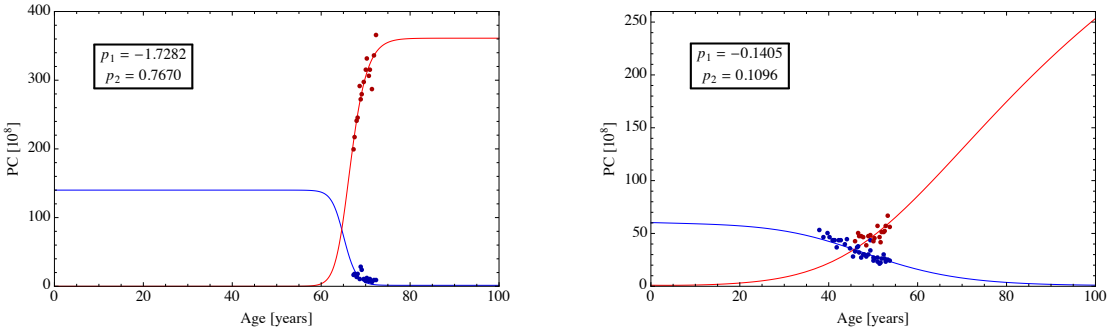

(b) Solution type B: Retarded increase in the number of malignant PCs. Left: Patient B1. Right: Patient B2.

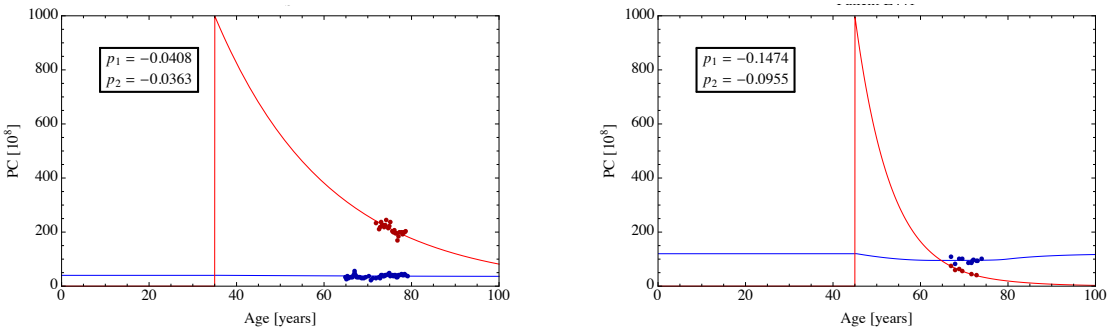

(c) Solution type C: Decrease in the number of malignant PCs. Left: Patient C1. Right: Patient C2.

Figure 11.2: Solution types of the myeloma model observed as best-fit solutions within the AMM- and MGUS-cohort of eligible patients. Different growth behaviour for the total number of healthy (blue) and malignant (red) plasma cells (PCs) is observed. For details, see text.

Solution type C: Figure 11.2 (c) exemplifies a solution type which is observed in 15% and 22% of the patients within the AMM- and MGUS-cohort, respectively. Mathematically, the model solution approaches the healthy equilibrium E_h (see Chapter 7), i.e. the population of malignant PCs decreases indicated by negative net growth rates $p_1, p_2 < 0$. This implies an increase in the number of healthy PCs to the level of healthy homoeostasis, see Patient C2.

Discussion

Relating the results to biology of myeloma, a solution of type A is the most plausible pattern describing the dynamics of the number of healthy and malignant PCs in the bone marrow, see also Figure 9.2. By the observations in Chapter 7, such a growth pattern implies a positive net growth of malignant PCs inside the niche (i.e. $p_2 > 0$), whereas the net growth of malignant PCs outside the niche is always smaller (i.e. $p_1 \leq p_2$) and can be negative. In that sense, residing in the niche is beneficial. Further, the model implies that PCs leave the niche due to faster accumulation inside the niche from advanced stages of the disease onwards (due to $z(t) < 0$ for t large enough), meaning that malignant PCs spill out of the niche.

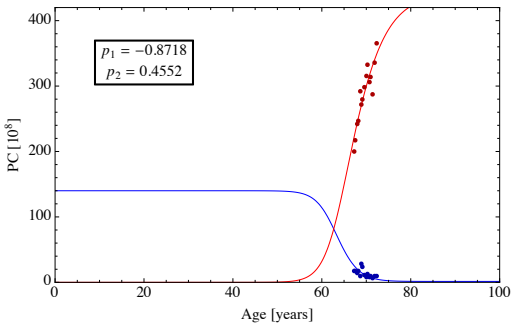

Figure 11.3: Another best-fit solution for Patient B1 out of the set of best-fit solutions, where the dynamics of the total number of healthy (blue) and malignant (red) plasma cells (PCs) are shown. The depicted solution reflects a more realistic biological scenario of retarded growth in the number of malignant PCs compared to Figure 11.2 (b). For details, see text.

A solution of type B is characterised by approaching the equilibrium E_m, see Chapter 7. In case of Patient B2, approaching the plateau takes a long time exceeding the lifetime

of the patient. This characterises a slow growth of the population of malignant PCs being in accordance with slow DTs, see Figure 9.2. A solution as observed for Patient B1 is not supported by any data which would justify the occurrence of a plateau [47], i.e. there is no single measurement in favour of such behaviour. The presented solution is chosen as one representative out of the set of best-fit solutions, see Definition 10.13. Choosing another best-fit solution gives a more realistic growth pattern as no plateau is reached within the patient's lifetime, see Figure 11.3.

A solution of type C is predominantly correlated with negative associated DTs. The decline in the malignant PC population would imply that myeloma would never manifest. Observe that this scenario depicts an unlikely high number of malignant PCs arriving at the bone marrow (10^{11} cells). Since the parameter estimation procedure considers orders of magnitudes for the initial number of malignant PCs (in particular 10^{10} and 10^{11} cells) and is based on a discretisation of time, a more realistic growth pattern is exemplified by Figure 11.4, where the number of malignant PCs initially arriving at the bone marrow is chosen to comprise $3 \cdot 10^{10}$ cells and $2 \cdot 10^{10}$ cells, respectively. Regarding Patient C2, the graph visualises how the myeloma model captures the replacement process of vanishing malignant PCs by healthy ones in analogy to the dynamics induced after vaccination, see Chapter 4. This implies an increase of the healthy PC population up to its healthy equilibrium.

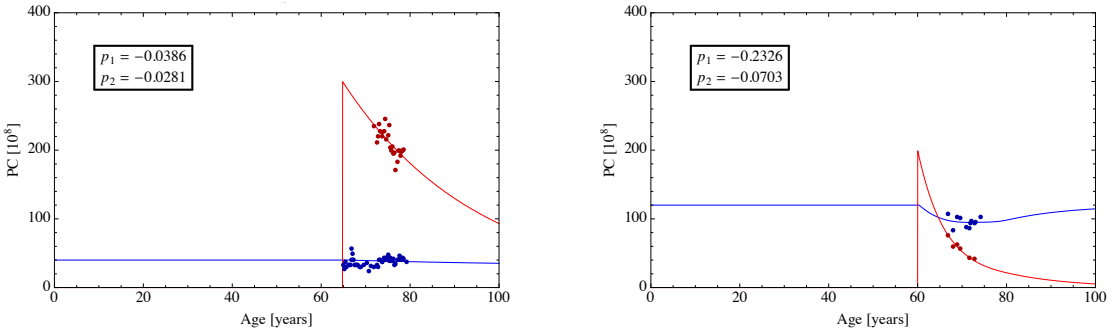

Figure 11.4: Another best-fit solution for Patients C1 (left) and C2 (right), respectively, where the dynamics of the total number of healthy (blue) and malignant (red) plasma cells (PCs) are shown. The initial number of malignant PCs arriving at the bone marrow is adapted to reflect a more realistic value compared to Figure 11.2 (c), respectively. For details, see text.

11.2.2 Dynamic doubling time

Chapter 2 introduced an exponential model

$$m(t) = be^{at}, \quad a \in \mathbb{R},\ b > 0 \ \text{ for } \ t \geq 0 \tag{2.0.1}$$

to explain growth of the malignant PC population. The constant growth rate was applied for defining the DT. By means of (7.4.1) it can be observed for the myeloma model that

$$x'_m(t) + y'_m(t) = \underbrace{\left(p_1 \frac{x_m(t)}{x_m(t) + y_m(t)} + p_2 \frac{y_m(t)}{x_m(t) + y_m(t)}\right)}_{=:\alpha(t)} (x_m(t) + y_m(t)) \,. \tag{11.2.1}$$

This motivates the forthcoming definition of the time-varying equivalent to the DT.

Definition 11.4 (Dynamic DT)**.** Consider the myeloma model (5.0.1) defined on $\mathcal{W}$. Let $\alpha(t)$ be given by (11.2.1). The dynamic doubling time (dynamic DT) of the population of malignant PCs is defined by

$$\tau(t) = \frac{\ln(2)}{\alpha(t)} \ \text{ if } \ \alpha(t) \neq 0.$$

Observe that a change in the sign of $\alpha(t)$ yields a singularity in $\tau(t)$. The dynamic DT allows characterising the growth of the total malignant PC population captured by the myeloma model. It enables to quantify the time-varying accumulation capacity of myeloma and offers means to compare the myeloma model with the exponential model.

Results

Figure 11.5 depicts the associated (constant) DT and the dynamic DT for the best-fit solutions of Patient A1 (left) and Patient A2 (right). Both graphs imply that the dynamic DT approaches a vicinity of the constant DT for large times. In case of Patient A1, the dynamic DT is always slower than the constant DT, whereas it can be faster than the constant DT in case of the right graph. Here, the dynamic DT is negative at the beginning. The singularity due to a change in the sign of $\tau(t)$ is illustrated by a vertical line.

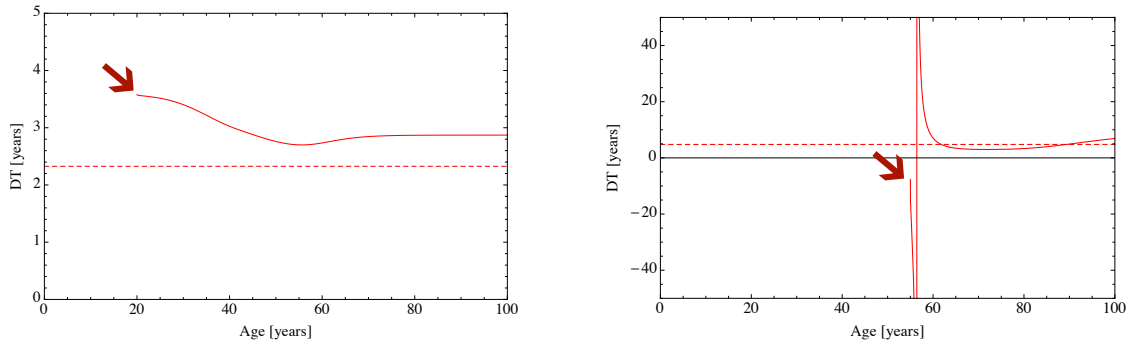

Figure 11.5: Comparison of the constant (dashed) and the dynamic (bold) doubling time (DT) for Patients A1 (left) and A2 (right). The dynamic DT is defined starting from the age of the patient at which the initial number of malignant plasma cells arrives at the bone marrow (red arrow). For details, see text.

Discussion

Biologically, a negative dynamic DT of the population of malignant PCs could be due to a large fraction of malignant PCs outside the niche (due to the initial population arriving at the bone marrow), implying predominant death of the total population. An increase of the fraction of malignant PCs inside the niche leads to predominant accumulation due to proliferation.

The dynamic DT allows explaining the occurrence of solution type B. Considering Patient B1, Figure 11.6 visualises a drastic change in the dynamic DT. This can be explained by a shift in the composition of the total number of malignant PCs in the bone marrow. Inflow of the initial population arriving at the bone marrow implies predominant death of the total population due to negative net growth of malignant PCs outside the niche. Residing in the niche is advantageous and malignant PCs accumulate comparably fast (due to positive net growth inside the niche) implying a fast DT of the total population. This yields malignant PCs spilling out of inside the niche, where a comparably large negative net growth of malignant PCs outside the niche implies cell death leading to a slow DT and retarded growth for the total population.

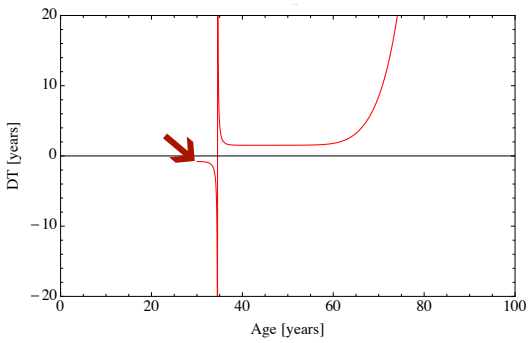

Figure 11.6: Dynamic doubling time (DT) for a best-fit solution of Patient B1 given by Figure 11.3. The dynamic DT is defined starting from the age of the patient at which the initial number of malignant plasma cells arrives at the bone marrow (red arrow). For details, see text.

11.2.3 Niche-dependence

Biologically plausible growth patterns are related to net growth rates satisfying $p_1 \leq p_2$ characterising the niche as a beneficial microenvironment.

Definition 11.5 (Niche-dependence)**.** Consider best-fit solutions of an eligible patient.

(i) If all estimates satisfy $p_1 < 0 < p_2$, the growth of the patient's population of malignant PCs is referred to as as niche-dependent.

(ii) If all estimates satisfy $p_1, p_2 > 0$, the growth of the patient's population of malignant PCs is referred to as niche-independent.

In case of $p_1 < 0 < p_2$, malignant PCs outside the niche die whereas those inside the niche grow. In this case, the niche is essential for the growth of the total population of malignant PCs. If $p_1, p_2 > 0$, the absence of malignant PCs inside the niche would not hinder the total population to increase.

Results

Investigation of niche-dependence for eligible patients within the AMM-cohort reveals that 36% of the patients (53 IgG-myeloma, 13 IgA-myeloma) are categorised as niche-dependent, and 35% of the patients (39 IgG-myeloma, 25 IgA-myeloma) as niche-independent. It is $p_1 < p_2$ true even in cases of niche-independence being

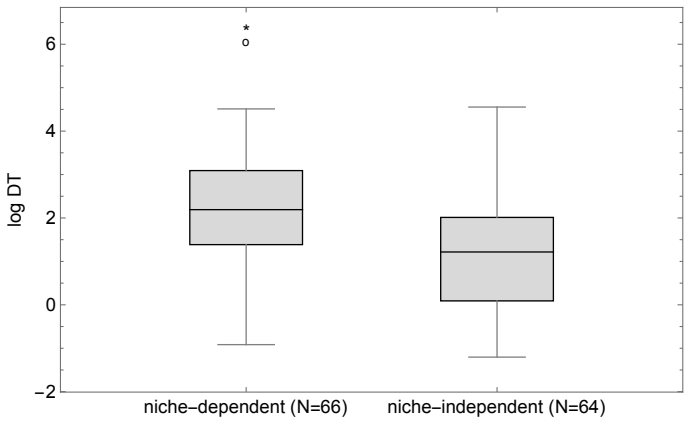

Figure 11.7: Box-Whisker plot of doubling times (DTs) of niche-dependent versus niche-independent populations of malignant plasma cells for patients within the AMM-cohort. The ordinate axis shows the natural logarithm of DTs. N is the total number of patients within the respective group. Significant difference between the groups is depicted by one asterisk for a level of $P < 0.05$. Significance testing was performed using a Wilcoxon rank-sum test [16]. For details, see text.

in agreement with the notion that the niche is a favourable microenvironment for healthy PCs as for malignant PCs. This is a result of the modelling and not an *a priori* assumption, see Chapter 5. Investigation of the relation between niche-dependence and the speed of growth of the malignant PC population yields that the median DT in patients with niche-dependent populations of malignant PCs is 9 years compared to 3.4 years in patients with niche-independent populations ($P < 0.05$), see Figure 11.7. Statistical analysis was performed using a Wilcoxon rank-sum test [16].

In view of Definition 11.5, further analysis was performed to relate niche-dependence to biological traits of malignant PCs. However, investigations do not imply significant evidence heretofore that niche-dependence is associated with any myeloma-related molecular aberration or gene expression. Likewise, this is the result for any tested predictor for progression of asymptomatic to therapy-requiring myeloma [49]. According to this, growth of malignant PCs could appear in- and outside the niche in all molecular entities of myeloma.

11.3 Initial number of malignant plasma cells

The question of how many malignant PCs initially arrive at the bone marrow and induce the growth of myeloma is of great interest for the understanding of myeloma dynamics but cannot be addressed by experimental methods. Unlike the more intuitive hypothesis that cancer arises from one mutated cell or a small group of cells, initial results regarding the DT suggest that that there is a population of initiating malignant PCs which proliferate in the bone marrow giving rise to myeloma. An explanation for this could be a malignant event occurring in or before the clonal expansion of plasma blasts (with DTs in the range of days) during the generation of healthy PCs (see Chapter 1) which could also appear as Gompertzian growth.

11.3.1 Equiprobable weighting

To exemplify the first approach, consider the three chosen AMM-patients from Chapter 10, i.e. Patients 1, 2 and 3. In Figure 11.9 on page 182, the selection of initial numbers of malignant PCs corresponding to best-fit solutions are visualised, where investigated initial numbers are marked with orange colour. For example, both a number of 10^9 or 10^{10} malignant PCs initially arriving at the bone marrow lead to best-fit solutions in case of Patient 2, see Figure 11.9 (b). Along these lines, the model does not differentiate between both scenarios. Observe that one malignant PC does not lead to a best-fit solution. With this in mind, one malignant PC initially arriving at the bone marrow is not able to explain the observed growth patterns on basis of the myeloma model, and is consequently ineligible as initial number. Similar holds for Patient 1, see Figure 11.9 (a). One initial malignant PC possibly explains the growth patterns in case of Patient 3, see Figure 11.9 (c), but this is only one of eight scenarios.

Assumption 11.6 (Equiprobable weighting)**.** Consider an eligible patient. The initial numbers of malignant PCs x_m^0 of best-fit solutions are equiprobable, i.e. a weight of 1 is equally distributed over all x_m^0 of all best-fit solutions.

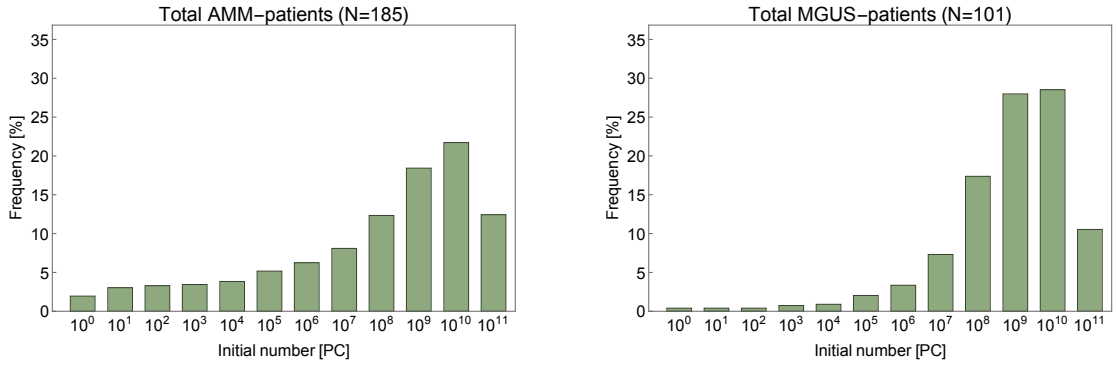

(a) Equiprobable weighting of initial numbers of malignant PCs corresponding to best-fit solutions.

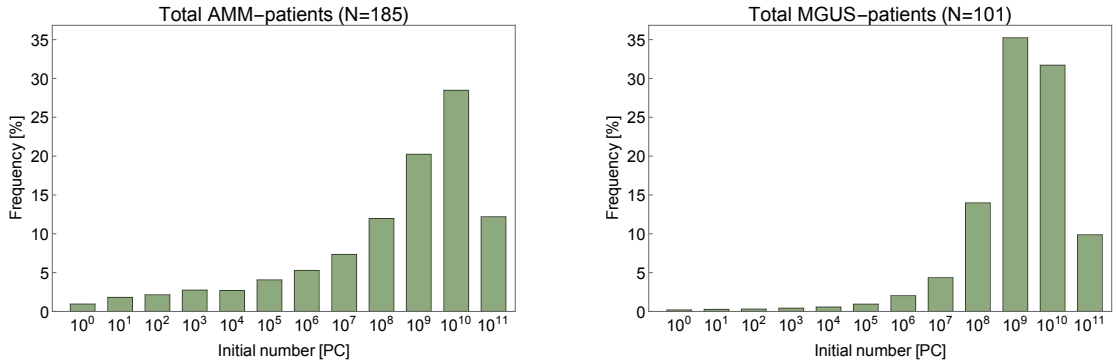

(b) Age-related weighting of initial numbers of malignant PCs corresponding to best-fit solutions.

Figure 11.8: Frequencies of initial numbers of malignant plasma cells (PCs) evaluated for the AMM- and MGUS-cohort of eligible patients, respectively. N is the total number of patients within the respective cohort. For details, see text.

In case of Patient 2, Assumption 11.6 implies that the probabilities of the occurrence of either 10^9 or 10^{10} malignant PCs initially arriving at the bone marrow are equal. Henceforth, both scenarios obtain the weighting factor 1/2. Likewise, each initial number corresponding to a best-fit solution acquires the weighting factors 1/4 and 1/8 in case of Patient 1 and 3, respectively.

This evaluation procedure is carried out for all eligible patients within the AMM-cohort and MGUS-cohort, see Table 11.1. Histograms visualise frequencies of the initial numbers of malignant PCs corresponding to best-fit solutions, see Figure 11.8 (a).

Results

In more than 90% of all eligible patients within the AMM-cohort and MGUS-cohort, the initial number of malignant PCs is in the magnitude of 10^3-10^{11} cells and 10^7-10^{11} cells, respectively. The most frequent initial number is 10^{10} cells for both the AMM-cohort (about 22%) and the MGUS-cohort (about 29%). In particular, an initial number of malignant PCs consisting of only one cell can explain the observed growth patterns in less than 2% and less than 1% of all eligible patients within the AMM-cohort and MGUS-cohort, respectively.

T \ xm0	E0	E1	E2	E3	E4	E5	E6	E7	E8	E9	E10	E11
0		360	223	114	57	73	187	401				
5		483	314	172	77	56	140	341				
10			440	260	121	54	97	276				
15				386	198	76	66	209				
20					322	133	53	144	422			
25						244	74	87	330			
30						433	155	54	230			
35							335	76	131			
40								212	60	413		
45									95	228		
50									452	66		
55										324		

(a) Patient 1.

T \ xm0	E0	E1	E2	E3	E4	E5	E6	E7	E8	E9	E10	E11
0							987	721	421	244	205	254	388
5								824	498	268	205	249	398
10								942	596	304	207	244	410
15									718	361	215	238	425
20									871	451	231	231	446
25										596	264	223	476
30										813	335	214	520
35											493	206	595
40											883	210	740
45												290	
50													

(b) Patient 2.

T \ xm0	E0	E1	E2	E3	E4	E5	E6	E7	E8	E9	E10	E11
0	451	617	802									
5	357	514	693	918								
10	265	408	578	800								
15	181	311	458	673	935							
20	115	224	338	537	795							
25	82	150	223	397	642	954						
30	86	97	128	259	478	782						
35	153	85	80	141	310	590	971					
40	441	125	107	80	160	384	747					
45		513	259	121	80	188	491	962				
50			720	560	172	79	229	642				
55					609	196	79	279	835			
60					681	521	305	86	308			
65							844	595	223	203		

(c) Patient 3.

Figure 11.9: Selection of initial numbers of malignant plasma cells (orange) corresponding to best-fit solutions (yellow) for Patients 1,2 and 3. For details, see text.

11.3.2 Age-related weighting

Assumption 11.6 can be further developed taking into account the patient's age at which the initial population of malignant PCs arrives at the bone marrow. As generation of healthy PCs is an error-prone process (see Section 1.1), a person at advanced age has been susceptible for such processes leading to malignant transformations much longer than a younger person. The probability that one wave of PCs arriving at the bone marrow each year [94] is comprised by a population of malignant PCs accumulates with ongoing time.

Assumption 11.7 (Probability of occurrence of a malignant PC population)**.** The probability of a malignant PC population arriving at the bone marrow given by $\gamma > 0$ is constant and small for each patient at any time, i.e. $\gamma \ll 1$. It is conservatively estimated as not to change as the patient ages.

The previous assumption justifies the usage of the cumulative exponential distribution [62] for a description of the probability of failure, i.e. the arrival of a malignant PC population at the bone marrow, up to an age t,

$$F\colon \mathbb{R}_+ \mapsto [0,1], \quad F(t) = 1 - e^{-\gamma t}.$$

This function captures the fact that a longer follow-up implies a greater probability that a mutation occurs. Note that since $\gamma \ll 1$, it follows that

$$F(t) \approx 1 - (1 - \gamma t) = \gamma t. \tag{11.3.1}$$

The expression on the right-hand side of (11.3.1) is often referred to as cumulative hazard function [61].

Equation (11.3.1) allows defining an age-dependent weight. Considering Patient 1 (see Figure 11.9 (a)), for each initial number of malignant PCs x_m^0 belonging to a best-fit solution, there is available information on the corresponding age of appearance T, see ages corresponding to yellow boxes. For example, $x_m^0 = 10^5$ corresponds to a best-fit solution if $T = 10$. Using the approximated cumulative exponential distribution (11.3.1) allows assigning the weight $F(10) = 10\gamma$. This can equally be done for all remaining initial numbers associated with best-fit solutions, i.e. $x_m^0 \in \{10^4, 10^6, 10^7\}$.

Normalisation yields that $x_m^0 = 10^5$ is weighted by

$$\frac{F(10)}{F(0)+F(10)+F(20)+F(30)} = \frac{10\gamma}{(0+10+20+30)\gamma} = \frac{1}{6}.$$

The mutation rate γ cancels out, implying no need for further assumptions on the exact value of γ. Observe that $x_m^0 = 10^4$ is rejected since $F(0) = 0$, i.e. the occurrence of a mutation at age zero is highly improbable.

For Patient 2, $x_m^0 = 10^{10}$ yields best-fit solutions if $T \in \{25, 30, 35, 40\}$. Hence, the malignancy-induced perturbation of the healthy equilibrium leading to a best-fit solution is not uniquely determined. Bearing in mind that $F(t)$ gives the probability that a mutation occurs up to time t, selecting the largest age T, i.e. $T = 40$, still leads to a best-fit solution.

The evaluation procedure is carried out for all eligible patients within the AMM-cohort and MGUS-cohort (see Table 11.1). Histograms visualise frequencies of the initial numbers of malignant PCs corresponding to best-fit solutions, see Figure 11.8 (b).

Results

In more than 90% of all eligible patients within the AMM-cohort and MGUS-cohort, the initial number of malignant PCs is in the magnitude of $10^4 - 10^{11}$ cells and $10^8 - 10^{11}$ cells, respectively. The most frequent initial number is 10^{10} cells for the AMM-cohort (about 28%), and 10^9 cells for the MGUS-cohort (about 35%). In particular, an initial number of malignant PCs consisting of only one cell can explain the observed growth patterns in less than 1% and less than 0.5% of all patients within the AMM-cohort and MGUS-cohort, respectively. Weighting by means of the corresponding age compared to equiprobable scenarios implies a shift of the distribution to the right. This is due to the fact that higher initial numbers of malignant PCs correspond to older ages of the patients as it is pointed out by the yellow boxes in the matrices for s^2, see Figure 11.9 on page 182.

11.3.3 Analysis of groups

In the following, it is investigated whether there are differences in the distributions of the initial numbers of malignant PCs between the AMM-cohort and the

MGUS-cohort. In particular, groups of both the AMM- and the MGUS-cohort are analysed. Grouping according to the type of myeloma, i.e. IgA- and IgG-myeloma is considered. Moreover, sub-groups of both cohorts with respect to the associated DT are investigated. The latter grouping is of particular interest since it allows analysing the correlation between the malignant growth kinetics (determined by an exponential model) and the initial number of malignant PCs (determined by the myeloma model). Recall the classification in four DT-groups, see Definition 9.3. Further, grouping according to niche-dependence is investigated, see Section 11.2.

For each analysis, patients are divided into the respective groups and the distributions of the initial numbers of malignant PCs are deduced using age-related weighting, see Sub-section 11.3.2.

Results for grouping according to AMM and MGUS

In order to investigate whether the histograms in Figure 11.8 (b) are identical across the two populations of AMM- and MGUS-patients, a chi-square test for homogeneity of categorical data was performed [33]. The null hypothesis stating that each population has the same proportion of observations is rejected ($P = 0.009$).

Results for grouping according to IgA- and IgG-myeloma

Part (a) and (b) of Figure 11.10 on page 187 show the fractions of each Ig type (yellow) within the total cohorts (green). In Figure 11.11 (a), the distributions of the initial numbers of malignant PCs is visualised for each group of the AMM-cohort separately. Performing a chi-square test for homogeneity of categorical data [33] yields that there is no significant difference in the frequencies of the initial numbers of malignant PCs between the group of IgA- and IgG-myeloma patients ($P > 0.99$). Figure 11.11 (b) shows the distributions of the initial numbers of malignant PCs for each group of the MGUS-cohort separately. The histograms significantly differ from each other (chi-square test for homogeneity of categorical data [33], $P = 0.0006$), bearing in mind that due to few numbers of patients in the IgA-myeloma group the result should be interpreted cautiously.

Results for grouping according to doubling times

For patients with a fast associated DT, small initial numbers of malignant PCs are more likely to explain the observed growth patterns than large numbers, see Figure 11.12 (a) and (b) on page 190. Vice versa, for a patient with a slow associated DT implying intermediate or infinitesimal increase of malignant PCs, large initial numbers of malignant PCs are preferably in line with best-fit solutions, see Figure 11.12 (c) and (d). Initial numbers of malignant PCs in the magnitude of $10^{10} - 10^{11}$ cells are almost exclusively determined by patients with a negative associated DT, see Figure 11.12 (e). Moreover, it is evident from Figure 11.13 on page 191 that the distributions are not identical across the DT-groups in case of the AMM-cohort approved by a chi-square test for homogeneity of categorical data [33] ($P < 0.001$). Similar holds true in case of the MGUS-cohort, see Figure 11.14 on page 192.

Results for grouping according to niche-dependence

Figure 11.15 on page 193 visualises the frequency of initial numbers of malignant PCs for AMM-patients analysed for niche-dependent and -independent patients according to Definition 11.5. By means of a chi-square test for homogeneity of categorical data [33], the distributions show a tendency to differ ($P = 0.08$).

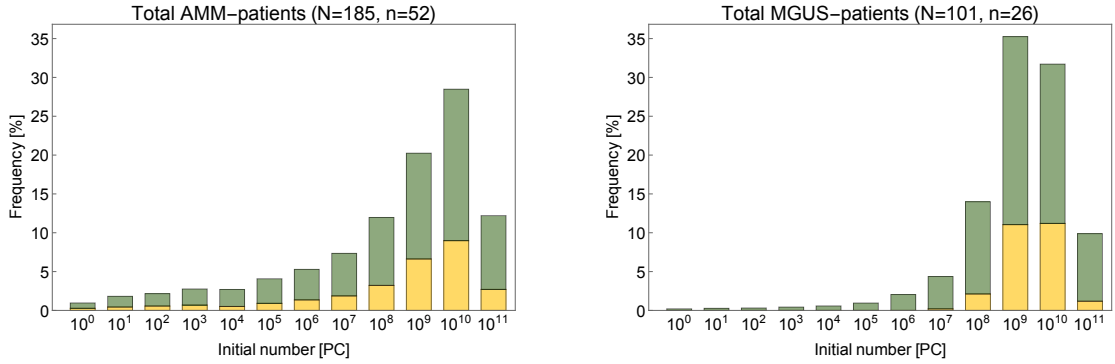

(a) Fraction of IgA-myeloma within each cohort.

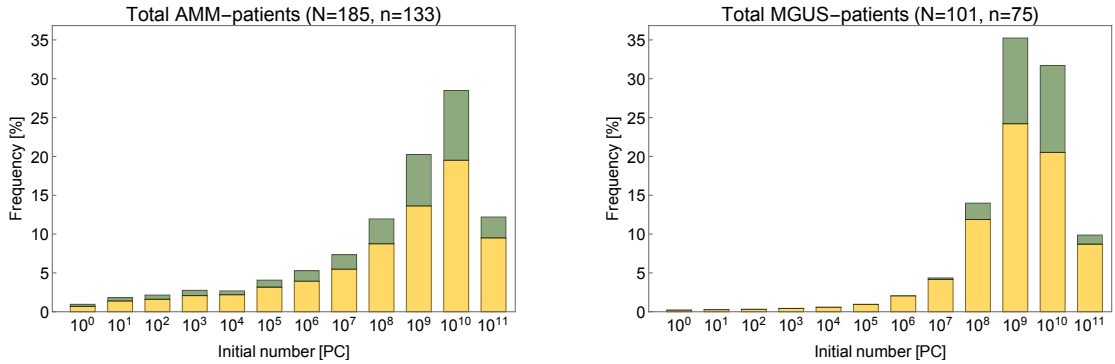

(b) Fraction of IgG-myeloma within each cohort.

Figure 11.10: Frequencies of initial numbers of malignant plasma cells (PCs) within the AMM- and MGUS-cohort of eligible patients (green) grouped according to IgA- and IgG-myeloma (yellow), respectively. N is the total number of patients within the respective cohort, whereas n is the number of patients within the respective group. Evaluation is based on age-related weighting of initial numbers of malignant PCs corresponding to best-fit solutions. For details, see text.

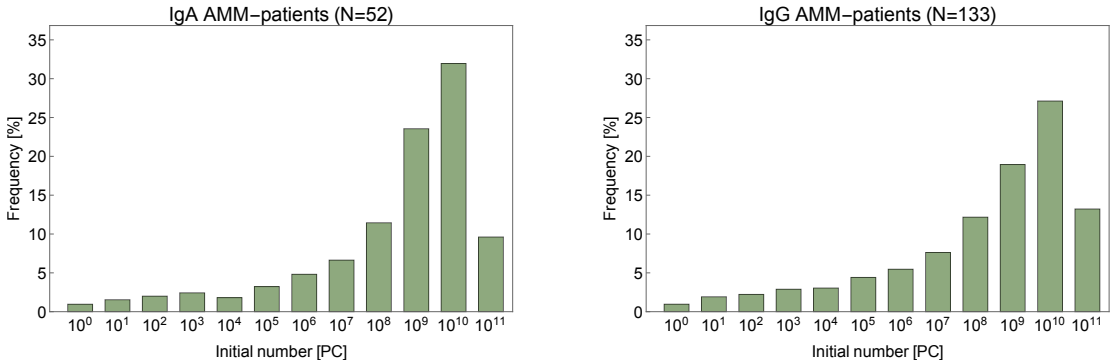

(a) Separate evaluation for each group within the AMM-cohort.

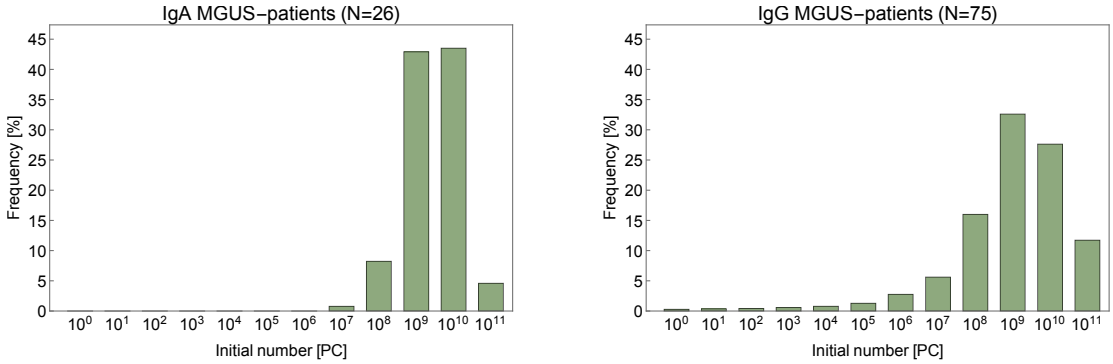

(b) Separate evaluation for each group within the MGUS-cohort.

Figure 11.11: Frequencies of initial numbers of malignant plasma cells (PCs) within the AMM- and MGUS-cohort of eligible patients evaluated for each IgA- and IgG-myeloma, respectively. N is the total number of patients within the respective group. Evaluation is based on age-related weighting of initial numbers of malignant PCs corresponding to best-fit solutions. For details, see text.

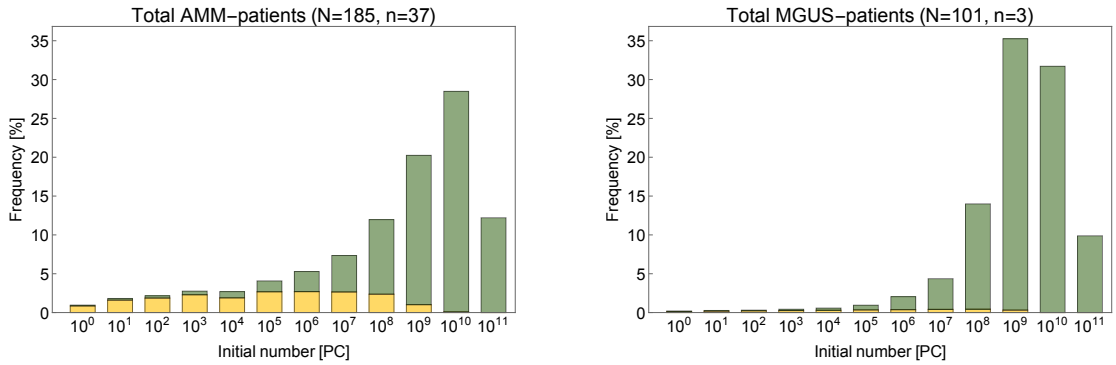

(a) Fraction of $0 < \tau < 2$ within each cohort.

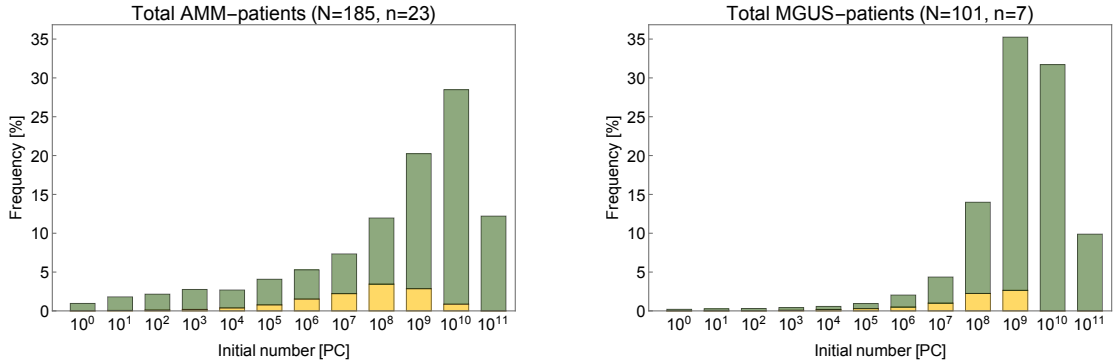

(b) Fraction of $2 \leq \tau < 4$ within each cohort.

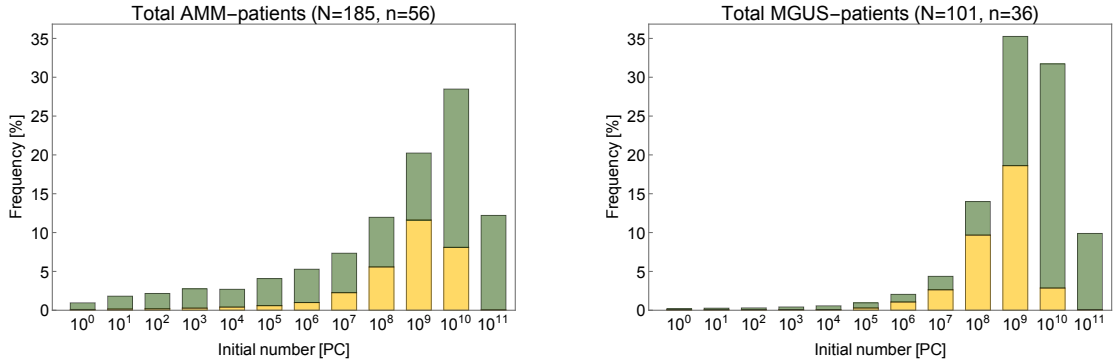

(c) Fraction of $4 \leq \tau < 16$ within each cohort.

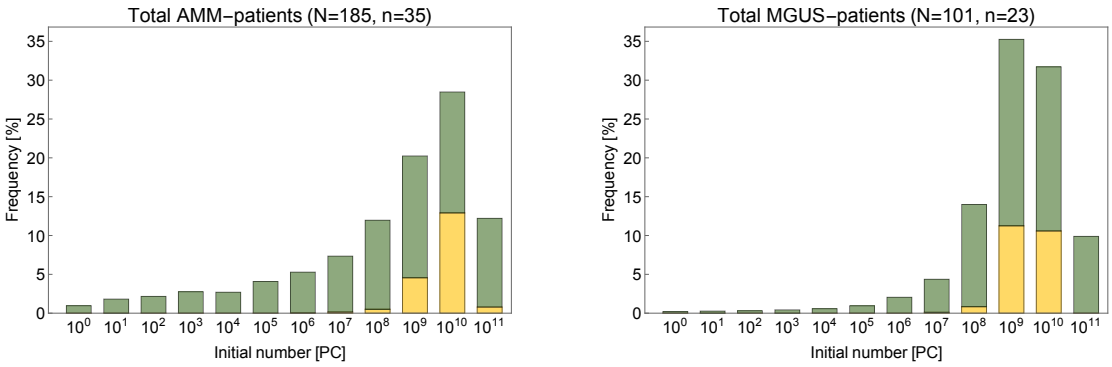

(d) Fraction of $\tau \geq 16$ within each cohort.

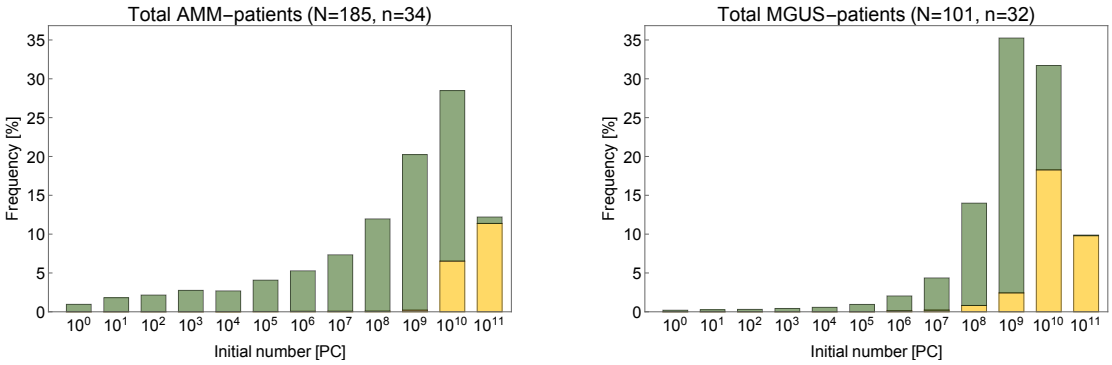

(e) Fraction of $\tau \leq 0$ within each cohort.

Figure 11.12: Frequencies of initial numbers of malignant plasma cells (PCs) within the AMM- and MGUS-cohort of eligible patients (green) grouped according to the associated doubling times (DTs) τ (yellow), respectively. N is the total number of patients within the respective cohort, whereas n is the number of patients within the respective group. Evaluation is based on age-related weighting of initial numbers of malignant PCs corresponding to best-fit solutions. For details, see text.

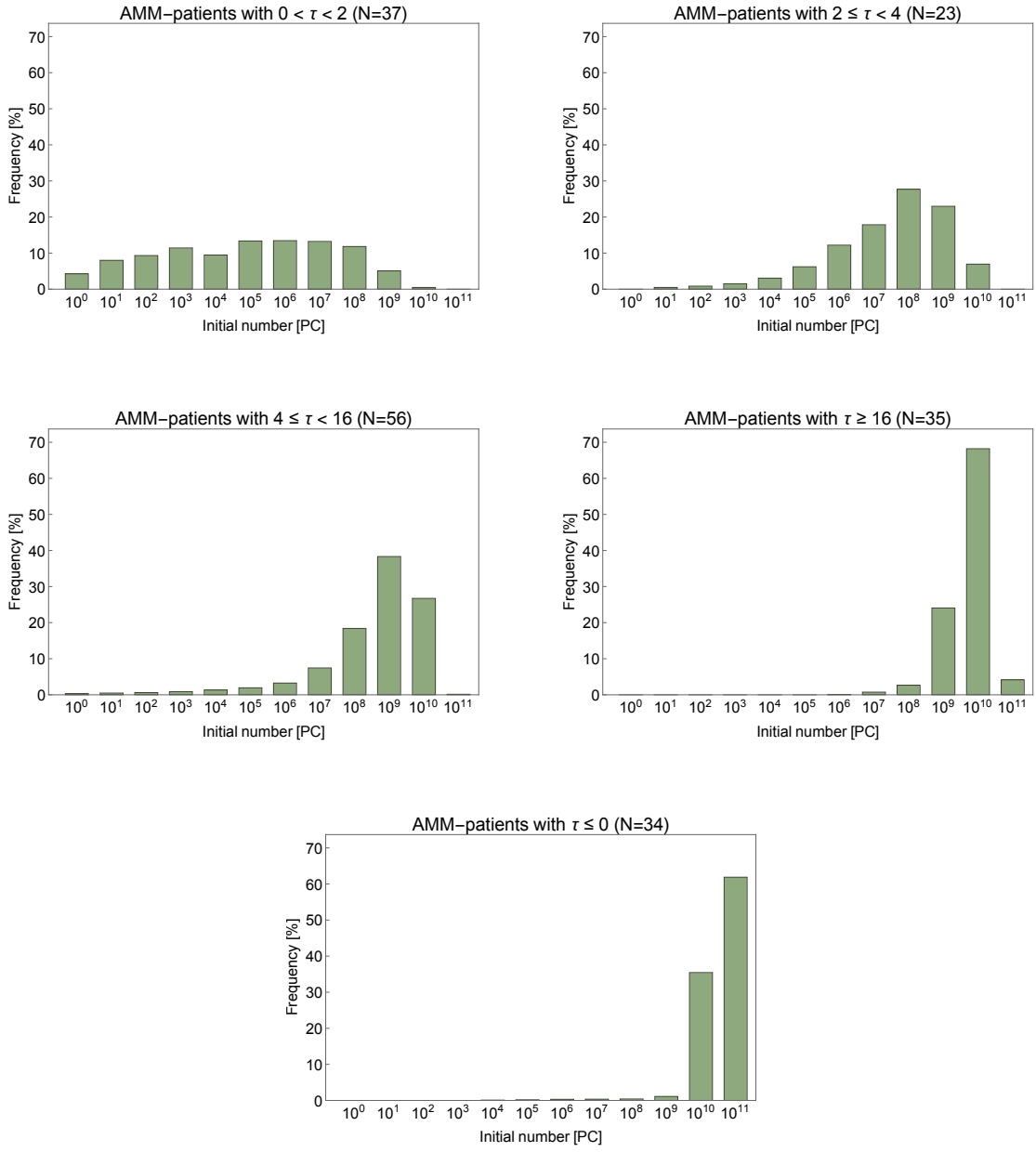

Figure 11.13: Frequencies of initial numbers of malignant plasma cells (PCs) within the AMM-cohort of eligible patients evaluated for each group of associated doubling times (DTs) τ. N is the total number of patients within the respective group. Evaluation is based on age-related weighting of initial numbers of malignant PCs corresponding to best-fit solutions. For details, see text.

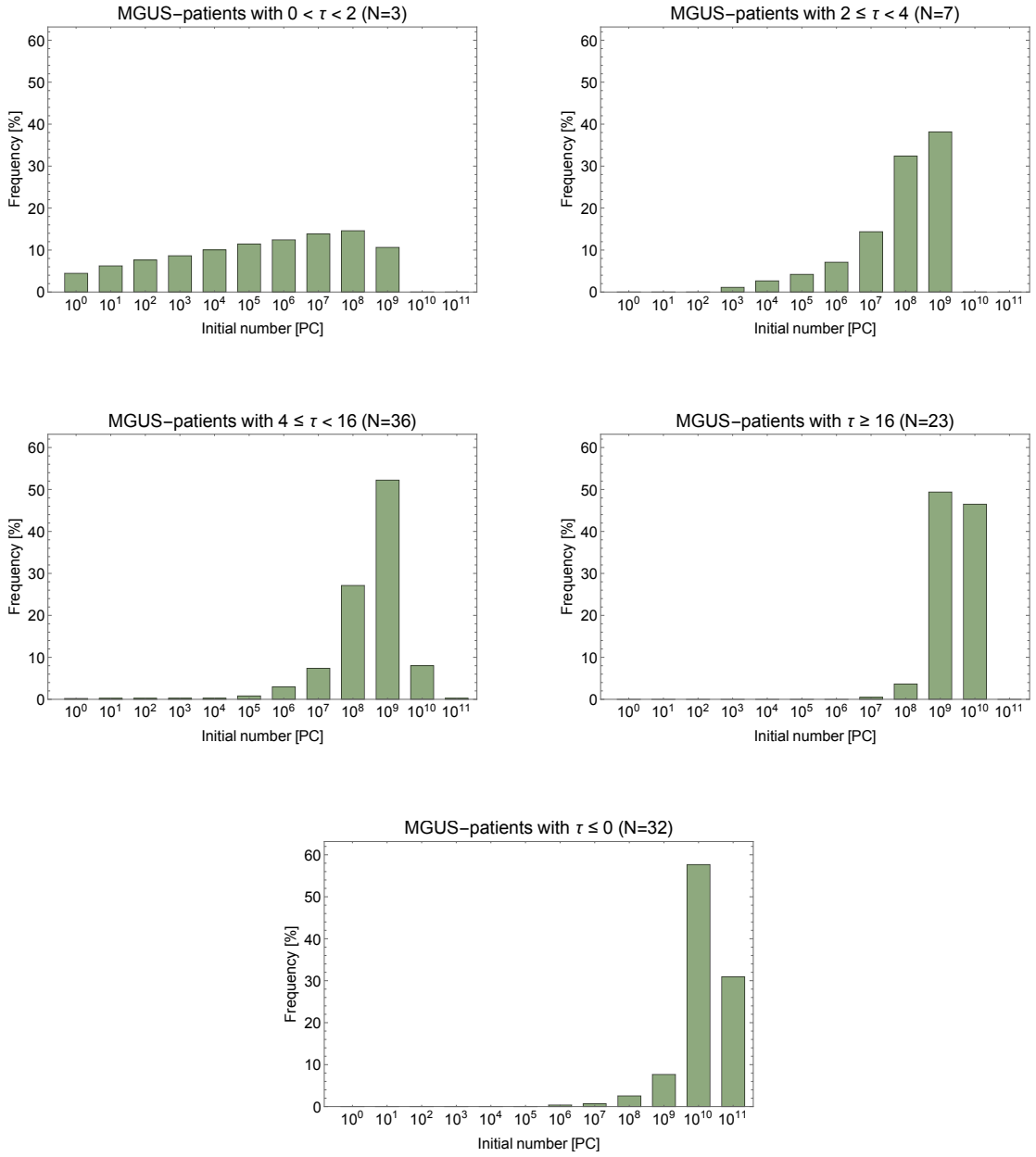

Figure 11.14: Frequencies of initial numbers of malignant plasma cells (PCs) within the MGUS-cohort of eligible patients evaluated for each group of associated doubling times (DTs) τ. N is the total number of patients within the respective group. Evaluation is based on age-related weighting of initial numbers of malignant PCs corresponding to best-fit solutions. For details, see text.

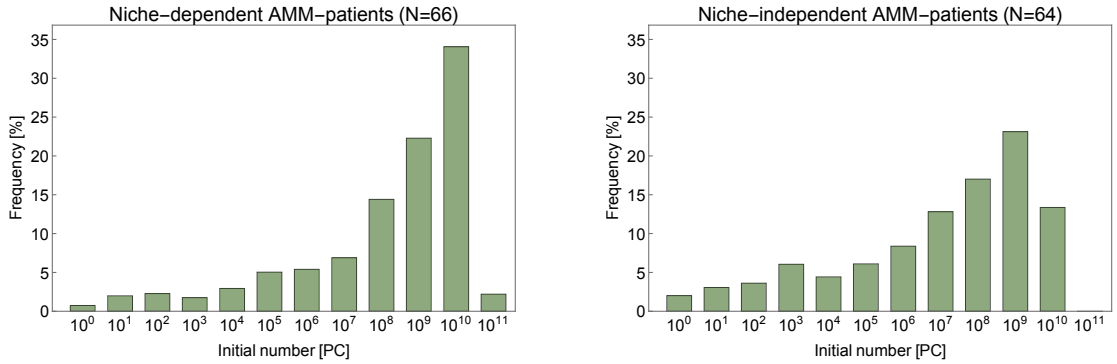

Figure 11.15: Frequencies of initial numbers of malignant plasma cells (PCs) within the AMM-cohort of eligible patients evaluated for niche-dependent and niche-independent populations of malignant PCs, see Section 11.2. N is the total number of patients within the respective group. Evaluation is based on age-related weighting of initial numbers of malignant PCs corresponding to best-fit solutions. For details, see text.

12 Integrating discussion and conclusions

Whereas many aspects have been discussed throughout the thesis, this chapter provides a comprehensive level of discussion and integration.

12.1 Discussion of aims

In this thesis, the following questions were addressed by mathematical modelling:

1. Characterisation of the growth of malignant plasma cells

The aim was to provide biologically plausible models of the growth of malignant PCs allowing investigating whether growth is continuous (such as in an exponential model) or associated with a change in the growth pattern (such as in a Gompertzian growth model). The following results were obtained:

- The dynamics of healthy PCs can be described by the basic model. The model is based on simplifications. Firstly, it is assumed that the inflow of healthy PCs is constant approximating the pathogen-induced waves of PCs arriving at the bone marrow per year [94]. Secondly, the niche is considered as separate compartment within the bone marrow. This is justified by healthy PCs being dependent on the niche for survival [60]. It is assumed that PCs outside the niche die at a constant rate [57]. Thirdly, transitions into and out of the niche are modelled depending on the surplus of PCs relative to the niche balance present at homoeostasis at which no transitions take place. This formalism allows describing the key elements impacting on PC dynamics in the bone marrow, whereby being adequate in terms of biological plausibility.

- The dynamics induced by antigen encounter and the concomitant production of healthy PCs can be described by the extended model as exemplified by a vaccination scenario. Inflow of vaccination-induced healthy PCs is modelled by a discrete-in-time event representing one of the extrapolated 30 waves of healthy PCs arriving at the bone marrow per year [94]. Being calibrated, the model is able to capture biologically plausible dynamics [9, 94].

- Growth of malignant PCs can be described by the myeloma model. Hypothesised to be similar to a vaccination-induced perturbation, malignancy-induced perturbation of homoeostasis is modelled by a discrete-in-time event representing one of approximately 30 waves of PCs arriving at the bone marrow per year [94]. The model allows for proliferation of the population of malignant PCs.

- Compared to the exponential growth model, the myeloma model describes more precisely the dynamics of malignant PC accumulation taking into account the bone marrow niche and the population of healthy PCs. The model is adequate in terms of biological plausibility, self-consistency, and well fitting data consisting of serum and urine samples ($n = 8398$) of patients with AMM and MGUS ($n = 322$ and $n = 196$, respectively).

- In case of PC dyscrasias, growth is characterised by an increase in the number of malignant PCs and a concomitant decrease in the number of healthy PCs. This results from both analytical results, numerical simulations and parameter estimation using clinical data. Increase in the number of malignant PCs is either unbounded (AMM: 62%, MGUS: 55%), retarded at late stages (23% each) or negative (AMM: 15%, MGUS: 22%). The latter is associated with a negative DT. This can imply either a decrease in the number of malignant PCs, i.e. myeloma never manifests, or a fairly constant number of malignant PCs, where progression is not driven by an increasing tumour mass (but for example by bone destruction). In contrast to a non-mechanistic Gompertzian model, retardation of the growth of the total population of malignant PCs can here be quantified by the dynamic DT and explained by a shift in the composition of the total number of malignant PCs in the bone marrow implying a time-varying accumulation speed. Malignant PCs spill out of the niche due to comparably

fast accumulation inside the niche. A comparably large negative net growth of malignant PCs outside the niche implies cell death.

- Positive growth of the population of malignant PCs is associated with faster proliferation of malignant PCs inside the niche compared to those outside the niche. In that sense, residing in the niche is beneficial for malignant PCs, which is not a model assumption. Net growth outside the niche can be negative (i.e. malignant PCs die) implying that the niche would not only be advantageous but also essential for survival of malignant PCs (i.e. malignant PCs are niche-dependent). Whereas it is traditionally assumed that the ability of malignant PCs to be niche-independent is obtained during disease progression [60], the definition at hand suggests that it can already exist at the beginning whereby its characteristic depends on the fraction of cells outside and inside the niche. Niche-dependence is seemingly independent of molecular aberrations or clinical variables. Niche-independent populations of malignant PCs possess a significantly faster DT compared to niche-dependent populations.

2. Characterisation of progression to symptomatic myeloma

Related to growth, the analysis addressed the question of how fast progression from early asymptomatic stages (MGUS, AMM) to therapy-requiring myeloma (MM) happens. The following results were obtained:

- The exponential growth model leads to the definition of the DT quantifying the rate of accumulation of malignant PCs. The identification of four DT-groups of patients with very fast, fast, intermediate and almost no accumulation delineates significantly different probabilities of progression from AMM to symptomatic myeloma [109].

3. Quantification of the initial number of malignant plasma cells

Further analysis investigated how many malignant PCs initiate myeloma. Hypothesising that initiation of myeloma is due to a population of malignant PCs arriving at the bone marrow similar to the dynamics occurring within a natural immune response [94], the analysis addressed the question whether one malignant PC is able

to induce accumulation in the bone marrow as it is assumed by the existing model, see Section 1.3. The following results were obtained:

- Results indicate that in more than 90% of the AMM- and MGUS-patients, there is a population of malignant PCs arriving at the bone marrow consisting of $10^4 - 10^{11}$ cells and $10^8 - 10^{11}$ cells, respectively. The most frequent initial number is 10^{10} cells for the AMM-cohort (28%), and 10^9 cells for the MGUS-cohort (35%). In less than 1% of the patients one initial malignant PC describes data best. A large initial number of malignant PCs could explain the occurrence of malignant PCs at different locations within the bone marrow from the beginning [43, 45, 58].

- The Gompertzian growth model of Salmon et al. [24, 103, 115] assumes that myeloma is initiated by one malignant *plasma cell*. The same is true for the exponential model of Hobbs [46] and the induced myeloma model of Jákó [53, Chapter 8]. Lacking biological plausibility for the severe retardation in the growth kinetics of malignant PCs as a consequence of this assumption has been criticised. In the light of our findings, the Gompertzian model could be interpreted in that the initial fast increase with DTs of $1 - 3$ days mirrors the clonal expansion analogue to the generation of *plasma blasts* (see Chapter 1), and the subsequent slow growth with DTs of $4 - 6$ months is given by the accumulation of *plasma cells* in the bone marrow. In the myeloma model, the initial fast increase in the number of plasma blasts is introduced by the number of malignant PCs arriving at the bone marrow. Similar to the dynamics induced by an antigen, where a wave consisting of a population of healthy PCs arrives at the bone marrow [94], the initial number of malignant PCs can be characterised as one „malignant wave“, which arrives at the bone marrow and perturbs healthy homoeostasis.

- Frequencies of initial numbers of malignant PCs belonging to best-fit solutions significantly differ between the DT-groups. A fast (slow or negative) associated DT correlates with a small (large) initial number of malignant PCs. These findings are coherent from a biological perspective, since a small initial number of malignant PCs would need to grow fast to reach the critical cell number for AMM or MGUS within the patient's lifetime. An initially high number

of malignant PCs has a chance of becoming clinically apparent also in case of a lower growth capacity. Frequencies of initial numbers of malignant PCs belonging to best-fit solutions significantly differ between the AMM- and MGUS-cohort. Biologically, this implies that a patient presenting at MGUS-stage is more likely to have a higher number of initial malignant PCs compared to a patient presenting at AMM-stage (where patients with low numbers of initial malignant PCs are less likely diagnosed). The former is associated with slower growth of malignant PCs and in turn in agreement with a lower progression rate, i.e. 1% per year in MGUS versus 10% per year in AMM [72].

12.2 Discussion of assumptions and resulting limitations

This section provides a discussion of assumptions and resulting limitations of the work presented in this thesis. Limitations are related to three areas: Firstly, mathematical modelling including assumptions and simplifications, and analysis. Secondly, the quantitative application of the models and defining a parameter estimation procedure. Thirdly, evaluation and biological interpretation of the parameter estimation results.

- One criticism of the models derived in this thesis comprises the simplification of a constant inflow of healthy PCs into the bone marrow, although knowing that it is rather periodic and given by waves consisting of populations of PCs arriving at the bone marrow [94]. The number and the shape of these waves may vary and depend on the ecosystem and the prevalences of infectious diseases an individual is exposed to. This is exemplified by seasonal infections (such as influenza), in which waves are not equally distributed over one year. Thus, variations in the number of healthy PCs at healthy equilibrium can take place. Since characteristics and serial dynamics of waves are not described biologically, a constant inflow of healthy PCs is assumed.

- Transition of PCs into the niche are assumed to take place if there is a surplus of PCs located outside the niche, pushing cells into the niche. Vice versa, transition of PCs out of the niche happens if there is a surplus of PCs inside the niche. This leads to piecewise-smooth continuous systems of equations, being shown

to reflect competitive dislocation of PCs out of the niche [94]. In case of the extended model, this implies existence of a manifold of equilibria representing re-established healthy equilibria after immune response, in agreement with long-term immunity [84, 94, 117]. In contrast, assuming constant transitions of PCs would yield a decreasing vaccination-induced PC population, and a stable immune characteristic would never manifest.

- From a mathematical point of view, the analysis lacks results for stability of equilibria of the myeloma model located on the switching manifold. Since the extension of established concepts for smooth dynamical systems to the case of non-smooth dynamical systems is an open research area [21], further investigation is necessary to provide an adequate theoretical framework, possibly similar to the theorem of Hartman and Grobman [36, Theorem 1.4.1].

- The presented models comprise interpretable and measurable parameters. Their values are derived from literature or evaluated by estimation using data. Information for the transition rates cannot be derived experimentally. Their values are fixed by assuming a biologically plausible range. As addressed by sensitivity analysis a certain level of uncertainty remains regarding their absolute value, but not regarding their order of magnitude.

- The parameter estimation procedure is based on discretisations of the malignancy-induced perturbation of the healthy equilibrium minimising the amount of executions. This can be criticised as being a too general approximation which might not be suited for each individual patient data set to identify the best fit. To overcome this issue, a selection criterion for the best-fit solutions is chosen to antagonise errors due to discretisation. Further, a fixed value for the individual healthy equilibrium might not be optimal for each patient data set. Individual weakness of the chosen algorithm can be compensated by the large number of patients ($n = 322$ for AMM and $n = 196$ for MGUS). Instead of fixing k and minimising the error variance with respect to T and x_m^0, optimisation could also be performed for T, x_m^0 and k simultaneously. However, this would imply an impractical amount of executions.

- Growth patterns of malignant PCs approaching an equilibrium are not supported by data [47]. Apart from the discussion depicted in this thesis, optimi-

sation could include constraints on the parameters p_1 and p_2 to avoid these patterns. However, such an approach could be criticised as being biased. Thus, estimation is performed using unconstrained optimisation methods.

- In about 30% of the patients within the AMM-cohort, the growth of the population of malignant PCs could not be attributed to being either niche-dependent or niche-independent. Klein et al. [60] propose malignant PCs to become partially independent of the niche due to self-reliant production of survival and growth factors. This could be seen as a potential description of the behaviour of malignant PCs. To account for the grade of dependence, an extension of the myeloma model including a continuous structure in terms of structured population equations [92] could be introduced. Since the dependences of the involved parameters, for example, death, proliferation and transitions, on the structural variable cannot be identified experimentally, further assumptions would be necessary, increasing the complexity of the model.

- The derived models consisting of ODEs are suited for describing the dynamics of large populations of PCs being well-mixed and spatially homogeneous. Although the investigation of the initial number of malignant PCs arriving at the bone marrow involves few cells located within transient regions between the peripheral blood and the bone marrow, results are still reliable since quantification does not address the absolute value of the initial number of malignant PCs but their order of magnitude.

12.3 Further directions

The work presented in this thesis could be continued in the following directions:

- Considering myeloma growth dynamics, further investigation could identify and, at the best, quantify the grade of niche-dependence of malignant PCs. The dynamic DT might be useful as a clinical parameter quantifying the time-varying accumulation capacity of myeloma. This is not only of theoretical interest but might also serve as foundation for improved treatment strategies, which might potentially be testable by means of the model framework.

- Considering myeloma bone disease, future research could elaborate a deeper investigation of the relationship between the cell and the bone remodelling dynamics. The myeloma model could be extended in order to capture the mutual interference of bone formation and degradation processes and malignant cell dynamics within the niche, which leads to bone destructions in MM [60]. This appears promising since existing models lack the explicit consideration of cells resident in the niche, see Section 1.3.

- Considering further research, the derived mathematical models might serve as frameworks for niche mechanisms in the bone marrow being present in other populations of healthy and malignant cell dynamics, as for example in general stem cell competitions [79, 114], healthy haematopoiesis and leukaemia [111, 134]. These would allow capturing the niche as a compartmental ingredient instead of a non-linear feedback, which has heretofore been suggested by a range of models, see for example [30, 82, 85, 113].

12.4 Conclusions

The new mathematical models describe the key elements impacting on the dynamics of healthy and malignant PC accumulation in the bone marrow, and are adequate in terms of biological plausibility, self-consistency, and well fitting data allowing exposing previously unknown mechanisms not being able to be investigated experimentally.

Modelling was achieved by tight collaboration between the Institute of Applied Mathematics at Heidelberg University and the Multiple Myeloma Research Laboratory at University Clinic Heidelberg, whereby biomedical hypothesis, advanced modelling approaches and subsequent validation of the model outputs were iteratively combined. Mathematical analysis reveals underlying mechanism responsible for observed dynamics. Evaluation of parameter estimation using clinical data consisting of serum and urine samples ($n = 8398$) of patients with AMM and MGUS ($n = 322$ and $n = 196$, respectively) allows characterising growth of malignant PCs and initiation of myeloma.

As for healthy PCs, modelling suggests the niche to be beneficial for survival and growth of malignant PCs. Accumulation of malignant PCs can be quantified by

the DT. A faster DT (significantly more frequent in niche-independent than in niche-dependent populations of malignant PCs) relates to a higher probability of progression to symptomatic myeloma, and correlates with a small initial number of malignant PCs. One initial malignant PC can rarely explain observed growth patterns, and initiation of myeloma can be characterised by a „malignant wave“ comprised of a population of malignant PCs arriving at the bone marrow and perturbing healthy homoeostasis.

13 Summary

Background

Plasma cell (PC) dyscrasias are characterised by accumulation of malignant PCs in the bone marrow. Asymptomatic multiple myeloma (AMM) evolves from monoclonal gammopathy of unknown significance (MGUS) and progresses to symptomatic myeloma involving end organ damage. Three main questions are addressed by mathematical modelling. Firstly, how is growth of malignant plasma cells characterised? Secondly, how fast does progression from early asymptomatic stages (MGUS, AMM) to symptomatic myeloma happen? Thirdly, how many malignant plasma cells initially arrive at the bone marrow?

Mathematical models

New mathematical models are formulated to analyse the dynamics of malignant PC accumulation in the bone marrow and its niche. Growth of healthy PCs can be described by the basic model. Healthy PCs are assumed to be constantly produced and enter the bone marrow through the peripheral blood where PCs outside the niche are distinguished from those inside the niche. Cell transitions between those two compartments are regulated by the function $z(t)$ representing the surplus of PCs outside (if $z(t) > 0$) or inside (if $z(t) < 0$) the niche relative to the niche balance (if $z(t) = 0$). The healthy equilibrium is identified as representative for healthy homoeostasis. As a refinement of the basic model, the extended model allows capturing the dynamics induced by a perturbation of the healthy equilibrium due to vaccination as example for a natural pathogen-induced production of healthy PCs. Derivation of the myeloma model is based on the extended model, where malignant PCs are considered as a population of „vaccination-induced“ PCs with the difference of being able to proliferate at net growth rates p_1 and p_2 for malignant PCs outside and inside the niche, respectively.

Analysis of the mathematical models

The mathematical models generate piecewise-smooth continuous dynamical systems. For the basic model, results about existence and uniqueness of non-negative solutions are provided. By means of a Lyapunov function, global asymptotic stability of the healthy equilibrium is shown. Invariant sets within the state space are identified which allow deducing that the function $z(t)$ may switch its sign at most once, and that $z(t)$ has at most one maximum or minimum. Results are visualised by qualitative simulations.

In case of the myeloma model, a domain of definition is identified assuring that the model equations are defined and solutions stay non-negative. Existence and uniqueness of solutions is proven and the set of equilibria is characterised. Two partial equilibria are shown to exist in dependence on the values p_1 and p_2, and on the choice of the initial conditions for malignant PCs. They extend the classical notion of equilibria. Further analysis focuses on their stability and the characterisation of their non-constant components. Results are visualised by qualitative simulations.

Existence and uniqueness of non-negative solutions of the extended model are deduced by previous results. Further analysis reveals global attractiveness of the one-dimensional manifold of non-isolated equilibria. Estimates for model solutions with initial conditions representing a vaccination-induced perturbation of the healthy equilibrium are provided, and results are visualised by qualitative simulation.

Quantitative application using clinical data

In a first step towards quantitative application of the mathematical models, clinical data consisting of serum and urine samples ($n = 8398$) of patients with AMM and MGUS ($n = 322$ and $n = 196$, respectively) are used to characterise growth of malignant PCs by means of an exponential model leading to the doubling time (DT). Having discussed surrogates for cell numbers, the parameter estimation procedure is carried forward addressing fixation of deducible parameter values, defining suitable fitting procedures, and selecting eligible patient data sets. The calibrated model is shown to reproduce biological observations. Model identifiability and sensitivity are addressed, indicating that certain variations in the transition rates of PCs still imply the validity of the obtained best-fit solutions. Parameter estimation of p_1 and p_2

results in adequate fittings, which on the one hand validate the models, and on the other hand are used to expose previously unknown biological mechanisms.

Biological results

The mathematical models are adequate in terms of biological plausibility, self-consistency, and well fitting data. Healthy PC dynamics induced by antigen encounter and the concomitant production of healthy PCs can be described by the extended model as exemplified by a vaccination scenario. The model is able to reproduce biological observations. Growth of malignant PCs can be described by an exponential model. More realistic dynamics involving healthy PCs and the bone marrow niche are captured by the myeloma model.

The DT quantifies the rate of accumulation of malignant PCs. The identification of four DT-groups of patients with very fast, fast, intermediate and almost no accumulation delineates significantly different probabilities of progression from AMM to symptomatic myeloma [109].

Growth of malignant PCs is associated with faster proliferation of malignant PCs inside the niche compared to those outside the niche. The median DT in patients with niche-independent populations of malignant PCs is significantly faster compared to patients with niche-dependent populations. In more than 90% of all eligible patients within the AMM-cohort and MGUS-cohort, the initial number of malignant PCs is in the magnitude of $10^4 - 10^{11}$ cells and $10^8 - 10^{11}$ cells, respectively. An initial number of malignant PCs consisting of only one cell can explain the observed growth patterns in less than 1% and less than 0.5% of all patients within the AMM-cohort and MGUS-cohort, respectively. A fast (slow or negative) associated DT correlates with a small (large) initial number of malignant PCs

Conclusions

As for healthy PCs, modelling suggests the niche to be beneficial for survival and growth of malignant PCs. Accumulation of malignant PCs can be quantified by the DT. A faster DT (significantly more frequent in niche-independent than in niche-dependent populations of malignant PCs) relates to a higher probability of progression to symptomatic myeloma, and correlates with a small initial number of malignant PCs. One initial malignant PC can rarely explain observed growth

patterns, and initiation of myeloma can be characterised by a „malignant wave“ comprised of a population of malignant PCs arriving at the bone marrow and perturbing healthy homoeostasis.

Bibliography

[1] V. Acary and B. Brogliato. *Numerical methods for nonsmooth dynamical systems: Applications in mechanics and electronics*, volume 35 of *Lecture notes in applied and computational mechanics*. Springer, Berlin/Heidelberg, 2008.

[2] I. J. Amanna and M. K. Slifka. Mechanisms that determine plasma cell lifespan and the duration of humoral immunity. *Immunological Reviews*, 236(1):125–138, 2010.

[3] M. Andraud, O. Lejeune, J. Z. Musoro, B. Ogunjimi, P. Beutels, and N. Hens. Living on three time scales: The dynamics of plasma cell and antibody populations illustrated for Hepatitis A virus. *PLoS Computational Biology*, 8(3):e1002418, 2012.

[4] B. Aulbach. *Continuous and discrete dynamics near manifolds of equilibria*, volume 1058 of *Lecture notes in mathematics*. Springer, Berlin/Heidelberg, 1984.

[5] B. P. Ayati, C. M. Edwards, G. F. Webb, and J. P. Wikswo. A mathematical model of bone remodeling dynamics for normal bone cell populations and myeloma bone disease. *Biology Direct*, 5(28), 2010.

[6] D. M. Bates and D. G. Watts. *Nonlinear regression analysis and its applications*. John Wiley and Sons, New York, 1988.

[7] A. Baur-Melnyk, S. Buhmann, H. Dürr, and M. Reiser. Role of MRI for the diagnosis and prognosis of multiple myeloma. *European Journal of Radiology*, 55(1):56–63, 2005.

[8] R. Benner, W. Hijmans, and J. Haaijman. The bone marrow: The major source of serum immunoglobulins, but still a neglected site of antibody formation. *Clinical and Experimental Immunology*, 46(1):1–8, 1981.

[9] N. L. Bernasconi, E. Traggiai, and A. Lanzavecchia. Maintenance of serological memory by polyclonal activation of human memory B cells. *Science*, 298(5601):2199–2202, 2002.

[10] P. R. Bevington and D. K. Robinson. *Data reduction and error analysis for the physical sciences*. McGraw-Hill, New York, 3rd edition, 2003.

[11] H. G. Bock. Randwertproblemmethoden zur Parameteridentifizierung in Systemen nichtlinearer Differentialgleichungen. *Bonner Mathematische Schriften*, 183, 1985.

[12] H. G. Bock, T. Carraro, W. Jäger, S. Körkel, R. Rannacher, and J. P. Schlöder, editors. *Model based parameter estimation: Theory and applications*, volume 4 of *Contributions in mathematical and computational sciences*. Springer, Berlin/Heidelberg, 2013.

[13] H. G. Bock, M. Diehl, C. Kirches, K. Mombaur, and S. Sager. *Skript Numerik 2*. Universität Heidelberg, 2014.

[14] O. H. Brekke and I. Sandlie. Therapeutic antibodies for human diseases at the dawn of the twenty-first century. *Nature Reviews Drug Discovery*, 2(1):52–62, 2003.

[15] R. Brink. New friends for bone marrow plasma cells. *Nature Immunology*, 12(2):115–117, 2011.

[16] H. Büning and G. Trenkler. *Nichtparametrische statistische Methoden*. Walter de Gruyter, Berlin, 1994.

[17] J. C. Butcher. *The numerical analysis of ordinary differential equations: Runge-Kutta and general linear methods*. John Wiley and Sons, New York, 1987.

[18] J. F. Butterworth, D. C. Mackey, and J. D. Wasnick. *Morgan and Mikhail's clinical anesthesiology*. McGraw-Hill, New York, 7th edition, 2013.

[19] V. Carmona, E. Freire, E. Ponce, and F. Torres. Invariant manifolds of periodic orbits for piecewise linear three-dimensional systems. *IMA Journal of Applied Mathematics*, 69(1):71–91, 2004.

[20] C. Chicone. *Ordinary differential equations with applications*, volume 34 of *Texts in applied mathematics*. Springer, New York, 2006.

[21] M. di Bernardo, C. Budd, A. R. Champneys, and P. Kowalczyk. *Piecewise-smooth dynamical systems: Theory and applications*, volume 163 of *Applied mathematical sciences*. Springer, London, 2008.

[22] M. di Bernardo and S. Hogan. Discontinuity-induced bifurcations of piecewise smooth dynamical systems. *Philosophical Transactions of the Royal Society of London A: Mathematical, Physical and Engineering Sciences*, 368(1930):4915–4935, 2010.

[23] L. Dieci and L. Lopez. Sliding motion in Filippov differential systems: Theoretical results and a computational approach. *SIAM Journal on Numerical Analysis*, 47(3):2023–2051, 2009.

[24] B. G. Durie and S. E. Salmon. Cellular kinetics, staging, and immunoglobulin synthesis in multiple myeloma. *Annual Review of Medicine*, 26(1):283–288, 1975.

[25] M. Eslami. *Theory of sensitivity in dynamic systems: An introduction*. Springer, Berlin/Heidelberg, 1994.

[26] A. F. Filippov. *Differential equations with discontinuous righthand sides: Control systems*, volume 18 of *Mathematics and its application*. Springer, Dordrecht, 1988.

[27] T. R. Fleming and D. P. Harrington. Nonparametric estimation of the survival distribution in censored data. *Communications in Statistics: Theory and Methods*, 13(20):2469–2486, 1984.

[28] R. Fonseca, B. Barlogie, R. Bataille, C. Bastard, P. L. Bergsagel, M. Chesi, F. E. Davies, J. Drach, P. R. Greipp, I. R. Kirsch, W. M. Kuehl, J. M. Hernandez, S. Minvielle, L. M. Pilarski, J. D. Shaughnessy, A. K. Stewart, and H. Avet-Loiseau. Genetics and cytogenetics of multiple myeloma: A workshop report. *Cancer Research*, 64(4):1546–1558, 2004.

[29] P. M. Frank. *Introduction to system sensitivity theory.* Academic Press, San Francisco, 1978.

[30] S. N. Gentry and T. L. Jackson. A mathematical model of cancer stem cell driven tumor initiation: Implications of niche size and loss of homeostatic regulatory mechanisms. *PloS ONE*, 8(8):e71128, 2013.

[31] P. E. Gill, W. Murray, and M. H. Wright. *Practical Optimization.* Emerald Group, Bingley, 1981.

[32] A. Gonzalez-Quintela, R. Alende, F. Gude, J. Campos, J. Rey, L. Meijide, C. Fernandez-Merino, and C. Vidal. Serum levels of immunoglobulins (IgG, IgA, IgM) in a general adult population and their relationship with alcohol consumption, smoking and common metabolic abnormalities. *Clinical and Experimental Immunology*, 151(1):42–50, 2008.

[33] P. E. Greenwood and M. S. Nikulin. *A guide to chi-squared testing.* John Wiley and Sons, New York, 1996.

[34] L. Grüne and O. Junge. *Gewöhnliche Differentialgleichungen: Eine Einführung aus der Perspektive der dynamischen Systeme.* Springer Spektrum, Wiesbaden, 2009.

[35] L. Grüne and P. E. Kloeden. Higher order numerical approximation of switching systems. *Systems and Control Letters*, 55(9):746–754, 2006.

[36] J. Guckenheimer and P. Holmes. *Nonlinear oscillations, dynamical systems, and bifurcations of vector fields*, volume 42 of *Applied mathematical sciences.* Springer, New York, 1983.

[37] P. Hahnfeldt, D. Panigrahy, J. Folkman, and L. Hlatky. Tumor development under angiogenic signaling: A dynamical theory of tumor growth, treatment response, and postvascular dormancy. *Cancer Research*, 59(19):4770–4775, 1999.

[38] E. Hairer, S. Nørsett, and G. Wanner. *Solving ordinary differential equations I. Nonstiff problems*, volume 8 of *Springer series in computational mathematics.* Springer, Berlin/Heidelberg, 1987.

[39] J. K. Hale. *Ordinary Differential Equations*. Krieger Publishing Company, Malabar, 1980.

[40] D. P. Harrington and T. R. Fleming. A class of rank test procedures for censored survival data. *Biometrika*, 69(3):553–566, 1982.

[41] W. Harrison. The total cellularity of the bone marrow in man. *Journal of Clinical Pathology*, 15(3):254–259, 1962.

[42] P. Hartman. *Ordinary Differential Equations*. John Wiley and Sons, New York, 1964.

[43] J. Hillengass, K. Fechtner, M.-A. Weber, T. Bäuerle, S. Ayyaz, C. Heiss, T. Hielscher, T. Möhler, G. Egerer, K. Neben, A. D. Ho, H. U. Kauczor, S. Delorme, and H. Goldschmidt. Prognostic significance of focal lesions in whole-body magnetic resonance imaging in patients with asymptomatic multiple myeloma. *Journal of Clinical Oncology*, 28(9):1606–1610, 2010.

[44] J. Hillengass, T. Möhler, and M. Hundemer. Monoclonal gammopathy and smoldering multiple myeloma: Diagnosis, staging, prognosis, management. In T. Möhler and H. Goldschmidt, editors, *Multiple Myeloma*, pages 113–131. Springer, Berlin/Heidelberg, 2011.

[45] J. Hillengass, M. Weber, K. Kilk, K. Listl, B. Wagner-Gund, M. Hillengass, T. Hielscher, A. Farid, K. Neben, S. Delorme, O. Landgren, and H. Goldschmidt. Prognostic significance of whole-body MRI in patients with monoclonal gammopathy of undetermined significance. *Leukemia*, 28(1):174–178, 2014.

[46] J. Hobbs. Growth rates and responses to treatment in human myelomatosis. *British Journal of Haematology*, 16(6):607–618, 1969.

[47] D. Hose. Asymptomatic multiple myeloma: Molecular background of progression, evolution, and prognosis. *Justus-Liebig-Universität Gießen, Dissertation*, 2015.

[48] D. Hose, J. Moreaux, T. Meissner, A. Seckinger, H. Goldschmidt, A. Benner, K. Mahtouk, J. Hillengass, T. Reme, J. De Vos, M. Hundemer, M. Condomines, U. Bertsch, J. F. Rossi, A. Jauch, B. Klein, and T. Möhler. Induction of

angiogenesis by normal and malignant plasma cells. *Blood*, 114(1):128–143, 2009.

[49] D. Hose, T. Rème, T. Hielscher, J. Moreaux, T. Messner, A. Seckinger, A. Benner, J. D. Shaughnessy, B. Barlogie, Y. Zhou, J. Hillengass, U. Bertsch, K. Neben, T. Möhler, J. F. Rossi, A. Jauch, B. Klein, and H. Goldschmidt. Proliferation is a central independent prognostic factor and target for personalized and risk-adapted treatment in multiple myeloma. *Haematologica*, 96(1):87–95, 2011.

[50] D. Hose, T. Rème, T. Meissner, J. Moreaux, A. Seckinger, J. Lewis, V. Benes, A. Benner, M. Hundemer, T. Hielscher, J. D. Shaughnessy, B. Barlogie, K. Neben, A. Kraemer, J. Hillengass, U. Bertsch, A. Jauch, J. De Vos, J. F. Rossi, T. Möhler, J. Blake, J. Zimmermann, B. Klein, and H. Goldschmidt. Inhibition of aurora kinases for tailored risk-adapted treatment of multiple myeloma. *Blood*, 113(18):4331–4340, 2009.

[51] International Myeloma Working Group. Criteria for the classification of monoclonal gammopathies, multiple myeloma and related disorders: A report of the international myeloma working group. *British Journal of Haematology*, 121(5):749–757, 2003.

[52] J. A. Jacquez and T. Perry. Parameter estimation: Local identifiability of parameters. *American Journal of Physiology, Endocrinology and Metabolism*, 258(4):E727–E736, 1990.

[53] J. Jákó. *Gammopathy*. Springer, Berlin/Heidelberg, 1993.

[54] B. Ji, P. G. Genever, R. J. Patton, and M. J. Fagan. Mathematical modelling of the pathogenesis of multiple myeloma-induced bone disease. *International Journal for Numerical Methods in Biomedical Engineering*, 30(11):1085–1102, 2014.

[55] C. Jolliff, K. Cost, P. Stivrins, P. P. Grossman, C. R. Nolte, S. Franco, K. Fijan, L. Fletcher, and H. Shriner. Reference intervals for serum IgG, IgA, IgM, C3, and C4 as determined by rate nephelometry. *Clinical Chemistry*, 28(1):126–128, 1982.

[56] F. Jonsson, Y. Ou, L. Claret, D. Siegel, S. Jagannath, R. Vij, A. Badros, S. Aggarwal, and R. Bruno. A tumor growth inhibition model based on M-protein levels in subjects with relapsed/refractory multiple myeloma following single-agent carfilzomib use. *CPT: Pharmacometrics and Systems Pharmacology*, 4(12):711–719, 2015.

[57] M. Jourdan, A. Caraux, J. De Vos, G. Fiol, M. Larroque, C. Cognot, C. Bret, C. Duperray, D. Hose, and B. Klein. An in vitro model of differentiation of memory B cells into plasmablasts and plasma cells including detailed phenotypic and molecular characterization. *Blood*, 114(25):5173–5181, 2009.

[58] E. Kastritis, L. Moulopoulos, E. Terpos, V. Koutoulidis, and M. Dimopoulos. The prognostic importance of the presence of more than one focal lesion in spine MRI of patients with asymptomatic (smoldering) multiple myeloma. *Leukemia*, 28(12):2402–2403, 2014.

[59] M. Kirkilionis and S. Walcher. On comparison systems for ordinary differential equations. *Journal of Mathematical Analysis and Applications*, 299(1):157–173, 2004.

[60] B. Klein, A. Seckinger, T. Möhler, and D. Hose. Molecular pathogenesis of multiple myeloma: Chromosomal aberrations, changes in gene expression, cytokine networks, and the bone marrow microenvironment. In T. Möhler and H. Goldschmidt, editors, *Multiple Myeloma*, pages 39–86. Springer, Berlin/Heidelberg, 2011.

[61] J. P. Klein and M. L. Moeschberger. *Survival analysis: Techniques for censored and truncated data*. Springer, New York, 2003.

[62] A. Klenke. *Wahrscheinlichkeitstheorie*. Springer Spektrum, Berlin/Heidelberg, 2006.

[63] M. Koenders and R. Saso. A mathematical model of cell equilibrium and joint cell formation in multiple myeloma. *Journal of Theoretical Biology*, 390:73–79, 2016.

[64] S. V. Komarova, R. J. Smith, S. J. Dixon, S. M. Sims, and L. M. Wahl. Mathematical model predicts a critical role for osteoclast autocrine regulation in the control of bone remodeling. *Bone*, 33(2):206–215, 2003.

[65] E. J. Kunkel and E. C. Butcher. Plasma-cell homing. *Nature Reviews Immunology*, 3(10):822–829, 2003.

[66] J. Kurzweil. *Ordinary differential equations: Introduction to the theory of ordinary differential equations in the real domain*, volume 13 of *Studies in applied mechanics*. Elsevier, Amsterdam, 1986.

[67] Y. A. Kuznetsov. *Elements of applied bifurcation theory*, volume 112 of *Applied mathematical sciences*. Springer, New York, 2nd edition, 1998.

[68] R. A. Kyle, B. G. Durie, S. V. Rajkumar, O. Landgren, J. Bladé, G. Merlini, N. Kröger, H. Einsele, D. H. Vesole, M. Dimopoulos, J. F. San Miguel, H. Avet-Loiseau, R. Hajek, W. M. Chen, C. Anderson, Kenneth, H. Ludwig, P. Sonneveld, S. Pavlovsky, A. Palumbo, P. Richardson, B. Barlogie, P. Greipp, R. Vescio, I. Turesson, J. Westin, and M. Boccadoro. Monoclonal gammopathy of undetermined significance (MGUS) and smoldering (asymptomatic) multiple myeloma: IMWG consensus perspectives risk factors for progression and guidelines for monitoring and management. *Leukemia*, 24(6):1121–1127, 2010.

[69] R. A. Kyle, M. A. Gertz, T. E. Witzig, J. A. Lust, M. Q. Lacy, A. Dispenzieri, R. Fonseca, S. V. Rajkumar, J. R. Offord, D. R. Larson, M. E. Plevak, T. M. Therneau, and P. R. Greipp. Review of 1027 patients with newly diagnosed multiple myeloma. In W. L. Lanier, editor, *Mayo Clinic Proceedings*, volume 78, pages 21–33, Amsterdam, 2003. Elsevier.

[70] R. A. Kyle and P. R. Greipp. Smoldering multiple myeloma. *New England Journal of Medicine*, 302(24):1347–1349, 1980.

[71] R. A. Kyle and S. V. Rajkumar. Criteria for diagnosis, staging, risk stratification and response assessment of multiple myeloma. *Leukemia*, 23(1):3–9, 2009.

[72] R. A. Kyle, E. D. Remstein, T. M. Therneau, A. Dispenzieri, P. J. Kurtin, J. M. Hodnefield, D. R. Larson, M. F. Plevak, D. F. Jelinek, R. Fonseca, L. J.

Melton III, and S. V. Rajkumar. Clinical course and prognosis of smoldering (asymptomatic) multiple myeloma. *New England Journal of Medicine*, 356(25):2582–2590, 2007.

[73] R. A. Kyle, R. A. Robinson, and J. A. Katzmann. The clinical aspects of biclonal gammopathies: Review of 57 cases. *The American Journal of Medicine*, 71(6):999–1008, 1981.

[74] R. A. Kyle, T. M. Therneau, S. V. Rajkumar, J. R. Offord, D. R. Larson, M. F. Plevak, and L. J. Melton III. A long-term study of prognosis in monoclonal gammopathy of undetermined significance. *New England Journal of Medicine*, 346(8):564–569, 2002.

[75] A. K. Laird. Dynamics of tumour growth. *British Journal of Cancer*, 18(3):490, 1964.

[76] O. Landgren, R. A. Kyle, R. M. Pfeiffer, J. A. Katzmann, N. E. Caporaso, R. B. Hayes, A. Dispenzieri, S. Kumar, R. J. Clark, D. Baris, R. Hoover, and S. V. Rajkumar. Monoclonal gammopathy of undetermined significance (MGUS) consistently precedes multiple myeloma: A prospective study. *Blood*, 113(22):5412–5417, 2009.

[77] R. I. Leine. Bifurcations of equilibria in non-smooth continuous systems. *Physica D: Nonlinear Phenomena*, 223(1):121–137, 2006.

[78] R. I. Leine and H. Nijmeijer. *Dynamics and bifurcations of non-smooth mechanical systems*, volume 18 of *Lecture notes in applied and computational mechanics*. Springer, Berlin/Heidelberg, 2013.

[79] L. Li and W. B. Neaves. Normal stem cells and cancer stem cells: The niche matters. *Cancer Research*, 66(9):4553–4557, 2006.

[80] D. Liberzon. *Switching in systems and control*. Birkhäuser, Basel, 2012.

[81] L. López-Corral, N. C. Gutiérrez, M. B. Vidriales, M. V. Mateos, A. Rasillo, R. García-Sanz, B. Paiva, and J. F. San Miguel. The progression from MGUS to smoldering myeloma and eventually to multiple myeloma involves a clonal

expansion of genetically abnormal plasma cells. *Clinical Cancer Research*, 17(7):1692–1700, 2011.

[82] A. L. MacLean, C. L. Celso, and M. P. Stumpf. Population dynamics of normal and leukaemia stem cells in the haematopoietic stem cell niche show distinct regimes where leukaemia will be controlled. *Journal of the Royal Society Interface*, 10(81):20120968, 2013.

[83] S. Mankarious, M. Lee, S. Fischer, K. Pyun, H. Ochs, V. Oxelius, and R. Wedgwood. The half-lives of IgG subclasses and specific antibodies in patients with primary immunodeficiency who are receiving intravenously administered immunoglobulin. *The Journal of Laboratory and Clinical Medicine*, 112(5):634–640, 1988.

[84] R. A. Manz and A. Radbruch. Plasma cells for a lifetime? *European Journal of Immunology*, 32(4):923–927, 2002.

[85] A. Marciniak-Czochra, T. Stiehl, A. D. Ho, W. Jäger, and W. Wagner. Modeling of asymmetric cell division in hematopoietic stem cells-regulation of self-renewal is essential for efficient repopulation. *Stem Cells and Development*, 18(3):377–386, 2009.

[86] A. Morell, W. D. Terry, and T. A. Waldmann. Metabolic properties of IgG subclasses in man. *Journal of Clinical Investigation*, 49(4):673, 1970.

[87] W. R. Moser. *Linear models: A mean model approach*. Academic Press, San Diego, 1996.

[88] J. D. Murray. *Mathematical Biology I: An Introduction*, volume 17 of *Interdisciplinary applied mathematics*. Springer, New York, 2nd edition, 1993.

[89] K. Neben, A. Jauch, T. Hielscher, J. Hillengass, N. Lehners, A. Seckinger, M. Granzow, M. S. Raab, A. D. Ho, H. Goldschmidt, and D. Hose. Progression in smoldering myeloma is independently determined by the chromosomal abnormalities del(17p), t(4;14), gain 1q, hyperdiploidy, and tumor load. *Journal of Clinical Oncology*, 31(34):4325–4332, 2013.

[90] J. A. Nelder and R. Mead. A simplex method for function minimization. *The Computer Journal*, 7(4):308–313, 1965.

[91] L. Perko. *Differential equations and dynamical systems*, volume 7 of *Texts in applied mathematics*. Springer, New York, 3rd edition, 2001.

[92] B. Perthame. *Transport equations in biology*. Birkhäuser, Basel, 2007.

[93] M. Qiao, D. Wu, M. Carey, X. Zhou, and L. Zhang. Multi-scale agent-based multiple myeloma cancer modeling and the related study of the balance between osteoclasts and osteoblasts. *PloS ONE*, 10(12):e0143206, 2015.

[94] A. Radbruch, G. Mühlinghaus, E. O. Luger, A. Inamine, K. G. Smith, T. Dörner, and F. Hiepe. Competence and competition: The challenge of becoming a long-lived plasma cell. *Nature Reviews Immunology*, 6(10):741–750, 2006.

[95] S. V. Rajkumar, M. A. Dimopoulos, A. Palumbo, J. Blade, G. Merlini, M.-V. Mateos, S. Kumar, J. Hillengass, E. Kastritis, P. Richardson, O. Landgren, B. Paiva, A. Dispenzieri, B. Weiss, X. LeLeu, S. Zweegman, S. Lonial, L. Rosinol, E. Zamagni, S. Jagannath, O. Sezer, S. Y. Kristinsson, J. Caers, S. Z. Usmani, J. J. Lahuerta, H. E. Johnsen, M. Beksac, M. Cavo, H. Goldschmidt, E. Terpos, R. A. Kyle, K. C. Anderson, B. G. Durie, and J. F. Miguel. International myeloma working group updated criteria for the diagnosis of multiple myeloma. *The Lancet Oncology*, 15(12):e538–e548, 2014.

[96] D. A. Ratkowsky. *Nonlinear Regression Modeling: A Unified Practical Approach*. Marcel Dekker, New York, 1983.

[97] A. Raue, V. Becker, U. Klingmüller, and J. Timmer. Identifiability and observability analysis for experimental design in nonlinear dynamical models. *Chaos: An Interdisciplinary Journal of Nonlinear Science*, 20(4):045105, 2010.

[98] A. Raue, J. Karlsson, M. P. Saccomani, M. Jirstrand, and J. Timmer. Comparison of approaches for parameter identifiability analysis of biological systems. *Bioinformatics*, 30(10):1440–1448, 2014.

[99] A. Raue, C. Kreutz, T. Maiwald, J. Bachmann, M. Schilling, U. Klingmüller, and J. Timmer. Structural and practical identifiability analysis of partially

observed dynamical models by exploiting the profile likelihood. *Bioinformatics*, 25(15):1923–1929, 2009.

[100] A. Raue, M. Schilling, J. Bachmann, A. Matteson, M. Schelke, D. Kaschek, S. Hug, C. Kreutz, B. D. Harms, F. J. Theis, U. Klingmüller, and J. Timmer. Lessons learned from quantitative dynamical modeling in systems biology. *PLoS ONE*, 8(9):e74335, 2013.

[101] I. Roitt. *Essential immunology*. Blackwell Science, Oxford, 9th edition, 1997.

[102] S. Salmon. Immunoglobulin synthesis and tumour cell number and the natural history of multiple myeloma. *British Medical Journal*, 2(5757):321, 1971.

[103] S. E. Salmon and B. A. Smith. Immunoglobulin synthesis and total body tumor cell number in IgG multiple myeloma. *Journal of Clinical Investigation*, 49(6):1114–1121, 1970.

[104] S. Sandkühler and E. Gross. Normal bone marrow total cell and differential values by quantitative analysis of particle smears. *Blood*, 11(9):856–862, 1956.

[105] G. A. F. Seber and A. J. Lee. *Linear Regression Analysis*. John Wiley and Sons, Hoboken, 2nd edition, 2003.

[106] G. A. F. Seber and C. J. Wild. *Nonlinear Regression*. John Wiley and Sons, Hoboken, 2003.

[107] A. Seckinger and D. Hose. Interaction between myeloma cells and bone tissue. *Der Radiologe*, 54(6):545–550, 2014.

[108] A. Seckinger and D. Hose. Dissecting the clonal architecture of multiple myeloma. In *20th Congress of the European Hematology Association, Vienna, Austria. Haematologica*, volume 9, pages 173–179, 2015.

[109] A. Seckinger, A. Jauch, M. Emde, S. Beck, M. Mohr, M. Granzow, T. Hielscher, T. Rème, R. Schnettler, N. Farid, K. Hinderhofer, P. T. Pyl, W. Huber, V. Benes, A. Marciniak-Czochra, V. Pantesco, A. D. Ho, B. Klein, H. Goldschmidt, J. Hillengass, and D. Hose. Asymptomatic multiple myeloma: Molecular background of progression, evolution, and prognosis. *Submitted*, 2016.

[110] A. Seckinger, T. Meissner, J. Moreaux, H. Goldschmidt, G. M. Fuhler, A. Benner, M. Hundemer, T. Rème, J. D. Shaughnessy, B. Barlogie, U. Bertsch, J. Hillengass, A. D. Ho, V. Pantesco, A. Jauch, J. De Vos, J. F. Rossi, T. Möhler, Klein, and D. Hose. Bone morphogenic protein 6: A member of a novel class of prognostic factors expressed by normal and malignant plasma cells inhibiting proliferation and angiogenesis. *Oncogene*, 28(44):3866–3879, 2009.

[111] Y. Shiozawa, A. Havens, K. Pienta, and R. Taichman. The bone marrow niche: Habitat to hematopoietic and mesenchymal stem cells, and unwitting host to molecular parasites. *Leukemia*, 22(5):941–950, 2008.

[112] A.-N. Spiess and N. Neumeyer. An evaluation of R^2 as an inadequate measure for nonlinear models in pharmacological and biochemical research: A Monte Carlo approach. *BMC Pharmacology*, 10(1):6, 2010.

[113] T. Stiehl and A. Marciniak-Czochra. Mathematical modeling of leukemogenesis and cancer stem cell dynamics. *Mathematical Modelling of Natural Phenomena*, 7(1):166–202, 2012.

[114] R. R. Stine and E. L. Matunis. Stem cell competition: Finding balance in the niche. *Trends in Cell Biology*, 23(8):357–364, 2013.

[115] P. W. Sullivan and S. E. Salmon. Kinetics of tumor growth and regression in IgG multiple myeloma. *Journal of Clinical Investigation*, 51(7):1697, 1972.

[116] M. Tang, R. Zhao, H. van de Velde, J. G. Tross, C. S. Mitsiades, S. Viselli, R. Neuwirth, D.-L. Esseltine, K. C. Anderson, I. M. Ghobrial, J. F. San Miguel, P. G. Richardson, M. H. Tomasson, and F. Michor. Myeloma cell dynamics in response to treatment supports a model of hierarchical differentiation and clonal evolution. *Clinical Cancer Research*, 10.1158/1078-0432.CCR-15-2793, 2016.

[117] D. Tarlinton, A. Radbruch, F. Hiepe, and T. Dörner. Plasma cell differentiation and survival. *Current Opinion in Immunology*, 20(2):162–169, 2008.

[118] L. W. Terstappen, S. Johnsen, I. M. Segers-Nolten, and M. R. Loken. Identification and characterization of plasma cells in normal human bone marrow by high-resolution flow cytometry. *Blood*, 76(9):1739–1747, 1990.

[119] G. Teschl. *Ordinary differential equations and dynamical systems*, volume 140 of *Graduate studies in mathematics*. American Mathematical Society, Providence, 2012.

[120] A. N. Tikhonov. Systems of differential equations containing small parameters in the derivatives. *Matematicheskii Sbornik*, 73(3):575–586, 1952.

[121] K. Tokoyoda, T. Egawa, T. Sugiyama, B.-I. Choi, and T. Nagasawa. Cellular niches controlling B lymphocyte behavior within bone marrow during development. *Immunity*, 20(6):707–718, 2004.

[122] K. van Herck, P. Beutels, P. van Damme, M. Beutels, J. van den Dries, P. Briantais, and E. Vidor. Mathematical models for assessment of long-term persistence of antibodies after vaccination with two inactivated Hepatitis A vaccines. *Journal of Medical Virology*, 60(1):1–7, 2000.

[123] H. C. van Houwelingen. Dynamic prediction by landmarking in event history analysis. *Scandinavian Journal of Statistics*, 34(1):70–85, 2007.

[124] V. I. Vorotnikov. Partial stability and control: The state-of-the-art and development prospects. *Automation and Remote Control*, 66(4):511–561, 2005.

[125] E. Walter. *Identifiability of state space models: With applications to transformation systems*, volume 46 of *Lecture notes in biomathematics*. Springer, Berlin/Heidelberg, 1982.

[126] E. Walter and L. Pronzato. *Identification of parametric models from experimental data*. Springer, London, 1997.

[127] W. Walter. *Gewöhnliche Differentialgleichungen: Eine Einführung*. Springer Berlin/Heidelberg, 7th edition, 2000.

[128] Y. Wang, P. Pivonka, P. R. Buenzli, D. W. Smith, and C. R. Dunstan. Computational modeling of interactions between multiple myeloma and the bone microenvironment. *PloS ONE*, 6(11):e27494, 2011.

[129] G. Wetzel. Geschichtliches zur Bestimmung der Größe des Markorgans. *Anatomy and Embryology*, 82(1):70–72, 1927.

[130] S. Wiggins. *Introduction to applied nonlinear dynamical systems and chaos*, volume 2 of *Texts in applied mathematics*. Springer, New York, 2nd edition, 2003.

[131] A. E. Williams. *Immunology: Mucosal and Body Surface Defences*. John Wiley and Sons, Hoboken, 2011.

[132] X. Yan and X. G. Su. *Linear regression analysis: Theory and computing*. World Scientific, Singapore, 2009.

[133] J. Zabalo. A mathematical model describing the early development of multiple myeloma. *University of Miami, Dissertation, Paper 366*, 2010.

[134] J. Zhang, C. Niu, L. Ye, H. Huang, X. He, W.-G. Tong, J. Ross, J. Haug, T. Johnson, J. Q. Feng, S. Harris, L. M. Wiedemann, Y. Mishina, and L. Li. Identification of the haematopoietic stem cell niche and control of the niche size. *Nature*, 425(6960):836–841, 2003.

List of symbols

A non-exclusive list of abbreviations and mathematical symbols is provided.

Abbreviations

Ig	Immunoglobulin
IgA	Immunoglobulin A
IgG	Immunoglobulin G
IgM	Immunoglobulin M
MM	Multiple myeloma
PC	Plasma cell
ODE	Ordinary differential equation
AMM	Asymptomatic multiple myeloma
MGUS	Monoclonal gammopathy of unknown significance
IMWG	International Myeloma Working Group
Basic model	Basic model of healthy PC dynamics in the bone marrow, see Chapter 3
Extended model	Extended model of healthy PC dynamics in the bone marrow, see Chapter 4
Myeloma model	Model of healthy and malignant PC dynamics in the bone marrow, see Chapter 5

Mathematical symbols

$\mathbb{N}$	Set of natural numbers
$\mathbb{R}$	Set of real numbers
$\mathbb{R}_+$	Set of non-negative real numbers, i.e. $\{x \in \mathbb{R} \colon x \geq 0\}$
$\mathbb{C}$	Set of complex numbers
$\mathbb{R}^n$	Set of n-dimensional vectors over $\mathbb{R}$, $n \in \mathbb{N}$
$\mathbb{R}^{n \times n}$	Set of $n \times n$-matrices over $\mathbb{R}$, $n \in \mathbb{N}$
$0^{n \times n}$	$n \times n$-zero matrix, $n \in \mathbb{N}$
$\mathbb{1}^{n \times n}$	$n \times n$-identity matrix, $n \in \mathbb{N}$
$C(\mathcal{U}, \mathcal{V})$	Set of continuous functions $\mathcal{U} \mapsto \mathcal{V}$. Abbreviation: C
$C^r(\mathcal{U}, \mathcal{V})$	Set of r-times continuously differentiable functions $\mathcal{U} \mapsto \mathcal{V}$. Abbreviation: C^r
$C^\infty(\mathcal{U}, \mathcal{V})$	Set of smooth functions $\mathcal{U} \mapsto \mathcal{V}$. Abbreviation: C^∞
∇	Gradient
$\dot{V}$	Lie derivative of V along a vector field, i.e. $\dot{V}(x) = \nabla V(x) \cdot g(x)$ with $x'(t) = g(x(t))$
x^T	Transposition of vector x
A^T	Transposition of matrix A
$\lvert A \rvert$	Determinant of matrix A
$\exp(x) = e^x$	Exponential function of x
$\ln(x)$	Natural logarithm of x
$\Re(x)$	Real part of $x \in \mathbb{C}$
$\lVert \cdot \rVert_1$	1-norm, i.e. $\lVert x \rVert_1 = \sum_{i=1}^n \lvert x_i \rvert$ for $x = (x_1, \ldots, x_n)^T \in \mathbb{R}^n$

t	Time variable
$x'(t)$, $\frac{d}{dt}x(t)$	Derivative of x with respect to t
$\frac{\partial f}{\partial x_i}(x_1, \ldots, x_n)$	Partial derivative of f with respect to x_i, $i = 1, \ldots, n$
max, min	Maximum or minimum of a function or set
argmin $f(x)$	Value of x such that f is minimal
id	Identity map
$\overline{\mathcal{U}}$	Closure of a set $\mathcal{U}$
$\partial\mathcal{U}$	Boundary of a set $\mathcal{U}$
$\mathcal{O}(g)$	Landau symbol, where $f \in \mathcal{O}(g)$ if $\left\lvert\frac{f(x)}{g(x)}\right\rvert < \infty$ for large x
Δ	Change of a parameter θ, i.e $\Delta(\theta)$, or difference/error of a function x, i.e. $\Delta(x)$
$\lfloor x \rfloor$	Largest integer less than or equal to x
P	p-value
$A \mathrel{\widehat{=}} B$	A corresponds to B
$x \ll y$	Significant strict inequality, i.e. x is much less than y
#	Number/amount

List of figures

List of tables

List of publications

- A. Seckinger, A. Jauch, M. Emde, S. Beck, M. Mohr, M. Granzow, T. Hielscher, T. Rème, R. Schnettler, N. Fard, K. Hinderhofer, P. Pyl, W. Huber, V. Benes, A. Marciniak-Czochra, V. Pantesco, A. D. Ho, B. Klein, J. Hillengass, D. Hose. Asymptomatic multiple myeloma: Molecular background of progression, evolution, and prognosis. *Submitted*, 2016.

Appendices

A Mathematical methods

A.1 Piecewise-smooth continuous dynamical systems

A.1.1 Basic definitions

While the theory of smooth dynamical systems is well understood [36, 67, 130], much less in known about non-smooth continuous vector fields. Piecewise-smooth systems exhibit a wide range of non-linear phenomena including bifurcations and chaos [22, 77]. For review, see di Bernardo et al. [21] or Leine and Nijmeijer [78].

Definition A.1 (Time-continuous dynamical system, adapted from Definition 2.1 in [21])**.** A state space $X \subseteq \mathbb{R}^n$, an index set $T \subseteq \mathbb{R}$ and an evolution operator $\Phi : T \times X \to X,\ (t, x) \mapsto \Phi(t, x)$, i.e. a flow, define a time-continuous dynamical system if

(i) $\Phi(0, x) = x$ for all $x \in X$

(ii) $\Phi(t + s, x) = \Phi\left(s, \Phi(t, x)\right)$ for all $x \in X,\ s, t \in T$.

Definition A.2 (Piecewise-smooth flow, adapted from Definition 2.20 in [21])**.** A piecewise-smooth flow is given by a finite set of autonomous ODEs

$$x'(t) = f_i(x(t)) \text{ for } x(t) \in \mathcal{S}_i,$$

where $\bigcup_i \mathcal{S}_i = \mathcal{D} \subseteq \mathbb{R}^n$ and each $\mathcal{S}_i$ has a non-empty interior. The intersection $\Sigma_{ij} := \bar{\mathcal{S}}_i \cap \bar{\mathcal{S}}_j$ is either an $(n-1)$-dimensional manifold included in the boundaries $\partial\mathcal{S}_i$ and $\partial\mathcal{S}_j$, or is the empty set. In the first case, Σ_{ij} is called a **switching manifold**. Each vector field f_i is smooth in the state x, and defines a smooth flow $\Phi_i(t, x)$ within any open set $\mathcal{U} \subseteq \mathcal{S}_i$.

Definition A.3 (Degree of smoothness, adapted from Definition 2.21 in [21])**.** The degree of smoothness at a point x_0 on a switching manifold Σ_{ij} of a piecewise-smooth flow is the highest order r such that the Taylor series expansions of $\Phi_i(t, x_0)$ and $\Phi_j(t, x_0)$ with respect to t, evaluated at $t = 0$, agree up to terms of $\mathcal{O}(t^{r-1})$. That is to say, the first non-zero partial derivative with respect to t of the difference $(\Phi_i(t, x_0) - \Phi_j(t, x_0))\,|_{t=0}$ is of order r.

By Definition A.3, a piecewise-smooth flow with degree of smoothness r is C^{r-1}. Thus, the respective vector field is one degree less smooth, i.e. C^{r-2} [21]. Systems with degree of smoothness one are called Filippov systems [21, 26].

The following consideration focuses on an ODE local to a single switching manifold $\Sigma := \Sigma_{12}$ given by

$$x'(t) = f(x(t)) = \begin{cases} f_1(x(t)) & \text{if } x(t) \in \mathcal{S}_1 \\ f_2(x(t)) & \text{if } x(t) \in \mathcal{S}_2, \end{cases} \tag{A.1.1}$$

where f_1 generates a flow Φ_1 and f_2 generates a flow Φ_2. As shown by di Bernardo et al. [21], if f_1 and f_2 differ in an m-th partial derivative with respect to the state x, the flows Φ_1 and Φ_2 differ in their $(m + 1)$-st partial derivative with respect to t. Observe that if $f_1(x(t)) = f_2(x(t))$ for $x(t) \in \Sigma$ and there is a difference in the Jacobian derivatives $\frac{\partial}{\partial x} f_1 \neq \frac{\partial}{\partial x} f_2$ at x, then the degree of smoothness is two.

Definition A.4 (Piecewise-smooth continuous dynamical system, see Section 2.2.2 in [21])**.** A dynamical system generated by a piecewise-smooth flow of the form (A.1.1) having degree of smoothness two or higher is called piecewise-smooth continuous dynamical system.

To summarise, a piecewise-smooth continuous dynamical system is continuous across the phase space boundaries but the Jacobian of the flow is discontinuous across the switching manifold. Note that system (A.1.1) does not specify the flow within the switching manifold in case of $\Sigma \notin \mathcal{S}_1 \cup \mathcal{S}_2$. Continuity allows assigning Σ as belonging to the region $\mathcal{S}_1$ or $\mathcal{S}_2$.

Using classical theory of ODEs [34, 39], (local) Lipschitz continuity of the vector field implies existence and uniqueness of solutions of the respective system.

Definition A.5 (Lipschitz continuity)**.** Let $g : \mathcal{U} \to \mathbb{R}^n$, $\mathcal{U} \subseteq \mathbb{R} \times \mathbb{R}^n$, be a (not necessarily autonomous) continuous vector field with $g : (t, x) \mapsto g(t, x)$. Then, g is locally Lipschitz continuous in x, uniformly in t, if for any closed bounded set $\mathcal{V} \subseteq \mathcal{U}$ there exists a constant $L > 0$ such that

$$\|g(t, x) - g(t, y)\| \leq L\|x - y\| \text{ for all } (t, x), (t, y) \in \mathcal{V}.$$

Theorem A.6 (Existence and uniqueness of solutions of piecewise-smooth continuous systems)**.** *Consider the piecewise-smooth continuous system* (A.1.1) *with initial condition* $x(t_0) = x_0$*. Then, the following holds true:*

(i) There exists a solution $x(t)$ *of* (A.1.1) *satisfying* $x(t_0) = x_0$ *which is defined for all* t *on an open maximal interval of existence* $I_{max} \subseteq \mathbb{R}$ *with* $t_0 \in I_{max}$*.*

(ii) In addition, if f *is (locally) Lipschitz continuous with respect to the state* x*, then there exists a unique solution* $x(t)$ *of* (A.1.1) *satisfying* $x(t_0) = x_0$ *which is defined for all* t *on an open maximal interval of existence* $I_{max} \subseteq \mathbb{R}$ *with* $t_0 \in I_{max}$*.*

Proof. Observe that f is continuous. Thus, the first statement follows by Peano's theorem [39, Theorem 1.1] and continuation of solutions [39, Theorem 2.1]. The latter follows by the theorem of Picard and Lindelöf [39, Theorem 3.1]. See also [34, Theorem 3.6]. □

Remark A.7 (Global existence and uniqueness of solutions)**.** If Lipschitz continuity holds on the entire domain, then $I_{max} = \mathbb{R}$, implying global existence and uniqueness of solutions. In general, the only obstruction to the solution propagating across the entire domain is unboundedness. That is if a blow-up of the solution $x(t)$ at a finite time $t_1 > t_0$ can be excluded, i.e. $\lim_{t \to t_1} x(t) = \infty$, then $x(t)$ exists globally.

Remark A.8 (Continuous dependence of solutions on initial conditions and parameters)**.** The unique solution $x(t)$ of (A.1.1) satisfying $x(t_0) = x_0$ is continuously dependent on the initial data x_0 and t_0 [119, Theorem 2.9]. If in addition to the hypotheses in Theorem A.6 (ii) the vector field f depends on a parameter $\lambda \in \mathcal{G}$, $\mathcal{G} \subseteq \mathbb{R}^k$, i.e. $f = f(x, \lambda)$, which is continuous for λ in $\mathcal{G}$, then the unique solution $x(t)$ satisfying $x(t_0) = x_0$ is continuously dependent on the parameter λ [66, Theorem 14.1.1].

Remark A.9 (Smooth dependence of solutions on initial conditions and parameters)**.** It is well known that if the right-hand side of an ODE has continuous first derivatives with respect to the state space and parameters, then the solution is continuously differentiable with respect to the initial conditions and parameters [39, Theorem 3.3]. Yet, since the vector field $f(x)$ is only piecewise-smooth, it cannot be deduced that the solutions of (A.1.1) are smoothly dependent on initial conditions and parameters. Piecewise-smooth systems may be approximated by smooth vector fields (see Appendix A.2), which in turn gives rise to approximate solutions. These depend smoothly on initial conditions and parameters.

A.1.2 Stability of equilibria

The extension of well-established concepts for smooth dynamical systems to the case of non-smooth dynamical systems is an open research area [21]. Linearised stability theory and the theorem of Hartman and Grobman [36, Theorem 1.4.1] cannot be applied to non-smooth vector fields. The following definitions are adapted from [119, Chapter 6].

Definition A.10 (Stability of an equilibrium)**.** Consider the piecewise-smooth system (A.1.1).

(i) An equilibrium $\bar{x}$ is said to be stable if for every $\varepsilon > 0$, there exists a $\delta > 0$ such that for every solution $x(t)$ satisfying $\|x(t_0) - \bar{x}\| < \delta$ it follows that $\|x(t) - \bar{x}\| < \varepsilon$ for all $t \geq t_0$.

(ii) An equilibrium $\bar{x}$ is said to be (locally) asymptotically stable if it is stable and if there is a neighbourhood $\mathcal{V}$ of $\bar{x}$ such that $\lim_{t\to\infty} x(t) = \bar{x}$ for all $x(t_0) \in \mathcal{V}$.

Definition A.11 (Invariant set)**.** Consider the piecewise-smooth system (A.1.1). Let $\mathcal{I} \subseteq \mathcal{D}$ be a set. Then, $\mathcal{I}$ is said to be (positively) invariant under the vector field of the piecewise-smooth system (A.1.1) if for any initial value $x(t_0) = x_0 \in \mathcal{I}$ the solution satisfies $x(t) \in \mathcal{I}$ for all $t > t_0$.

If an invariant set is located in either $\mathcal{S}_1$ or $\mathcal{S}_2$, the theory of smooth vector fields may be applied to analyse the stability of an equilibrium. However, if the invariant set straddles the boundary Σ between $\mathcal{S}_1$ and $\mathcal{S}_2$, the derivation of necessary and sufficient conditions that guarantee asymptotic stability are not definite. The application of

the theory for smooth dynamical systems may lead to incorrect conclusions as the following example illustrates.

Example A.12 (Unstable piecewise-linear system, adapted from Example 2.11 in [21], see also [19])**.** We consider the following piecewise-linear system in $\mathbb{R}^3$ with $x(t) = (x_1(t), x_2(t), x_3(t))^T$ given by

$$x'(t) = \begin{cases} A^+ x(t) & \text{if } x_1(t) \geq 0 \\ A^- x(t) & \text{if } x_1(t) < 0, \end{cases}$$

where

$$A^+ = \begin{pmatrix} -3.2 & -1 & 0 \\ 25.61 & 0 & -1 \\ -75.03 & 0 & 0 \end{pmatrix}, \quad A^- = \begin{pmatrix} -1 & -1 & 0 \\ 1.28 & 0 & -1 \\ -0.624 & 0 & 0 \end{pmatrix}.$$

Since

$$A^+ x(t) = A^- x(t) \text{ with } x_1(t) = 0,$$

the system is continuous across the switching manifold $\Sigma = \{x(t) \in \mathbb{R}^3 \colon x_1(t) = 0\}$. A straightforward calculation yields that the eigenvalues of A^+ are $-0.1 \pm 0.5i$ and -3, whereas the eigenvalues of A^- are $-0.2 \pm i$ and -0.6. For each linear system separately, this would imply stability of the origin $(0, 0)^T$ due to the negative real parts of the eigenvalues [36]. Trajectories of the piecewise-linear system starting in the neighbourhood of the origin tend to infinity, as indicated by Figure A.1.

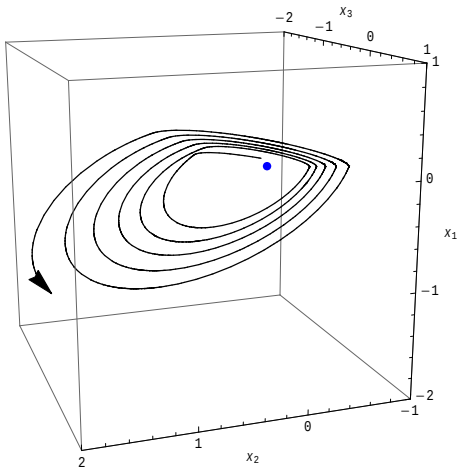

Figure A.1: A trajectory of the piecewise-linear system in Example A.12, which starts in the neighbourhood of the trivial equilibrium (blue), tends to infinity.

The previous example shows that stability properties of equilibria located on the switching manifold Σ cannot be deduced from the sub-system dynamics in $\mathcal{S}_1$ and $\mathcal{S}_2$. As proposed in [80], one way of proving stability of an equilibrium located on Σ is to find a common Lyapunov function, i.e. a function that is Lyapunov for each of the vector fields defining the systems dynamics in each of the phase space regions $\mathcal{S}_1$ and $\mathcal{S}_2$. The definition of a Lyapunov function and its application for determination of the stability of an equilibrium originating from the classical theory of smooth dynamical systems are provided [36, Chapter 1]. Thereby, the definition of the Lie derivative of a function along a vector field is recalled [119, Chapter 6]. This is a major tool for proving (positive) invariance of a set under a given vector field.

Definition A.13 (Lyapunov function)**.** Let $\mathcal{U} \subseteq \mathbb{R}^n$ be open and $g \in C(\mathcal{U}, \mathbb{R}^n)$ be (locally) Lipschitz continuous. A Lyapunov function of the system $x'(t) = g(x(t))$ is a function $V \in C^1(\mathcal{U}, [0, \infty))$ with non-positive **Lie derivative**, that is to say,

$$\dot{V}(x) = \nabla V(x) \cdot g(x) \leq 0 \text{ for all } x \in \mathcal{U}.$$

If the Lie derivative is strictly negative, that is to say,

$$\dot{V}(x) = \nabla V(x) \cdot g(x) < 0 \text{ for all } x \in \mathcal{U}$$

with $g(x) \neq 0$, then V is called a strict Lyapunov function.

Theorem A.14 (Lyapunov stability)**.** *Let $\mathcal{U} \subseteq \mathbb{R}^n$ be open and $g \in C(\mathcal{U}, \mathbb{R}^n)$ be (locally) Lipschitz continuous. Let $\bar{x}$ be an equilibrium of the system $x'(t) = g(x(t))$. Moreover, let $\mathcal{V} \subseteq \mathcal{U}$ be an open neighbourhood of $\bar{x}$.*

(i) If there exists a Lyapunov function V on $\mathcal{V}$ satisfying $V(\bar{x}) = 0$ and $V(x) > 0$ for all $x \in \mathcal{V}$ with $x \neq \bar{x}$, then $\bar{x}$ is stable.

(ii) If there exists a strict Lyapunov function V on $\mathcal{V}$ satisfying $V(\bar{x}) = 0$ and $V(x) > 0$ for all $x \in \mathcal{V}$ with $x \neq \bar{x}$, then $\bar{x}$ is (locally) asymptotically stable.

Observe that if the statement of Theorem A.14 (ii) is satisfied globally (i.e. on the complete domain $\mathcal{U}$ of the right-hand side g of the system), then $\bar{x}$ is globally asymptotically stable. Moreover, g is only required to be continuous. This justifies the usage of Lyapunov stability for piecewise-smooth continuous dynamical systems.

Remark A.15. In Chapters 6, 7 and 8, the bar notation $\bar{x}$ for designation of equilibria is omitted. Instead, equilibria are labelled differently, or the time dependence is dropped.

A.1.3 Numerical methods

As observed by Acary and Brogliato [1], dynamical systems consisting of piecewise-smooth ODEs with Lipschitz continuous right-hand side can be solved numerically with standard methods which apply to dynamical systems consisting of smooth ODEs with Lipschitz continuous right-hand side [17, 38]. Due to non-differentiability of the right-hand side, these methods have only order of convergence one. To maintain the order, so-called event-driven schemes are used. The times at which the system becomes non-smooth are accurately solved using, for instance, the Runge-Kutta method [21, 35].

Within this thesis, the software package *Mathematica, Version 9* by Wolfram Research is used for solving piecewise-smooth continuous systems. This is done by applying the function `NDSolve`, which uses methods based on an implicit assumption that the right-hand side of the system of ODEs is Lipschitz continuous. In addition, *Mathematica* allows event location and restarting of the numerical integration using `WhenEvent`. For more details on implemented methods, see *Mathematica's* online documentation (http://reference.wolfram.com; last accessed: April 2016).

A.2 Smoothing method

Consider the piecewise-smooth continuous dynamical system introduced in Appendix A.1, i.e.

$$x'(t) = f(x(t)) = \begin{cases} f_1(x(t)) & \text{if } x(t) \in \mathcal{S}_1 \\ f_2(x(t)) & \text{if } x(t) \in \mathcal{S}_2 \end{cases} \tag{A.1.1}$$

with $f_1(x) = f_2(x)$ for $x \in \Sigma$. Furthermore, assume that

$$\begin{aligned} \mathcal{S}_1 &= \{x \in \mathbb{R}^n \mid h(x) > 0\} \\ \Sigma &= \{x \in \mathbb{R}^n \mid h(x) = 0\} \\ \mathcal{S}_2 &= \{x \in \mathbb{R}^n \mid h(x) < 0\}. \end{aligned}$$

The non-smooth right-hand side $f(x)$ can be approximated by a smoothed vector field [78]. For a smooth approximation of the sign-function, the arctangent approximation may be used, i.e.

$$\operatorname{sign}(x) \approx \frac{2}{\pi} \arctan(\varepsilon x), \quad \varepsilon \gg 1.$$

By using this approximation, the smoothed system of (A.1.1) reads

$$x'(t) = \frac{1}{2}\left(f_1 + f_2 + \frac{2}{\pi} \arctan(\varepsilon h)(f_1 - f_2)\right) \tag{A.2.1}$$

with $f_{1,2} := f_{1,2}(x(t))$ and $h := h(x(t))$.

Example A.16 (Smoothed version of the basic model)**.** Let $h = h(x_h, y_h) = z = x_h - y_h + n$. Applying the smooth approximation (A.2.1) yields

$$\begin{aligned} x_h' &= f - \frac{1}{2}\left(b_h + c_h + \frac{2}{\pi} \arctan(\varepsilon z)(b_h - c_h)\right) z - d x_h \\ y_h' &= \frac{1}{2}\left(b_h + c_h + \frac{2}{\pi} \arctan(\varepsilon z)(b_h - c_h)\right) z, \end{aligned}$$

where the time dependence is skipped. Consequently, the approximated rates of

transition are given by the function

$$\frac{1}{2}\left(b_h + c_h + \frac{2}{\pi}\arctan(\varepsilon z)(b_h - c_h)\right).$$

To give an illustration, the approximation of the transition rates dependent on the sign of z are shown in Figure A.2 for different values of ε. Smoothing of the basic model requires the transition rates to be approximated by a continuous version.

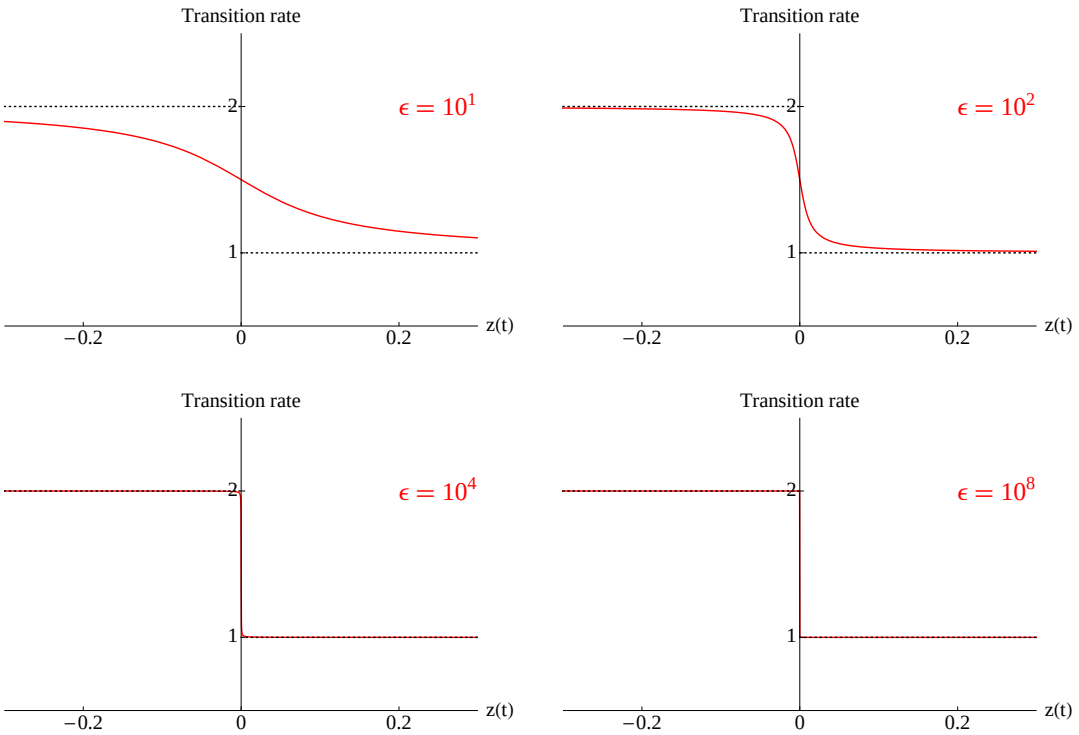

Figure A.2: Approximations of the transition rates for different values of ε. Black dotted: Transition rates for $z \geq 0$ and $z < 0$, respectively. Red: Smooth approximation of transition rates. For details, see text.

Example A.17 (Smoothed version of the myeloma model)**.** Let $h = h(x_h, x_m, y_h, y_m) = z = x_h + x_m - y_h - y_m + n$. Applying the smooth approximation (A.2.1) yields

$$x_h' = f - \frac{1}{2}\left(b_h \frac{x_h}{x_h + x_m} + c_h \frac{y_h}{y_h + y_m} + \frac{2}{\pi}\arctan(\varepsilon z)\left(b_h \frac{x_h}{x_h + x_m} - c_h \frac{y_h}{y_h + y_m}\right)\right) z - d x_h$$

$$x_m' = p_1 x_m - \frac{1}{2}\left(b_m \frac{x_m}{x_h + x_m} + c_m \frac{y_m}{y_h + y_m} + \frac{2}{\pi}\arctan(\varepsilon z)\left(b_m \frac{x_m}{x_h + x_m} - c_m \frac{y_m}{y_h + y_m}\right)\right) z$$

$$y_h' = \frac{1}{2}\left(b_h \frac{x_h}{x_h + x_m} + c_h \frac{y_h}{y_h + y_m} + \frac{2}{\pi}\arctan(\varepsilon z)\left(b_h \frac{x_h}{x_h + x_m} - c_h \frac{y_h}{y_h + y_m}\right)\right) z$$

$$y_m' = p_2 y_m + \frac{1}{2}\left(b_m \frac{x_m}{x_h + x_m} + c_m \frac{y_m}{y_h + y_m} + \frac{2}{\pi}\arctan(\varepsilon z)\left(b_m \frac{x_m}{x_h + x_m} - c_m \frac{y_m}{y_h + y_m}\right)\right) z,$$

where the time dependence is skipped. Considering IgA-myeloma Patient 1, a best-fit solution was found within the framework of the myeloma model, see Chapter 10. In Figure A.3, dotted functions represent solutions of the smoothed approximation using the identical set of parameters. The relative error of an approximate solution $s_a(t)$ is defined by

$$\frac{s_a(t) - s(t)}{s(t)},$$

where $s(t)$ is the solution to be approximated. By this definition, the relative error of the smoothed approximation in case of $\varepsilon = 10^{12}$ is in the order of 10^{-7}. Along these lines, the smooth approximation of the piecewise-smooth continuous dynamical system (A.1.1) yields a good approximation for large values of ε. Although it often results in stiff differential equations which are numerically expensive to solve [78], it allows applying the stability theory of equilibria for smooth vector fields [36].

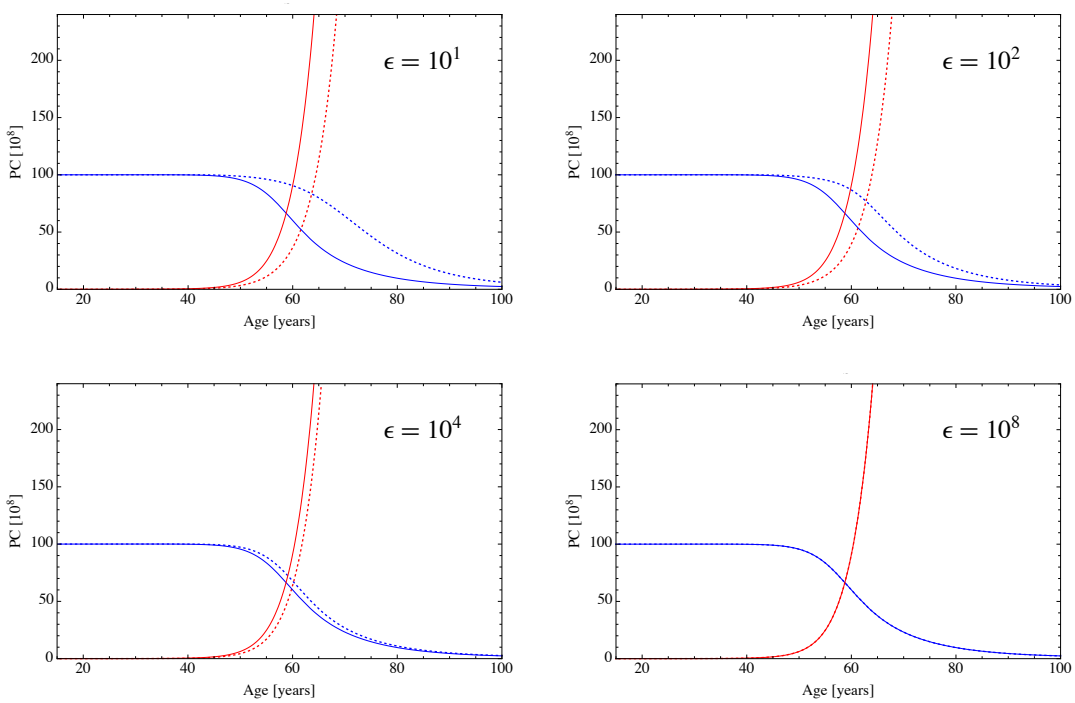

Figure A.3: Approximations (dotted) of a best-fit solution (solid) for IgA-myeloma Patient 1 for different values of ε. The total number of healthy (blue) and malignant (red) plasma cells (PCs) are visualised. For details, see text.

A.3 Principles of parameter estimation

A.3.1 Linear regression models

This chapter reviews basic results about linear regression. This is due to the fact that methods for non-linear regression are mainly based on the linear findings. Basic knowledge about probability theory is presumed [62]. For more details, see Seber and Lee [105], Moser [87] or Yan and Su [132].

Definition A.18 (Multivariate normal distribution)**.** Let $\mu \in \mathbb{R}^n$ and $\Sigma \in \mathbb{R}^{n \times n}$ be a symmetric and positive definite matrix. The multivariate normal distribution is defined by the probability density function

$$p(x) = \frac{1}{(2\pi)^{n/2}|\Sigma|^{1/2}} \exp\left(-\frac{1}{2}(x-\mu)^T\Sigma^{-1}(x-\mu)\right).$$

A random vector X is said to be normally distributed with mean μ and covariance matrix Σ if it has probability density $p(x)$. In that case, we write

$$X \sim \mathcal{N}_n(\mu, \Sigma).$$

Definition A.19 (Chi-squared distribution)**.** Let $X_1, \ldots, X_n$ with $X_i \sim \mathcal{N}(0,1)$ be independent. The chi-squared distribution with n degrees of freedom is defined as the distribution of the random variable

$$Z = \sum_{i=1}^{n} X_i^2$$

and denoted as $Z \sim \chi_n^2$.

Definition A.20 (F-distribution)**.** Let $X_1 \sim \chi_{n_1}^2$ and $X_2 \sim \chi_{n_2}^2$ be independent. The F-distribution with n_1 and n_2 degrees of freedom is defined as the distribution of the random variable

$$Z = \frac{X_1/n_1}{X_2/n_2}$$

and denoted as $Z \sim F_{n_1,n_2}$.

Definition A.21 (Student's t-distribution)**.** Let $X_1 \sim \mathcal{N}(0,1)$ and $X_2 \sim \chi^2_n$. The Student's t-distribution with n degrees of freedom is defined as the distribution of the random variable

$$Z = \frac{X_1}{\sqrt{X_2/n}}$$

and denoted as $Z \sim t_n$.

Next, the definition of the linear regression model is stated.

Definition A.22 (Linear regression model)**.** Let $Y \in \mathbb{R}^n$ be the vector of observations or responses, $X \in \mathbb{R}^{n\times m}$ the design matrix of explanatory or predictor variables, $\beta \in \mathbb{R}^m$ the vector of parameters and $\varepsilon \in \mathbb{R}^n$ the vector of random variables representing disturbances which perturb the responses. The linear regression model reads

$$Y = X\beta + \varepsilon \;\text{ with }\; \varepsilon \sim \mathcal{N}_n(0, \sigma^2 \mathbb{I}_n). \tag{A.3.1}$$

The following notation is used:

$$Y = \begin{pmatrix} y_1 \\ y_2 \\ \vdots \\ y_n \end{pmatrix}, \quad X = \begin{pmatrix} x_{11} & x_{12} & \dots & x_{1m} \\ x_{11} & x_{12} & \dots & x_{1m} \\ \vdots & \vdots & \ddots & \vdots \\ x_{n1} & x_{n2} & \dots & x_{nm} \end{pmatrix} \quad \beta = \begin{pmatrix} \beta_1 \\ \beta_2 \\ \vdots \\ \beta_m \end{pmatrix}, \quad \varepsilon = \begin{pmatrix} \varepsilon_1 \\ \varepsilon_2 \\ \vdots \\ \varepsilon_n \end{pmatrix}.$$

At first, the variance σ^2 is required to be known. Assuming that the linear model is appropriate for the given data represented by Y, the goal of parameter estimation is to find an estimate or a preferably good approximation $\hat{\beta}$ of the true but unknown parameter β.

The assumptions on ε imply that $\varepsilon_i,\ i = 1,\dots,n$, are mutually independent and $Y \sim \mathcal{N}(X\beta, \sigma^2\mathbb{I}_n)$, see [105, Theorem 2.1]. Thus, the joint probability density function for Y, given β and σ^2, reads

$$p(Y|\beta,\sigma^2) = (2\pi\sigma^2)^{-\frac{n}{2}} \exp\left(\frac{-\|Y - X\beta\|^2}{2\sigma^2}\right).$$

Regarding this probability density function as a function of the parameters conditional on the observed data yields the likelihood function $L = L(\beta, \sigma^2|Y)$ [105], which is maximised with respect to the parameter vector β when the **residual sum of squares**

$$S(\beta) = \|Y - X\beta\|^2 = \sum_{i=1}^{n} \left(y_i - \sum_{j=1}^{m} x_{ij}\beta_j \right) \tag{A.3.2}$$

is minimised. Thus, the residual sum of squares is a suitable goodness-of-fit expression.

Proposition A.23 (Least squares estimate)**.** *Consider the linear regression model* (A.3.1)*. If the design matrix X has full rank, the optimisation problem*

$$\min_{\beta \in \mathbb{R}^m} S(\beta)$$

possesses a unique solution $\hat{\beta}$, the least squares estimate, which is given by

$$\hat{\beta} = \left(X^T X\right)^{-1} X^T Y.$$

Proof. See [105, Section 3.1]. □

Due to the assumption on the distribution of the error ε, the least squares estimate is also the maximum likelihood estimate for β, see [105, page 43].

Proposition A.24 ($\hat{\beta}$ is unbiased)**.** *Consider the linear regression model* (A.3.1)*. Let $\hat{\beta}$ be the least squares estimate for β. It holds true that*

$$\hat{\beta} \sim \mathcal{N}_m \left(\beta, \sigma^2 \left(X^T X\right)^{-1} \right).$$

In particular, $\hat{\beta}$ is an unbiased estimate for the parameter β.

Proof. The proof is stated in [105, Section 3.2]. □

If the variance σ^2 cannot be assumed to be known, it needs to be estimated, too.

Proposition A.25 (An unbiased estimate for σ^2)**.** *Consider the linear regression model* (A.3.1)*. Let $\hat{\beta}$ be the least squares estimate for β. If the design matrix X has full rank and $n > m$, it holds true that*

$$s^2 = \frac{S(\hat{\beta})}{n - m} \tag{A.3.3}$$

is an unbiased estimate for σ^2, which satisfies

$$s^2 \sim \frac{\sigma^2}{n-m}\chi^2_{n-m}.$$

Proof. See [105, Section 3.3]. □

Next, the uncertainty of the least squares estimate $\hat{\beta}$ is addressed. Although $\hat{\beta}$ gives the value of β that fits the given data optimally, other values for β may also be compatible with the observations.

For an individual parameter $\beta_j,\ j = 1, \ldots, m$, the **confidence interval** of $\hat{\beta}_j$ contains the true parameter value of β_j with a certain probability, for example 95% (level of confidence). The multi-dimensional generalisation of a confidence interval is the confidence region. A **confidence region** of $\hat{\beta}$ contains the true parameter value of β with a certain probability. In contrast to this concept, a confidence band encloses the area that contains the true responses with a certain probability. It is closely related to prediction bands, which enclose the area that one expects future data points with a certain probability.

Theorem A.26 (Inference)**.** *Consider the linear regression model* (A.3.1)*. Let $\hat{\beta}$ be the least squares estimate for β. The following inference statements hold:*

(i) A $1-\alpha$ confidence region for β is the ellipsoid

$$\left(\beta - \hat{\beta}\right)^T X^T X \left(\beta - \hat{\beta}\right) \leq m s^2 F_{m,n-m;\alpha}$$

where $F_{m,n-m;\alpha}$ is the upper α quantile for the F-distribution with m and $n-m$ degrees of freedom.

(ii) A $1-\alpha$ confidence interval for the j-th parameter $\beta_j,\ j = 1, \ldots, m$, is given by

$$\hat{\beta}_j \pm se(\hat{\beta}_j) t_{n-m;\alpha/2}$$

where $t_{n-m;\alpha/2}$ is the upper $\alpha/2$ quantile for Student's t-distribution with $n-m$ degrees of freedom and the standard error of the estimate $\hat{\beta}_j$ given by

$$se(\hat{\beta}_j) = s\sqrt{(X^T X)^{-1}_{jj}}$$

with the j-th diagonal element of the matrix $(X^T X)^{-1}$.

(iii) A $1-\alpha$ confidence interval for the expected response at x_0 is given by

$$x_0^T\hat{\beta} \pm s\sqrt{x_0^T(X^TX)^{-1}x_0}t_{n-m;\alpha/2}.$$

(iv) A $1-\alpha$ confidence band for the response function at any x is given by

$$x^T\hat{\beta} \pm s\sqrt{x^T(X^TX)^{-1}x}\sqrt{mF_{m,n-m;\alpha}}.$$

Proof. See [105, Chapter 4]. □

Remark A.27. The matrix $s^2(X^TX)^{-1}$ is also known as the covariance matrix of the estimate $\hat{\beta}$.

Criteria of model goodness are mostly based on standard goodness-of-fit measures, on estimating the prediction error, on estimating the number of non-zero coefficients, or on estimating some measure of distance between the model based on the estimate and the true model [105].

Consider the residual sum of squares $S(\beta)$ given by (A.3.2). Let $\hat{Y}$ be the predicted (or modelled) output of the linear model (A.3.1) given the data Y. The value of $\beta = \hat{\beta}$ has been determined such that $S(\beta)$ is minimal, and $\hat{Y} = X\hat{\beta}$. Then, the residual sum of squares reads

$$S(\hat{\beta}) = \|Y - \hat{Y}\|^2 = \sum_{i=1}^{n}\left(Y_i - \hat{Y}_i\right)^2.$$

Furthermore, let $\bar{Y} = \frac{1}{n}\sum_{i=1}^{n} Y_i$ be the mean of the observed data. Then, consider the two sums given by

$$\sum_{i=1}^{n}\left(Y_i - \bar{Y}\right)^2 \quad \text{and} \quad \sum_{i=1}^{n}\left(\hat{Y}_i - \bar{Y}\right)^2,$$

where the first sum is denoted as the total sum of squares, and the latter is denoted as the regression sum of squares. The following theorem holds true:

Theorem A.28 (Coefficient of determination, adapted from Theorem 4.2 in [105])**.**

(i)

$$\sum_{i=1}^{n} \left(Y_i - \bar{Y}\right)^2 = \sum_{i=1}^{n} \left(Y_i - \hat{Y}_i\right)^2 + \sum_{i=1}^{n} \left(\hat{Y}_i - \bar{Y}\right)^2$$

(ii)

$$R^2 := \frac{\sum_{i=1}^{n} \left(\hat{Y}_i - \bar{Y}\right)^2}{\sum_{i=1}^{n} \left(Y_i - \bar{Y}\right)^2} = 1 - \frac{S(\hat{\beta})}{\sum_{i=1}^{n} \left(Y_i - \bar{Y}\right)^2}$$

The quantity R^2 is known as the coefficient of determination. It relates the squared residuals with respect to the linear regression to the squared residuals with respect to the average value. The greater the value of R^2, the closer is the predicted model output to the observed data. If the curve fits the data perfectly, then it is $S(\hat{\beta}) = 0$ and therefore $R^2 = 1$. Otherwise, in general, $R^2 < 1$.

The residual sum of squares $S(\hat{\beta})$ and the estimated variance s^2 (see (A.3.3)) are suitable measures for the goodness of the fit if one aims to compare models with the same number of variables [105].

A.3.2 Non-linear regression models

In linear regression, the relationship between the explanatory variables and the observations was considered to be linear in the parameters. Most physical and biological models involve responses to be non-linear functions of the parameters. As in linear regression, non-linear estimation of parameters seeks to find those parameter values that minimise the sum of squared residuals. Yet one usually cannot solve the equation for the parameters analytically. For that reason various iterative numerical procedures are applied.

Definition A.29 (Non-linear regression model)**.** Let $Y_i,\ i = 1, \ldots, n$ be the i-th observation or response, $x_i \in \mathbb{R}^k$ a vector of associated independent variables for the i-th observation and $\theta \in \mathbb{R}^m$ the vector of parameters. Furthermore, let $f = f(x_i, \theta) \colon \mathbb{R}^k \times \mathbb{R}^m \to \mathbb{R}$ be the expectation function which is supposed to be

non-linear in the parameters θ. The random variable ε_i represents the disturbance which perturbs the i-th response. The non-linear regression model reads

$$Y_i = f(x_i, \theta) + \varepsilon_i \text{ with } \varepsilon_i \sim \mathcal{N}(0, \sigma^2) \tag{A.3.4}$$

or, in vector notation for n observations,

$$Y = \eta(\theta) + \varepsilon \text{ with } \varepsilon \sim \mathcal{N}_n(0, \sigma^2 \mathbb{I}_n) \tag{A.3.5}$$

where $\eta(\theta) = (f(x_1, \theta), \ldots, f(x_n, \theta))^T$.

As in linear regression, the least squares estimate $\hat{\theta}$ of the parameter θ is of interest. Geometrically, this means that the vector function $\eta(\theta)$ defines an m-dimensional surface, called expectation surface, in the response space. The least squares estimate corresponds to the point on the expectation surface, $\hat{\eta} = \eta(\hat{\theta})$, which is closest to Y. Again, this implies that $\hat{\theta}$ minimises the residual sum of squares

$$S(\theta) = \|Y - \eta(\theta)\|^2.$$

Finding the best estimate $\hat{\theta}$ of the parameter θ in the non-linear regression model (A.3.5) given the data typically involves the optimisation of a function, i.e. minimisation of $S(\theta)$. Since this optimisation problem can rarely be solved analytically, iterative numerical procedures have to be applied to find the optimal value of θ. In general, the involved functions possess one or more local optima in addition to their global optimum. This further complicates the optimisation procedure. Moreover, reliable global optimisation methods are still subject of research and only available for very restrictive classes of objective functions. Local optimisation methods can be applied to find a local minimum. For a detailed survey on non-linear regression methodology, see [6, 96, 106].

Remark A.30 (Embedding differential equation models in the regression framework)**.** Models describing biological or medical phenomena are formulated using differential equations, for example

$$x'(t) = f(x(t), \theta)$$

where $x(t) \in \mathbb{R}^k$ is the state at time t, and $\theta \in \mathbb{R}^m$ is the vector of parameters. For piecewise-smooth systems, it is $f : \mathbb{R}^k \times \mathbb{R}^m \to \mathbb{R}^k$ piecewise-smooth in the state-space $x(t, \theta)$. Let $g : \mathbb{R}^k \to \mathbb{R}^l,\ l \leq k$, be the function which associates the internal states $x(t, \theta)$ with the observations $y(t)$, that is to say,

$$y(t) = g(x(t, \theta)) + \varepsilon,$$

where ε represents the normally distributed measurement noise. In particular, if all internal states can be observed, it is $g = id$. Consequently

$$y(t) = x(t, \theta) + \varepsilon$$

with $y(t) \in \mathbb{R}^k$. In general, the relationship between x and t is non-linear in the parameters θ. Moreover, $x(t, \theta)$ (and therefore $g(x(t, \theta))$) cannot be expected to be differentiable with respect to the parameters θ, see Remark A.9. Note that if $l < k$, the model is said to be partially observed. Observations can be measurements taken at discrete time points $t_j,\ j = 1, \ldots, n$. If $n \geq m$, then the model parameters θ can be (not necessarily uniquely - see Appendix A.4) determined on basis of the observations [106].

In case of the parameter estimation problem in the framework of the myeloma model (5.0.1), data describe the total number of both healthy and malignant PCs and do not distinguish between cells out- or inside the niche. Hence, the observables are sums of the internal states. In this view, since $k = 4$ and $l = 2$, the myeloma model is partially observed.

Linear approximation

In this section, the linear approximation for the non-linear regression model given by (A.3.4) or (A.3.5), respectively, is introduced. Let $f \in C^1(\mathbb{R}^k \times \mathbb{R}^m, \mathbb{R})$.

The most basic numerical approach for finding the least squares estimate given the data vector Y, the expectation function $f(x_i, \theta)$ and a set of design vectors $x_i,\ i = 1, \ldots, n$, is the Gauss-Newton method. It uses a linear approximation of the function f to iteratively improve an initial guess θ^0 for θ and keeps improving the estimates until there is no further improvement. The function $f(x_i, \theta)$ is expanded

in a first order Taylor series about θ^0 as follows:

$$f(x_i, \theta) = f(x_i, \theta^0) + \nu_{i1}(\theta_1 - \theta_1^0) + \nu_{i2}(\theta_2 - \theta_2^0) + \cdots + \nu_{im}(\theta_m - \theta_m^0)$$

with

$$\nu_{ij} = \left.\frac{\partial f(x_i, \theta)}{\partial \theta_j}\right|_{\theta^0} \quad \text{for} \quad j = 1, \ldots, m.$$

In vector notation, this reads

$$\eta(\theta) = \eta(\theta^0) + V^0(\theta - \theta^0)$$

where $V^0 \in \mathbb{R}^{n \times m}$ is the Jacobian matrix of η evaluated at θ^0 with elements $\{\nu_{ij}\}$. Setting $\varepsilon^0 = Y - \eta(\theta^0)$ and $\delta = \theta - \theta^0$, this is equivalent to

$$\varepsilon(\theta) = Y - \Big(\eta(\theta^0) + V^0\delta\Big) = \varepsilon^0 - V^0\delta,$$

which is an approximation of the residuals. Observe that we derived a linear regression model (A.3.1) given by

$$\varepsilon^0 = V^0\delta + \varepsilon(\theta)$$

with the preliminary residuals ε^0 as observation variable, the rows of V^0 as vectors of associated independent variables, and the coefficients $\delta \in \mathbb{R}^m$. This linear model approximates the non-linear regression model, allowing the use of methods in the framework of linear regression.

Continuing the Gauss-Newton method, an increment is calculated based on the geometry of the linear regression model in order to minimise the approximate residual sum of squares $\|\varepsilon^0 - V^0\delta\|^2$. This yields an improved value θ^1, for which again, the approximated model is calculated. This iteration step is continued as long as the correction of the previous estimate is negligible. Information about the technical details can be found in [6, 12]. An overview of further common numerical methods can be found in [13, 106].

Remark A.31 (Linear approximation)**.**

(i) The adequacy of the linear approximation is essential both for the quality of the numerically determined estimate with respect to the non-linear model, and the convergence properties of the numerical methods. Beside this, reasonably chosen initial guesses may help the iterative procedure to find a solution more quickly and surely. Since the Gauss-Newton method is a local optimisation method, the algorithm tends to stop in a local minimum. Consequently, the initial guess θ^0 should be varied to assure the identification of the global minimum.

(ii) If f is a piecewise-smooth function, then the partial derivatives ν_{ij} do not exist at non-differentiable points. However, most algorithms based on derivatives (such as the Gauss-Newton method) still tend to perform well as long as the discontinuities are isolated, few and do not occur in the neighbourhood of the minimum [106].

(iii) The derivatives ν_{ij} are also called sensitivities, which shall be discussed in Appendix A.4.

The linear approximation is used to derive appropriate statistical inference about the least squares estimate $\hat{\theta}$. For that, let $\hat{V}$ denote the Jacobian matrix of η evaluated at $\hat{\theta}$. The linear approximation is given by

$$\eta(\theta) = \eta(\hat{\theta}) + \hat{V}(\theta - \hat{\theta}).$$

Analogously to the results in Theorem A.26, an approximate $1 - \alpha$ confidence region for a non-linear model is given by

$$\left(\theta - \hat{\theta}\right)^T \hat{V}^T \hat{V} \left(\theta - \hat{\theta}\right) \leq m s^2 F_{m,n-m;\alpha},$$

where the linear approximation $\hat{V}$ takes the place of the design matrix X. Similarly, approximate confidence bands may be constructed.

Remark A.32 (Goodness-of-fit measures for non-linear regression)**.** In contrast to linear regression models, the sums of the squared errors in non-linear regression generally do not add up as stated in Theorem A.28. As a consequence, using R^2 to

evaluate the fit of non-linear models leads to incorrect conclusions [112]. Instead, the unbiased estimate of the error variance given by

$$s^2 = \frac{S(\hat{\theta})}{n-m} \tag{A.3.3}$$

can be used, where n is the number of measurements and m is the number of parameters. In particular, it can be used to compare the goodness of a fit of different models given the same set of data. A smaller value of s^2 indicates a better fit.

In the following, a numerical method is addressed which does not incorporate derivatives. The so-called direct search methods do not approximate $\eta(\theta)$ in the vicinity of θ^0. Instead, they compare function values. These methods are generally recommended for non-smooth functions [31].

The method of Nelder and Mead

The algorithm of Nelder and Mead [90] is the most common direct search method. It is based on a simplex, which is a polytope of $n+1$ vertices in n dimensions. In the following, the algorithm is delineated.

Let g be the function to minimise. At each iteration, $n+1$ points $x_1, \ldots, x_{n+1}$ form the corners of a regular polytope or simplex. For instance, for $n = 2$, the polytope is a triangle. The points are ordered such that $g(x_1) \leq g(x_2) \leq \cdots \leq g(x_{n+1})$. The worst point x_{n+1} is replaced by a newly generated point. Let

$$c = \sum_{i=1}^{n} x_i$$

be the centroid of the remaining points. A new trial point x_t is generated by reflecting the worst point through the centroid, i.e.

$$x_t = c + \alpha(c - x_{n+1}),$$

where $\alpha > 0$ is a parameter of the algorithm. The following action to be taken depends on x_t:

- If $g(x_1) \leq g(x_t) \leq g(x_n)$, then replace x_{n+1} by x_t.

- If $g(x_t) < g(x_1)$, the search direction is promising, thus one more reflection can be carried out by

$$x_e = c + \beta(x_t - c) \quad \text{with} \quad \beta > 1.$$

  If $g(x_e) < g(x_t)$, then x_e replaces x_{n+1}. Otherwise, x_t replaces x_{n+1}.

- If $g(x_t) > g(x_n)$, i.e. x_t is still the worst point, a smaller contraction step needs to be taken. The new trial point is defined as

$$x_c = \begin{cases} c + \gamma(x_{n+1} - c) & \text{if } \; x_t \geq x_{n+1} \\ c + \gamma(x_t - c) & \text{if } \; x_t < x_{n+1} \end{cases}$$

  with $0 < \gamma < 1$. If $g(x_c) < \min\{g(x_{n+1}), g(x_t)\}$, replace x_{n+1} by x_c. Otherwise, a further contraction is carried out.

As possible stopping rule, a maximal amount of iterations can be predetermined. Another possibility is to stop the algorithm if the difference between the best function values in the new and old polytope, or the distance between the new best point and the old best point are less than prescribed tolerances, see Wolfram Research *Mathematica's* online documentation (http://reference.wolfram.com; last accessed: April 2016). In contrast to derivative-based optimisation methods, the Nelder-Mead algorithm is more robust, though its rate of convergence is lower [106].

Estimation with *Mathematica*

Non-linear regression analysis is performed using the software package *Mathematica, Version 9* by Wolfram Research. The numerically solved system is used to fit the (transformed) data to the obtained system of equations.

Mathematica has a built-in function called `NonlinearModelFit` which returns a `FittedModel` object representing the constructed non-linear model based on the given data. The software also returns properties and diagnostics of the model which rely on linear approximations. In case of the myeloma model (5.0.1), this is at the expense of the routine's execution time. Consequently, the residual sum of squares is directly minimised using built-in functions for numerical non-linear optimisation. The function `NMinimize` is able to cope with functions that are not differentiable.

The algorithm of Nelder and Mead is used by specifying the method `NelderMead`. To identify the global minimum, we choose different initial guesses for the values of the parameters and run optimisation several times.

A.4 Sensitivity and identifiability

A.4.1 Sensitivity analysis

Sensitivity analysis investigates how a perturbation of the value of an independent variable (for example a parameter) influences a particular dependent variable (for example an observation) [29]. Global sensitivity analysis considers model behaviour over a wide range of parameter values, whereas local sensitivity analysis focuses on investigation of model behaviour near a particular point in the parameter space.

Consider the following initial value problem

$$x'(t) = f(x(t,\theta),\theta), \quad x(t_0) = x_0 \tag{A.4.1}$$

with $x(t,\theta) \in \mathbb{R}^k$ and parameters $\theta \in \mathbb{R}^m$. We assume that $f\colon \mathbb{R}^k \times \mathbb{R}^m \to \mathbb{R}^k$ is sufficiently smooth. In case of piecewise-smooth continuous dynamical systems, the right-hand side f is in general not smooth. However, it can be approximated by a smoothed vector field [78]. For details, see Appendix A.2. In order to interpret the initial value x_0 as parameter, let $\tilde{\theta} = (\theta, x_0)^T \in \mathbb{R}^{m+k}$. In the following, the tilde is skipped. Let $x(t,\theta)$ denote the solution of (A.4.1).

Changing the value of the j-th parameter, $j = 1,\ldots,m$, in the parameter vector θ, from θ_j to $\theta_j + \Delta(\theta_j)$ yields the corresponding solution to become

$$x = x(t, \theta_j + \Delta(\theta_j)), \tag{A.4.2}$$

where for brevity, only θ_j is mentioned explicitly. Since x is a continuous function of θ_j, (A.4.2) can be expanded into a Taylor series. For small $\Delta(\theta_j)$, the Taylor series can be truncated after the linear term, yielding

$$\Delta(x) = x(t, \theta_j + \Delta(\theta_j)) - x(t,\theta_j) \approx \frac{\partial x(t,\theta_j)}{\partial \theta_j}\Delta(\theta_j).$$

$\Delta(x)$ is the variation of x due to the change of the input parameter θ_j given by $\Delta(\theta_j)$. Taking the limit $\Delta(\theta_j) \to 0$ results in

$$\frac{\partial x(t,\theta_j)}{\partial \theta_j},$$

which is known as the (first order) local sensitivity of the dependent variable x with respect to the input parameter θ_j.

In the following, established definitions in sensitivity analysis are summarised [25].

Definition A.33 (Nominal value)**.** The nominal value of a parameter vector θ, which is assigned by θ^0, is that value of θ whose corresponding experimental and analytical system responses are initially very close to each other, or, ideally, these two values are identical. It also refers to the estimate of θ.

Definition A.34 (Parameter variation)**.** If θ changes its nominal (or initial) value θ^0 to a new value $\theta^0 + \Delta(\theta)$, then $\Delta(\theta)$ is defined as parameter variation relative to the nominal condition θ^0. It is assumed that this change is static.

Definition A.35 (Primitive sensitivity function)**.** Assume that $\Delta(\theta_j)$ is the parameter variation of the j-th component of θ, i.e. θ_j. Suppose that x_i, i.e. the i-th component of the response of system (A.4.1), changes to $x_i + \Delta(x_i)$ as θ_j changes to $\theta_j + \Delta(\theta_j)$. Then, the ratio $\Delta(x_i)/\Delta(\theta_j)$ is defined as the primitive sensitivity function.

As shown above, if the parameter variation $\Delta(\theta_j)$ is small, it is

$$\lim_{\Delta(\theta_j)\to 0} \frac{\Delta(x_i)}{\Delta(\theta_j)} = \frac{\partial x_i}{\partial \theta_j},$$

which exists due to smoothness of f in (A.4.1) [39]. Then the following time-dependent matrix can be constructed:

Definition A.36 (Sensitivity matrix and sensitivity function)**.** The matrix

$$S(t) = \frac{\partial x}{\partial \theta}(t,\theta) = \begin{pmatrix} \frac{\partial x_1}{\partial \theta_1}(t,\theta) & \frac{\partial x_1}{\partial \theta_2}(t,\theta) & \cdots & \frac{\partial x_1}{\partial \theta_{m+k}}(t,\theta) \\ \frac{\partial x_2}{\partial \theta_1}(t,\theta) & \frac{\partial x_2}{\partial \theta_2}(t,\theta) & \cdots & \frac{\partial x_2}{\partial \theta_{m+k}}(t,\theta) \\ \vdots & \vdots & \ddots & \vdots \\ \frac{\partial x_k}{\partial \theta_1}(t,\theta) & \frac{\partial x_k}{\partial \theta_2}(t,\theta) & \cdots & \frac{\partial x_k}{\partial \theta_{m+k}}(t,\theta) \end{pmatrix}$$

is called sensitivity matrix with respect to the parameters θ. The element $S_{ij}(t)$ is called sensitivity function of x_i with respect to θ_j.

The sensitivity function

$$S_{ij}(t) = \frac{\partial x_i}{\partial \theta_j}(t, \theta)$$

describes how the state $x_i,\ i = 1, \ldots, k$, changes if the parameter $\theta_j,\ j = 1, \ldots, m$, is infinitesimally altered. In order to eliminate the physical dimension of the sensitivity functions and to normalise the magnitudes of the input parameter θ_j and the variable x_i, the sensitivities are multiplied by a weighting factor, which yields relative or normalised sensitivity functions.

Definition A.37 (Normalisation of the sensitivity)**.** Consider the following types of normalisation of the sensitivity function $S_{ij}(t)$:

(i) Normalisation relative to the numerator (species quantity): $\frac{1}{x_i(t,\theta)} S_{ij}(t)$

(ii) Dimensionless normalisation: $\frac{\theta_j}{x_i(t,\theta)} S_{ij}(t)$

The normalised sensitivity relative to the species quantity can be interpreted as follows: An infinitesimal increase in θ_j near θ_j^0 leads to a $\frac{1}{x_i(t,\theta)} S_{ij}(t) \times 100\ \%$ increase in $x_i(t, \theta)$ at time t.

Remark A.38 (Large changes of the parameter)**.** If the change $\Delta(\theta)$ of the parameter θ is not infinitesimal but large, the error $x(t, \theta^0 + \Delta(\theta)) - x(t, \theta^0)$ needs to be addressed instead of using sensitivity functions. For that, it is sufficient for f in (A.4.1) to be Lipschitz continuous.

Sensitivities can be calculated using numerical methods which are based on external and internal numerical differentiation, for example using the **variational differential equation** or sensitivity equations, respectively [11, 12, 100]. Differentiation of the sensitivity matrix with respect to the time t, and reversing the order of differentiation, yields

$$\frac{d}{dt}\frac{\partial x}{\partial \theta}(t, \theta) = \frac{\partial}{\partial \theta}\left(\frac{d}{dt} x(t, \theta)\right) = \frac{\partial f}{\partial \theta}(x(t, \theta), \theta).$$

Using the chain rule for differentiation, it follows that the variational differential equation,

$$\frac{d}{dt}\frac{\partial x}{\partial \theta}(t,\theta) = \frac{\partial f}{\partial x}(x(t,\theta),\theta)\frac{\partial x}{\partial \theta}(x(t,\theta),\theta) + \frac{\partial f}{\partial \theta}(x(t,\theta),\theta). \tag{A.4.3}$$

Since $\theta \in \mathbb{R}^{m+k}$ includes the m-dimensional vector of parameters and the k-dimensional vector of initial conditions for the solution vector $x(t,\theta)$, the initial conditions for system (A.4.3) at $t = t_0$ are given by

$$\frac{\partial x}{\partial \theta}(t_0,\theta) = \left(0^{k\times m}\ \mathbb{1}^{k\times k}\right),$$

where $0^{k\times m}$ denotes the $k \times m$-dimensional zero matrix and $\mathbb{1}^{k\times k}$ is the $k \times k$-dimensional identity matrix. The sensitivities in (A.4.3) are to be solved simultaneously with the respective state equations (A.4.1).

Beside other applications, sensitivity can be used as a tool for model calibration, i.e. determining numerical values for model parameters. This is a key issue in fitting models to given data. Sensitivity can address model identifiability, i.e. the question of whether or not parameter values for a model can be determined from a given set of data.

A.4.2 Local structural identifiability

Identifiability analysis investigates if it is possible to assign unique values for the unknown parameters for one model prediction. This is fundamental for parameter estimation since the presence of non-identifiable parameters may result in bad convergence of the numerical method for solving the optimisation problem leading to wrong results.

According to Raue et al. [99], a parameter is said to be identifiable if the confidence interval of its estimate is finite. A very large confidence interval may already indicate non-unique identification of the corresponding parameter, particularly if the interval includes zero. In the following, structural identifiability is considered, which is related to model structure independent of data. In contrast, practical identifiability takes into account the amount and quality of the data, being less well defined in literature [97–99].

Definition A.39 (Structural identifiability, adapted from Chapter 2 in [126])**.** Let $M(\theta)$ represent a mathematical model with vector $\theta \in \mathbb{R}^m$ of unknown parameters.

(i) A parameter $\theta_i,\ i = 1, \ldots, m$, is globally structurally identifiable if for almost any $\theta^* \in \mathbb{R}^m$, it follows that $M(\theta) = M(\theta^*)$ implies $\theta_i = \theta_i^*$.

(ii) A parameter $\theta_i,\ i = 1, \ldots, m$, is locally structurally identifiable if for almost any $\theta^* \in \mathbb{R}^m$, there exists a neighbourhood $\mathcal{U}(\theta^*)$ such that $M(\theta) = M(\theta^*)$ implies $\theta_i = \theta_i^*$ for all $\theta \in \mathcal{U}(\theta^*)$.

(iii) A parameter $\theta_i,\ i = 1, \ldots, m$, is structurally non-identifiable if for almost any $\theta^* \in \mathbb{R}^m$, there exists no neighbourhood $\mathcal{U}(\theta^*)$ such that $M(\theta) = M(\theta^*)$ implies $\theta_i = \theta_i^*$ for all $\theta \in \mathcal{U}(\theta^*)$.

For the subsequent analysis of local structural identifiability of parameters and its relation to sensitivity functions, consider the system

$$\begin{aligned} x'(t) &= f(x(t), \theta), \quad x(t_0) = x_0 \\ y(t) &= g(x(t), \theta) \end{aligned}$$

where $x(t) \in \mathbb{R}^k$ describes the state, $\theta \in \mathbb{R}^m$ is the vector of parameters, and $y(t)$ is the model output. Furthermore, $f : \mathbb{R}^k \times \mathbb{R}^m \to \mathbb{R}^k$, and $g : \mathbb{R}^k \times \mathbb{R}^m \to \mathbb{R}^l,\ l \leq k$. The function g describes the observations in terms of the state variable and the parameters. Again, the parameter vector may be extended to capture the initial condition x_0, i.e. $\tilde{\theta} = (\theta, x_0)^T \in \mathbb{R}^{m+k}$. In the following, the tilde is skipped. For sake of simplicity, the derivation for one observation is provided, i.e. $y(t)$ is a scalar. Note that the results may be extended to multiple observations. The descriptions follow Walter [125].

For an initial estimate $\hat{\theta}$ for θ, a large number of predictions at $n > m + k$ time points can be computed, where $y(t_i) = y(i, \hat{\theta}),\ i = 1, \ldots, n$. If $y(i, \theta) = y(i, \hat{\theta})$ for $\theta \neq \hat{\theta}$, then both outputs are indistinguishable, resulting in non-identifiability of $\hat{\theta}$. Let the map G be defined by

$$G : \theta \mapsto y(i, \theta), \quad i = 1, \ldots, n.$$

Identifying $\hat{\theta}$ from the set of predictions $\{y(i, \theta) \colon i = 1, \ldots, n\}$ can be viewed as looking for an inverse mapping G^{-1}. The inverse function theorem implies that this

exists (locally) if the matrix H defined by

$$H = \begin{pmatrix} \frac{\partial y}{\partial \theta_1}(1,\theta) & \frac{\partial y}{\partial \theta_2}(1,\theta) & \cdots & \frac{\partial y}{\partial \theta_{m+k}}(1,\theta) \\ \frac{\partial y}{\partial \theta_1}(2,\theta) & \frac{\partial y}{\partial \theta_2}(2,\theta) & \cdots & \frac{\partial y}{\partial \theta_{m+k}}(2,\theta) \\ \vdots & \vdots & \ddots & \vdots \\ \frac{\partial y}{\partial \theta_1}(n,\theta) & \frac{\partial y}{\partial \theta_2}(n,\theta) & \cdots & \frac{\partial y}{\partial \theta_{m+k}}(n,\theta) \end{pmatrix}$$

has a rank equal to the number of unknown parameters. Observe that H is a sensitivity matrix with entries giving the sensitivities of the model output $y(t,\theta)$ to infinitesimal perturbations of parameters at time points $t_j,\ 1,\ldots,n$. For identification of insensible and therefore locally non-identifiable parameters, the columns of H have to be examined. For insensible parameters the corresponding columns have only (nearly) zero entries. If some components of θ are a priori known, it implies that corresponding columns of H are zero, and they have to be discarded [52, 125]. Investigation of parameter sensitivity allows drawing conclusions on local structural identifiability. Along these lines, a parameter is likely to be identifiable if the system output is highly sensitive to small perturbations of this parameter. Otherwise, locally insensible parameters are likely to be non-identifiable. Moreover, narrow confidence intervals for the estimates of the parameters under consideration may imply their identifiability. If the use of different methods for parameter estimation and different values for initial guesses lead to the same estimates, this indicates that the parameter of interest is identifiable.

Available data should not be disregarded since structural identifiability does not necessarily imply practical identifiability [97]. An insufficient amount and quality of data or of the chosen time points can lead to large confidence intervals.

B Contributions

Table B.1: Contributions to the scientific work depicted in this thesis.

Subject	**Item**	**Contribution**
Modelling	Discussion and development of model formulation and interpretation of results	PD Dr. Dr. Dirk Hose (2) Prof. Dr. Anna Marciniak-Czochra (1) Dr. Anja Seckinger (2)
	Statistical analysis and interpretation of doubling times (Section 9.1)	PD Dr. Dr. Dirk Hose (2) Dr. Anja Seckinger (2)
Mathematical analysis	Discussion of relevant issues	Prof. Dr. Anna Marciniak-Czochra (1)
Sampling and plasma cell purification	Scientific, administrative and organisational responsibility	PD Dr. Dr. Dirk Hose (2)
	Performing bone marrow aspiration	Responsible physician
	Performing purification	Technicians (2)
	Data analysis and interpretation	PD Dr. Dr. Dirk Hose (2) Dr. Anja Seckinger (2)
Clinical data	Scientific responsibility	PD Dr. Dr. Dirk Hose (2) Dr. Anja Seckinger (2)
	Data collection	PD Dr. Dr. Dirk Hose (2) Dr. Anja Seckinger (2) Sybille Seyfried (2)
	Data analysis and interpretation	PD Dr. Dr. Dirk Hose (2) Dr. Anja Seckinger (2)

Legend:

(1) Applied Analysis and Modelling in Biosciences (Head: Prof. Dr. Anna Marciniak-Czochra), Institute of Applied Mathematics, Interdisciplinary Center for Scientific Computing (IWR) and BIOQUANT Center, Im Neuenheimer Feld 205, D-69120 Heidelberg, Germany.

(2) Multiple Myeloma Research Laboratory (Head: PD Dr. Dr. Dirk Hose), Medical Clinic V, University Clinic Heidelberg, Im Neuenheimer Feld 410, D-69120 Heidelberg, Germany.